The University of Adelaide
Department of Physics and Mathematical Physics

FIDELITY OF OPTICAL PHASE CONJUGATION USING STIMULATED BRILLOUIN SCATTERING

Vladimyros Devrelis

MechEng *SAIT*, BAppSc *SAIT*, BSc(Hons) *Flinders*, GradDipBus *UniSA*

Thesis submitted for the degree of

Doctor of Philosophy

in

The University of Adelaide

September, 1997

CONTENTS

ABSTRACT

This thesis describes the experimental study of stimulated Brillouin scattering (SBS) used in optical phase conjugation (OPC) of laser beams. The OPC-SBS process was investigated for a variety of pumping conditions and focusing geometries in order to establish regimes of best operation. The main interest was in understanding the parameters that govern the process for the purpose of developing practical laser systems and improving current theoretical models. The findings should assist in the application of OPC-SBS to current laser technology for aberration correction as well as to new designs of Q-switched laser oscillators for high beam quality.

The thesis is divided into five chapters. Chapter one contains the theory of OPC and SBS, and presents the plan for the thesis. Chapter two is concerned with the generation of phase conjugate Stokes waves from laser pump pulses with long coherence length (~ 3.3 m). Any phenomena in the Stokes waves that detracted from a perfect OPC performance are presented with extensive experimental detail and an understanding of the processes dynamics is discussed. This study showed that the time of relaxation of the hypersound in the medium under a specific focusing geometry plays an important role in determining whether that OPC mirror would be able to reconstruct the input laser beam. High reflectivity and phase fidelity OPC-SBS is also successfully demonstrated in this study.

Chapter three investigates the effect that the rise time of the input laser pulse has on Stokes phase fidelity. Pulses with long coherence length but rise times much faster than the hypersound relaxation time are found to degrade the fidelity of the Stokes wave. This finding is in qualitative agreement with other existing studies.

Chapter four details the effects that input laser pulses with short coherence length have on the OPC-SBS process. Specifically optical breakdown and cavitation bubbles are examined and discussed closely. This regime of OPC-SBS is the most difficult to work in, as it produced Stokes returns with both poor reflectivity and fidelity. This regime does not appear promising for phase conjugation.

The conclusions based on the knowledge gained from this thesis are presented in the final chapter.

Declaration

Except as stated herein, this thesis contains no material which has been accepted for the award of any other degree or diploma in any University. To the best of my knowledge and belief, this thesis contains no copy or paraphrase of material previously published or written by another person, except where due reference is made in the text of this thesis.

I give my consent for this thesis to be made available for photocopying and loan.

V. Devrelis

ACKNOWLEDGEMENTS

In the course of an Ph.D. project assistance inevitably comes from many different people in many different ways.

I recognise with gratitude the direction, and support given to me by my supervisor Professor Jesper Munch. I also thank him for the quite critical reading of this thesis. I am thankful to him for the opportunity to transform a room with a wooden table into an optics laboratory and become a member of the newly formed 'Laser and Nonlinear Optics' group which grew from 3 to around 20 people.

I am indebted to the much appreciated assistance accorded to me by Martin V O'Connor who collaborated on the work in sections 2.2, 2.3, 4.2 and 4.3, Dr. Changjiang Wei who collaborated in section 2.3.2, Sahraam Afshaarvahid for collaborating on the modelling of the transient SBS process in section 1.3, Petar Atanackovic for his assistance with the GPIB programming and Tim Bubner for the use of the distillation and NMR equipment. Most of them at various times, throughout this project, fulfilled a role as sounding boards for many ideas and valuable collaborators. Their valuable contribution to the work covered by this thesis is represented in the co-authorship of the published papers. I am also indebted to the staff and students of the Department of Physics and Mathematical Physics, at Adelaide, for their help and friendship.

My thanks go to my employers at DSTO (Defence Science and Technology Organisation) for the opportunity to do a PhD and for their financial assistance during the candidature.

Last but not least, I would like to thank my family and friends for their never-ending support.

Αυτη η διατριβη ειναι αφιερωμενη στην Αφροδιτη καθως και σε ολα τα αλλα αγαπητα μου προσωπα.

Πασα επιστημη χωριζομενη δικαιοσυνης και της αλλης αρετης πανουργια, ου σοφια φαινεται.

(Πλατων)

Chapter 1

Introduction

Diffraction limited beam quality and low beam jitter are desirable but not easily obtained characteristics of most high power lasers. In high power solid state lasers, for example, the beam quality is often degraded by thermal and mechanical stress in the laser rod. However, Optical Phase Conjugation via Stimulated Brillouin Scattering (OPC-SBS) could potentially offer laser systems with beams that are diffraction limited and have excellent pointing stability in any situation. Unfortunately, even SBS has its own limitations which have been reported by many researchers.

This thesis is concerned with my work on the problem of spatial beam quality degradation in Optical Phase Conjugation. The purpose of this chapter is to outline the basic concepts and structure of the work. These concepts should assist in clarifying (i.e. interpret) some of the processes that will be encountered in the following chapters (2, 3 and 4). An explanation of optical phase conjugation and stimulated Brillouin scattering in relation to beam quality is to be presented.

1.1 Optical Phase Conjugation

Real time optical phase conjugation (OPC) in nonlinear processes, also referred to as wave-front reversal, was first observed in 1971.[1] Optical Phase Conjugation permits aberration correction through a double pass technique. In a way, it resembles time reversal as the output reconstructed wavefront is identical to the input reference beam, but propagates in the opposite direction. It is for this reason that the process of OPC can be used in particular optical systems such as lasers, to remove optical aberrations. The practical importance of the process is that it can correct both static and dynamic aberrations. This is a truly "magical" reflector when compared to a typical bathroom mirror.

The basic nature of OPC can best be understood by comparing its behaviour to that of an normal mirror. Consider an example, where a plane light wave enters a medium which has a spatial variation in refractive index across its aperture (e.g. a lens). As Figure 1.1.1 indicates the transmitted wavefront is no longer plane but has been altered. Some parts of the wave have been advanced in respect to the rest. The wave now strikes the normal mirror and is reflected towards the medium. It is critical here to notice that the advanced part of the wavefront is reflected first and then the rest follows. The reflected wave enters the medium (i.e. lens) for a second time and after exiting, the wave has suffered a further second alteration. We see that the original input light wave and the new output wave are different from each other. In Figure 1.1.2 we have replaced the normal mirror with a phase conjugate mirror. Now the transmitted wave having passed through the medium strikes the OPC mirror. It is here that we note that the reflected wave has the inverse wavefront to that of the incident.

Again the reflected wave enters the medium for a second time and after exiting, the wave is recovered, as the retarded part of the wave is now advanced by an equal amount. Comparison between the original input light wave and the new output wave shows no difference in the wavefront of these two. A complete reconstruction of the original wave has been achieved.

Together with the phase reversal property, the OPC mirror must also maintain the intensity distribution which is associated with each wave in the beam.[2] It is these two properties that allow the OPC mirror to correct distortions.

The concept of optical phase conjugation can be understood by introducing a mathematical description of the process. We will assume that the incident wave on the phase conjugate mirror is monochromatic with angular frequency ω_L, wave number k_L and is propagating in the negative z direction. This wave is represented as:

$$E_L(r,t) = \frac{1}{2}\left[A_L(r)e^{i(\omega_L t + k_L z)} + A_L^*(r)e^{-i(\omega_L t + k_L z)}\right] \qquad (1.1.1)$$

where $A_L(r)$ is a slowly varying field amplitude that describes the transverse extent of the wave.

A counter propagating wave to 1.1.1 (i.e. a reflection) will be expressed as:

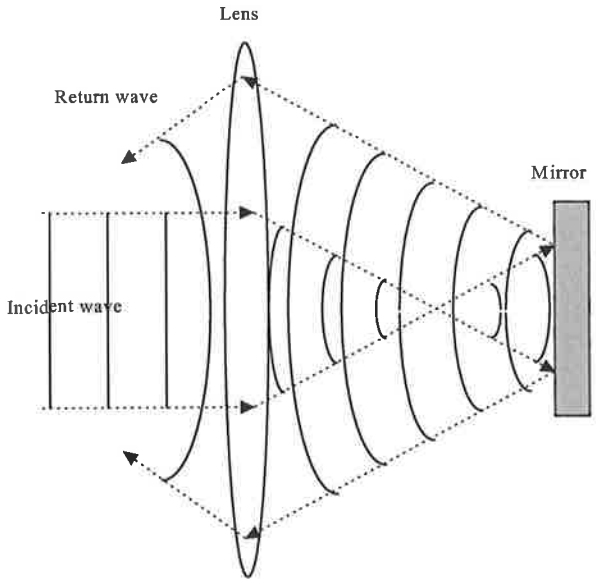

Figure 1.1.1: Diagram indicates the transmitted wavefront after reflection from normal mirror is no longer plane but has been altered.

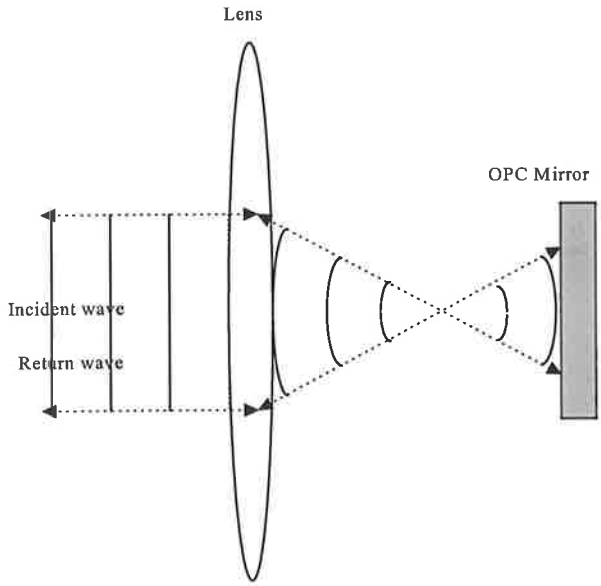

Figure 1.1.2: Diagram indicates the transmitted wavefront after reflection from the OPC mirror reproduces the incident wave.

$$E_S(r,t) = \frac{1}{2}\left[A_S(r)e^{i(\omega_S t - k_S z)} + A_S^*(r)e^{-i(\omega_S t - k_S z)} \right] \quad (1.1.2)$$

When an ideal PC mirror is illuminated by the incident wave (i.e. equation 1.1.1) it produces a reflected (backward scattering) wave, called the phase conjugate wave, given by

$$E_S(r,t) = \frac{1}{2}\left[RA_L^*(r)e^{-i(\omega_L t - k_L z)} + RA_L(r)e^{i(\omega_L t - k_L z)} \right] \quad (1.1.3)$$

Where R represents the amplitude reflection coefficient of the PC mirror and we assume $\omega_S = \omega_L$ (the incident and return wavelength is the same). We note from these expressions (1.1.1-3) that

$$E_S(r,t) = RE_L(r,-t)$$
if
$$A_S(r) = RA_L^*(r) \quad (1.1.4)$$

That is to say the electric field amplitude can be replaced by its complex conjugate amplitude. Due to this result the process of wave-front reversal is called phase conjugation. The reflected wave is essentially a time reversed replica of the input. This treatment is suitable for the description of an ideal phase conjugate mirror.

When a wave enters a medium, its amplitude can be described mathematically as a function of z and t, and we often assume for simplicity that the wave has plane wavefront and that the second order derivatives can be ignored. This approach uses the

fact that the amplitude of the wave will always change slowly compared to the oscillating part of the expression $E_L(z,t)$ (e.g. the scale of the variation of the amplitude along z is larger than the optical wavelength). When substituting this expression into Maxwell's equations, the differentials with respect to the amplitude will be small compared to those of the oscillating part. Thus, by ignoring all negligible terms a great deal of simplification of the resulting equations can be obtained. This process of simplification is known as the slowly varying envelope approximation (SVEA).

Insight into the phase conjugation process can be gained through a mathematical description of the practical case where a beam of light passes twice in opposite directions through an aberrating medium (e.g. atmospheric turbulence). The incident wave $E_L(r,t)$, propagates through a lossless material of nonuniform refractive index $n(r)=[\varepsilon(r)]^{1/2}$, where $\varepsilon(r)$ is the dielectric permittivity.[3] The scale of the spatial variation of $\varepsilon(r)$ is assumed to be much larger than the laser wavelength. The monochromatic incident and return waves must satisfy Maxwell's paraxial wave equation.

$$\nabla^2 A_L + \left(\frac{\varepsilon(r)\omega^2}{c^2} - k^2 \right) A_L + 2ik \frac{\partial A_L}{\partial z} = 0 \qquad (1.1.5)$$

The mean direction of propagation is along the z (longitudinal) direction only. Since this wave equation is valid, then so should its complex conjugate be (as long as $\varepsilon^*(r) = \varepsilon(r)$, no absorption) since it too satisfies Maxwell's paraxial wave equation (i.e. it can exist physically as a real wave):

$$\nabla^2 A_L^* + \left(\frac{\varepsilon(r)\omega^2}{c^2} - k^2 \right) A_L^* - 2ik \frac{\partial A_L^*}{\partial z} = 0 \qquad (1.1.6)$$

This equation describes the wave

$$E_S(r,t) = \frac{1}{2}\left[A_L^*(r) e^{-i(\omega_L t - k_L z)} + A_L(r) e^{i(\omega_L t - k_L z)} \right] \qquad (1.1.7)$$

which is a wave propagating in the negative z direction and whose complex amplitude is everywhere the complex conjugate of the incident wave $E_L(r,t)$. This shows that if the PC mirror can produce a return wave whose amplitude is the complex conjugate of that of the incident wave, then the field amplitude of the return wave will be the complex conjugate of that of the incident wave at all points in front of the mirror. Therefore this can be used to unravel optical distortions.

This corrective property of phase conjugation has been utilised for a large variety of applications. laser amplifier heads are commonly used in MOPA (Master Oscillator Power Amplifier) configurations to increase the power of laser beams. Under pulsed operation these systems suffer from thermal lensing and birefringence effects which reduce the quality and power of the beam. In a double pass arrangement with a PC mirror these brightness decreasing effects in the amplifier can be reduced, and near diffraction limited performance can be obtained in practice.[1,4] Provided that the gain which the phase conjugate wave experiences when passing through the amplifier is only in the z direction, then the output will have the same phase as the input but a much higher intensity. PC mirrors can also be used to replace either one or both mirrors in a laser oscillator for the correction of intracavity distortions.[5,6]

Optical phase conjugation has also been used for reconstruction of images when viewed through low quality optics or distorting media (i.e. atmosphere), for automatic tracking of satellites, image up-conversion,[7] laser beam combination,[8] pulse compression[9] and photolithographic[10] applications among others.

1.2 Phase Conjugation Techniques

The concept of optical phase conjugation was initially demonstrated in holography[11,12] and adaptive optical systems.[13] In the 1970's, phase conjugation based on nonlinear interactions was performed for real-time (i.e. dynamic) phase correction in solids, liquids, gases and plasmas. Most of this activity related to applications in image processing and dynamic compensation for distortion in laser amplifiers and oscillators. In the literature often the terms optical phase conjugation and wavefront reversal are used interchangeably.

Various nonlinear processes can be used for optical phase conjugation, including:

- Four-wave mixing (degenerate, nearly degenerate) in transparent, absorbing and amplifying material.
- Stimulated (Brillouin, Rayleigh and temperature) Scattering.
- Photorefractive

One property that most of the above nonlinear processes have in common is the creation of a phase or amplitude grating in the medium. Each of these techniques has its

unique characteristics and limitations which dictate its particular application. The most widely applied of these are degenerate four-wave mixing and stimulated Brillouin scattering.

The work in this thesis is concerned with the limitations of optical phase conjugation by SBS and the resulting temporal effect on the beam quality under various experimental conditions. Four wave mixing will receive some mention as this process was combined with SBS in the application of the loop phase conjugation scheme.[14]

1.3 Stimulated Brillouin Scattering Theory

The scattering of light from thermally excited acoustic waves (spontaneous Brillouin scattering) was first predicted by Brillouin in 1922.[15] The phenomenon of stimulated Brillouin scattering (SBS) requires high intensity and thus had to wait for the development of lasers and was discovered in 1964.[16] SBS is also referred to as Stimulated Mandel'shtram-Brillouin Scattering (SMBS) in the Russian literature. The process of Stimulated Brillouin Scattering has been studied theoretically and experimentally in solids, liquids, gases and plasmas. SBS is an inelastic process, meaning that the medium is left excited and the photon energies will not be conserved. In SBS the scattered light has its frequency shifted down (Stokes component) by an amount determined by the bulk characteristics of the medium. The light is scattered by a hyper-acoustic wave which is created in the SBS medium by the input light wave itself. The frequency shift is a Doppler shift arising from the acoustic wave moving away from the input laser beam.

SBS is a nonlinear optical effect. In an isotropic medium this effect can be described by assuming that the induced polarisation P is related to the applied optical field. As all nonlinear effects are small for small field amplitudes, the polarisation can be expressed as:

$$P = \varepsilon_0\left(\chi E + \chi_2 E^2 + \chi_3 E^3 + ...\right) \tag{1.3.1}$$

$$P = \varepsilon_0 \chi E + P_{NL} \tag{1.3.2}$$

where χ is the susceptibility, ε_0 is the permittivity of free space and P_{NL} represents the nonlinear part of the polarisation. Each term of the expression can describe some optical effect. Terms with χ_2 can describe second harmonic generation whereas terms with χ_3 can describe stimulated Brillouin scattering, stimulated Raman scattering and other nonlinear effects.

Intense laser beams provide a medium with a time varying electric field which produce a corresponding time varying electrostrictive strain which drives an acoustic wave in the medium. Electrostriction is the tendency of materials to become compressed in the presence of an electric field.[17]

Most text books in nonlinear optics[18,19] offer a steady-state (stationary) theoretical treatment of stimulated Brillouin scattering. The classical theory presented in this section is for transient stimulated Brillouin scattering in a focusing geometry. Transient SBS is also known in the wider literature as travelling SBS and nonsteady-state. The process discussed in this section is noise initiated and includes the effects of pump depletion and of a finite phonon lifetime τ_B which introduces a memory into the

process. A numerical model was developed for this theory[20] based on fast algorithm by Chu et al[21] and used a SBS focusing idea by Menzel and Eichler.[22]

The basic equations that describe the SBS process are derived from Maxwell's equations for the electric fields and Navier-Stokes equations for the medium response with input laser field E_L, backscattered Stokes field E_S and acoustic (sound) field q represented in the form[23]

$$E_L(z,t) = \frac{1}{2}\left[A_L(z,t)e^{i(\omega_L t + k_L z)} + A_L^*(z,t)e^{-i(\omega_L t + k_L z)}\right]$$

$$E_S(z,t) = \frac{1}{2}\left[A_S(z,t)e^{i(\omega_S t - k_S z)} + A_S^*(z,t)e^{-i(\omega_S t - k_S z)}\right] \qquad (1.3.3)$$

$$q(z,t) = \frac{1}{2}\left[Q(z,t)e^{i(\omega_Q t + k_Q z)} + Q^*(z,t)e^{-i(\omega_Q t + k_Q z)}\right]$$

We assume that the total optical field E_T in the medium is given by

$$E_T(z,t) = E_L(z,t) + E_S(z,t) \qquad (1.3.4)$$

The conservation of energy and linear momentum in the SBS process requires that the scattered light's (photon) acoustic frequency and wavenumber be expressed as

$$\omega_Q = \omega_L - \omega_S$$
$$k_Q = k_L + k_S \qquad (1.3.5)$$

As the acoustic frequency (though hypersonic) is always considerably smaller than the optical frequencies, then the frequency of the scattered light is very close to that of the input laser light. Therefore $|k_S| \approx |k_L|$.

$$|k_Q| \approx 2n|k_L|\sin\left(\frac{\theta}{2}\right) \tag{1.3.6}$$

where θ is the angle between k_L and k_S, i.e. the scattering angle (see figure 1.3.1). This is the Bragg condition for the diffraction of light by sound.

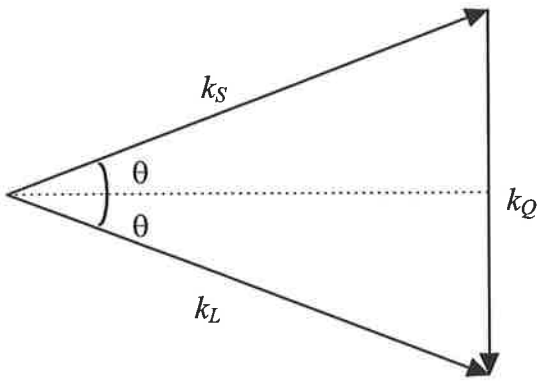

Figure 1.3.1: Vector diagram of Brillouin scattering.

Since $\omega_Q = k_Q v$, where v is the speed of sound in the medium, the Brillouin shift is

$$\omega_Q = 2n\omega_L \frac{v}{c}\sin\frac{\theta}{2} \tag{1.3.7}$$

where n is the refractive index, and c is the speed of light. The maximum value for ω_Q is obtained for $\theta=\pi$, i.e. backscattering (see figure 1.3.2).

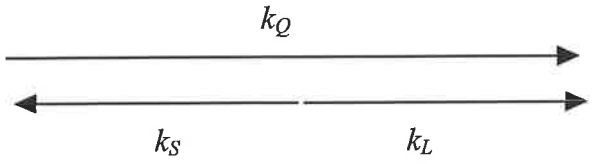

Figure 1.3.2: Vector diagram for Stokes scattering in the backward direction.

The description of the coupling between these fields is simplified by assuming that they have slowly varying amplitudes (SVEA) compared to their temporal and spatial frequencies ($\omega\tau>>1$, where τ is the pulse duration and ω the field frequency). The electric fields easily satisfy this assumption. The acoustic field can also satisfy the SVEA condition even though in practice it can have an $\omega\tau\sim8$ or less. Further, variations in the laser and Stokes transverse field are neglected but the intensity variation with z, due to focusing in the medium, is considered. Any linear optical absorption in the medium is also neglected in this treatment.

The following coupled wave equations can be found, in a similar treatment to that given by G. C. Valley in reference 24 for the basic equations of the pump, Stokes, and phonon.

$$\left(\frac{\partial}{\partial z}-\frac{n\partial}{c\partial t}\right)A_L = ig_2QA_s$$

$$\left(\frac{\partial}{\partial z}+\frac{n\partial}{c\partial t}\right)A_S = -ig_2QA_L \qquad (1.3.8)$$

$$\left(\frac{\partial}{\partial t}+\Gamma\right)Q = -ig_1A_LA_s + f_1$$

Here g_1 and g_2 are coupling coefficients, f_1 describes the thermal fluctuations of acoustic waves in the medium and Γ is the damping rate of the medium.

In general the initial phase relationship of the fields $(\varphi_L,\varphi_S,\varphi_Q)$ in the medium is variable as the SBS process initiates from noise. For this reason the fields are redefined as $A_L = A_Le^{-i\varphi_L}$, $A_S = A_Se^{-i\varphi_S}$, and $Q = Qe^{-i\varphi_Q}$. These fields can also be presented in cosine and sine terms by applying Euler's formula, $e^{i\varphi} = \cos\varphi + i\sin\varphi$. We can now substitute these fields in place of those given in equation 1.3.8 for the basic equations for the SVEA of the pump, Stokes, and phonon. In a similar treatment to A. Kummrow et al,[25] coupled equations for the phases can also be obtained.

Six coupled equations result from these assumptions, describing the amplitudes and associated phases for the fields. These also include the spontaneous growth from noise:

$$\left(\frac{\partial}{\partial z}-\frac{n\partial}{c\partial t}\right)A_L = -g_2 sin\left(\varphi_L-\varphi_S-\varphi_Q\right)QA_s$$

$$\left(\frac{\partial}{\partial z}+\frac{n\partial}{c\partial t}\right)A_S = g_2 sin\left(\varphi_S+\varphi_Q-\varphi_L\right)QA_L \qquad (1.3.9)$$

$$\left(\frac{\partial}{\partial t}+\Gamma\right)Q = -g_1 sin\left(\varphi_S+\varphi_Q-\varphi_L\right)A_L A_s + f_1$$

and

$$\left(\frac{\partial}{\partial z}-\frac{\partial}{c\partial t}\right)\varphi_L = -g_2 cos\left(\varphi_L-\varphi_S-\varphi_Q\right)\frac{Q A_S}{A_L}$$

$$\left(\frac{\partial}{\partial z}+\frac{\partial}{c\partial t}\right)\varphi_S = g_2 cos\left(\varphi_S+\varphi_Q-\varphi_L\right)\frac{Q A_L}{A_S} \qquad (1.3.10)$$

$$\left(\frac{\partial}{\partial t}\right)\varphi_Q = g_1 cos\left(\varphi_S+\varphi_Q-\varphi_L\right)\frac{A_L A_S}{Q} + f_2$$

The fields have an initial phase φ which can effect the Brillouin gain i.e. the gain is maximum when the collective phase is $\varphi_L-\varphi_S-\varphi_Q = \pi/2$, or is reduced when phase pulling (i.e. $\varphi_L-\varphi_S-\varphi_Q \neq$ constant) can take place. From equations 1.3.10 we can see that in the absence of noise (i.e. f_2=0) the field phases will be constant (i.e. phase locked) only when $\varphi_L-\varphi_S-\varphi_Q = \pi/2$. The Stokes wave will have its maximum gain only under this condition. The phase locked condition has been widely used by past authors in their theoretical treatment and its validity is based on the fact that only a phase conjugate wave would receive maximum amplification. The significance of this has also been discussed by H. Hsu in his treatment of phase conjugation.[26]

The input laser pulse enters at z=L as shown in figure 1.3.3. The input laser field amplitude A_L, the Stokes field amplitude A_S and the acoustic field amplitude Q, are normalised to the maximum value of input laser amplitude incident on the medium of the SBS cell. The spontaneous bandwidth is $\Gamma = 1/2\tau_B$ where τ_B is the Brillouin phonon lifetime of the medium. The Brillouin coupling constants g_1, g_2 are the normalised electric field and acoustic wave coupling coefficients, respectively. These coupling coefficients are proportional to the maximum amplitude of the input laser field. A spatial derivative is also omitted from the acoustic wave equation since the sound wave does not significantly propagate during the interaction (v<<c). The Langevin noise[27] sources $f_{1,2}$ describe the thermal fluctuations of acoustic waves in the medium that lead to spontaneous Brillouin scattering and thus to the initiation of the SBS process. We make the standard physical assumptions here, that f_1 and f_2 are Gaussian distribution random noise generators with zero mean, $\langle f(z,t)\rangle = 0$ (i.e. the average value over space and time is zero). The noise is δ correlated (i.e. has an infinite value for the average of the product of the two sources when they have an absolute correlation with any previous value of the source, $\delta(z-z') = \infty$ for z=z') in space and time in the sense that $\langle f(z,t)f^*(z',t')\rangle = Q\delta(z-z')\delta(t-t')$. The value of Q has been derived[28] using thermodynamic arguments and is given by

$$Q = \frac{2K_B T \rho_0 \Gamma}{A v^2} \qquad (1.3.11)$$

where K_B is Boltzmann's constant, T is the temperature, ρ_0 is the mean density of the material, v is the sound speed and A is the cross-sectional area of the interaction region.

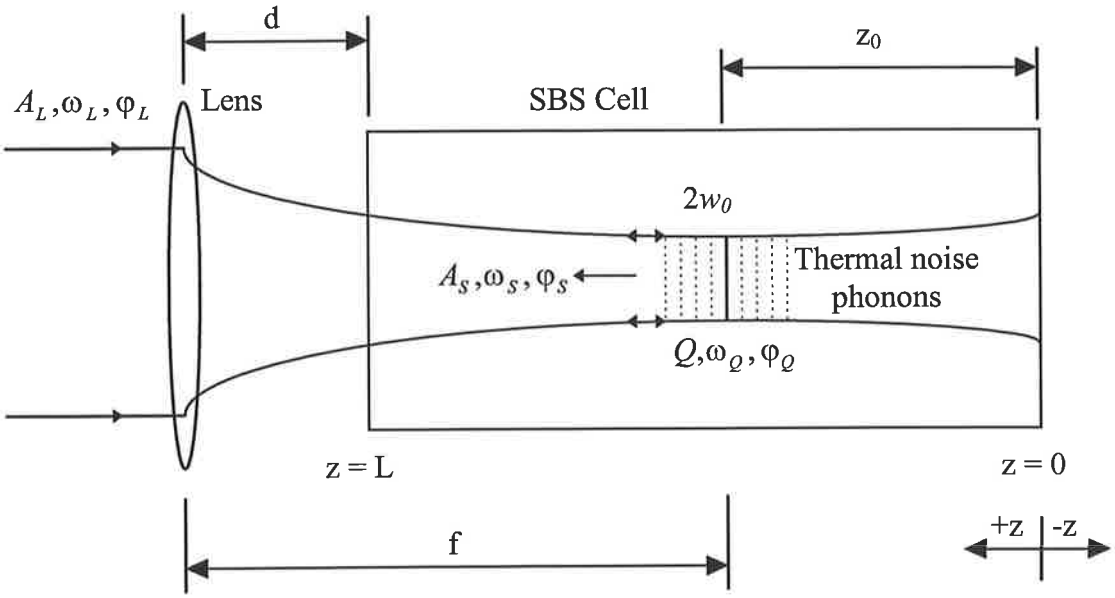

Figure 1.3.3: Geometry of the Stimulated Brillouin scattering interaction. The input beam is incident at z=L.

For the variation in intensity due to focusing, the reduction in the beams cross-sectional area A is considered. Let the distance between the lens and the SBS cell be d. Assuming a spatially Gaussian beam of $1/e^2$ value radius, then the radius of the beam, $w(z)$, will vary according to the relation:

$$w^2(z) = w_0^2\left[1+\left(\frac{(z-z_0)\lambda}{\pi w_0^2 n(z)}\right)^2\right] \qquad (1.3.12)$$

where the $n(z)$ refractive index value depends on the medium that the beam traverses, λ is the laser wavelength, and w_0 is the focal waist radius at position $z=L+d-f$. Thus, the input beams cross-sectional area $A(z)$ along the length of the medium can now be obtained.

By redefining the electric field amplitude as $A_{L,S} = \frac{A'_{L,S}}{w_0(z)}$, (where $A^2_{L,S} = \frac{Power}{Area}$), then the SBS coupled set of equations can be altered to account for any intensity variations due to changes in the beams area. This system of partial differential equations was solved, using a non-iterative, numerical algorithm.[29] Numerical solutions are obtained by integrating the Q phonon from the partial differential equation and substituting it into the input laser and Stokes partial differential equations.

In modelling the SBS process, the following analytical expression for the Gaussian input laser pulse was used:

$$A_L(t,L) = e^{-2\left[\frac{(t-t_0)}{\tau_Q}\right]^2} \qquad (1.3.13)$$

This input was normalised with respect to its peak value which occurs at time t_0.

It takes a certain amount of power to produce detectable stimulated Brillouin scattered light. The onset of the SBS process requires that an intensity threshold is exceeded. At threshold a phenomenological expression is defined for the SBS threshold in terms of the threshold intensity existing over the interaction length which must have sufficient gain to sustain a positive feedback.

$$g_B I_L l_i = C \qquad (1.3.14)$$

where g_B is the mediums steady state SBS gain ($g_B = g_1 g_2 / \Gamma$), usually expressed in cm/MW; I_L is the intensity of the input laser beam; l_i is the length of interaction (for

figure 1.3.3, l_i=L-z_0 where z_0 is the value of z at w_0) and C is a numerical constant, usually in the range $20<C<25$ for organic liquids. Here $g_B I_L l_i$ is the single-pass intensity gain of the Stokes field. As the value of g_B is small the single-pass intensity gain is increased by maximising the product of $I_L l_i$. In practice, instead of increasing the power, the intensity can be increased by focusing the beam.[16] Alternatively, the interaction length can be increased by using a waveguide (e.g. optical fibre)[30]. A typical threshold energy is around few millijoules for a Q-switched pulse of several nanosecond duration.

Figures 1.3.4-6 give typical examples of a laser input pulse, SBS (Stokes) return pulse and transmitted pulse, calculated by the aid of this theoretical model. For a given input pulse the corresponding SBS return and transmitted pulse portion through the SBS cell are calculated. From these outputs other parameters such as reflectivity as a function of Input Energy to Threshold Energy ratio can be plotted (see figure 1.3.7). This plot shows a monotonic increase in reflectivity after the SBS threshold value is exceeded. The computer modelled results of this theoretical work exhibit features similar to those seen from experiments. Recently, intensity fluctuations due to phase jumps were predicted by this model.[20,29,31] This model has become a useful tool in helping to understand some of the mechanisms of the SBS process and thus in the interpretation of experimental results.

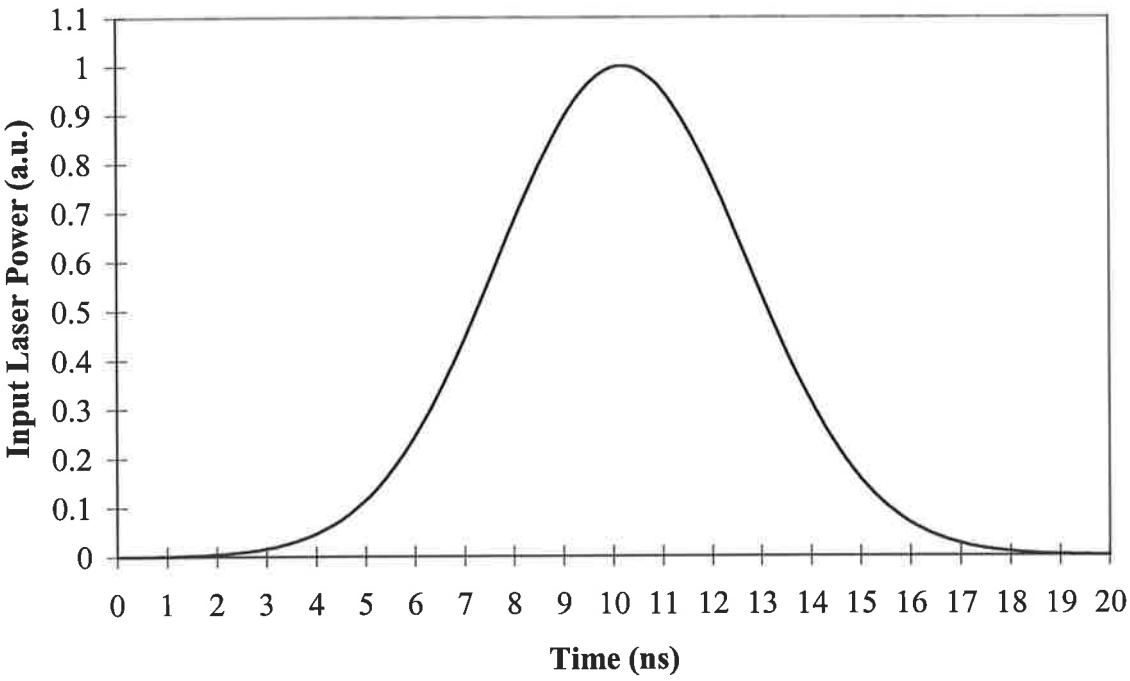

Figure 1.3.4: Plot shows typical example of a laser input pulse, for theoretical model.

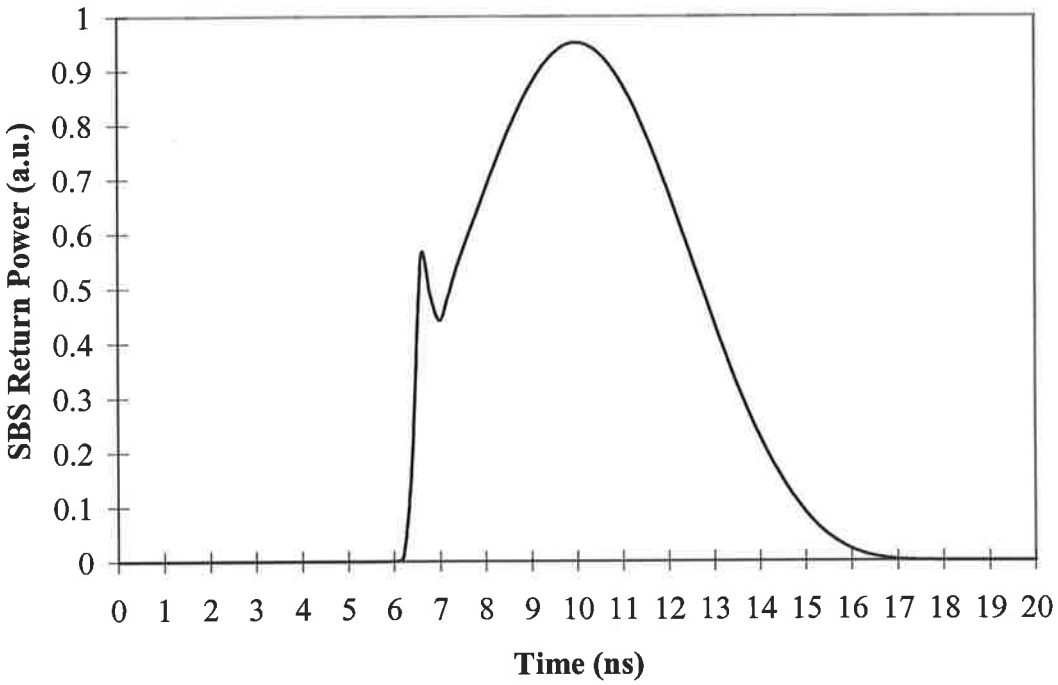

Figures 1.3.5: Plot shows a typical example of a SBS (Stokes) return pulse, calculated by the aid of this theoretical model.

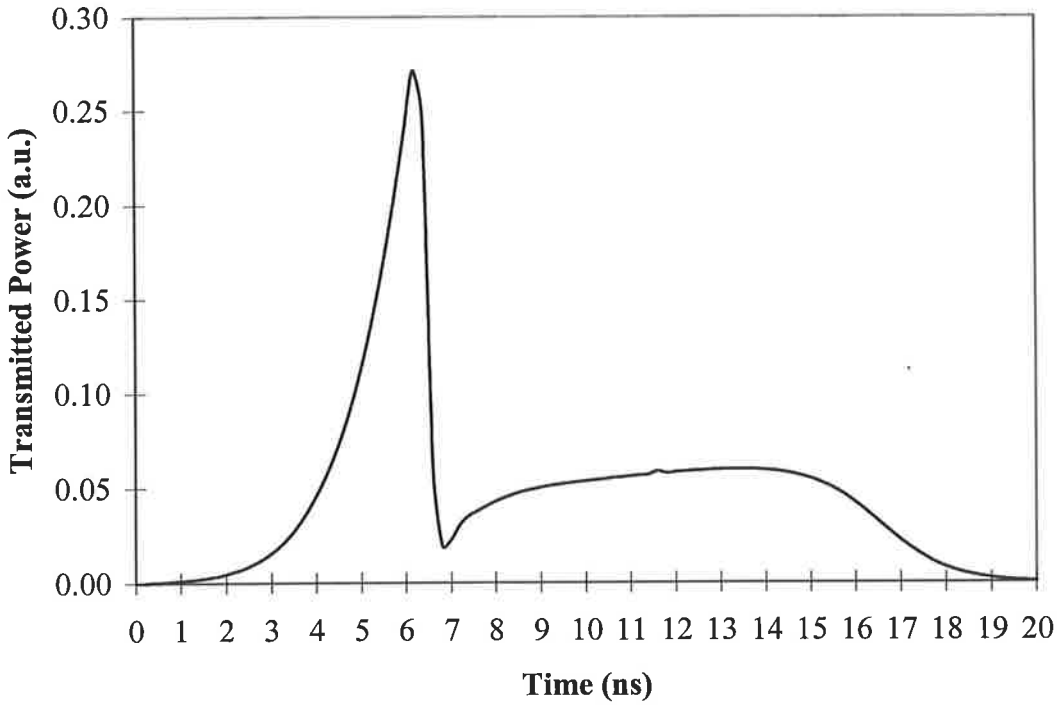

Figures 1.3.6: Example of a theoretically modelled laser transmitted pulse.

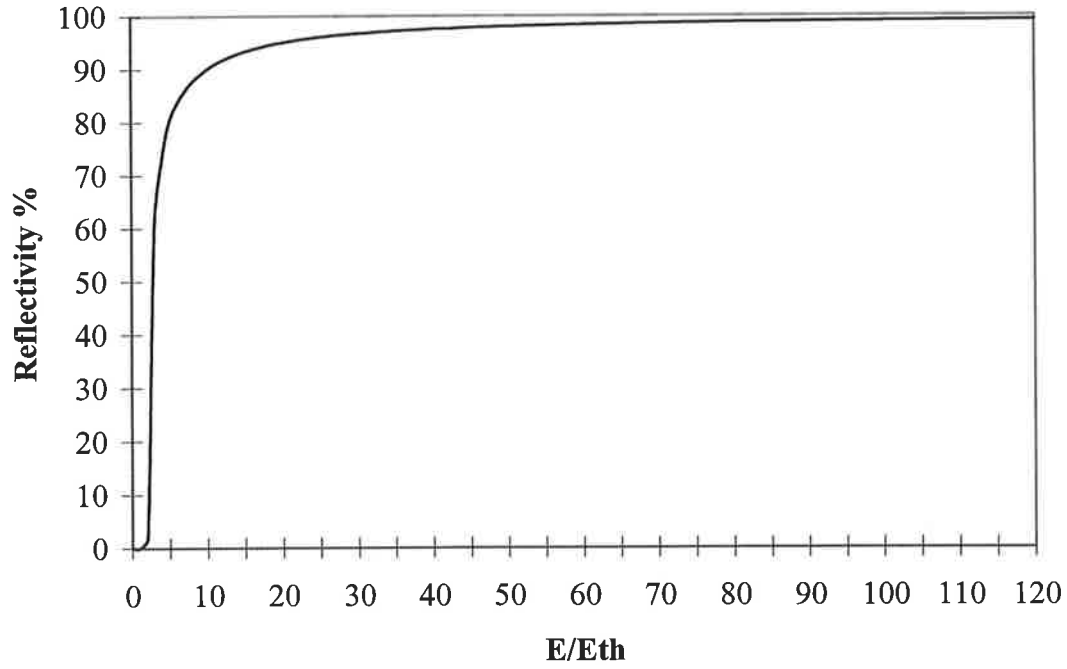

Figures 1.3.7: Plot shows a typical example of Reflectivity as a function of input energy/threshold energy ratio, calculated by the aid of this theoretical model.

1.4 Fidelity of OPC-SBS in the Saturation Regime

A basic description of the way in which SBS generates a OPC wave will now by presented. Envisage an aberrated laser beam being focused in the SBS interaction region (i.e. in a similar arrangement to figure 1.3.3). The aberrated beam creates a non-uniform intensity distribution (i.e. speckle) in the focal region of the lens. The Stokes wave which depends on the local intensity will also experience a non-uniform gain distribution. As SBS is initiated by noise (i.e. spontaneous Brillouin scattering) it initially has all possible spatial Fourier components. However, only that Fourier component whose intensity distribution matches the non-uniform gain distribution will receive maximum amplification. This component has a wavefront that match that of the aberrated input laser beam and therefore corresponds to the phase conjugate of the input. The degree by which Stokes reconstructs the input is referred as fidelity.

Most experiments are conducted in the saturation regime of SBS where the input laser pulse is depleted. For this reason a theoretical description of the reproduction of the original input by the SBS process is useful. By predicting the Stokes behaviour under pumping conditions that exceed the SBS threshold by many times, a comparison with experimental results can later be made. As a quantitative measure of the inaccuracy of OPC, Zel'dovich et al (Reference 32) defined the phase conjugate beam fidelity H, as:

$$H = \frac{\left|\int A_L(r,z)A_S(r,z)d^2r\right|^2}{\int|A_L|^2 d^2r \int|A_S|^2 d^2r}, \quad 0 \le H \le 1 \qquad (1.4.1)$$

Here $r=(x,y)$ and H describes the degree of overlap of the input laser A_L and Stokes A_S fields. It is based on the Schwartz-Cauchy inequality[33] and holds for all A_L and A_S fields. When H is zero, then there is a total absence of correlation, whereas when H=1 then the Stokes field is the exact phase conjugate of the input laser field. The only property of a beam that the OPC-SBS mirror can not conjugate is the polarisation of the input beam. With respect to this, it behaves as a normal metallic mirror does. This is because the acoustic wave is scalar and does not have information about the direction of the vector field that drives it.

Based on the steady-state picture of SBS and including depletion, then the wave equations for the input laser and Stokes fields are be given by

$$\left(\frac{\partial}{\partial z}+\frac{i}{2k_L}\nabla_\perp^2\right)A_L = \frac{g_B}{2}\left|A_S\right|^2 A_L$$
$$\left(\frac{\partial}{\partial z}-\frac{i}{2k_S}\nabla_\perp^2\right)A_S = \frac{g_B}{2}\left|A_L\right|^2 A_S \qquad (1.4.2)$$

where $\nabla_\perp^2 = \left(\partial^2/\partial x^2 + \partial^2/\partial y^2\right)$ and g_B is the Brillouin gain coefficient for the medium.

At the entrance of the medium (z=L) the input laser field has a developed speckle structure. In the course of the depletion by a nonuniform Stokes wave, both the structure and intensity of the beam will vary along z. The Stokes wave is excited by spontaneous noise and thus has Gaussian statistics. We assume that both fields obey Gaussian statistics throughout the interaction volume. An expression for H as a function of z can be obtained if we assume plane waves. The SBS system equations then reduce to

$$\frac{\partial A_L}{\partial z} = \frac{g_B}{2}|A_S|^2 A_L$$
$$\frac{\partial A_S}{\partial z} = \frac{g_B}{2}|A_L|^2 A_S \qquad (1.4.3)$$

By taking the complex conjugate of these simple coupled differential equations and multiplying the first by A_L and the second by A_S and then adding each equation to its conjugate, we obtain:

$$A_L^* \frac{\partial A_L}{\partial z} + A_L \frac{\partial A_L^*}{\partial z} = g_B A_S A_S^* A_L^* A_L$$
$$A_S^* \frac{\partial A_S}{\partial z} + A_S \frac{\partial A_S^*}{\partial z} = g_B A_S A_S^* A_L^* A_L \qquad (1.4.4)$$

By defining the average intensities $I_{L,S} = \left\langle |A_{L,S}|^2 \right\rangle$ (i.e. assume the integration over the transverse coordinates is equivalent to averaging over an ensemble of random realisations)[34] then we get

$$\frac{dI_L}{dz} = \frac{dI_S}{dz} = g_B \left\langle A_S A_S^* A_L^* A_L \right\rangle \qquad (1.4.5)$$

where $\left\langle A_S A_S^* A_L^* A_L \right\rangle = \left\langle A_S A_S^* \right\rangle \left\langle A_L^* A_L \right\rangle + \left\langle A_S A_L^* \right\rangle \left\langle A_S^* A_L \right\rangle + \left\langle A_S A_L \right\rangle \left\langle A_S^* A_L^* \right\rangle$ based on the assumption that the complex field amplitudes are random Gaussian quantities (i.e. due to bad aberrations) and $\left\langle A_S A_L \right\rangle = 0$ (i.e. ignore forward scattering), $\left\langle A_S^* A_L^* \right\rangle = 0$.

The differential equation can be transformed to

$$\frac{dI_L}{dz} = \frac{dI_S}{dz} = g_B I_L I_S \left(1 + \frac{\left| \left\langle A_S A_L^* \right\rangle \right|^2}{I_L I_S} \right) \qquad (1.4.6)$$

We have thus obtained expressions for the intensity variation in the medium as a function of fidelity.

$$\frac{dI_L}{dz} = \frac{dI_S}{dz} = g_B I_L I_S (1+H) \tag{1.4.7}$$

Using this result, Zel'dovich et al (Reference 32) also obtained an expression describing the variation in Stokes wave fidelity as a function of input laser intensity.

$$\frac{dH}{dz} = g_B \left(I_L + I_S\right) H(1-H) \tag{1.4.8}$$

From these two equations a number of observations can be made. When H=1, the Stokes wave is the phase conjugate of the input wave and the Brillouin gain of the PC portion of the noise field will be twice as large than any other mode of the noise field. A number of analytic theories agree with this.[35,36] At H=0 the correlation between the Stokes wave and the input laser wave disappears and there is energy transfer between uncorrelated waves at gain g. The value of dH/dz becomes zero for both H=0 (the field remains uncorrelated over the interaction length) and at H=1 (exact phase conjugation in all cross sections). Further, from these equations we may derive:

$$H(z)\left[1-H(z)\right]^{-2} = \text{constant} \cdot I_L(z) I_S(z) \tag{1.4.9}$$

$$\frac{H(z)}{\left(1-H(z)\right)^2}\left[\frac{\left(1-H(0)\right)^2}{H(0)}\right] = \frac{I_L(z) I_S(z)}{I_L(0) I_S(0)} \tag{1.4.10}$$

The initial Stokes field is of the form $I_S(0)=I_L(0)e^{-G}$ where G~25 under experimental conditions. By applying SBS boundary conditions ($I_L(z)$-$I_S(z)$=$I_L(0)$-$I_S(0)$=constant, conservation of energy) for the case of saturation, the following expressions are obtained: $I_S(z)=I_L(z)-I_L(L)(1-R)$ and $I_L(0) \approx I_L^{th} \approx I_L(L)(1-R)$, giving $I_S(L) \approx I_L(L) - I_L^{th}$

where R denotes the reflectivity (with respect to intensity) and I_L^{th} is the threshold intensity.

Thus, the fidelity expression can be simplified to:

$$\frac{H(z)}{(1-H(z))^2}\left[\frac{(1-H(0))^2}{H(0)}\right] = X(X-1)e^{25}, \quad X>1 \tag{1.4.11}$$

where X is the ratio of input laser intensity over that of the threshold intensity.

In practice, phase conjugation starts from spontaneous noise thus $H<<1$ but never equal to zero. A detailed examination of H(z) requires numerical calculation for different values of $H(0)$. Such studies have already been reported for a number of parameters in reference 32. It has been shown[37] that a value for $H(0)$ can be obtained for which H(L)=1 to within a tolerance δ. Thus from the previous equation we obtain:

$$H(0) > \frac{1}{\delta^2 X(X-1)e^{25}}, \qquad X>1 \tag{1.4.12}$$

The behaviour of H(L) for increasing input laser intensity in multiples of the threshold intensity is shown in figure 1.4.1 for δ=0.1 and $H(0)$=6.94x10^{-11} (chosen as it best fits our experimental results).

We can see from this plot that as the input laser intensity reaches values of reflectivity saturation, the fidelity of the Stokes return also approaches unity. According to this approach, an increase in input intensity brings an improvement to the quality of the optical phase conjugation. Comparing the fidelity plot to that of the reflectivity we note that the fidelity reaches unity at a faster rate and for a smaller value of input

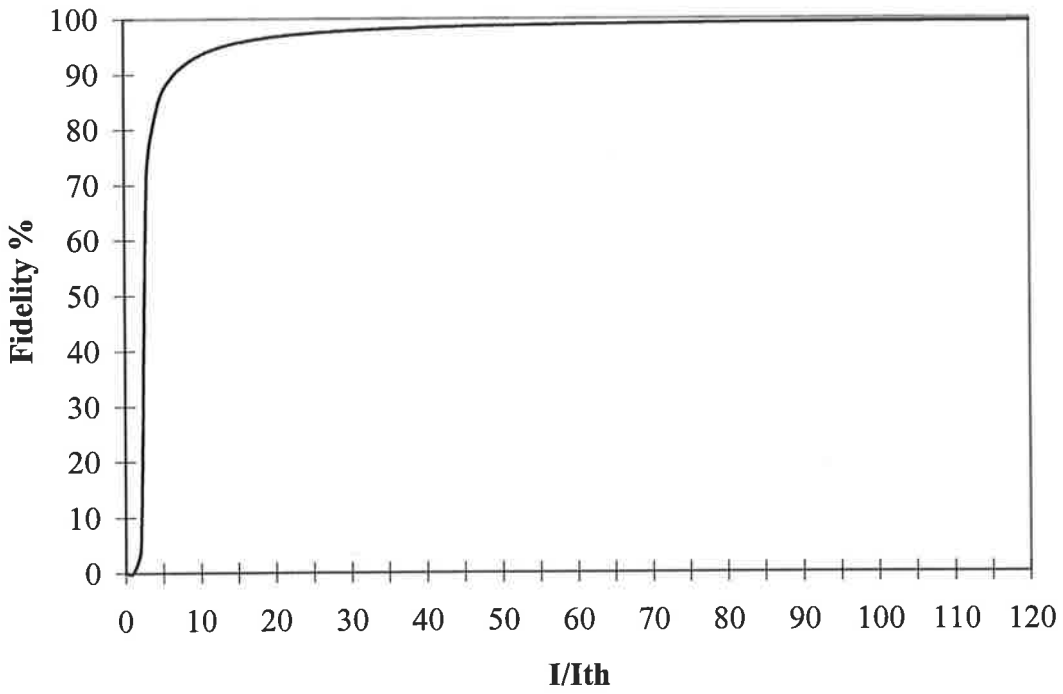

Figure 1.4.1: Plot of PC fidelity H(L) as a function of input laser intensity in multiples of the threshold intensity

intensity. Two-dimensional numerical simulations of OPC-SBS by Lehmberg[38] for focused, aberrated beams in unbounded medium and waveguides, also showed that (for pump depletion cases) the conjugate fidelity is significantly improved as the incident intensity is increased. It should be noted here that fidelity values of near unity do not imply a TEM_{00} mode but rather a true reproduction of the input mode structure. Finally, in real experiments the input laser beam will not be a plane wave but rather will have some finite diameter and the intensity will usually vary across the beam thus causing effects (e.g. spatial narrowing) that could reduce the fidelity. Such limiting effects can be eliminated in practice by use of two-lens systems which distribute the Stokes gain more evenly (see figure 1.4.1a).[39] In the two-lens system the beam profile of the SBS is made to coincide with that of the pump by imaging the end face of a laser in the SBS cell so it is located in front of the plane of the equivalent focus.

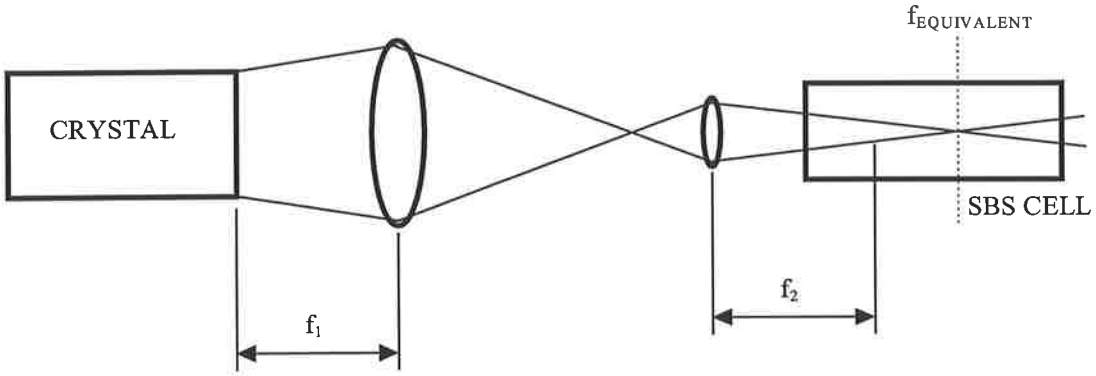

Figure 1.4.1a: Two-lens scheme for the input of the pump radiation into the medium for SBS.

Measurement of the OPC during a single pulse, based on the Zel'dovich definition of fidelity H, is difficult as it requires knowledge of both intensity and wavefront phase as a function of space (across the beam) for the input laser and Stokes beam. In this Thesis, information about the OPC fidelity was obtained by measuring the Reflectivity and the Beam Quality which in turn provides the Phase Fidelity of the beams (see section 2.2.5 for definition of these terms). These two parameters (i.e. Reflectivity and Phase Fidelity) allow experimental results to be interpreted in a simple manner. The Phase Fidelity gives information about the beam's wavefront phase by measuring parameters relating to the Beam Quality of the input and Stokes return beams. These parameters will be expressed in chapter 2 as the 'Beam Merit' function. The parameters relating to the Beam Quality (i.e. Beam merit) were measured using power-in-the-bucket (i.e. measure at the far-field the pulse power that passes through an aperture the size of the diffraction limited divergence of the beam). The Reflectivity gives information about the beams spatially averaged intensity by measuring the pulse power at near-field.[40,41] As we will see in the next chapter the Phase fidelity in a similar way to

the Fidelity H, gives a quantitative measure of the quality of phase conjugation characterised by the ratio of the scattered power to that of the that of the perfectly conjugated beam.

1.5 Four-Wave Mixing

Four-wave mixing is the most widely applied technique in optical phase conjugation. It was shown[42,43] in 1977 that phase conjugation could be obtained by the process of degenerate four-wave mixing (DFWM) using the geometry shown in figure 1.5.1. The process is degenerate because all four interacting waves have the same frequency. There is an analogy between four-wave mixing OPC and holography which suggests that all of the applications envisaged or demonstrated with conventional holography can be performed using real-time phase conjugate optics.

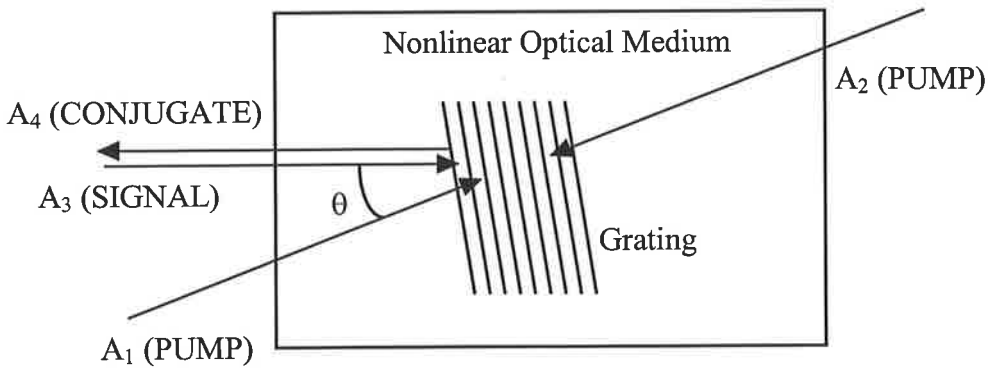

Figure 1.5.1: Configuration in phase conjugation by degenerate four-wave mixing.

In this geometry, two pump waves, A_1 and A_2, are incident on the nonlinear medium from opposite directions. The wave front carrying the information to be conjugated is the signal wave A_3 and the conjugate wave A_4 that is produced in the interaction $\omega_4=\omega_1+\omega_2-\omega_3$ propagates in the direction opposite to A_3. Since the pairs of waves are counter-propagating and have the same frequency, the interaction is automatically phase matched for any angle q between the signal and the pump waves.

This interaction creates a diffraction grating (volume hologram) in the medium through the interference of the waves. The grating is formed by the signal wave A_3 whose phase conjugate is required, and a reference pump wave A_1. The grating refractive index contours contains the information of both the signal and reference pump waves. The conjugate wave A_4 is produced by the scattering of the pump wave A_2 off the diffraction grating created by A_3 and A_1. The information of the grating is transferred to the phase contours of A_4 as it is created but with its sense reversed (phase conjugate). A similar interference occurs between all pairs of the incident waves, and each interference contributes to the phase conjugate wave.

As a result of the third order nonlinearity the polarisation induced in the χ_3 medium by A1, A2 and A3 will contain a term having the form:[44]

$$P = \text{constant} \cdot A_1 A_2 A_3^* e^{i(\omega t + kz)} \qquad (1.5.1)$$

Thus this polarisation acts as a source for the spontaneous build-up of a backward propagating wave that is the phase conjugate to the signal, $A_4 = A_3^*$.

It is possible to do nondegenerate four-wave mixing by using SBS, which is also a third order nonlinear effect. This is known as Brillouin induced four-wave mixing

(BIFWM) or Brillouin enhanced four-wave mixing (BEFWM).[45] From very weak signal beams, BEFWM can produce a phase conjugate return whose reflectivity can be well in excess of 100%.[46] Although none of the work in this thesis is directly concerned BEFWM, the part of the work in chapter two that deals with the Loop Scheme is closely related.[47] In the Loop Scheme we need to consider a system of two coupled nonlinear region. A region where SBS and four-wave mixing occur and one where Brillouin amplification takes place.

1.6 Conclusion and Objective of Thesis

As already mentioned there are number of stimulated scattering processes (i.e. Raman, Rayleigh, Thermal) which compete with SBS but of these, long coherence length SBS has a much higher gain in the time region of 1-10 ns and thus dominates. Often though these processes occur in the presence of SBS and thus reducing the amount of backscattered Brillouin light. The phase conjugation technique contained in this thesis uses stimulated Brillouin scattering in the backward direction. Some of these competing processes can also provide wavefront reversal but their wavelength shift is larger than that of SBS.

The original idea for the transient theoretical model was born out of a necessity to explain the experimental results and observations that are presented within this thesis. I felt that an appropriate theory should include the temporal behaviour of SBS, a focusing geometry and be initiated from noise. Initially a theoretical model was developed based on the work of Dianov et al (see Chapter 2, reference 2) with the extra improvement of

including a focusing geometry. With the arrival of S. Afsharvahid into our research group a collaboration started and a new theoretical model was quickly developed. This model is presented in the Appendix 1 (The Nature of Intensity and Phase Modulations in Stimulated Brillouin Scattering).

The presentation of the theoretical background in this chapter leads to the following conclusions: SBS can be used to obtain OPC beams whose reflectivity and fidelity is close to 100%; both reflectivity and fidelity maintain a high value even at intensities many times that of the SBS threshold. As shown in the Appendix 1 the field phases may not remain locked throughout the SBS process due to noise. The importance of these concepts will become clearer through the discussion of the experimental results in the following chapters.

The main emphasis of the thesis is the study of the SBS process although its application to laser technology was also considered. Understanding of the process from this work was applied by Martin O'Connor to the development of an improved laser oscillator with an intracavity phase conjugating mirror.[6] At the beginning of this work there were no commercial devices utilising SBS phase conjugation and there was a motivation to study OPC-SBS in order to finally develop a commercial device. More recently, in addition to a number of Russian companies selling this technology in their lasers, a company in the U.S.A. has produced a Nd:YAG (MOPA) laser.[48] The phase conjugate mirror has finally moved from the laboratory to the market place.

The overall objective of this research program is to demonstrate that optical phase conjugation has regimes were the temporal fidelity (amplitude and phase) can be

maintained in the SBS process. This is required, together with the correction of spatial aberrations, in useful applications. The specific objectives are:

a) Characterise OPC under long coherence pumping for various focusing geometries, and understand reasons for any bad performance in OPC-SBS

b) Characterise OPC with long coherence length pumping for laser pulses with fast rise edge.

c) Characterise OPC with short coherence length pumping as well as any competing phenomena that take place during the SBS process.

In order to meet these specific objectives a series of experiments were designed and performed. Each of the following chapters deals with each of these specific objectives.

In chapter two some of the properties of the spontaneous noise produced in a Brillouin generator (which can effect the maximum attainable reflectivity and fidelity) are experimentally investigated. The length of interaction necessary to produce good returns is determined from a set of different focusing geometries. These experiments raise issues and explore the fidelity in a Brillouin generator. The question as to 'why does the fidelity occasionally degrade, under apparently good operating conditions?' has now been answered.

Chapter three looks at fidelity under long coherence pumping conditions where the leading edge of the input pulse, rises fast compared to the hypersound relaxation time of

the medium. Chapter four examines fidelity for inputs of short coherence length and in addition detailed observations of the behaviour of the medium are made.

Finally chapter five contains a summary of this works findings on SBS and identifies those areas where further research is necessary.

Although optical phase conjugation is examined under various conditions, the primary reason for this study is not aberration correction but rather temporal behaviour. For this reason the use of any aberrators is minimum and it is only done to show that OPC occurs.

1.7 References

1 B. Ya. Zel'dovich, V. I. Popovichev, V. V. Ragul'skii and F. S. Faizullov, "Connection between the wave fronts of the reflected and exciting light in stimulated Mandel'shtram-Brillouin scattering", Soviet Physics JETP Letters, Vol. 15, 109, 1972

2 R. A. Fisher, *Optical Phase Conjugation*, Academic Press, 1983

3 A. Yariv, *Optical Electronics*, Saunders College Publishing, 4th edition, 610, 1991

4 S. G. Anderson, "Diode-pumped Nd:YAG laser provides high energy at high repetition rates", Laser Focus World, Vol. 30, No. 2, 15, February 1994

5 I. M. Bel'dyugin, B. Ya. Zel'dovich, M. V. Zolotarev and V. V. Shkunov, "Lasers with wavefront-reversing Mirrors", Soviet Journal of Quantum Electronics, Vol. 15, 1583, 1986

6 M. O'Connor, V. Devrelis and J. Munch, "SBS phase conjugation of a Nd:YAG laser for high beam quality", The Society for Optical & Quantum Electronics, Lasers 95, 500-504, 4-8 December 1995

7 J. Feinberg, "Self-pumped, continuous-wave phase conjugator using internal reflection", Optics Letters, Vol. 7, 486, 1982

8 J. Falk, M. Kenefsky and P. Suni, "Limits on the Efficiency of Beam Combination by Stimulated Brillouin Scattering", Optics Letters, Vol. 13, No. 1, 39, 1988

9 D. T. Hon, "Pulse Compression by Stimulated Brillouin Scattering", Optics Letters, Vol. 5, No. 12, 516, 1980

10 L. A. Hackel, C. B. Dane, M. R. Herman and L. E. Zapata, "Phase Conjugated Lasers Applied to Commercial X-ray Lithography", Second International School and Topical Meeting on Applications of Non-Linear Optics, Prague, 1993

11 H. Kogelnik and K. S. Pennington, "Holographic imaging through a random medium", Journal of Optical Society of America, Vol. 58, No. 2, 273-274, 1968

12 J. Upatnieks, A. Vander Lugt and E. N. Leith, "Correction of lens aberrations by means of holograms", Applied Optics, Vol. 5, No. 4, 589-593, 1966

13 W. T. Cathey, C. L. Hayes, W. C. Davis and V. F. Pizzurro, "Compensation for atmospheric Phase effects at 10.6 μ", Applied Optics, Vol. 9, 701-707, 1970

14 A. M. Scott, W. T. Whitney, and M. T. Duignan, "Stimulated Brillouin scattering and loop threshold reduction with a 2.1-μm Cr,Tm,Ho:YAG laser" J. Opt. Soc. Am. B, Vol. 11, No 10, 2079-2088, October 1994

15 L. Brillouin, "Diffusion de la lumiere et des rayons par un corps trasparent homogene", Ann. Physique, Vol. 17, 88, 1922

16 R. Y. Chiao, C. H. Townes and B. P. Stoicheff, "Stimulated Brillouin Scattering and Coherent Generation of Intense Hypersonic Waves", Physical Review Letters, Vol. 12, 592, 1964

17 A. Yariv, *Quantum Electronics*, 3nd Edition, J. Wiley, N.Y., p. 476, 1975

18 Y. R. Shen, *The principles of Nonlinear Optics*, Wiley, New York, pp 187-195, 1984

19 P. W. Milloni and J. H. Eberly, *Lasers*, Wiley Publication, pp 692-701, 1988

20 S. Afshaarvahid, J. Munch and V. Devrelis, "Numerical Study of Stimulated Brillouin Scattering Initiated from Noise", CLEO/Pacific Rim '97, ThM1, July 1997.

21 R. Chu, M. Kanefsky and J. Folk, "Numerical Study of Transient Stimulated Brillouin Scattering", J. Appl. Phys., Vol. 71, No. 10, 4653-4658, 15 May 1992

22 R. Menzel and H. J. Eichler, "Temporal and Spatial Reflectivity of Focused Beams in Stimulated Brillouin Scattering for Phase Conjugation", Physical Review A, Vol. 46, 7139-7149, 1992

23 W. Kaiser and M. Maier, "Stimulated Rayleigh, Brillouin and Raman Spectroscopy", Laser Handbook, Vol. 2, edited by F.T. Arecchi and E. O Schuls-DuBois, 1077-1149, 1972

24 G. C. Valley, "A Review of Stimulated Brillouin Scattering Excited with a Broad-Band Pump Laser", IEEE Journal of Quantum Electronics, Vol. 22, No. 5, 704-712, May 1986 (see equations 1-3)

25 A. Kummrow and H. Meng, "Pressure dependence of stimulated Brillouin Backscattering in gases", Optics Communications, Vol. 83, No. 5,6, 342-348, 15 June 1991 (see equations 13)

26 H. Hsu, "Fundamentals of Parametric interaction and Phase Conjugation", International Journal of Nonlinear Optical Physics, Vol. 1, No. 4, 743-764, 1992

27 L. A. Coldren and S. W. Corzine, *Diode Lasers and Photonic Integrated Circuits*, John Wiley & Sons, Inc.,1996, Appendix 13, pp 540-551

28 R. W. Boyd and K. Rzazewski, P. Narum, "Noise initiation of stimulated Brillouin scattering", Physical Review A, Vol. 42, No 9, 5514-5521, 1990

29 S. Afshaar Vahid, V. Devrelis and J. Munch, "The Nature of Intensity and Phase Modulations in Stimulated Brillouin Scattering", submitted for publication in IEEE Journal of Quantum Electronics, 1997

30 M. P. Petrov and E. A. Kuzin, Pisma Zh. Tech. Fiz., Vol. 8, 729-732, 1982, English translation: Soviet Technical Physics Letters, Vol. 8, 316-317, 1982

31 V. Devrelis, M. O'Connor, J. Munch, S. Afsharvahid, C-J. Wei and A-M. Grisogono, "Fidelity of Optical Phase Conjugation using Stimulated Brillouin Scattering", XX IQEC 96, Sydney, WL59, p.165, July 1996

32 B. Ya. Zel'dovich, N. F. Pilipetsky and V. V. Shkunov, *Principles of Phase Conjugation*, Springer Series in optical Sciences, Vol 42, Springer-Verlag, p. 115, p. 134, 1985

33 H. Anton, *Elementary Linear Algebra*, J. Wiley, 2nd Edition, p. 165, 1977

34 G. G. Kochemasov and V. D. Nikolaev, "Investigation of the spatial characteristics of Stokes radiation in stimulated scattering under saturation conditions", Soviet Journal of Quantum Electronics, Vol. 9, 1155-1157, 1979

35 R. W. Hellwarth, "Optical beam phase conjugation by stimulated Backscattering", Optical Engineering, Vol. 21, 257-262, 1982

36 B. Ya. Zel'dovich and T. V. Yakovlea, "Calculations of the accuracy of wavefront reversal utilizing pump radiation with one-dimensional transverse modulation", Soviet Journal of Quantum Electronics, Vol. 11, 186-189, 1981

37 R. A. Lamb, "The Application of Phase Conjugation to High Power Lasers Using Stimulated Brillouin Scattering", Ph.D. Thesis, University of London, January 1994

38 R. H. Lehmberg, "Numerical study of phase conjugation in stimulated backscatter with pump depletion", Optics Communications, Vol. 43, No. 5, 369-374, 1 November 1982

39 Yu. V. Dolgopolov, V. A. Komarevskii, S. B. Kormer, G. G. Kochemasov, S. M. Kulikov, V. M. Murugov, V. D. Nikolaev and S. A. Sukharev, "Experimental investigation of the feasibility of application of the wavefront reversal phenomenon in stimulated Mandel'shtam-Brillouin scattering", Soviet Physics JETP, Vol. 49, No. 3, 458-466, March 1979

40 V. I. Bespalov, A. A. Betin and G. A. Pasmanik, "Experimental investigation of the threshold of the stimulated scattering (SS) of multimode light beams and the degree of regeneration of the pumping in scattered radiation", Radiophys. Quantum Electron., Vol. 20, 544, 1977

41 R. Mays and R. J. Lysiak, "Phase conjugated wavefronts by stimulated Brillouin and Raman scattering", Optics Communications, Vol. 31, 89, 1979

42 R. W Hellwarth, "Generation of time-reversed wave fronts by nonlinear refraction", Journal of Optical Society of America, Vol. 67, No. 1, 1, 1977

43 A. Yariv and D. M. Pepper, "Amplified reflection, phase conjugation, and oscillation in degenerate four-wave mixing", Optics Letters, Vol. 1, No. 1, 16, 1977

44 R. W. Boyd, *Nonlinear Optics*, Academic Press Inc., p246, 1992

45 A. M. Scott and K D Ridley, "A review of Brillouin enhanced four-wave mixing", IEEE Journal of Quantum Electronics, Vol. 25, 438, 1989

46 N. F. Andreev, V. I. Bespalov, A. M. Kiselev, A. Z. Matveev, G. A. Pasmanik and A. A. Shilov, "Wavefront inversion of weak optical signals with a large reflection coefficient", JETP Letters, Vol. 32, 625, 1981

47 A. M. Scott, W. T. Whitney, and M. T. Duignan, "Stimulated Brillouin scattering and loop threshold reduction with a 2.1-μm Cr,Tm,Ho:YAG laser" J. Opt. Soc. Am. B, Vol. 11, No 10, 2079-2088, October 1994

48 T. Moss, "Coherent introducing new high-performance pulsed YAG", Photonics Spectra, Vol. 28, No. 2, 24, February 1994

Chapter 2

Long Coherence OPC-SBS

2.1 Introduction

Temporal intensity fluctuations on Stimulated Brillouin Scattering (SBS) return pulses have been reported in gases, liquids and solids.[1,2,3] These fluctuations have been attributed to the acoustic noise from which the SBS process initiates.[2] Simultaneous temporal variations in SBS reflectivity and phase fidelity have also been reported,[4] but their origin was unresolved.

The objective of our work was to understand and establish design parameters for the effective control of phase fidelity in Optical Phase Conjugation (OPC) by SBS, using a pulsed Nd:YAG laser. The experimental approach relies on both time averaged and time resolved measurements of all input and output pulses during the SBS process. Observations of SBS returns with intensity fluctuations similar to References 1-3 were made under certain operating conditions. A reduction in the fidelity of the reconstructed laser beam was also observed during these pulses.[4] With the aid of a heterodyne detection system,[3] we have observed time resolved phase jumps in coincidence with the intensity fluctuations. These jumps in phase were observed even at high input energies, up to 100 times above the SBS threshold value. Thus a correlation between reduction of

fidelity and phase jumps has been established. These experimental findings support the theoretical model predictions by Wandzura.[5,6] We have found that the phase fluctuations are a function of the interaction length and phonon relaxation time of the SBS cell, similar to Gaeta et al.[7]

In addition we have investigated various geometries to reduce phase fluctuations, including the triple pass four-wave mixing enhanced approach by Scott et al.[8] The results have been promising.

I shall present the latest experimental results from a variety of SBS geometries, to determine an extended parameter regime in which SBS works reliably.

"Noise" in this study refers to spontaneously scattered light due to quantum fluctuations in the response of the SBS medium (atomic, molecular, plasma)[9].

2.2 Experimental Technique

This section describes the apparatus assembled and used to perform the experiments, and the techniques employed to extract information from the measurements.

2.2.1 Laser

The laser used for the experiments in this section was a flash lamp pumped, Q-switched multiple longitudinal mode Nd:YAG built by Spectra-Physics, that could also have a single longitudinal mode output when injection seeded by a diode pumped, single frequency Nd:YVO_4 laser. The laser output was linearly polarised at 1.064 μm with a linewidth of 90 MHz. Substantial effort (i.e. alignment of oscillator and seeder to obtain good near and far field) was placed into obtaining a good quality beam, as diffraction effects can change the spatial intensity profile of pulsed solid-state lasers.[10] The two parameters that were considered for the improvement of the laser beams quality were its divergence and its intensity profile at selected distances. The spatial profile of the beam was supergaussian with a beam diameter (at $1/e^2$) of 8.5 mm at a near field distance of 1 m. The beam divergence (full angle) was ~ 0.2 mrad and the pointing stability was better than 10 μrad over an eight hour period (once the laser was allowed one hour to reach thermal equilibrium). The M^2 method for evaluating the beam quality was not used as it was inappropriate for our time resolved studies. Instead the power-in-the-bucket method was used (see section 2.2.5) since only two high bandwidth measurement channels, were available. The pulse duration was 8 nsec full width at half maximum although wider pulses (14 nsec) could also be obtained at the cost of maximum pulse energy. The pulse energy could be delivered in a quasi-gaussian temporal profile, and it could be varied by either changing the laser flash lamp voltage or using a half-wave plate with polariser combination. The maximum Q-Switched energy was 780 mJ per pulse with an pulse to pulse energy stability of 2%. The pulse repetition frequency could be varied from 1 to 15 Hz, but the laser was mostly operated at either 4 or 10 Hz (due to thermal effects and computer acquisition limitations). A

typical temporal profile of a laser pulse is shown in figure 2.2.1.1. The pulse shows a smooth profile indicating single mode operation.

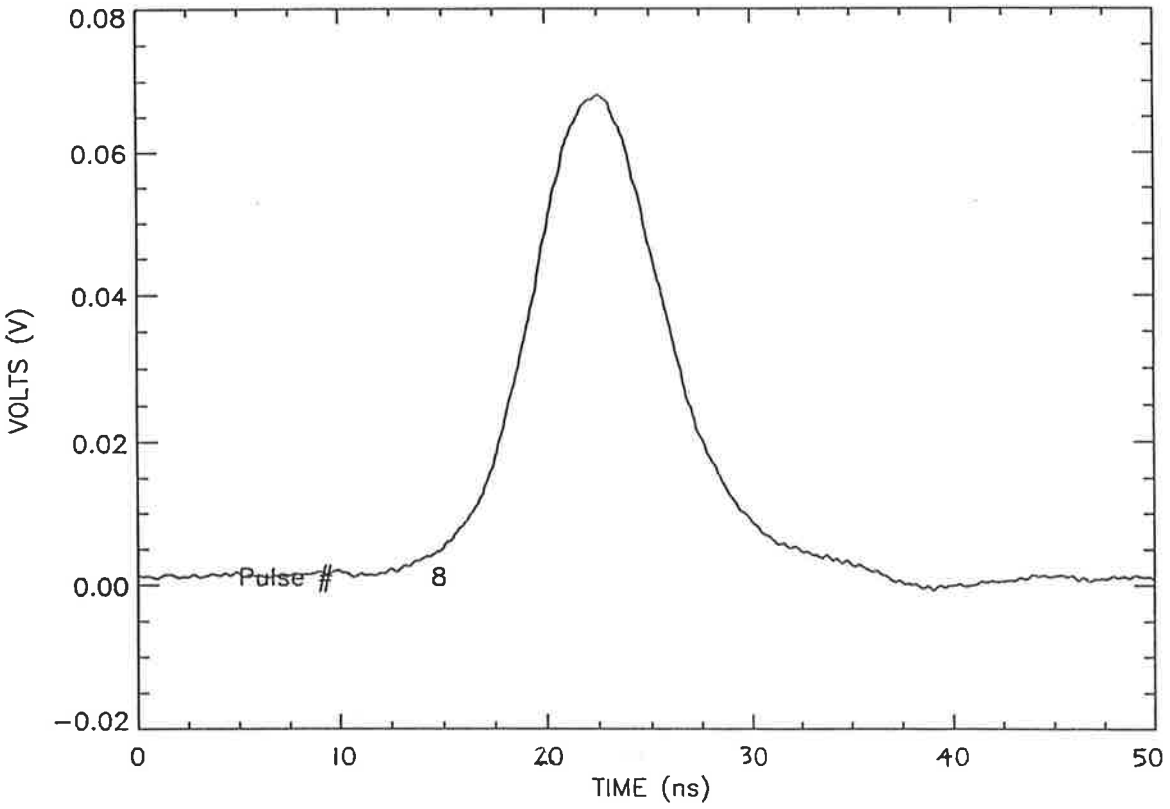

Figure 2.2.1.1: Typical temporal profile of laser pulse.

2.2.2 Detectors

The design and assembly of the detection system had to provide for the time coincident capture of all input and output pulses to the SBS cell. The captured information included the beam energy, power variation in time and beam images. All input laser beams and output beams from the SBS cell had their pulse shapes monitored with silicon PIN photodiodes (Electro-Optics Technology ET2000) which have a rise time of <200 psec and a cut off frequency of >1.75 GHz. Some high speed photodetectors with a bandwidth of >2.5 GHz were also made using InGaAs detectors (EG&G C30617) in a positive bias circuit. Lengths of two meter UR67 coaxial cable were used with N-type connectors in order to maintain the high bandwidth of the signals. In addition, high responsivity detectors were made using large area InGaAs detectors (EG&G C30619). The temporal profiles of the pulses were recorded using two, 1.86 GHz (3db frequency) transient digitizers (Tektronix SCD1000). The transient digitizer traces were stored in a 486 computer via a GPIB interface (National Instruments). For the pulse energy measurements a dual channel Joulemeter/Ratiometer (Molectron JD2000) was used with calibrated pyroelectric energy heads (Molectron J25). The energy readings were stored in a 486 computer via a RS-232 interface card. The time integrated intensity profile of the pulses was imaged onto an asynchronously triggered CCD video array (Pulnix TM-620) and recorded on a 486 computer with a frame grabbing card (PC Vision+). All stored data in the 486 computer's memory could be processed and printed on a laser printer (HP Laserjet 4L). The capture of data relied on output trigger pulses from the Nd:YAG laser power supply. Figure 2.2.2.1 gives a schematic representation of the data acquisition system. The computer programs required to run the above diagnostic systems were written using VisualBasic and C++.

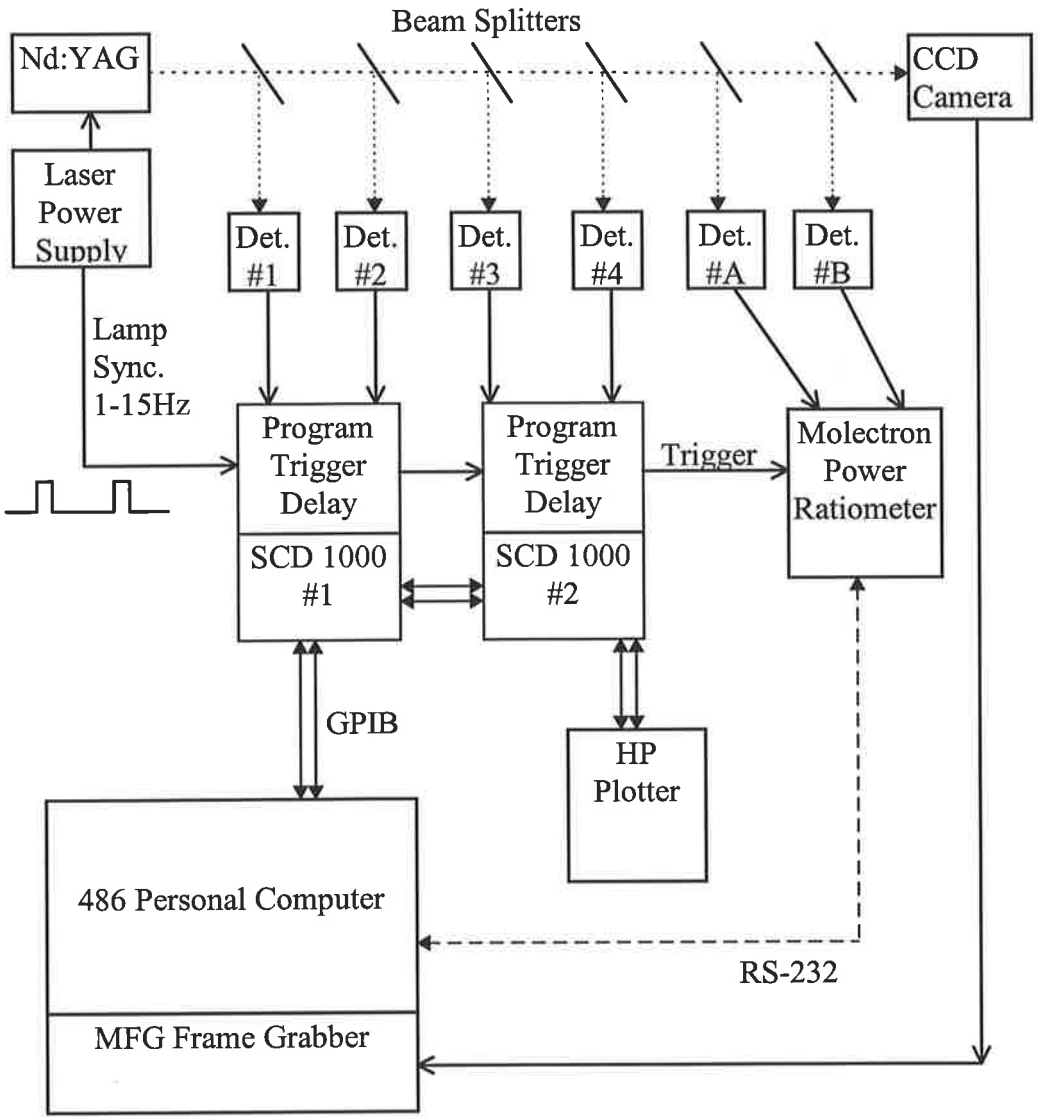

Figure 2.2.2.1: Diagram of the Data Acquisition using SCD 1000 Tranzient Digitizers, Molectron Power Meter and National Instruments GPIB Communications.

2.2.3 SBS Material

The liquid, Freon-113 (1,1,2-trichlorotrifluoroethane, $ClCF_2$-CCl_2F), was selected as the SBS medium due to its small optical absorption at 1.064 μm, its good physical and chemical properties[11,12] when in contact with other materials, its good SBS reflectivity[13] and its low toxicity (safe for laboratory handling) when compared to the tetrachlorides of group IV elements.[14] It had been previously suggested by Pasmanik as an excellent SBS material for 1.064 μm, and was in extensive use in many laboratories in the world by 1990. The minimum purity of the Freon-113 was specified by the manufacturer to be 99.8%. In practice the commercially available Freon contained floating particles which were found to be detrimental to the SBS process and thus needed to be removed. A tall multistage fractionating column was used to distil one litre of the Freon over a period of two to three days. The distilled liquid was passed twice through a 0.2 μm pore teflon filter to remove any micro-particles. This distillation and filtering cycle was repeated another two times before the Freon-113 was tested for scatter. A 70 mW He-Ne laser beam was focused by a 150 mm focal length lens into the Freon container and the amount of light scattered by particles in the liquid was visually observed in dark room conditions. Figure 2.2.3.1 indicates the difference in scattered light between the original dirty liquid and the clean liquid. The original liquid showed a lot of scatter (specular glow), where as the clean liquid showed a faint beam (soft glow) mostly near the focus. A Carbon-13 Nuclear Magnetic Resonance (NMR) spectra was measured in order to identify any impurities within the clean Freon. These NMR scans showed no impurities to be present to within 100 ppm resolution. Ideally, longer distillation times and finer size filters should produce an even cleaner liquid. The clean Freon was placed into a suitably cleaned cell for use (see below). The optical breakdown threshold of the liquid

under laser pumping conditions now exceeded the maximum output energy available from the laser, thus eliminating any problems due to suspended particles. The reasons the optical breakdown threshold was not measured as an intensity are a) as energy was the parameter used to measure SBS threshold direct comparison needed to be made and b) in the presence of self focusing it is difficult to measure as the focal spot diameter is not known. Two other SBS media were also investigated: methanol (CH_3OH) and gaseous SF_6 at 22 atm. A mathematical analysis on the feasibility of methanol as an SBS medium was carried out based on the work of reference 15. In practice, methanol was a poor SBS medium probably due to the presence of hydrogen-containing impurities and suspended particles which can increase absorption. The importance of purifying organic liquids for use in SBS has been emphasised also by other researchers who have applied similar distillation and filtering techniques.[16,17]

In order to characterise the new clean material the SBS gain was needed to be measured. The measurement of the gain was based on a technique demonstrated by Scott et al[18] where the back-scattered light from a cell at energies below the SBS threshold was detected. With the aid of an Newport Silicon avalanche photodiode and a 600 mm SBS cell the logarithm of the pulses peak value was obtained as a function of pump intensity. The length of interaction was the length of the SBS cell i.e 600mm. The slope of the logarithm of the pulses peak against the pump intensity gave the value of gL=0.360 where L was the length of the SBS cell. The SBS gain factor of the medium g (small signal gain), was measured for Freon-113 and was 0.0058 cm/MW which is in excellent agreement with published values (reference 13 gives g=0.0062 cm/MW and reference 19 gives g=0.0055 cm/MW). The quality of the liquid was thus established.

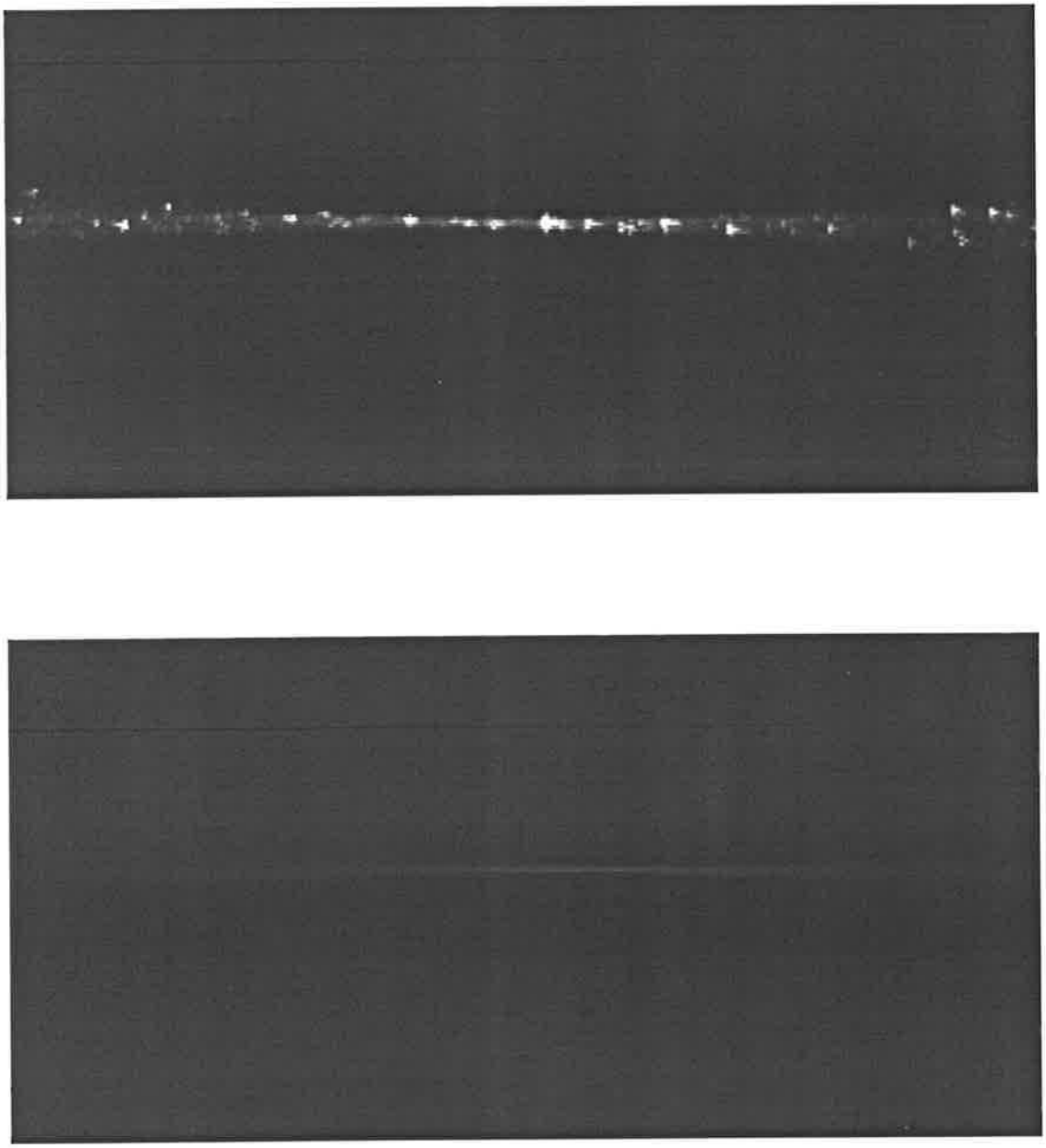

Figure 2.2.3.1: Indicates the difference in scattered light between the original dirty liquid (top) and the clean liquid (bottom).

2.2.4 SBS Cells

A number of SBS cells was made out of Pyrex borosilicate glass. The cells were tubular with a diameter of 50 mm and at each end, flat windows were fused on, which were tilted by 5 to 10 degrees. The tilting of the windows on the cells was important in avoiding backreflections which can cause parasitic behaviour in SBS or the laser during operation. Both horizontal and vertical cells were made at lengths of 100, 200, 400, and 600 mm. A number of smaller cells (10 to 50 mm) was also used. The vertical cells were required for avoiding front window damage whenever there was shallow focusing into the SBS medium. A PTFE (polytetrafluoroethylene or Teflon) plug was used to seal the Freon-113 in the cells. All glassware were initially cleaned and soaked for a day using a pyrogenically negative cleaner (Pyroneg by Diversey). After a day the cells were rinsed with de-ionised, de-mineralised, filtered water and were dried in a bio-clean (sterilisation) furnace. The cells were rinsed with clean Freon before being filled and then, the amount of scattered light was again checked with a He-Ne laser. The ambient room temperature was kept at a steady value during the taking of measurements and was not allowed to ever fall bellow 22°C or above 24°C. In this way thermal distortions (refractive index changes) in the liquid were reduced. This was important when we had long or multiple beam paths through the SBS cell.

The cells overall had a simple design, were inexpensive, convenient to use and did not contaminate the liquid (e.g. Freon-113).

2.2.5 Experimental Layout and Techniques Used

A schematic of the experimental layout for the single pulse simultaneous monitoring of laser and SBS reflectivity and fidelity is shown in figure 2.2.5.1. Both time integrated and time resolved measurements of reflectivity and phase fidelity could be made by using energy detectors and photodetectors respectively. The near field measurement of the laser input and the SBS return pulses gave the reflectivity for that shot.

$$\text{Reflectivity} = \frac{\text{Near Field SBS return}}{\text{Near Field Laser input}} \qquad (2.2.5.1)$$

The PC fidelity of the SBS backscattered beam was determined by using the power-in-bucket technique.[4,28] Here, the transmission of the SBS return pulse was measured through a single diffraction limited pinhole located at the far field of a concave mirror. The measurement of the pinhole transmission (T) relates to the beams wavefront. The terms Fidelity and Phase Fidelity will share the same meaning for the rest of this thesis (see section 1.4). Figure 2.2.5.2 gives a schematic of the near field and far field diagnostic techniques.

$$\text{Phase Fidelity} = \frac{\text{SBS beam merit}}{\text{Laser beam merit}} \qquad (2.2.5.2)$$

where we define

$$\text{SBS beam merit} = \frac{\text{Far Field SBS power through pinhole}}{\text{Near Field SBS power} \times \text{T\%}} \qquad (2.2.5.3)$$

and

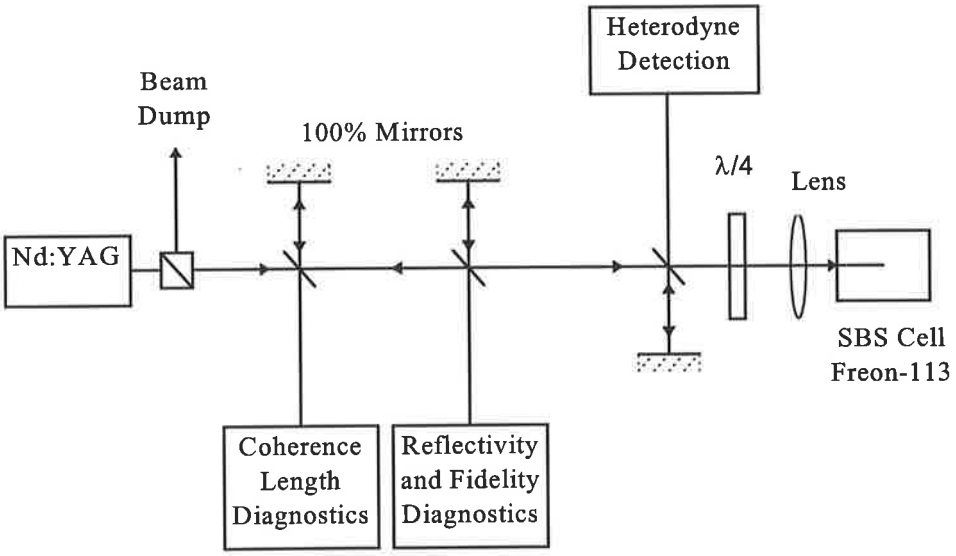

Figure 2.2.5.1: Diagram of the experimental layout for the pulse-to-pulse simultaneous monitoring of laser and SBS reflectivity and fidelity

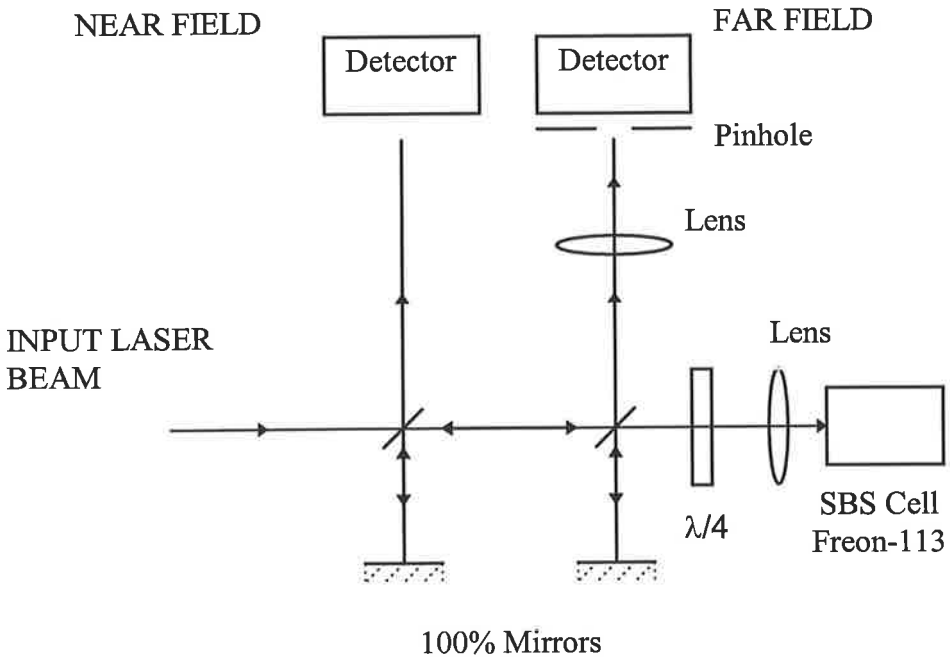

Figure 2.2.5.2: Block diagram of the near field and far field diagnostic technique for the measure of time resolved and time averaged power-in the-bucket. Here the lens in front of the pinhole replaces the curved mirror.

$$\text{Laser beam merit} = \frac{\text{Far Field Laser power through pinhole}}{\text{Near Field Laser power} \times \text{T\%}} \qquad (2.2.5.4)$$

Equations 2.2.5.3 and 2.2.5.4 can be expressed in terms of TDL (i.e. Times Diffraction Limited) Beam Quality by taking the square-root of their reciprocals. Therefore for the SBS beam we have

$$BQ_{SBS} = \sqrt{\frac{\text{Near Field SBS return} \times \text{T\%}}{\text{Far Field SBS return through pinhole}}}, \qquad (2.2.5.5)$$

where the value of BQ_{SBS} is equal or greater than one.

A Fidelity of 1 corresponds to the exact reconstruction of the input laser beam's angular divergence. Any Fidelity value that deviates from 1, indicates a reduction in the degree of correlation between input and output beams.

Using the energy-in-the-bucket method, a number of pinhole sizes were tested before the selection was made using a 1.5 m focal length mirror. The far field in absence of a pinhole was imaged by a microscope objective lens[4] onto a CCD camera to assure the presence of a diffraction limited intensity distribution. This was the most simple and practical way out of several others[20,21] for measuring the laser OPC fidelity, especially for obtaining time resolved data. The transmission percentage T, of each pinhole was determined by measuring the far field energy with and without the pinhole. It is well known that a beam with a top-hat spatial profile will produce an Airy-disk in the far field. The central lobe of the Airy-disk contains about 85% of the beams energy. The diffraction-limited angle (at which the first null of the Airy pattern occurs) for a top-hat is $\theta = 2.44\lambda / D = 305$ μrad and for a Gaussian $\theta = 1.27\lambda / D = 160$ μrad where

D=8.5 mm, the beam diameter and λ is the laser wavelength 1.064 μm. The intensity distribution of the near field was not a top-hat or a perfect Gaussian but was super-gaussian (i.e. like a top-hat but with slightly rounded edges). A range of increasing aperture diameters was used to measure the energy percentage into the far field aperture and thus find the point of inflection (where the first Airy null occurs). The final selected size of the pinhole resulted in a beam transmission of T~85%. The pinhole was 0.3 mm in diameter and corresponded to the$\theta \times f = 200 \times 10^{-6} \times 1.5 = 300$ μm, where θ is the measured divergence angle of the laser beam and f is the mirrors focal length. The laser had a measured beam quality better than 1.25 times diffraction limit.

The measure of the fidelity refers to the phase reproduction of a laser beam. Although this method of phase fidelity does not measure the beams spatial amplitude fidelity, it is important as it relates to a beams angular direction. There are other ways in which fidelity can be measured[22,23] but this is the only practical one which could provide both integrated and resolved temporal information.

The beam merit of the input laser beam was measured simultaneously with the SBS beam merit. The laser beam merit had a value of 100% with less than 1% variation from pulse to pulse and over the whole energy range. Any laser pulses whose beam merit was other than the above stated value were rejected as important information about the process can be lost when reproducing poor input beams (i.e. the results can become ambiguous when interpreting the fidelity). The SBS Phase Conjugate (PC) fidelity was determined by taking the ratio of the SBS beam merit over the laser beam merit. The monitoring of all input and output pulses guaranteed that no two bad beam merits could

be divided to result to a seemingly good SBS PC fidelity. This insured that no false results were attributed a high PC fidelity.

The coherence length of the laser and the SBS return of most pulses (i.e. depending on what experiment was ran) was measured using a modified Michelson interferometer.[24] The details of this diagnostic system are discussed in chapter four. Based on the specific needs of the experiments other diagnostic systems were also used from time to time such as Mach-Zehnder interferometers and Schlieren imaging[25] to provide information on thermal effects or off-axis scattering.

The laser beam energy was set through a variable attenuator (combination of half-wave plate ($\lambda/2$) and thin-film polarising beam splitter) rather than varying the laser flash-lamp voltage, as this caused changes to the beam through varying thermal lensing on the YAG rods. The input laser pulse and the SBS return reflected/passed through a 5° uncoated glass wedge beam splitter which provided the input to all the diagnostic systems. The SBS return was outcoupled (stopped from returning into the laser) by the placement of a quarter-wave plate ($\lambda/4$) in front of the SBS cell which in combination with the thin-film polarising beam splitter appropriately changed the polarisation state of the beam. To further avoid parasitic effects due to feedback into the laser, the SBS cell was placed at least half a laser pulse width away. The outcoupled beam was dumped into a box of bricks were it was absorbed and scattered. The laser input beam was focused into the SBS cell with a lens which was placed against the front window of the cell. Both aberrators (i.e distorted glass) and YAG dielectric mirrors could be inserted in front of the cell and along the laser input beam path.

Figure 2.2.5.3 shows the heterodyne beat experimental layout (used in section 2.3.3), which was designed to compare the instantaneous phase of the SBS return with that of the input laser. Here portions of the laser input pulse and the SBS return pulse simultaneously arrive at a high speed detector after travelling two different paths but with equal lengths. Part of the laser pulse is reflected by a mirror and acts as a frequency reference, while the signal pulse (i.e. the SBS return) comes from the cell. The two pulses although similar in their spatial and temporal profile have different frequencies due to the SBS shift. This difference manifests itself as a beat frequency when the two pulses are made to overlap temporally. The captured data were analysed as follows: Since the data are composed of low and high frequencies functions, a FFT (fast Fourier transform) was applied to subtract the low frequency, smoothly varying function. The remainder high frequency function has a sinusoidal appearance. By measuring the period of this function the beat frequency can be determined. This beat frequency is the SBS frequency shift. By comparing this high frequency sinusoidal signal function to a mathematical sine function of similar but fixed frequency, then any changes in the phase of the former can be determined. The stability of the laser input frequency during the pulse lifetime was determined by placing a mirror in front of the SBS cell and moving it so the two pulses arrive at the detector at different times over the pulse duration. Under these conditions no beating was observed. The laser pulse was also mixed with the pulse that is transmitted through the SBS cell and still beating was not found, which means that no other process but SBS is responsible for the phase changes. The use of the laser pulse as a frequency reference was thus an appropriate choice.

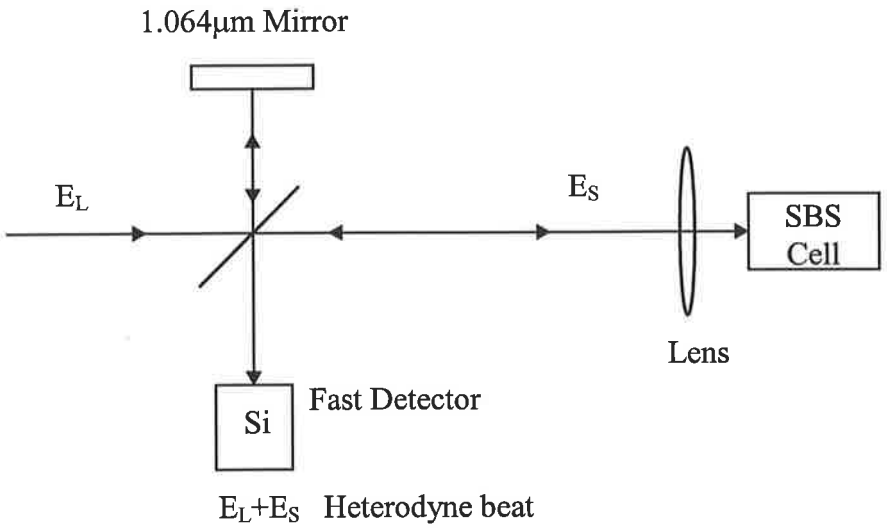

Figure 2.2.5.3: Diagram shows the heterodyne beat detection system for the laser EL and the SBS return ES pulses.

The Heterodyne Diagnostic System was calibrated with the aid of a sine-wave generator (Rohde & Schwarz, Signal Generator, 5 kHz-3.0 GHz). A fixed amplitude sine-wave was added through a T-connector to a smooth Gaussian-like laser pulse from a fast Si-detector and the result was fed into the tranzient digitizers. The recorded signals were analysed by the computer and the output frequency and amplitude of the sine-wave was compared to its input values. Figure 2.2.5.4 shows the attenuation in signal as a function of frequency for the whole detection system. The measured output frequency corresponded with the input frequency to within 5 MHz at the worst case (see figure 2.2.5.5). These calibrations showed that a phase measurement of better than $\pi/25$ in accuracy could be obtained with the entire diagnostic system (hardware and software). Throughout the study this accuracy was more than adequate for phase measurements (at least 10x better than any of the phase changes that were analysed).

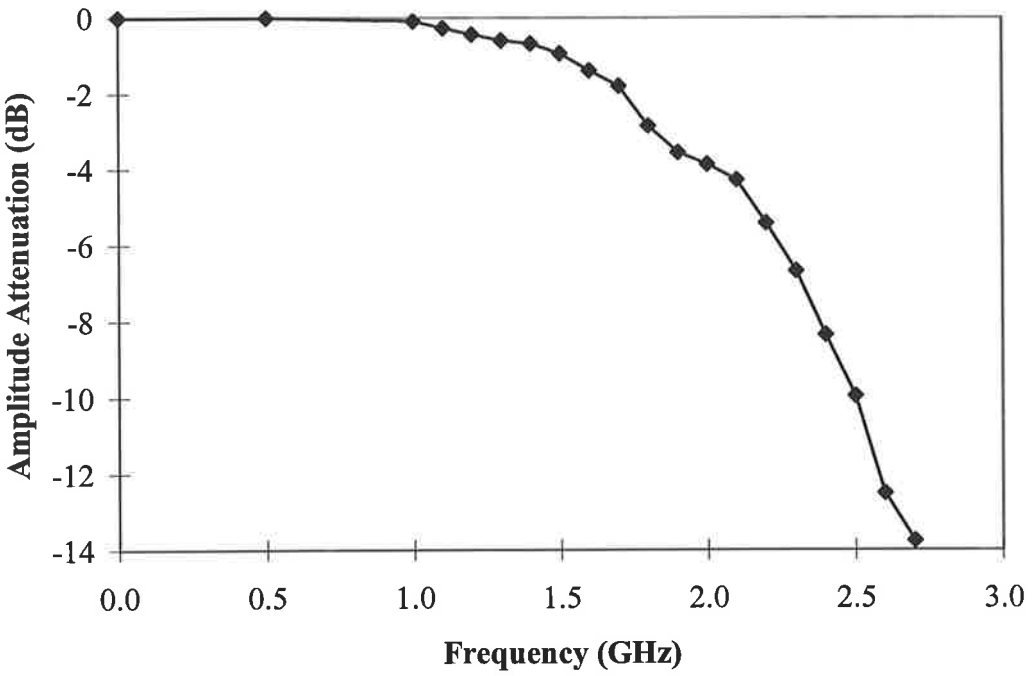

Figure 2.2.5.4: Diagram of the measured amplitude attenuation in signal as a function of frequency.

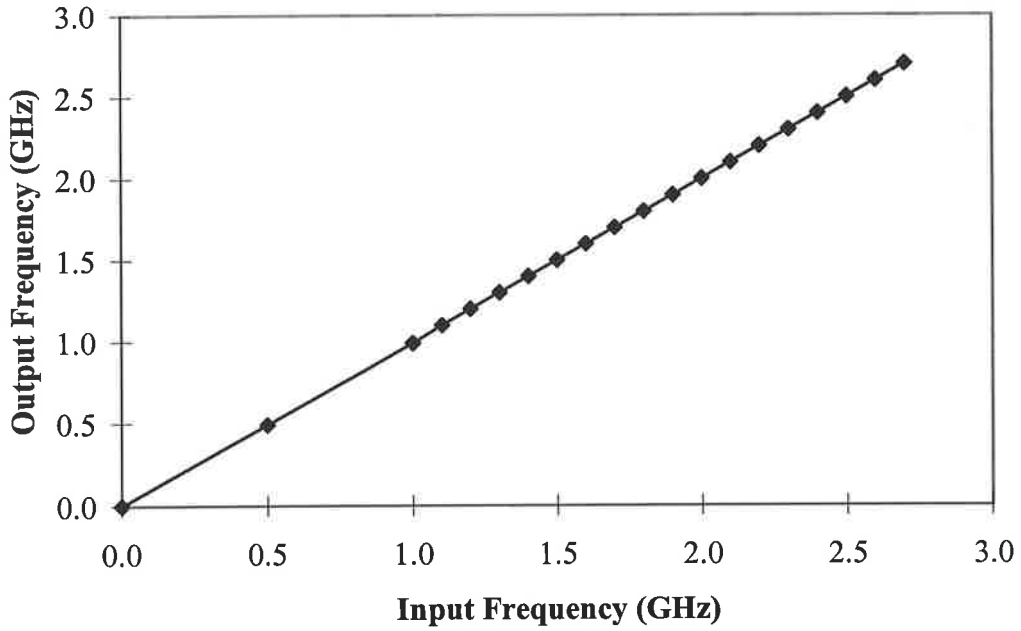

Figure 2.2.5.5: Diagram of the measured output frequency as function of the input frequency.

As part of this study into the effects of noise on the Stokes phase, the simple lens and SBS cell set-up was replaced by a more complicated cell (More explanations about this set-up are given in section 2.3.5). The introduction of this set-up allows the measurement of reflectivity and fidelity for the SBS process without any interference from noise. Figure 2.2.5.6 shows the experimental geometry of the multipass SBS loop with overlap at the foci. The SBS cell now has a confocal lens pair and tilted mirrors at the front and the back window. The laser input beam enters the cell as in a single focus SBS PC mirror but here is focused into the SBS cell a total of three times. The transmitted beam is recollimated and backreflected so that it focuses into the cell in an adjacent position to the first focus. This acts as an intermediate SBS amplifier. The beam transmitted through the front window is again recollimated and backreflected so that it focuses into the cell with the third focus overlapping the first. Brillouin four wave mixing takes place at the overlap region. After the third focus the beam exits the cell and is dumped. This more complex arrangement has the ability of phase locking the phases of the pump and Stokes fields throughout the duration of the pump pulse.

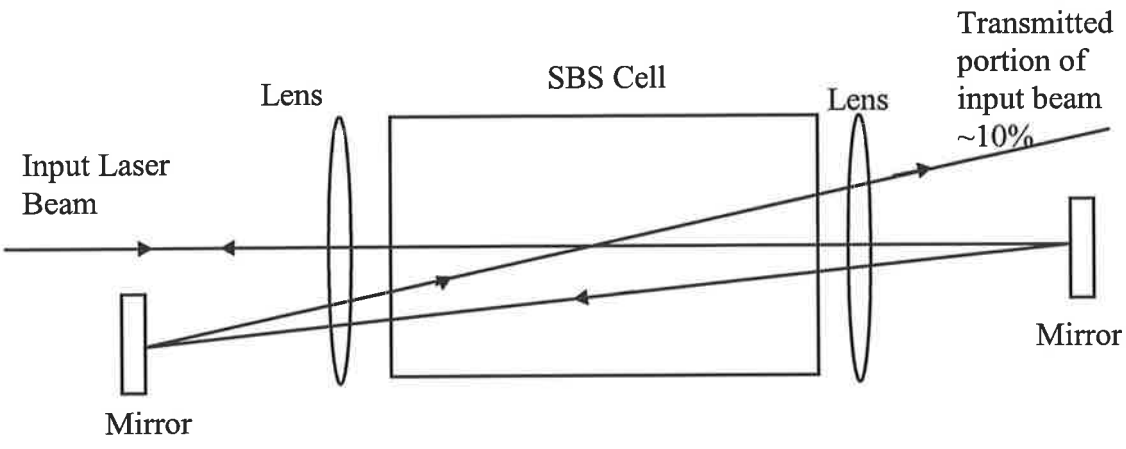

Figure 2.2.5.6: Diagram shows the experimental geometry of the multipass SBS loop with overlap of the first and third foci.

2.3 Results and Discussion

2.3.1 Short Interaction Length

In this section the long coherence, temporal and spatial data are both presented and discussed. With the experiment set up as discussed in the previous section, the reflectivity of the SBS cell was measured as a function of the pump pulse energy in multiples of SBS threshold. To calibrate the reflectivity, a 100% reflecting dielectric mirror was also placed in front of the SBS cell. Typical results are presented in figure 2.3.1. The shape of the reflectivity curve with a steep rise which gradually approaches unity compares well with other experimental[26] and theoretical predictions (see figure 1.3.7). The SBS threshold energy for the 8 ns pump pulse was 3.0 mJ. Here the SBS threshold energy is the total energy in the pump pulse at the point where the reflectivity reaches the value of 2% (see figure 2.3.1). This corresponds to an instantaneous power (i.e. Power=Energy/time=3mJ/8ns=375KW) which is higher than the steady state value for threshold power (i.e. $P_{threshold}=C\lambda/\pi g=(25x1.064mm)/(\pi x0.0058x10\text{-}8)=146KW$). The threshold is stated in terms of energy rather than power simply because that was the measured parameter throughout the study. Similar reflectivity results have been reported by others.[13,27] The reflectivity in the saturation region does not approach unity asymptotically as in the case of theoretical curves but it levels off. This may be due to the very high intensities generated in the volume ahead of the focus which could cause additional non-linear competing effects (i.e. nonlinear absorption, SHG, self-focusing

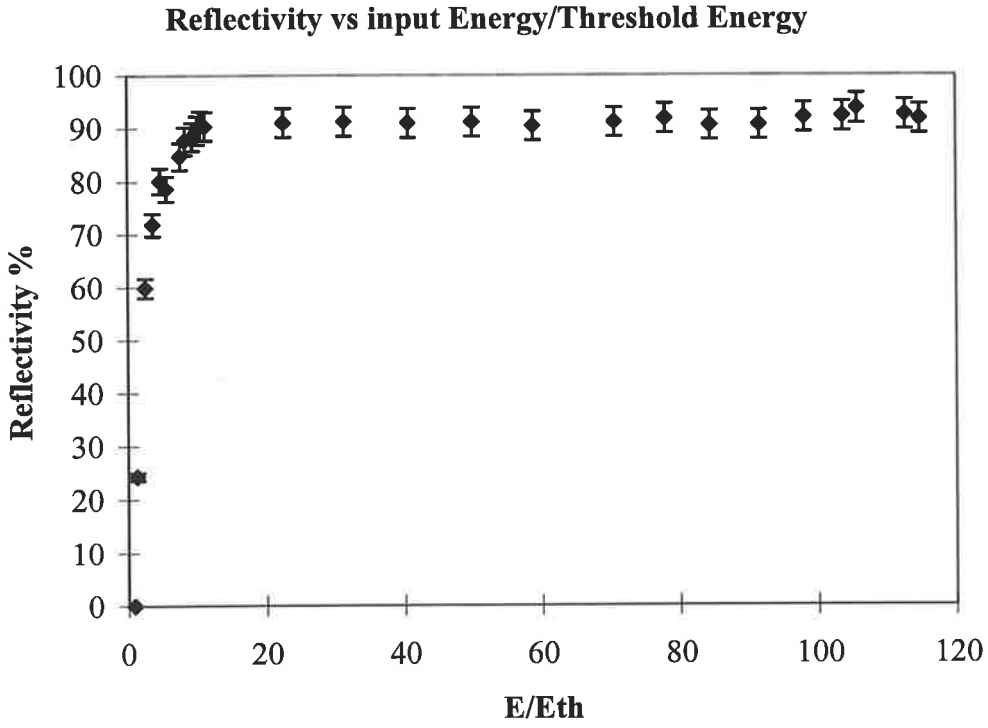

Figure 2.3.1: Diagram shows the long coherence reflectivity of Freon-113 as a function of input Energy/Threshold Energy ratio

and optical breakdown) that clamp the reflectivity. The experimental parameters for the data in figure 2.3.1, include a long coherence length (> 3.0 m), a short length of interaction (< 100 mm), a short Rayleigh range (< 2 mm) and a high purity liquid (distilled and filtered Freon-113). The reflectivity in the case of commercially available, undistilled liquid (micro-particles and other substances) is shown in figure 2.3.2. Although the curve maintains its characteristic shape, the maximum reflectivity is reduced to below 50%.

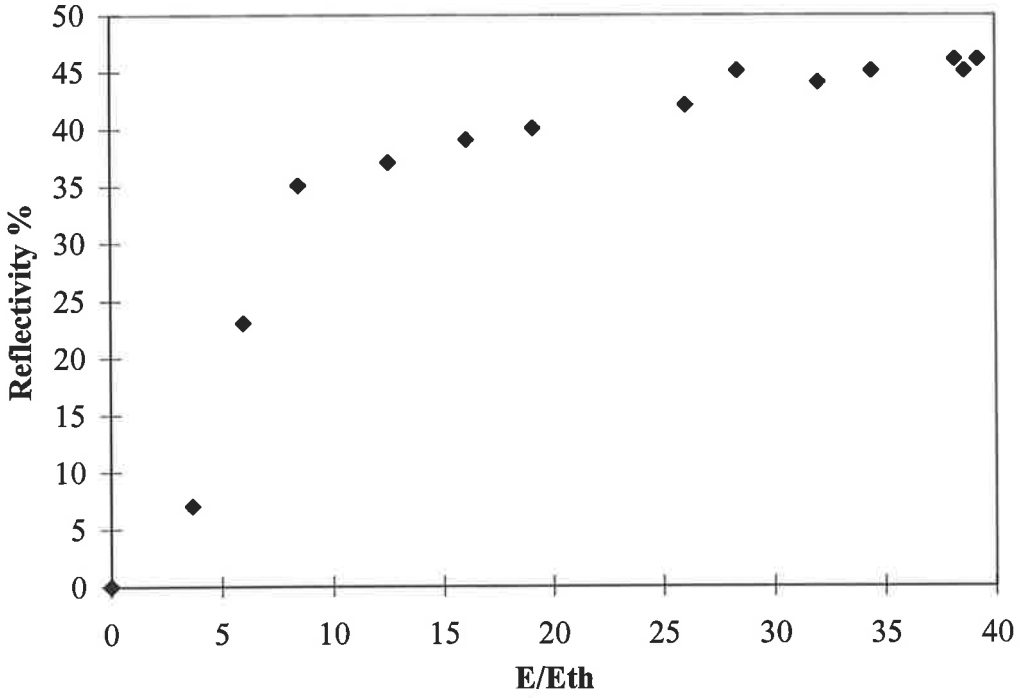

Figure 2.3.2: Diagram of reflectivity of dirty Freon-113 as a function of input Energy/Threshold Energy ratio

The SBS threshold in this case has also slightly increased. Also, for a pure liquid, no optical breakdown was observed in this energy region, whereas with a contaminated liquid, breakdown occurred about 40% of the time at all energies. The importance of using clean, pure liquids to avoid other undesirable competing nonlinear effects will also be highlighted in section 4.3.

The corresponding Phase fidelity (as defined in equation 2.2.5.2) over the range of pump pulse energies is presented in figure 2.3.3. Each of the points on the graph is the average of 99 pulses, with the error bar representing the standard deviation of the fidelity at that particular input energy. The measurements obtained here are in good agreement with other published data,[28,29] but were found to differ to the results of

Ottusch et al.[30] for reasons to be discussed in chapter three. The monotonic rise to unity above the SBS threshold was also a

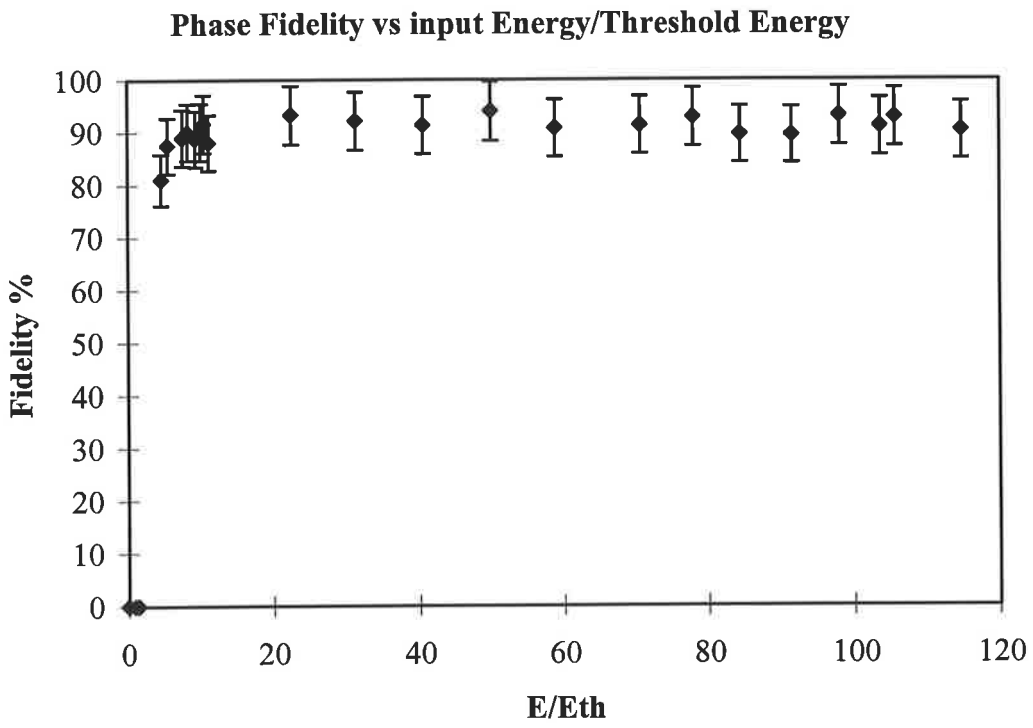

Figure 2.3.3: Plot of long coherence phase fidelity of Freon-113 as a function of input Energy/Threshold Energy ratio

characteristic of other studies[30,31] in which the fidelity as function of input intensity was made. The average value of fidelity is in the order of 90% with a standard deviation of less than 10%. This spread in fidelity continues well above threshold and probably arises because of thermal effects, air currents, acoustic noise, slight pulse to pulse variations in the laser pulse's rise time etc. This means that the pointing stability of the Stokes beam relative to the laser can be slightly affected. Results of aberration correction by phase conjugation in this study, have already been published,[32] (see Appendix 5) showing typical laser beam spatial intensity patterns for an unaberrated

input beam, an aberrated beam, and the phase conjugated SBS beam having passed back through the aberrator. The aberrator was the distorted bottom of a glass beaker and was used to show that OPC occurs. The experimental phase fidelity data compare favourably with theoretical plots of phase conjugate beam fidelity *H* (see figure 1.4.1) as was defined by Zel'dovich et al.[33,34] Both the results for reflectivity and phase fidelity are close to unity in spite of any competing effects that might be involved there. The presented results contradict the findings of reference 35 and disagreed with the supposition of Ottusch and Rockwell in reference 30, that the cause of the PC fidelity instability is connected with a decrease of the spatial mode discrimination for above SBS threshold. Although a reduction in PC fidelity can be connected with a decrease of the spatial mode discrimination,[36] was shown by Dane et al. (reference 31) and confirmed in section 3.3 that this was not the case in their study.

An example of typical far field and near field traces for the laser input and SBS return pulses with their corresponding time resolved Phase fidelity are presented in figure 2.3.4. The error in the values of reflectivity and fidelity are due to quantisation (i.e. intensity value of corresponding time bins) of the pulses and do not exceed 5.0%. Here, it can be seen, that the high fidelity implies that the SBS return pulses reconstruct the laser input pulses very closely.

2.3.2 Intensity Fluctuations

These excellent results were not observed under all operating conditions. A second new regime was investigated, which is characterised a long coherence length (> 3.0 m), a

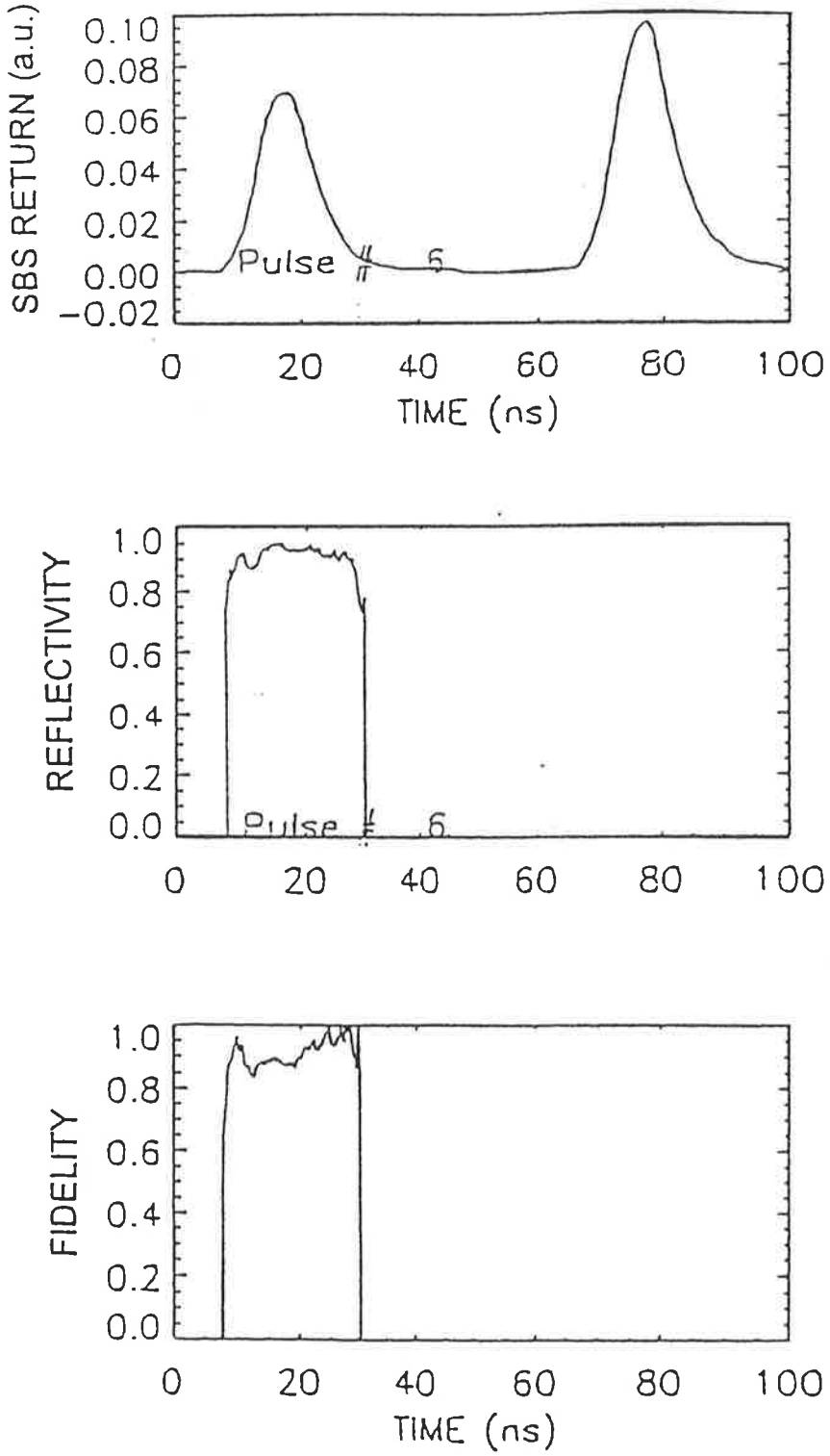

Figure 2.3.4: An example of typical far field (left) and near field (right) traces for a SBS return pulse with its corresponding calculated, time resolved Reflectivity and Phase fidelity.

long length of interaction (> 170 mm), a long Rayleigh range (2 mm to 22 mm) and a high purity liquid (distilled and filtered Freon-113). The longer interaction length is the major difference between this and the previous regime.Under these new conditions intensity fluctuations were seen in about one out of ten (on average) SBS return pulses. Near field fluctuations in SBS have previously been reported by others,[1,37,38] and inferred to be due to stokes phase fluctuations but no direct experimental evidence as to their origin had been given. The intensity fluctuation has a particular temporal shape associated with it. Examples of intensity fluctuations in the SBS return pulses are presented in figure 2.3.5. The fluctuation starts with a decrease in intensity reaching a minimum value and then it very quickly increases reaching a maximum followed by a drop in intensity down to the normal expected value for that specific pulse. The shape of the fluctuation resembles a dispersion curve. These fluctuations can occur anywhere during the pulse (i.e. their occurrence is random in time). Figure 2.3.5 also shows corresponding intensity fluctuations in the transmitted beam. By simultaneously measuring the transmitted part of the input pulse through the SBS cell and the SBS return, we have determined a one to one correspondence where for every decrease in intensity in the SBS return there is a corresponding increase in the transmitted beam. Also for every increase in intensity in the SBS return there is a corresponding decrease in the transmitted beam (i.e. Both SBS return and transmission fluctuations are time coincident). Furthermore as can be seen in figure 2.3.6, the intensity fluctuations can vary in size from small to large and were found to be almost independent of the input pulses energy (with the exception of very high energies where they are suppressed).

When observing intensity fluctuations in the near field of the SBS return, corresponding phase fluctuations always occurred. Figure 2.3.7 gives examples of both

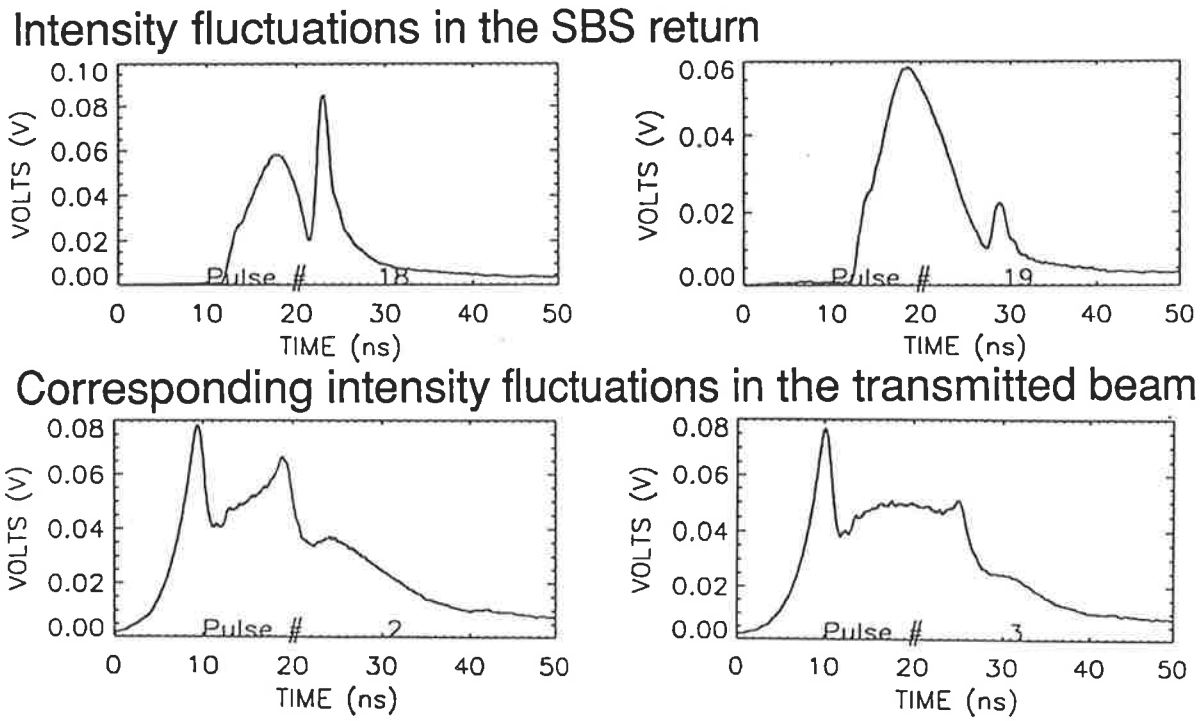

Figure 2.3.5: Examples of intensity fluctuations in the SBS return pulses (top) and corresponding transmitted beams (bottom).

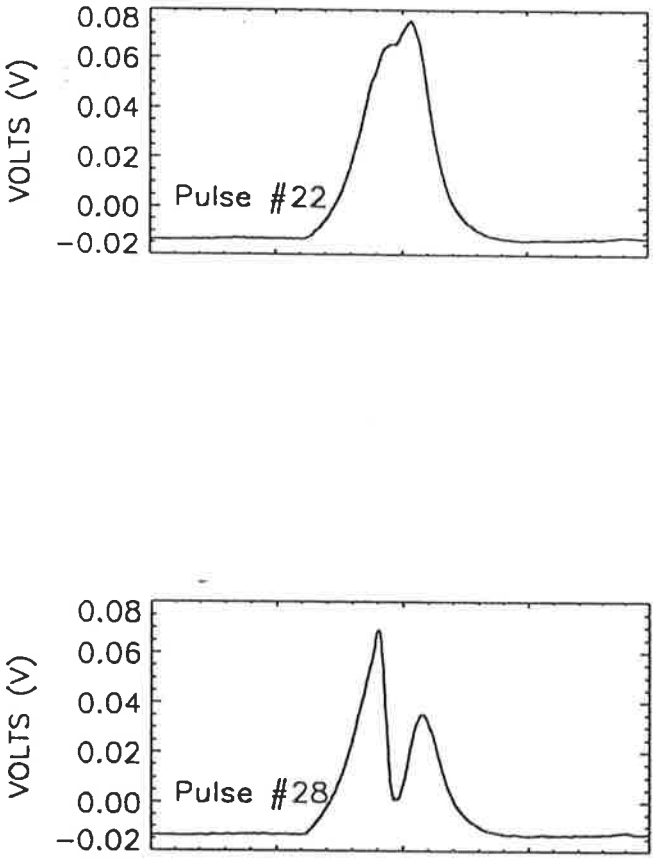

Figure 2.3.6: The intensity fluctuations on the Stokes pulses can vary in size from small (top) to large (bottom).

far field (i.e. transmitted through pinhole) and near field pulses for the laser input and SBS return. It can be clearly seen that although there are no intensity fluctuations in the laser input pulses, there are intensity fluctuations in the SBS return. In fact the third trace of the SBS return pulses shows the occurrence of more than one fluctuation. Similar type of fluctuations in the far field have been reported by others.[4] The data of figure 2.3.7 show that there is a correlation between the near field fluctuations and the reduction of phase in the far field. Figure 2.3.8 shows the time resolved fidelity in the presence of these fluctuations.

The near field fluctuating pulses observed in this study are qualitatively similar to the amplified noise pulses seen by K. Ridley.[39] In reference 39 the intensity fluctuations of the noise pulses were interpreted as thermally excited acoustic fluctuations with temporal variation on the timescale of the phonon relaxation lifetime. With increasing laser input, the intensity of the spontaneously scattered Brillouin light in the medium is amplified in the backwards direction as it travels along the laser path. Furthermore, oscillations on a Stokes temporal gain signal have been observed[40] when the Stokes wave is detuned from resonance (resonance is determined by the conservation of energy and momentum for the scattering process). These losses on the Stokes wave were measured[40] in the transient regime and were interpreted as a slip of phase between the Stokes and the driving force from the acoustic and pump waves. The reason suggested for the loss of signal was that the acoustic wave persists over time scales comparable to the duration of the input pulse. A theoretical study by Kummrow[41] also showed that since SBS grows from noise, fluctuations in reflectance and fidelity as a function of the changed Stokes seed phase can be obtained. Based on the above publications, the intensity fluctuation effects in this experimental study, could take place only if the noise

on which the SBS process relies, was to change phase and cause detuning from SBS resonance during a pulse. One objective of this study was to confirm this by experiments.

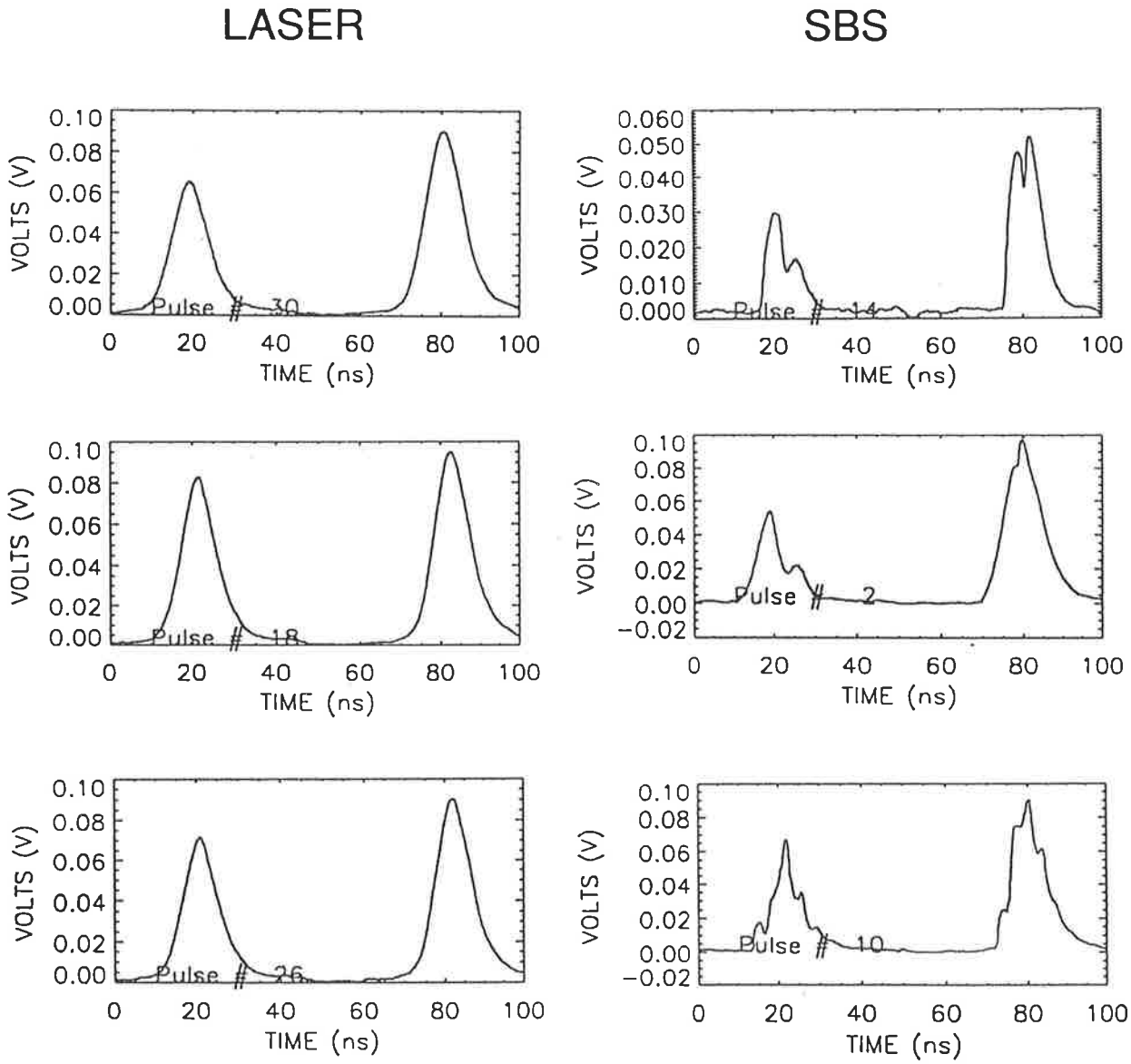

Figure 2.3.7: Plots give examples of both far field (left pulse) and near field pulses (right pulse) for the laser input (left column) and SBS return (right column).

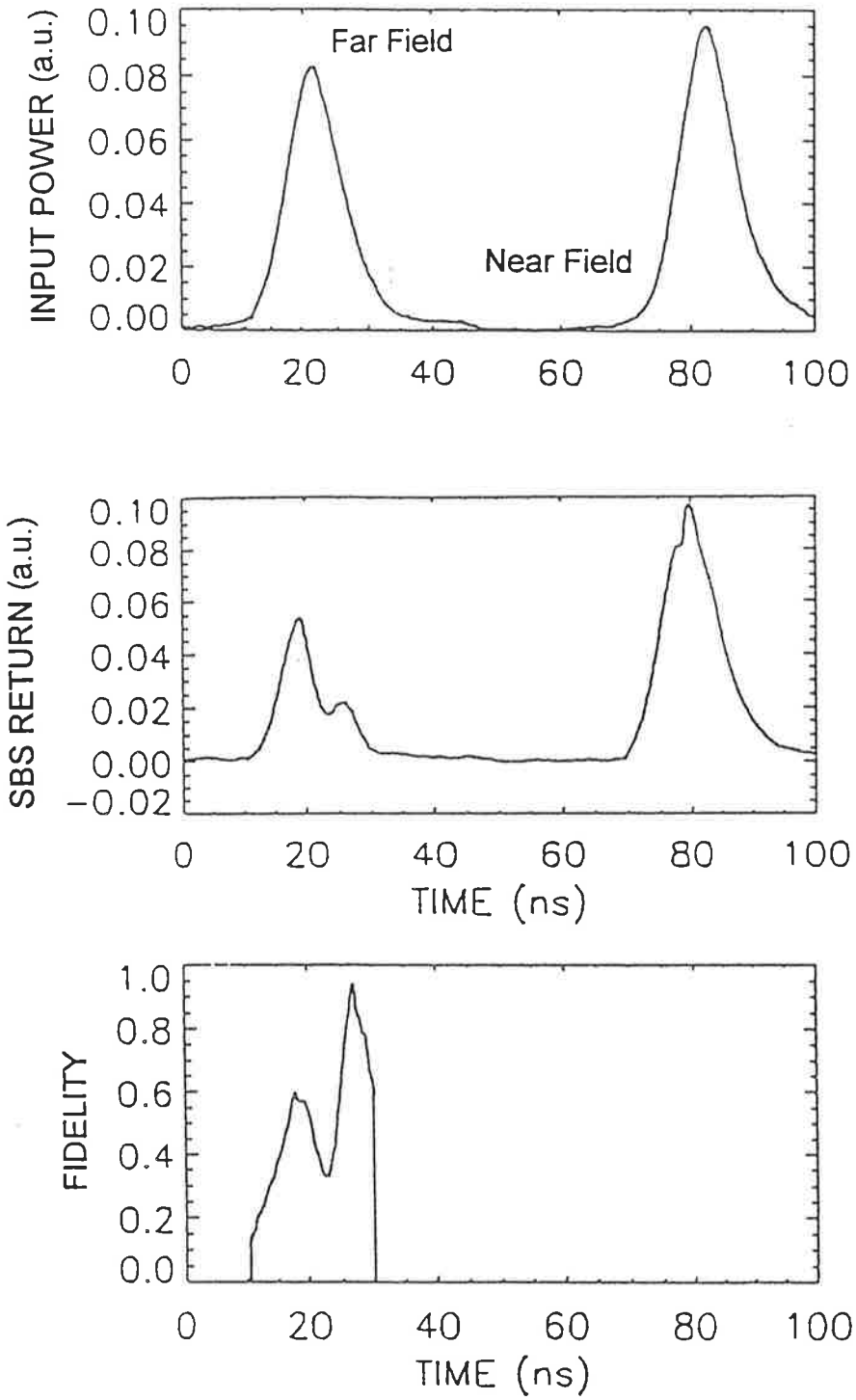

Figure 2.3.8: Plot shows the time resolved fidelity in the presence of these fluctuations. laser pulse (top), SBS return pulse (middle) and phase fidelity of SBS return (bottom).

2.3.3 Phase Changes

A closer examination of the origin of these intensity fluctuations used heterodyne detection to measure the relative phase of the laser input and the SBS return pulses. This technique as suggested in reference 42 is a high-resolution frequency measurement technique for small Brillouin shift changes. The experimental approach used here was discussed in section 2.2.5. An example of data from this experimental study is shown in figure 2.3.9. From these data information such as the Stokes phase, the SBS frequency shift and the speed of the acoustic grating in the medium can be measured. From published data[43] the Brillouin shift for Freon-113 at 1.064 μm is 1.86 GHz. Since the 3 dB level for the bandwidth of the transient digitiser is also at 1.86 GHz, it was possible to detect the beat frequency of the two pulses but with some attenuation in amplitude (see Figure 2.2.5.4). Most other liquids (i.e. CCl_4) have a Brillouin shift of about 2.3 to 9.3 GHz, which makes the direct measurement of their frequency shift, difficult, from a technical point of view. Detection of the shift in this study could be enhanced by increasing the temperature of the liquid thus reducing the Brillouin shift[44,45] but this option was not practical for Freon-113, due to its low boiling point (47.6 °C). Time resolved measurements of beat frequency and phase were made from the heterodyne beat signals as described in section 2.2.5. Figure 2.3.10 presents data of a SBS return whose beat frequency and phase are both steady with respect to the laser input pulse over its pulse duration. The great majority of pulses fall under this category. The Brillouin frequency shift, ν_B is given by the beat frequency and was measured here to be, ν_b=1.8 ± 0.08 GHz. This value is close to other published values[13,43] (e.g. ν_b=1.86 GHz) for Freon-113. Having measured the Brillouin frequency shift, other SBS parameters can

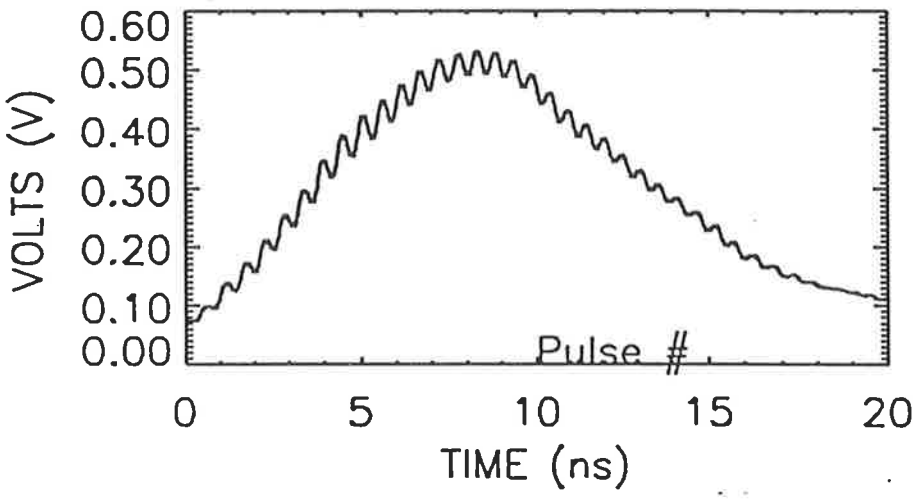

Figure 2.3.9: Example of heterodyne beat between input laser and SBS return pulses.

now be calculated. According to the classical steady state theory of SBS,[46] the speed of the sound, v, in the medium can be calculated from the following relation:

$$v = \frac{\nu_B \lambda}{2n \sin(\theta/2)} \qquad (2.3.1)$$

$$v \approx 704 \text{ m/s}$$

Now having calculated v, the hypersonic absorption can be obtained[47] from $\alpha_s = 1/(2v\tau_B)$ where τ_B=0.72ns.[43] From this expression the distance that the sound wave will travel before it is absorbed, is about 1.0 μm. This propagation is negligible for the timescale of the scattering ($v << c$) and justifies the elimination of the spatial variation of sound from theoretical treatment (see section 1.3).

The pulses that showed intensity fluctuations also had phase jumps associated with them. These phase jumps are presented in figure 2.3.11 to 2.3.13 together with a plot (see figure 2.3.14) from a simple interpretive model which was used as an aid in understanding of the behaviour of the beat frequency (see Appendix 2). Figures 2.3.11 and 2.3.12 show a phase jump of ~ π and ~ π/2 amplitude. As can be seen in this data, both positive and negative phase jumps took place and there were furthermore observed with apparently equal probability of occurrence. The amplitudes of the phase jumps were not necessarily π or π/2 but varied in a random manner. The change in phase was fast with a duration of about 2 to 4 phonon lifetimes. Phase jumps with less than a π/3 amplitude were not observed (even though they could be measured) and phase changes of this order did not show an associated intensity fluctuation on the SBS return. It was observed that the intensity fluctuations on the SBS return were correlated to the

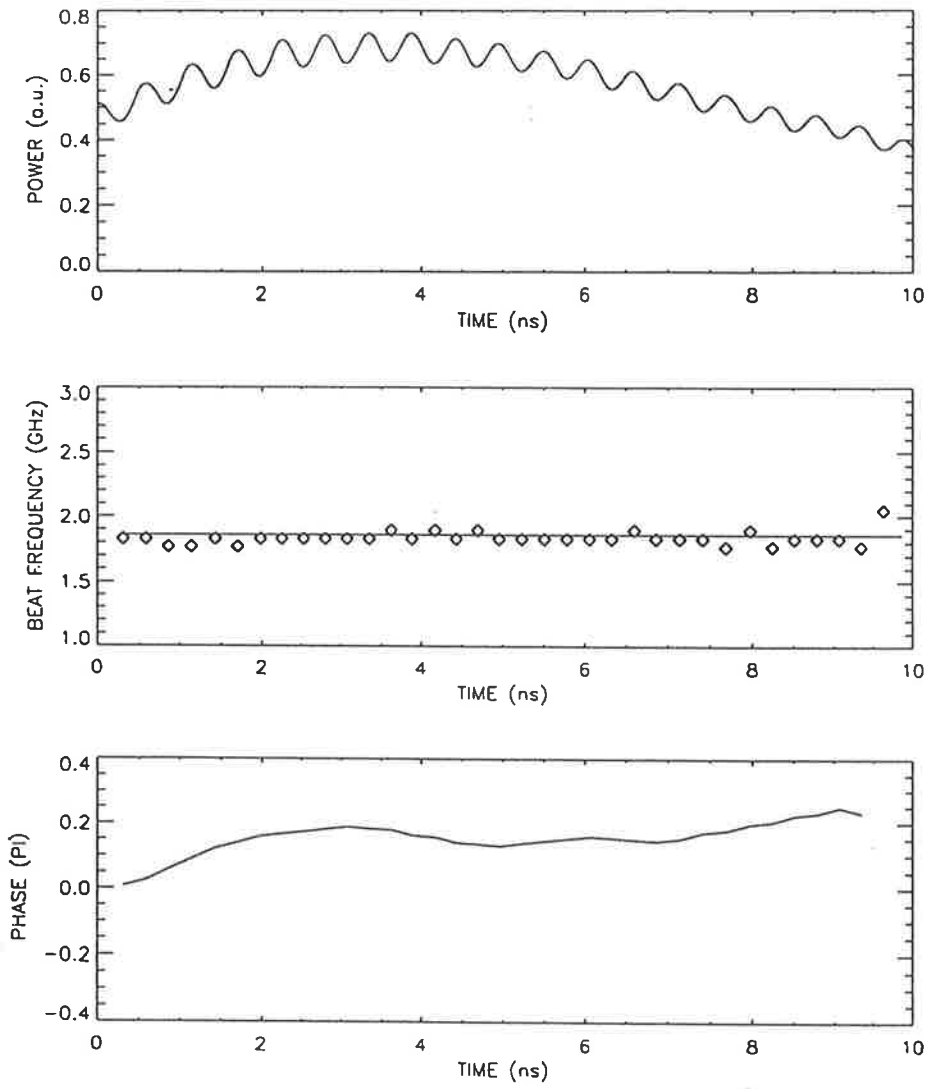

Figure 2.3.10: Plot presents data of a SBS return whose beat frequency and phase are both steady over its lifetime with respect to the laser input pulse. Heterodyne signal (top), beat frequency (middle) and phase of SBS return (bottom).

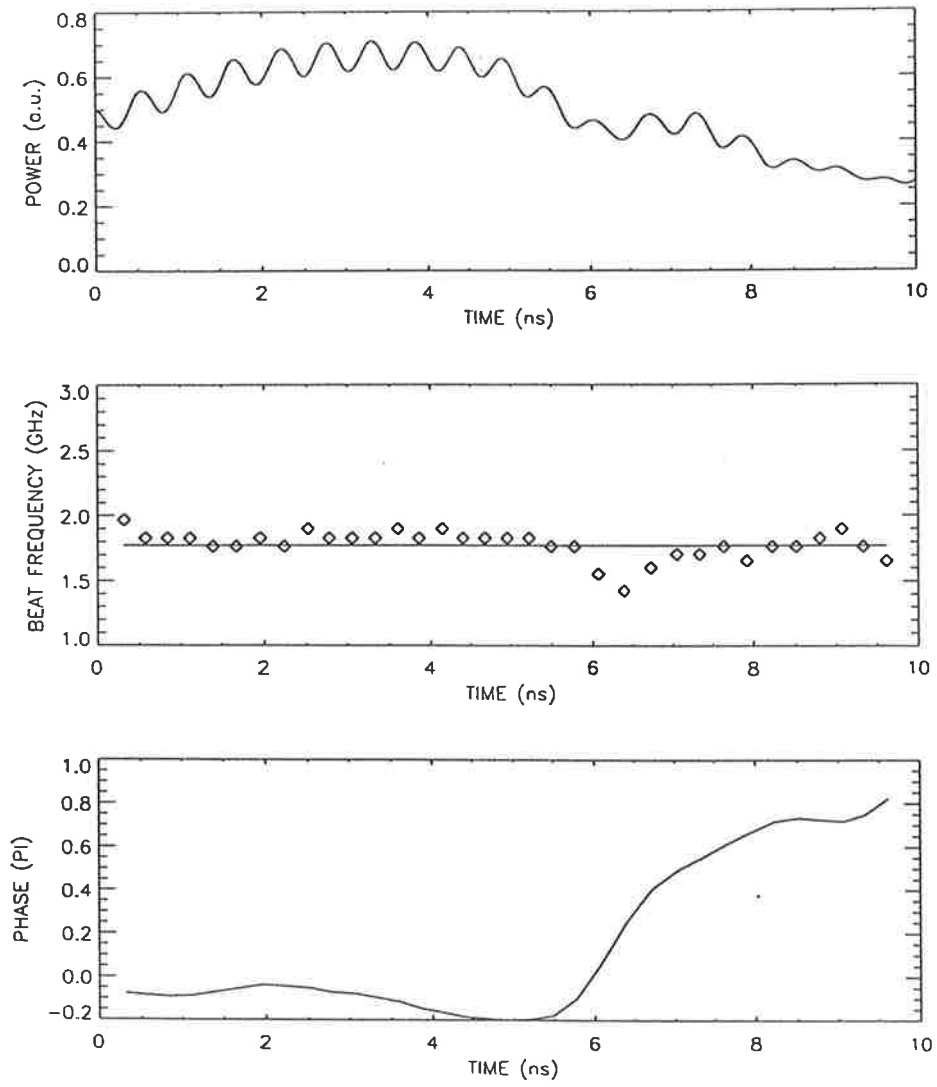

Figure 2.3.11: Plot presents data of a SBS return phase jump (~π).

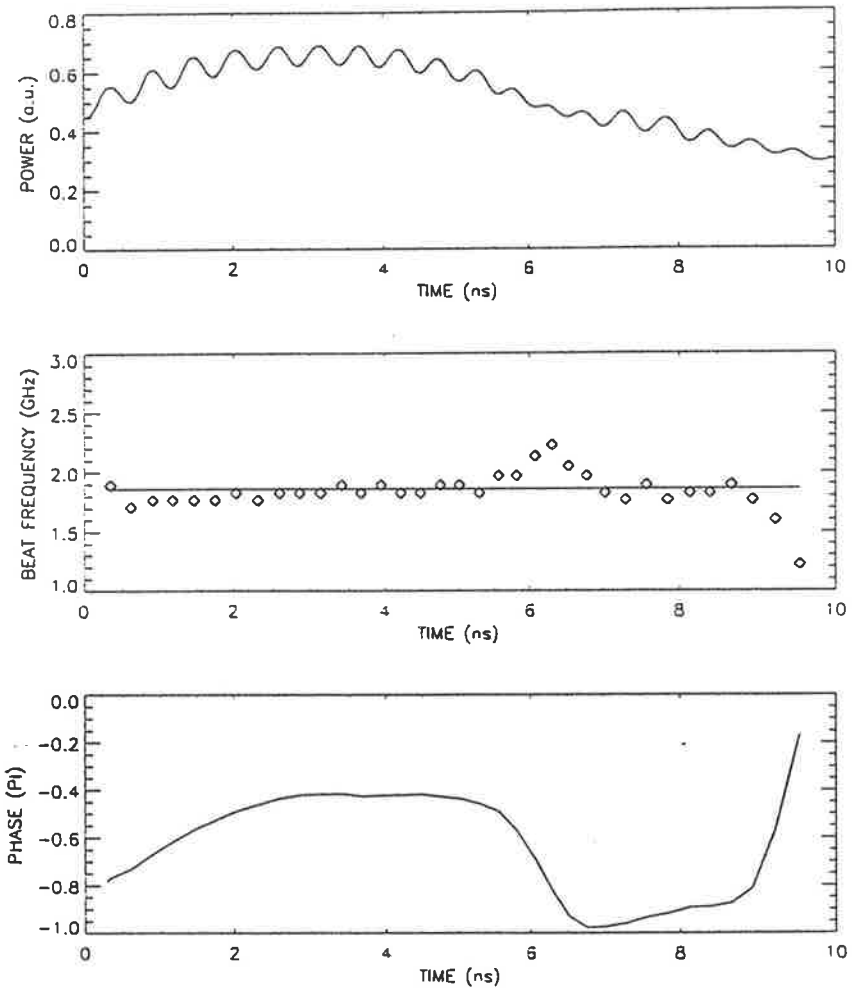

Figure 2.3.12: Plot presents data of a SBS return phase jump (~π/2).

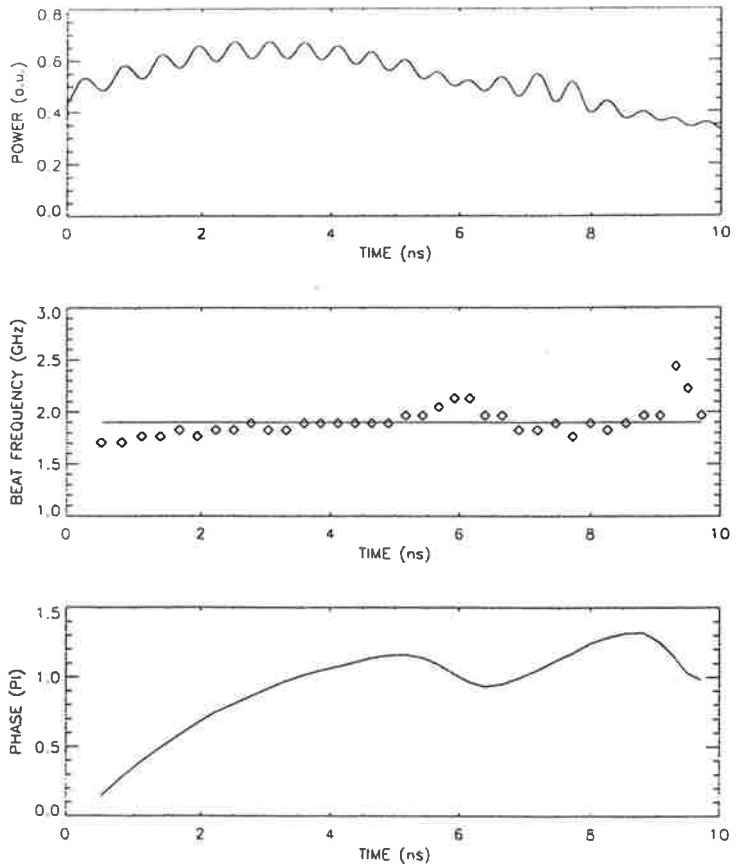

Figure 2.3.13: Plot presents data of a SBS return phase drift.

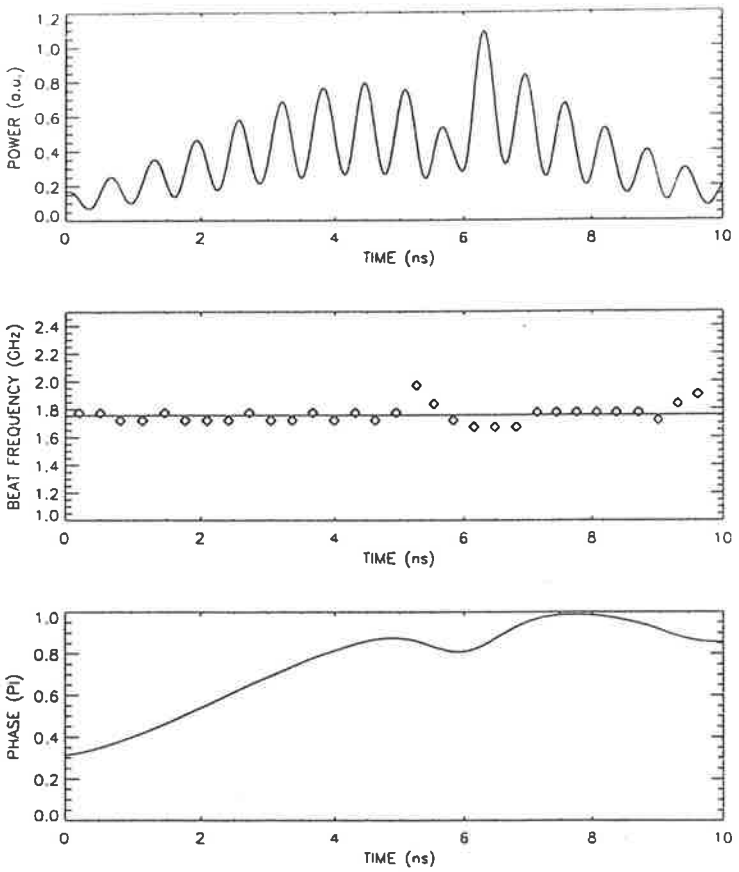

Figure 2.3.14: Plot presents data of a modelled SBS return phase drift. The interpretive model was used to simulate plot from figure 2.3.13.

presence of the phase jumps and their amplitudes were directly related i.e. a π phase jump produced a larger intensity fluctuation than a $\pi/2$ phase jump did. We know from theory that phase and intensity of the Stokes wave are coupled. Thus the larger the phase change, the greater is the intensity fluctuation. Similar phase jumps in SBS have been measured in gases[3] and solids[2,7]. Although some phase changes in liquids have been reported[48] in a study of spectral structure of SBS in CCl_4, the absence of a stable reference beam (the reference beam was reflected from a $TiCl_4$ SBS mirror and was presumed not to contribute to the phase changes) placed some doubt on the validity of that investigation. The authors appear to have ignored that phase changes can take place in both of the SBS returns from the two different liquids (i.e. CCl_4 and $TiCl_4$) and can not guarantee that the observed changes in the heterodyne signal are due to one (i.e. CCl_4) of the two liquids only. This present study does not have such problem, thus providing accurate data on the phase changes in Freon-113.

Similar effects (i.e. phase jumps) have already been predicted[49] and observed[50,51] for stimulated Raman scattering (SRS). The Stokes intensity fluctuations and the phase jumps are thought in these SRS studies to arise from the same underlying mechanism: quantum-noise-driven temporal fluctuations of the Stokes field as it builds up from the zero-point motion of the medium's molecular oscillators (or, equivalently, spontaneous Raman scattering from the material). In SRS as the Stokes gain becomes saturated due to the depletion of the pump field, the noise amplitude fluctuations, which determine the statistical property of the Stokes pulse energy, are almost completely suppressed. By contrast, the phase fluctuations, which induce shot-to-shot variations of the single-shot Stokes spectrum, still grow in the region of high gain (pump depletion).

Further to this effect, temporal instabilities and deterministic chaos arising from counterpropagating laser beams in nonlinear-optical media were experimentally examined in this study. The possibility of chaotic temporal fluctuations in the SBS return due to optical feedback[52] and/or due to resonance detuning[53] was discounted as no periodicity or period-doubling[54] on the SBS Stokes return was observed in this study. All optical surfaces in this experimental study were appropriately tilted to avoid feedback into the SBS cell. When intentionally imposing optical feedback during the SBS process whereby the transmitted portion of the pump and/or the Stokes were reflected back into the SBS interaction volume, then undesirable amplitude fluctuations were produced on the Stokes output. Thus feedback and chaos were eliminated as sources of intensity fluctuation in our experiments.

Figures 2.3.13 and 2.3.14 also show examples of phase drifts, defined here as events where the phase deviates from the original value in a smooth fashion only to return again to its original value. Both the amplitude and duration of the phase drifts were found to be random in character. Qualitatively similar fast and slow fluctuations on the SBS return from liquids had been reported previously,[55] but for broadband (4.5GHz) pumping conditions. In our experiments the possibility of these phase changes being due to absorption[6] is unlikely because the distilled liquid (Freon-113) has very small optical absorption,[55] $\alpha<3.3\times10^{-7}$ cm^{-1} and further, the phase change did not move towards the start of the pulse when the input power was increased.

So far it can be said that changes in phase of the SBS return are associated with fluctuations in intensity of the near field which in turn are associated with reduction of the phase fidelity. The possibility of intensity fluctuations at the far field[38] due to the

finite phonon lifetime had been suggested by Chu et al.[56] The nature of those intensity oscillations was based on a deterministic Stokes input and was not related to the noise input. In reference 57, it was reported that 2-D and 3-D computer models predicted fluctuations in SBS reflectivity and conjugation fidelity to occur simultaneously with jumps in the overall phase of the Stokes wave. However, this present study is the first direct high resolution experimental measurement of fidelity reduction due to noise initiated intensity fluctuations and phase jumps in SBS. This statement will be further supported in a later section by the experimental results of the loop scheme which show that SBS in the absence of noise does not produce phase jumps nor fidelity reductions. Also it has been shown theoretically that the exclusion of noise from the SBS equations does not produce phase jumps (see Appendix 1).

2.3.4 Effect of Focusing Condition

The intensity fluctuations and corresponding phase jumps are consistent with the theory discussed (see section 1.3), and are due to the acoustic noise which helps start and maintain the SBS process. The strength of the intensity fluctuation for 112 pulses at four energy settings, was measured. The strength of the intensity fluctuation at a given energy, was defined as the intensity amplitude modulation measured from its depth to its height, divided by the maximum intensity of the normal SBS return pulse (in the absence of a fluctuation). For two sets of lenses (100 mm and 300 mm focal length) and interaction lengths of 100 and 400 mm respectively, the strength of intensity fluctuations versus energy was measured as summarised in Table 2.3.1. Figure 2.3.15

shows the scatter of the strength of intensity fluctuations for energies above ~8X threshold energy.

	Energy/Threshold energy	8	16	22	26
Focal Length (100 mm), Interaction Length (100 mm)	Strength of intensity fluctuations (average value, %)	35.6	28.5	18.6	8.2
Focal Length (300 mm), Interaction Length (400 mm)	Strength of intensity fluctuations (average value, %)	37.8	37.6	32.8	30.2

Table 2.3.1: Strength of intensity fluctuations vs energy over threshold

The average value of the fluctuation strengths as well as the spread of values appear to decrease as the energy is increased but less dramatically in the case of the longer interaction length. This finding, is consistent with Dianov et al,[2] where the depth of Stokes amplitude modulation decreased with increasing pump intensity but increased with increasing interaction length.[58,59] The number of fluctuations at low energies is higher, because the range of phase change angles becomes wider[59] (i.e. the Stokes return behaves as amplified noise and as such has a continuous random phase). The shape of the fluctuation near threshold energy appears as a dip in the pulse intensity (see figure 2.3.6) but at higher energies it becomes narrower and acquires a characteristic shape (see figure 2.3.5). Both findings of this work as well as those of other studies (e.g. Dianov et al), show that the fluctuations in the SBS return tend to be suppressed at high pump power/intensity at the saturation regime. Accurate measurements of intensity fluctuations at SBS threshold and slightly above it were difficult to make as the SBS

return is shorter (i.e. ~2 nsec) than the input (i.e. ~8 to 10 nsec), thus giving less of an opportunity for detection.

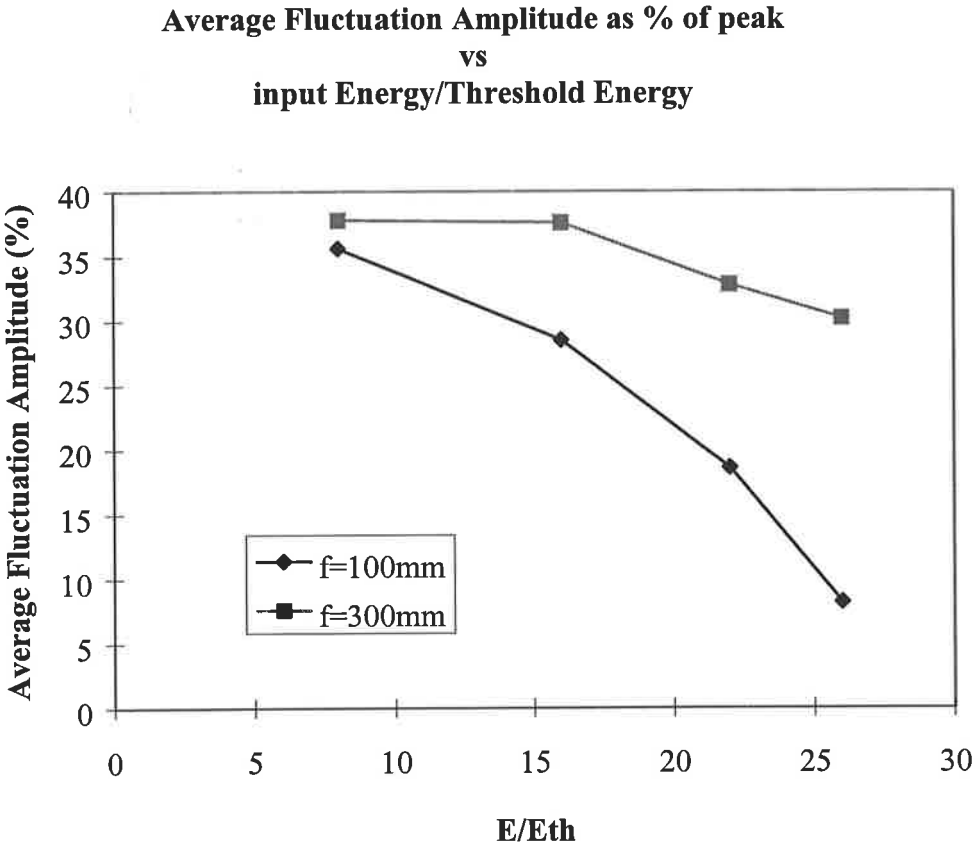

Figure 2.3.15: Average Fluctuation Amplitude strength as % of peak amplitude versus the ratio of input energy over threshold energy (for energies above ~8X threshold energy).

It was observed during the experiments, that the different focal lengths caused either a decrease or an increase in the occurrence of phase jumps. This prompted the examination of focal length as a parameter affecting phase jumps. A set of lenses with focal lengths varying from 50 mm to 1000 mm, were placed in front of a 600 mm SBS cell. The distance between the lens and the front window of the cell was kept to a

minimum. The input pulse energy was ~120 times above SBS threshold. The experimental parameters are presented in Table 2.3.2. The length of the SBS cell was a limiting factor. The strength of intensity fluctuations was suppressed, (as also reported in reference 7), for increased pump energy and short focal lengths.

Focal Length (mm)	50	100	140	200	300	500	800	1000
Interaction Length (mm)	50	100	140	200	300	500	600	600
Strength of intensity fluctuations (average value, %)	0.0	0.0	0.0	5.8	7.0	9.5	12.2	12.1

Table 2.3.2: Strength of intensity fluctuations vs interaction length

One hundred sets of 16 sequential SBS return pulses (1600 pulses) were captured on the transient digitiser for each focal length. From these pulses only those that had a phase jump between $\pi/2$ and π were counted since only these appeared to produce an intensity fluctuation. Furthermore, the ratio of the amplitude of the intensity fluctuation over the average of the maximum intensity of the normal SBS return pulses was measured. From experimental results during this work and from the reported work of Gaeta and Boyd[58,60] on SBS stochastic dynamics, it became clear that it was not the focal length which was the most critical parameter but rather the length of interaction. The length of interaction, l_i, is defined here to be the distance from the front window of the SBS cell to the focal plane in the medium for the particular lens used (i.e the immersion length). Alternatively, the time of propagation, τ_p, is the time it takes the

input laser pulse to go from the front window of the SBS cell to the focal plane in the medium.

$$\tau_p = \frac{nl_i}{c} \tag{2.3.2}$$

Also the phonon lifetime (phonon relaxation), τ_B, appeared to be an important parameter in this case as well. In figure 2.3.16 the relative strength of the intensity fluctuations was plotted against τ_p/τ_B. From this it can be seen that for values of τ_p/τ_B less than one, the relative strength of the fluctuations is close to 0%, whereas for values larger than one the relative strength of the fluctuations increases.

Experimental results reported by others,[61] have shown that, in the $\tau_p/\tau_B>1$ regime there is a deviation in the Stokes amplitude that has a random nature from pulse to pulse, (i.e. fluctuational Stokes return), and which also depends strongly on the sharpness of the focusing and on the energy of the laser beam. Our own study showed that in the regime of $\tau_p/\tau_B <1$ the time of propagation is shorter than the time of the phonon relaxation on which the intensity fluctuations of the SBS return take place. Under this condition, it has been suggested[49] that during the time that a intensity fluctuation lasts, the amount of pump depletion can vary noticeably, thus smoothing the intensity fluctuations in the SBS return. Numerical results from our own theoretical model of SBS

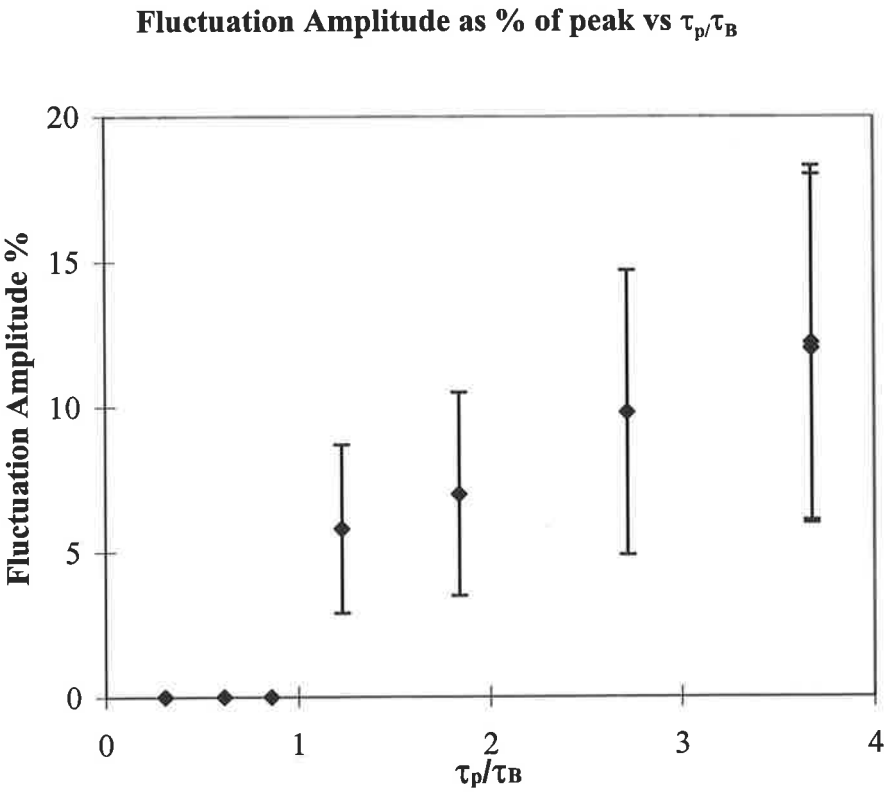

Figure 2.3.16: Diagram shows the relative strength (amplitude %) of the intensity fluctuations against τ_p/τ_B.

also support this behaviour.[63] Therefore, both the amplitude fidelity and the phase fidelity of the SBS return pulse depend on the geometrical and physical characteristics of the Brillouin medium. In addition to this it has also been suggested in Reference 62 that the time of pulse propagation in the SBS medium should not greatly exceed τ_B for the material, as strong pulse reshaping in the Stokes return in the form of pulse compression can result.

Using the above information, experimental predictions can be made from our study. When $\tau_p/\tau_B=1$, then l_i=163 mm for Freon-113, with τ_B=0.74 nsec and n=1.36. This

means that any lens whose focal length is longer than 163 mm will produce some phase jumps on the SBS return pulse in Freon. This result (as predicted) is shown in Figure 2.3.16.

The behaviour of the phase jumps measured in this study (seen in figures 2.3.15-16) is qualitatively similar to the predictions of the theoretical model[63] in section 1.3 (see Appendix 1). Our results show that an increase in fluctuation strength is observed by decreasing energy or by increasing interaction length. The above mentioned results are in qualitative agreement with reference 64 (see Appendix 4) where amplitude and phase fluctuations in SBS were found to depend critically on the length of the interaction region (τ_p/τ_B). Also, in other studies[65,66] (SBS in optical fibers) it has been shown that the value of the τ_p/τ_B ratio affects the Stokes gain coefficient thus causing selective amplification of the amplitude fluctuations to take place.

In order to test further the validity of this condition i.e. no phase jumps when $\tau_p/\tau_B<1$, a set of lenses (from 50 to 500 mm focal length) were now placed some distance in front of the SBS cell. The length of interaction, l_i for each lens was restricted to either half of its focal length or 80 mm, which ever distance was the smallest for that lens. The experimental parameters are presented in Table 2.3.3. The input pulse energy was ~120 times above SBS threshold. The strength of intensity fluctuations in the Stokes return had to be greater than 2% in order to be counted. Lenses with longer focal length at this energy caused optical breakdown to the cell window.

Focal Length (mm)	50	100	140	200	300	500
Interaction Length (mm)	50	50	70	80	80	80
Strength of intensity fluctuations (%)	0	0	0	0	0	0

Table 2.3.3: Strength of intensity fluctuations at decreased length of interaction for $\tau_p/\tau_B<1$ condition.

The strength of the intensity fluctuations versus focal length, for the $\tau_p/\tau_B<1$, is zero for all of the above lengths. The data show an absence of intensity fluctuations observed as compare to table 2.3.2. The major difference here is in the reduction of the interaction length in the SBS cell and the intensity at focus. In the case of the 500 mm focal length lens some smooth intensity changes in the shape of the SBS return were observed however. No satisfactory explanation could be given for these smooth changes as they were not due to ~π angle phase jumps. Here the intensity along the interaction length is higher than in the previous cases and the distribution of the Stokes gain and acoustic grating in different parts of the medium is altered due to the faster growth rate in the Stokes wave, thus possibly causing these smooth changes to take place.[67,68] Therefore, it appears that τ_p/τ_B is an important parameter as it holds the key to the suppression of phase jumps.

A review of the published articles in which SBS amplitude or phase fluctuations were reported, allows the construction of the following table.

Material	τ_p/τ_B	Reference Article No.
CCl_4	1.2	1 (Vasil'ev et al)
CCl_4	1.6	38 (Bespalov et al)
CCl_4	1.2	48 (Erokhin et al)
CCl_4	3.8	64 (Moore et al)
Methanol	1.9	4 (Munch et al)
N_2 @ 5.5 atm	>1.5	3 (Mangir et al), (for 1.5mm beam diameter)

Table 2.3.4: τ_p/τ_B data from articles with SBS fluctuations

The above data indicate that for $\tau_p/\tau_B>1$ SBS fluctuations have already been observed in these materials.

All of this work was concentrated on the temporal evolution/behaviour of the SBS process. I suggest at this point that future work (i.e. experimental and theoretical) relating to spatial effects/conditions should be undertaken as it would offer a more precise picture of OPC-SBS. For instance, further insight could be obtained for figures 2.3.15-16 by examining the behaviour of SBS speckles that may be generated by the process. Speckle patterns have spatial frequencies which depend on the focusing geometry and since the SBS process starts from noise then a large number of spatial frequencies can exist. The Stokes wave at the focal region is initially uncorrelated with the laser input wave as the excited noise sources are independent in phase and propagation. Therefore the SBS return beam can consist of a diverging speckle pattern (i.e. non-phase conjugate return) if spatial frequencies other than these which correspond to the laser input could receive gain (e.g. poorly defined far field). The effects of excess spontaneous noise associated with the transverse modes of a gain-

guided SRS amplifier have already been shown to induce beam-pointing fluctuations.[69] As there is some theoretical similarity between SBS and SRS (SRS can be described as the scattering of light from optical phonons), future work in this area could have a significant implication in laser applications that utilise SBS cells.

During pumping but near the SBS threshold, some spontaneous scattering also takes place in all directions but in a focusing geometry only those photons which are scattered in the backward direction to that of the input beam would receive maximum amplification and thus could cause Stokes phase jumps. The spontaneous noise can be related to the mean number, $\bar{n}$ of phonons per mode of the acoustic field in Freon-113. Even for one mode the number of phonons is large:

$$\bar{n} = \frac{1}{\exp\left[\hbar\nu_B / k\mathrm{T}\right] - 1} \qquad (2.3.4)$$

$\bar{n} = 3{,}470$ for T=300 K and ν_B =1.8 GHz.

The more spatial modes in a laser beam, the higher will be the number of spontaneous photons that are generated at the initiation of the SBS process. The number of temporal modes in the volume is given by the product of the bandwidth, $\Delta\omega$ of the thermal phonons and τ_p.[70] The total number of spatial-temporal modes in practice, could be large. The pulse-to-pulse fluctuations in the SBS return occur because many independent modes can contribute to the Stokes emission, making it spatially and/or temporally incoherent. In the case of stimulated Raman scattering a theory of spatial and temporal coherence has already been developed[71] which predicts pulse fluctuations. More recent theoretical work for transient SBS using a zero-order approximation of the

Maxwell wave equation has failed to include phase-mismatched terms.[72] A comprehensive SBS theory is still to be developed.

2.3.5 Loop Scheme

During this thesis work, it was reported[73] that noise in SBS could be eliminated by use of a loop scheme, originally designed to reduce threshold.[8] We immediately set out to confirm the validity of this report, as it provides us with an extra tool to study the effects of noise on SBS. Although the loop scheme was initially designed and applied[8] with laser pulses with duration from 200 nsec to 1.0 μsec, by contrast, in this experiment only 8-10 nsec laser pulses were used. In studies by others,[74] similar schemes have also been applied for the reduction of threshold in SBS using variable pulse lengths from 15-100 nsec.

Since the source of all phase jumps is due to the spontaneous noise which helps start the SBS process, an experiment was set up where the noise was replaced with an imposed (simulated) acoustic grating at or near the far field.[8,73,75] This set-up (based on work of reference 8) was described in section 2.2.5, refer to figure 2.2.5.6. Scott et al in reference 8, gave a very good theoretical and experimental description of the loop geometry. In this scheme the laser input beam is looped so that it overlaps itself near the focal plane where it writes an acoustic grating using four-wave mixing. Even though the process starts from noise, the acoustic grating is rapidly amplified. The Stokes beam no longer scatters from spontaneous noise but is directly seeded by the continuously written acoustic grating. SBS can still take place and as an added benefit its threshold is

also reduced (i.e. due to 4-wave mixing). As long as the looped (feedback) beam intersects at the front of the focal region where the acoustic wave was strongest, appreciable seeding would be generated.[76] For favourable operating conditions it is important that the angle of intersection at the overlap region be small, since the amount of the SBS shift relies on it, and that a long overlap is obtained between the crossing beams for maximum gain conditions.[77] Figure 2.3.19 gives a typical example of the far field and near field of the laser input and SBS return pulses. No phase jumps were observed during the experiment under these operating conditions thus resulting in high SBS fidelity. These findings agree with those of reference 78. Figure 2.3.20 presents an example of the time resolved phase fidelity. This loop scheme was insensitive to the τ_p/τ_B ratio. By blocking out the overlapping (feedback) beam the SBS process had only noise to rely on for its start and maintenance, thus bringing about the return of the phase jumps (i.e. became sensitive to the τ_p/τ_B ratio), which in turn caused the reduction of the PC fidelity.

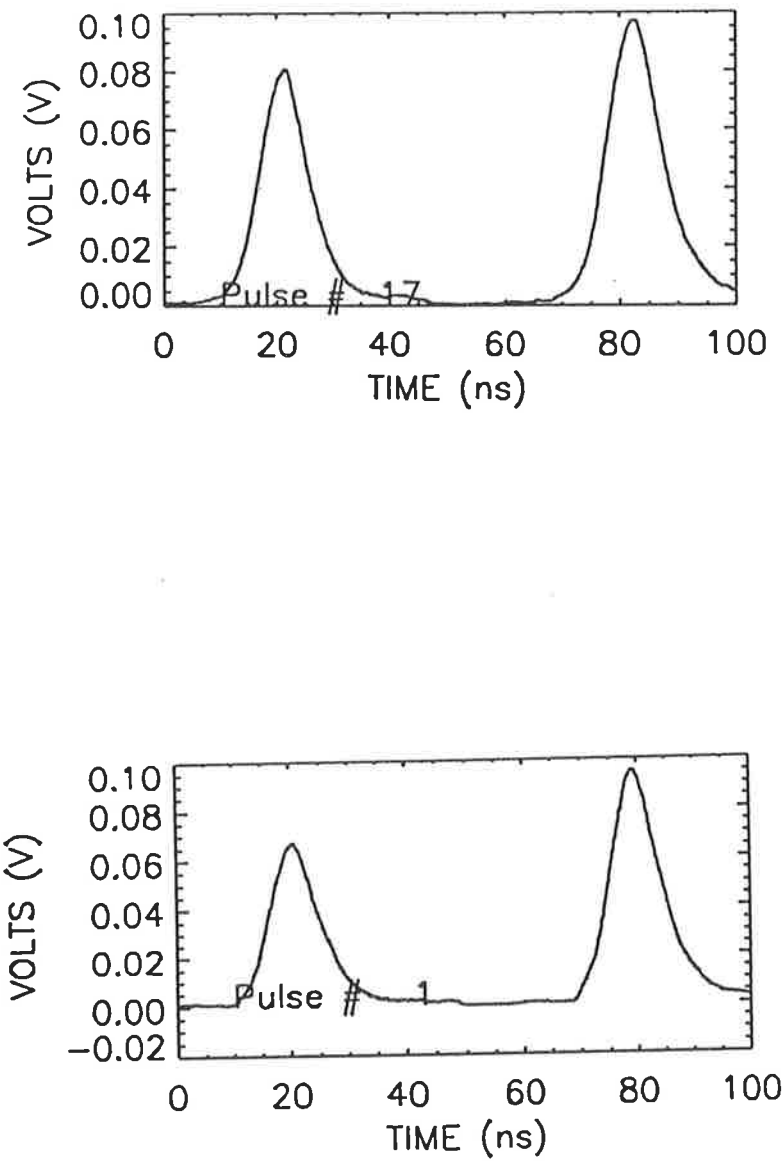

Figure 2.3.19: A typical example of the far field (left) and near field (right) of the laser input (top) and SBS return (bottom) pulses.

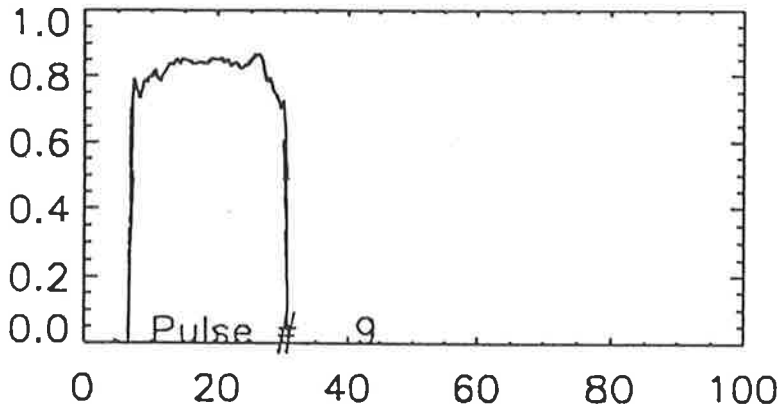

Figure 2.3.20: Plot presents an example of the time resolved phase fidelity.

2.4 CONCLUSION

The aim of this work was to resolve discrepancies in the literature and in the process establish design parameters for high fidelity in OPC-SBS. Unlike what was reported by others, no shot-to-shot fluctuations in the far-field fidelity were observed due to operation in the saturated reflectivity regime alone. Rather, it was found that the careful balance of SBS process parameters can assure high fidelity even in the saturated reflectivity regime.

Use of long coherence length pulses alone in the OPC-SBS process does not guarantee a high fidelity on every laser shot regardless of whether their energy is near threshold or well above saturation. The thermal relaxations or spontaneous emissions (noise) of the medium in an SBS cell play an important role in the initiation as well as throughout the duration of the SBS process. This experimental investigation has shown that the effects of noise are responsible for the intensity fluctuations, phase changes and fidelity reduction of the SBS return (Stokes backscattered radiation). These effects were not observable under all types of SBS optical configurations, thus providing OPC-SBS with a regime in which the process works reliably. At energies close to threshold the SBS return can have up to 100% intensity fluctuations but as the energy in a pulse increases then the fluctuations are reduced. Large intensity fluctuations can occasionally be experienced even at the reflectivity saturation, gain depletion regime. The suppression of fluctuations depends strongly on the ratio of the propagation time to that of the phonon relaxation time in the medium. The smaller this ratio is, the larger the suppression of these fluctuations becomes. By better understanding the various medium

parameters and applying appropriate pumping geometries, this process will find a wider commercial application.

This work has showed (or confirmed) that the appropriate choice of focusing geometry or use of direct seeding can eliminate the presence of phase jumps and intensity fluctuations which noise normally creates in OPC-SBS. The best performance of OPC-SBS required the following conditions: high input energy, and short length of interaction (i.e. immersion length). Although the loop scheme works well it is still complex in its construction. Thus there is a real need for identifying a stable operating regime where a single, simple SBS cell works well. All of the experimental results have been related wherever possible to the published results and findings of other experimental and theoretical studies.

In an attempt to provide greater insight into the process of OPC-SBS, the results of this work have been useful as a test to theory but could also serve as a guide for theory. Experiments can only offer information about a restricted range of parameters in the OPC-SBS process due to practical restrictions (e.g. laser source, SBS material). It is for this reason that we have also undertaken a theoretical modelling approach which is already providing useful information on the behaviour of the SBS process under various focused geometries.

2.5 References

1 M. V. Vasil'ev, A. L. Gyulameryan, A. V. Mamaev, V. V. Ragul'skii, P. M. Semenov, and V. G. Sidorovich, "Recording of phase fluctuations of stimulated scattered light", Pis'ma Zh. Eksp. Teor. Fiz. 31, 673-677 (1980) [JETP Lett., Vol 31, No 11, 634-368, 5 June 1980]

2 E. M. Dianov, A. Ya. Karasik, A. V. Lutchnikov and A. N. Pilipetskii, "Saturation effects at backward-stimulated scattering in the single-mode regime of interaction", Optical and Quantum Electronics, Vol. 21, 381-395, 1989

3 M. S. Mangir, J. J. Ottusch, D. C. Jones and D. A. Rockwell, "Time-resolved measurements of Stimulated-Brillouin-Scattering phase jumps", Physical Review Letters, Vol. 68, No 11, 1702-1705, 16 March 1992

4 J. Munch, R. F. Wuerker and M. J. LeFebvre, "Interaction length for optical phase conjugation by stimulated Brillouin scattering: an experimental investigation", Applied Optics, Vol. 28, No 15, 3099-3105, 1 August 1989

5 S. M. Wandzura, "Stimulated scattering does not have a steady state", CLEO'88, Nonlinear Optics: 1, MC3, 25 April 1988

6 S. F. Grigor'ev, O. P. Zaskal'ko and V. V. Kuz'min, "Some features of stimulated Brillouin scattering in light-absorbing media", Sov. Phys. JETP, Vol. 65, No 4, 697-702, April 1987

7 A. L. Gaeta, R. W. Boyd and T. R. Moore, "Stochastic dynamics in stimulated light scattering", IEEE publication, IQEC'94, 1994

8 A. M. Scott, W. T. Whitney, and M. T. Duignan, "Stimulated Brillouin scattering and loop threshold reduction with a 2.1-μm Cr,Tm,Ho:YAG laser" J. Opt. Soc. Am. B, Vol. 11, No 10, 2079-2088, October 1994

9 R. E. Slusher, L. W. Hollberg, B. Yurke, J. C. Mertz and J. F. Valley, "Squeezed states in optical cavities: A spontaneous-emission-noise limit" Phys. Rev. A, Vol. 31, No 5, 3512-3515, May 1985

10 A. C. Ashmead, "Watch out for diffraction effects on laser-beam profiles", Laser Focus World, 83-92,August 1991

11 Freon Product Information, "Freon Fluorocarbons: Properties and Applications", Du Pont, Wilmington, DE 19898, Barley Mill Plaza, 1985

12 "Thermodynamic properties of FREON 113, TRICHLOROTRIFLUORO-ETHANE, ClCF2-CCl2F, With Addition of Other Physical Properties", Du Pont, Wilmington, DE 19898, Barley Mill Plaza, 1979

13 N. F. Andreev, E. Khazanov, G. A. Pasmanik, 'Applications of Brillouin Cells to High Repetition Rate Solid-State Lasers', IEEE Journal of Quantum Electronics, Vol. 28, NO 1, pp. 330-341, January 1992

14 V. M. Volynkin, K. V. Gratsianov, A. N. Kolesnikov, Yu. I. Kruzhilin, V. V. Lyubimov, S. A. Markosov, V. G. Pankov, A. I. Stepanov and S. V. Shklyarik, "Reflection by stimulated Brillouin Scattering mirrors based on tetrachlorides of group IV elements", Soviet Journal of Quantum Electronics, Vol. 15, No. 12, 1641-2, December 1985

15 V. Yu. Zalesskii and A. M. Kokushkin, "Liquid media for stimulated Brillouin scattering in the middle infrared", Sov. J. Quantum Electron., Vol. 15, No. 4, 541-543, April 1985

16 H. J. Eichler, R. Menzel, R. Sander and B. Smandek, "Reflectivity enhancement of stimulated Brillouin scattering liquids by purification", Optics Communications, Vol. 89, No. 2,3,4, 260-262, 1 May 1992

17 C. B. Dane, L. E. Zapata, W. A. Neuman, M. A. Norton and L. A. Hackel, "Design and Operation of a 150 W Near Diffraction-Limited Laser Amplifier with SBS Wavefront Correction", IEEE Journal of Quantum Electronics, Vol. 31, No. 1, 148-163, January 1995

18 A. M. Scott, D. E. Watkins and P. Tapster, "Gain and noise characteristics of a Brillouin amplifier and their dependence on the spatial structure of the pump beam", Journal of the Optical Society of America B, Vol. 7, No. 6, 929-935, June 1990

19 E. L. Budis, V. V. Vargin, L. R. Konchalina and A. A. Shilov, "Study of low-absorption media for SBS in the near-IR spectral range", Opt. Spektrosk. (Optics and Spectroscopy), Vol. 65, No 6, 1281-1285(759-9), Dec. 1988

20 T. D. Milster and J. P. Treptau, "Measurement of Laser Spot Quality", SPIE, Laser Beam Diagnostics, Vol. 1414, 91-96, 1991

21 J. A. Ruff and A. E. Siegman, "Single-pulse laser beam quality measurements using a CCD camera system", Applied Optics, Vol. 31, No. 24, 4907-4909, 20 August 1992

22 J. Munch, R. F. Wuerker and M. LeFebvre, "Michelson Interferometer with a Holographic Memory for Measuring Fidelity of Aberrated Phase Conjugated Beams", Appl. Opt., Vol. 28, 1731-1733, 1989

23 A. Petris, S. Tibuleac and L. Voicu, "Measuring the phase conjugation fidelity by computer image analysis", Romanian Journal of Physics, Vol. 38, N0 7, 669-673, 1993

24 V. Devrelis, M. O'Connor and J. Munch, "Coherence length of single laser pulses as measured by CCD interferometry", Applied Optics, Vol. 34, No 24, 5386-5389, 20 August 1995

25 S. G. Lipson and H. Lipson, *Optical Physics*, Cambridge University Press, 2nd edition, p. 286, 1981

26 S. Jackel, P. Shalev and R. Lallouz, "Experimental and theoretical investigation of statistical fluctuations in phase conjugate mirror reflectivity", Optics Communications, Vol. 101, No 5,6, 411-415, 1 September 1993

27 M. J. Dyer and W. K. Bischel, "Stimulated Brillouin Spectroscopy of liquids", CLEO'92, CTuN5, 182, 12 May 1992

28 R. St. Pierre, H. Injeyan and J. Berg, "Investigation of SBS phase conjugation fidelity fluctuations in Freon-113", CLEO 92, CTuN3, Vol. 12, 180, 12 May 1992

29 C. B. Dane, W. A. Neuman and L. A. Hackel, "Fidelity fluctuation in SBS phase conjugation at high input energies", Nonlinear Optics III, OE LASE 92, SPIE, Vol. 1626, 308-316, 1992

30 J. Ottusch and D. Rockwell, "Stimulated Brillouin Scattering phase-conjugation fidelity fluctuations", Optics Letters, 24,No 6 369-371, 1991

31 C. B Dane, W. A Newman and L. A. Hackel, "Pulse Shape Dependence of Stimulated Brillouin Scattering Phase Conjugation Fidelity For High Input Energies", Optics Letters, Vol. 17, No 18, 1271, 1992

32 J. Munch, V. Devrelis, A-M. Grisogono, M. V. O'Connor and C. J. Wei, "Phase Conjugation in Solid State Lasers", Australian Optical Society News, Vol. 10, Issue 2, pp. 8-12, June 1995

33 B. Ya. Zel'dovich, N. F. Pilipetsky and V. V. Shkunov, "Principles of Phase Conjugation", Springer Series in Optical Science, Vol. 42, Springer-Verlag, 1985.

34 B. Ya. Zel'dovich, N. F. Pilipetsky and V. V. Shkunov, "Phase Conjugation in Stimulated Scattering", Sov. J. Polymer Physics Usp, Vol. 25, No 10, 713, 1982

35 N. F. Andreyev, E. A. Khazanov, O. V. Palashov and G. A. Pasmanik, "Phase-conjugation fidelity fluctuations for various stimulated-Brillouin-scattering mirror geometries", J. Opt. Soc. Am. B, Vol. 11, No 5, 786-788, May 1994

36 M. Lefebvre, S. Pfeifer and R Johnson, "Dependence of stimulated-Brillouin-scattering phase-conjugation correction on the far-field intensity distribution of the pump light", J. Opt. Soc. Am. B, Vol. 9, No 1, 121-131, January 1992

37 N. G. Basov, I. G. Zubarev, A. B. Miranov, S. I. Mikhailov, and A. Yu. Okulov, "Phase fluctuations of the Stokes wave produced as a result of stimulated scattering of light", Pis'ma Zh. Eksp. Teor. Fiz. 31, 685-689 (1980) [JETP Lett., Vol. 31, No 11, 645-649, 5 June 1980]

38 V. I. Bespalov, A. A. Betin, G. A. Pasmanik, and A. A. Shilov, "Observation of transient field oscillations in the radiation of stimulated Mandel'shtam-Brillouin scattering" Pis'ma Zh. Eksp. Teor. Fiz. 31, 668 (1980) [JETP Lett., Vol. 31, No 11, 630-633, 5 June 1980]

39 K. D. Ridley, "Novel Phase Conjugation Techniques Based on Stimulated Brillouin Scattering", PhD Thesis, Imperial College, University of London, p. 31, 1993

40 G. W. Faris, M. J. Dyer and A. P. Hickman, "Transient effects on stimulated Brillouin scattering", Optics Letters, Vol. 17, No 15, 1049-1051, 1 August 1992

41 A. Kummrow, "Hermite-gaussian theory of focused beam SBS cells", Optics Communications, Vol. 96, No 1,2,3, 185-194, 1 February 1993

42 J. Czarske and H. Muller, "Heterodyne detection technique using stimulated Brillouin scattering and a multimode laser", Optics Letters, Vol. 19, No 19, 1589-1591, 1 October 1994

43 M. J. Weber, 'CRC Handbook of Laser Science and Technology, Supplement 2: Optical Materials', CRC Press, Table 12.1, 1995

44 D. P. Eastman, A. Hollinger, J. Kenemuth and D. H. Rank, "Temperature Coefficient of Hypersonic Sound and Relaxation Parameters for Some Liquids", The Journal of Chemical Physics, Vol. 50, No. 4, 1567-1581

45 M. J. Cardamone, W. Rhodes, D. Egan and N. Spotts, "Brillouin scattering and Vibrational relaxation in Benzene", J. Opt. Soc. Am. B, Vol. 2, No. 10, 1612-1614, October 1985

46 I. L. Fabelinskii, "Stimulated Mandelstam-Brillouin Process", *Quantum Electronics: A Treatise*, Edited by H. Rabin and C. L. Tang, Academic Press, Volume I, Nonlinear Optics, Part A, p. 365, 1975

47 A. Laubereau, W. Englisch and W. Kaiser, "Hypersonic Absorption of Liquids Determined from Spontaneous and Stimulated Brillouin Scattering", IEEE J. Quantum Electr., Vol. 5, No 8, 410-415, August 1969

48 A. I. Erokhin, V. V. Oleinikov and A. A. Putilin, 'Spectral structure of Stimulated Brillouin scattering', Pis'ma Zh. Eksp. Teor. Fiz. 61, 873 (1995) [JETP Lett. 61, 887(1995)]

49 J. C. Englund and C. M. Bowden, "Spontaneous Generation of Raman Solitons from Quantum Noise", Physical Review Letters, Vol. 57, No 21, 2661-2663, 24 November 1986

50 M. G. Raymer, Z. W. Li and I. A. Walmsley, "Temporal Quantum Fluctuations in Stimulated Raman Scattering: Coherent-Modes Description", Physical Review Letters, Vol. 63, No 15, 1586-1589, 9 October 1989

51 K. Druhl, R. G. Wenzel and J. L. Carlsten, "Observation of Solitons in Stimulated Raman Scattering", Physical Review Letters, Vol. 51, No 13, 1171-1174, 26 September 1983

52 P. Narum, A. L. Gaeta, M. D. Skeldon and R. W. Boyd, "Instabilities of laser beams counterpropagating through a Brillouin-active medium", J. Opt. Soc. Am. B, Vol. 5, No 3, 623-628, March 1988

53 C. C. Chow and A. Bers, "Chaotic stimulated Brillouin scattering in a finite-length medium", Physical Review A, Vol. 47, No 6, 5144-5149, June 1993

54 O. Kulagin, G. A. Pasmanik, A. L. Gaeta, T. R. Moore, G. J. Benecke and R. W. Boyd, "Observation of Brillouin chaos with counterpropagating laser beams", J. Opt. Soc. Am. B, Vol. 8, No 10, 2155-2157, October 1991

55 O. M. Vokhnik and V. I. Odintsov, "Slow field fluctuations of the Stokes wave due to SMBS with a wide-band pumping", JETP Letters, Vol. 33, No 9,421-424, 5 May 1981

56 R. Chu, M. Kanefsky and J. Folk, "Numerical study of transient stimulated Brillouin scattering", J. Appl. Phys., Vol. 71, No. 10, 4653-58, 15 May 1992

57 W. P. Brown and S. M. Wandzura, "Computer modelling of time-dependent SBS in two and three dimensions", CLEO'88, Nonlinear Optics: 1, MC5, 25 April 1988

58 A. L. Gaeta and R. W. Boyd, "Stochastic dynamics of stimulated Brillouin scattering in an optical fiber", Physical Review A, Vol. 44, No 5, 3205-3209, 1991

59 Y. Akiyama, K. Midorikawa, M. Obara and H. Tashiro, "Measurement of a π Stokes phase jump in spontaneously initiated stimulated Raman scattering", J. Opt. Soc. Am. B, Vol. 8, No 12, 2459-2465, December 1991

60 R. W. Boyd and K. Rzazewski, P. Narum, "Noise initiation of stimulated Brillouin scattering", Physical Review A, Vol. 42, No 9, 5514-5521, 1990

61 Z. M. Benenson, F. V. Bukin, D. V. Vlasov, E. M. Dianov, A. Ya. Karasik, A. V. Luchnikov, E. P. Shchebnev and T. V. Yakovleva, "Stimulated Mandel'shtam-Brillouin scattering in a "travelling" regime", JETP Letters, Vol. 42, No 4, 202-205, 25 August 1985

62 L. A. Hackel, C. B. Dane, L. E. Zapata and M. R. Herman, "Phase conjugated lasers applied to X-ray generation", International Journal of Nonlinear Optical Physics, Vol. 3, No 2, 137-167, 1994

63 S. Afshaarvahid, J. Munch and V. Devrelis, "Numerical study of stimulated Brillouin scattering initiated from noise", CLEO/Pacific Rim, ThM1, 4-17 July 1997

64 T. R. Moore, A. L. Gaeta and R. W. Boyd, "Amplitude and phase fluctuations in stimulated Brillouin scattering", CLEO'93, CThD5, 394-396, 6 May 1993

65 A. A. Fotiadi and E. A. Kuzin, "Selective amplification of the amplitude Stokes fluctuations in stimulated Brillouin scattering", CLEO'94, CTuK3, 84, 1994

66 E. A. Kuzin, M. P. Petrov and A. A. Fotiadi, "Phase Conjugation by SMBS in Optical Fibers", *Optical Phase Conjugation*, editors M. Gower and D. Proch, Spinger-Verlag, 75-96, 1995

67 R. Menzel and H. J. Eichler, "Temporal and spatial reflectivity of focused beams in stimulated Brillouin scattering for phase conjugation", Physical Review A, Vol. 46, 7139-7149, 1992

68 E. A. Kuzin, M. P. Petrov, A. E. Sitnikov and A. A. Fotiadi, "Amplitude modulations of the intensities of the scattered and transmitted light during stimulated Brillouin scattering in an optical fiber because of hypersound relaxation", Sov. Phys. Tech. Phys., Vol. 33, No. 12, 1420-1423, December 1988

69 S. J. Kuo, D. T. Smithey and M. G. Raymer, "Beam-Pointing Fluctuations in Gain-Guided Amplifiers", Physical Review Letters, Vol. 66, No 20, 2605-2608, 20 May 1991

70 N. F. Andreev, V. I. Bespalov, M. A. Dvoretsky and G. A. Pasmanik, "Phase Conjugation of Single Photons", IEEE J. Quantum Elect., Vol. 25, No 3, 346-350, March 1989

71 M. G. Raymer, I. A. Walmsley, J. Mostowski and B. Sobolewska, "Quantum theory of spatial and temporal properties of stimulated Raman scattering", Physical Review A, Vol. 32, No 1, 332-344, July 1985

72 R. Chu, M. Kanefsky and J. Falk, "Transient phase conjugation by stimulated Brillouin scattering: numerical analysis of zero-order solutions", J. Opt. Soc. Am. B, Vol. 11, No 2, 331-338, February 1994

73 C. Brent Dane, L. A. Hackel and M. J. Lefebvre, "Long-coherence-length, low-threshold 1-μm SBS phase conjugation", CLEO'95, CMA1, 1, 1995

74 S. Pfeifer, R. Johnson and W. Carrion, "Experimental investigation of threshold reduction techniques in stimulated Brillouin scattering", CLEO'91, CMG3, 50, 13 May 1991

75 A. M. Scott and W. T. Whitney, "Characteristics of a Brillouin ring resonator used for phase conjugation at 2.1 μm", J. Opt. Soc. Am. B, Vol. 12, No 9, 1634-1641, September 1995

76 G. K. N. Wong and M. J. Damzen, "Investigations of Optical Feedback Used to Enhance Stimulated Scattering", IEEE Journal of Quantum Electronics, Vol. 26, No 1, 139-148, January 1990

77 Y. Glick and S. Sternklar, "Angular bandwidth for Brillouin amplification", J. Opt. Soc. Am. B, Vol. 11, No 9, 1539-1543, September 1994

78 A. M. Scott, W. T. Whitney and M. T. Duignan, "Low threshold phase conjugation for 2-μm lasers", CLEO'93, CThJ3, 426, 6 May 1993

Chapter 3

Sharp Rise Effects in OPC-SBS

3.1 Introduction

The dependence of the phase conjugate (PC) SBS fidelity on the input laser pulse energy has been a source of great debate over the last 10 or more years. Two camps were formed. The one claiming that their theoretical[1,2] and experimental[3,4,5] work showed PC fidelity to be high for increasing input energy. The other, also based on their theoretical[6,7] and experimental[8,9] work, showed PC fidelity to be decreasing to low values for increasing input energy. The use of SBS in these and many other studies has been towards the correction of rapidly varying aberration (i.e. those encountered in laser amplifiers, resonators, atmosphere, etc), which raises the question as to how fast the SBS process responds to temporally varying input pulses.

In SBS the acoustic grating's spatial structure is determined by the interference pattern of the laser and Stokes fields. The acoustic grating contours the input laser wavefront in a way that it retroreflects all the points on the input wavefront and thus the scattered Stokes wavefront becomes an OPC return. The field of the acoustic

grating maintains a phase which is fixed in relation to that of the input beam. When the input wave-front changes slowly compared to the acoustic relaxation in the nonlinear medium then good PC can be achieved. However, if the input wave were to change its phasefront instantaneously by a large amount, then the acoustic grating would have the wrong phase structure and a non-phase conjugate SBS return would result. In reference 2 the temporal response of the grating was related to the damping time of the hypersound in the medium. The damping time creates a memory in the SBS process which can cause a lag in the response time of the Stokes beam. Some semi-analytical theoretical and experimental work,[10] indicated, that the temporal response of the SBS conjugation fidelity can be effected by input beam profiles which change on timescales faster than the phonon lifetime. According to reference 11 if the duration of an input pulse is less or comparable to the SBS phonon lifetime of the medium, then the material response time would produce observable transient effects which create losses in the Stokes wave. The Stokes return can be treated as the response to the system's interaction time determined from a large intensity input pulse.[12,13] The impulse response for the undepleted pump case depends on the SBS gain coefficient and the ratio of the pulse duration over the phonon relaxation time τ_B. It has been reported[6] that input pulses with widths smaller than the SBS phonon relaxation time of the medium can result in poor phase conjugation. However, medium reflectivity ($50 \pm 15\%$) with qualitatively good (near field) fidelity SBS in a rapid transient regime had been demonstrated[14] for pulse trains of 200 psec pulses at 1.064 μm. In that study though, close inspection revealed that the (near field) PC fidelity was not perfect and other effects including optical breakdown, were assumed (but not proven) as possible explanations for its degradation. The above

studies indicate the fast temporal changes of the input in relation to the phonon relaxation time can result in poor Stokes returns and poor PC fidelity.

Reduction in PC has also been shown both experimentally and theoretically in some studies[15,16] to be due to multiphoton absorption effects. Competing scattering mechanisms due to multiphoton absorption (i.e. stimulated temperature scattering) were ruled out in our study as the measured frequency shift corresponded only to the SBS shift.

Work done in the early 80's showed that the onset of SBS and its competing processes (i.e. SRS, optical breakdown) is determined by the input pulse power and the shape of its leading edge[17]. Dudov et al[17] have shown experimentally that for sharp rise pulses the pump power necessary to reach threshold for competing non-linear effects can be achieved prior to the SBS threshold energy, thus suppressing initially the development of the process. Thus competing processes can disturb the initilisation of SBS. Also, recent results by C. Brent Dane et al.[18] indicate that the lack of fidelity in reference 8 may be traceable to the rapid turn on of the laser pulse even though the pulse width is larger than the SBS phonon relaxation time. This explanation is consistent with the moving gain model proposed by J. Munch et al,[19] for the lack of phase fidelity at short coherence lengths (where rapid transients are also present). The fast turn-on can discriminate against the PC mode in favour of the other non-PC modes that exist in the mediums noise field.[8,19] A laser input pulse with a fast leading edge could prevent the formation of an initial grating in the far field resulting in fidelity fluctuations. The SBS return, seeded by the non-PC modes can be amplified and will deplete the input beam so that other modes remain below

threshold. This can last throughout the duration of the input pulse (i.e. tens of nanoseconds) thus resulting in a less than perfect Stokes return. Additionally, stimulated Raman scattering could become a problem.[20] The question of the rate of increase in an input leading edge, up to which good PC can still take place needs to be studied.

The experiments reported in this chapter look closely at the effect that sharp rise pulses have on the phase conjugation of the SBS process. The work was part of the plan to resolve a controversy[3,8,21] which existed at the commencement of this study but was resolved by Dane et al[18] during my thesis work. In this chapter we shall declare what we did, which essentially confirm the findings of Dane et al.[18]

3.2 Experimental Technique

The equipment and diagnostic tools used for this experiment are those described in section 2.2.5 of the previous chapter. The coherence length diagnostics are discussed in section 4.2.1 in the next chapter. The experimental setup is shown in figure 3.2.1. The aim of the setup was to create a sharp rise input pulse and for this purpose the SBS process itself was utilised. The laser beam is first directed into SBS cell-1 and it's the output from this cell that is now used as the input beam to the SBS cell-2. It is the input and output from SBS cell-2 that is under investigation in these experiments. Both SBS cells were manufactured from 50 mm diameter glass tube, with SBS cell-1 being 600 mm long and SBS cell-2 being 400 mm long. The energy

of the laser pulses was governed with a λ/2 plate, plus polariser combination. The output from SBS cell-1 was coupled into the SBS cell-2 and the diagnostic instruments (i.e. reflectivity, fidelity, coherence length and heterodyne), by using a

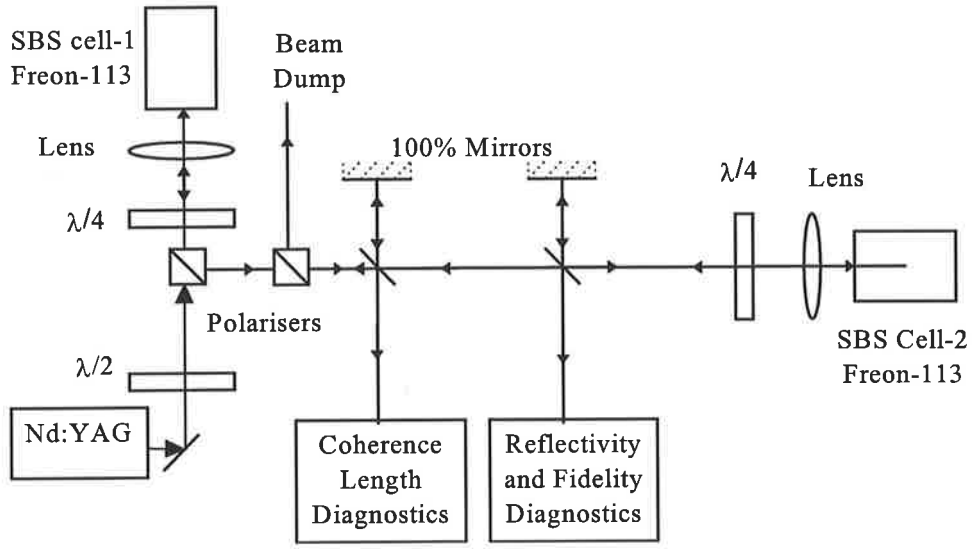

Figure 3.2.1: Schematic diagram of experimental set-up for the generation of sharp-rise pulses and for the pulse-to-pulse monitoring of laser and SBS reflectivity and fidelity.

λ/4 plate, plus polariser combination. Figure 3.2.2 gives a typical example of the output pulses from the laser, SBS cell-1 and SBS cell-2. By choosing both the lens in front of SBS cell-1 appropriately and the immersion of focus into the cells liquid (e.g. long focal length lens with long immersion length), some pulse shaping could be obtained due to pulse compression. Similar types of pulses (i.e. pulse compressed at the front edge of the pulse) have been reported by others as well.[22] Examples of

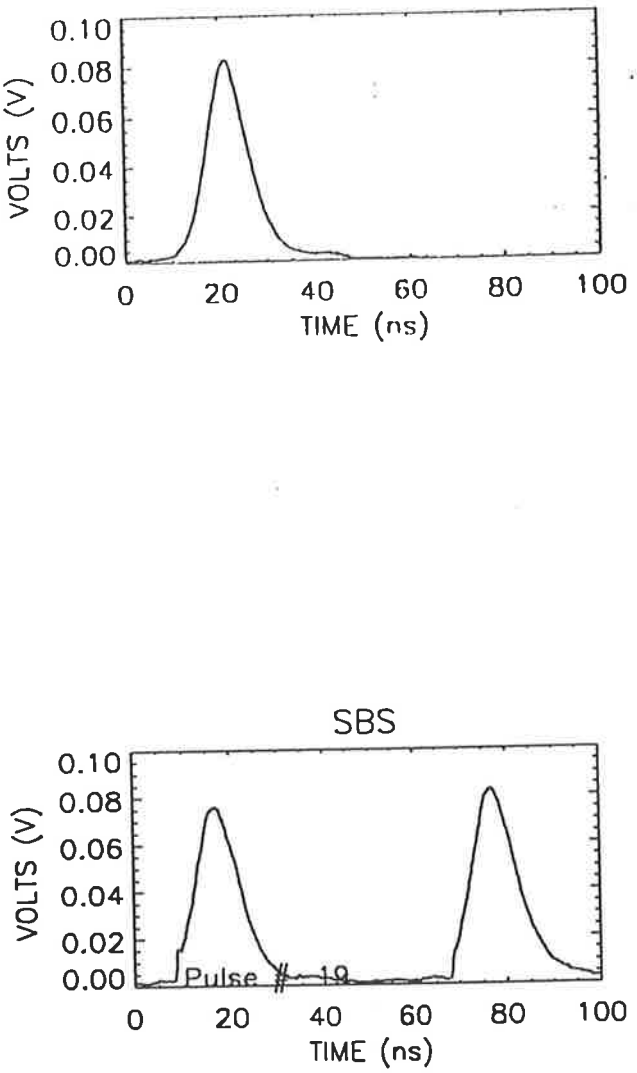

Figure 3.2.2: Plot gives a typical example of the output pulses from the laser, SBS cell-1 (left) and SBS cell-2 (right).

two tailored output pulses from SBS cell-1 are shown in figure 3.2.3. It is the initial spike on these pulses which was of interest. The round-trip time ($t_c = 2nl_i/c$ where l_i is the distance from the SBS cell entrance to the focal plane in the medium) of the interaction region could be varied from 1 nsec to 5.5 nsecs. The leading edge spike could be made to have a faster risetime by increasing the power of the input pulse. It should be noted here that the compression of the input pulse is not complete but rather is followed by a smooth pulse shape similar to that of the input pulse. The reason for the incomplete compression is twofold. First, the round-trip time in the SBS cell is too small for the compression of a 8-10 nsecond input pulse. Second, at the higher input pulse powers the SBS process starts upstream of the focus thus reducing the length of interaction and compressing only the front part of the input pulse. For complete pulse compression the SBS amplifier-generator systems are best suited. No finite-cell oscillations (the type predicted by Marburger et al in reference 23) were observed during the SBS process.

The measurement of the input and output pulses from the SBS cell was used to determine the reflectivity and fidelity for that pulse. The calculations were made according to the following equations (see also section 2.2.5, equations 2.2.5.1-4):

$$\text{Reflectivity} = \frac{\text{Near Field SBS return energy}}{\text{Near Field Laser input energy}}, \text{ and}$$

$$\text{Phase Fidelity} = \frac{\text{SBS beam merit}}{\text{Laser beam merit}}$$

where we define

$$\text{beam merit} = \frac{\text{Far Field beam return through pinhole}}{\text{Near Field beam return} \times \text{T\%}}$$

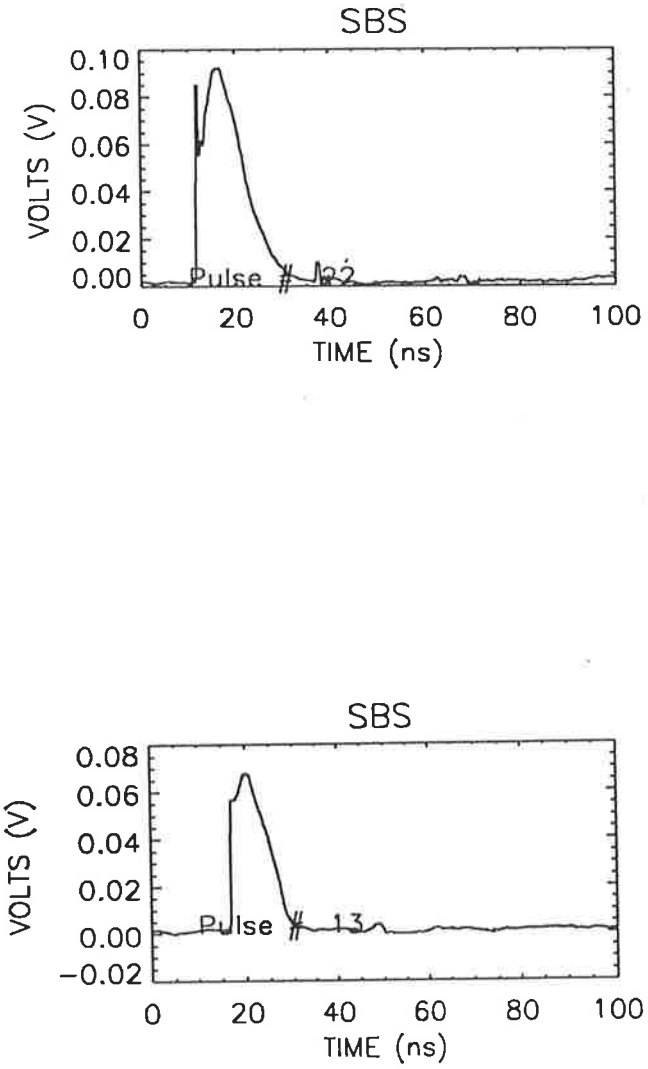

Figure 3.2.3: Examples of tailored output pulses from SBS cell-1. Long immersion length (top) and short immersion length (bottom).

3.3 Results and Discussion

The set up for this experiment is as shown in section 3.2. The coherence length throughout these measurements was maintained at ~ 3.3 m (this was measured with a variable arm length Michelson interferometer). The only difference between these input pulses and those used in the previous chapter, is that they have a fast leading edge compared to the phonon relaxation time of the medium. The lasers pulse repetition frequency was run at 4, 10 and 15 Hz. This parameter was not found to have any effect on the collected results. The data presented and discussed in this section were all obtained at a laser prf of 4 Hz. The gaussian-like temporal pulse of chapter two (fig 2.2.1), depending on its pulse energy had a leading edge rise time of about 3-4 nsec. The measured reflectivity reached a value of 90% (fig 2.3.1) and the corresponding phase fidelity was also 90% (fig 2.3.3). In comparison the new sharp rise input pulse had a leading edge rise time of 0.2 nsec. Two typical sequential input pulses are shown in figure 3.3.1. These pulses have similar pulse width (FWHM) at low energies and identical widths at high energies to the gaussian-like pulses. Figure 3.3.2 show the experimentally measured near field (total pulse energy) reflectivity of sharp rise input pulses versus input energy to threshold energy for a Freon-113 SBS cell. Input energies up to 86 times threshold were used in this measurements. At each input energy setting there are 99 pulses showing the average value and the standard deviation. This reflectivity compares well with figure 2.3.1 with the only exception that the variation is slightly larger. The time resolved diagnostics showed that the SBS return pulse closely follows the input pulse except near the transient onset where the intensity can overshoot. However, it was observed that if the input pulse

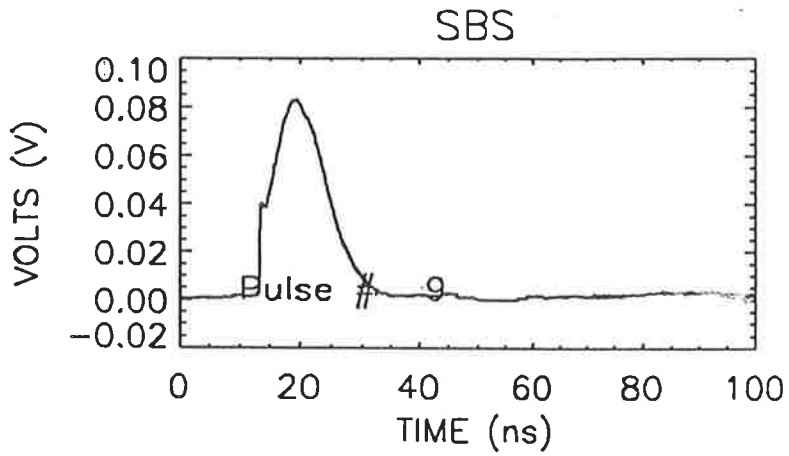

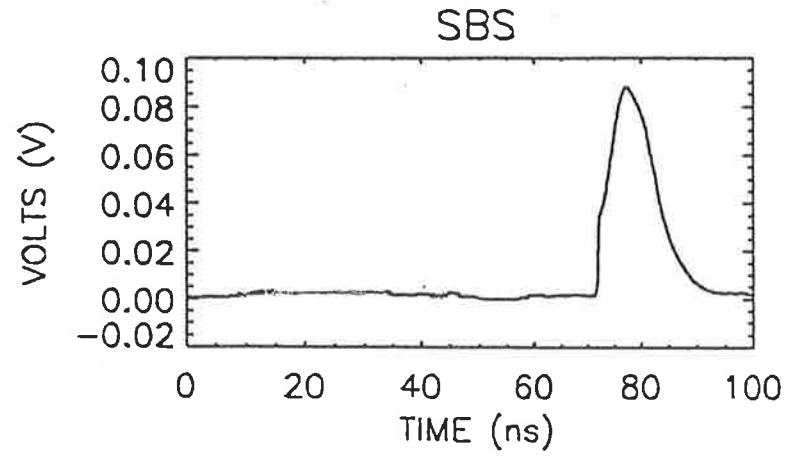

Figure 3.3.1: A typical set of input pulses is presented.

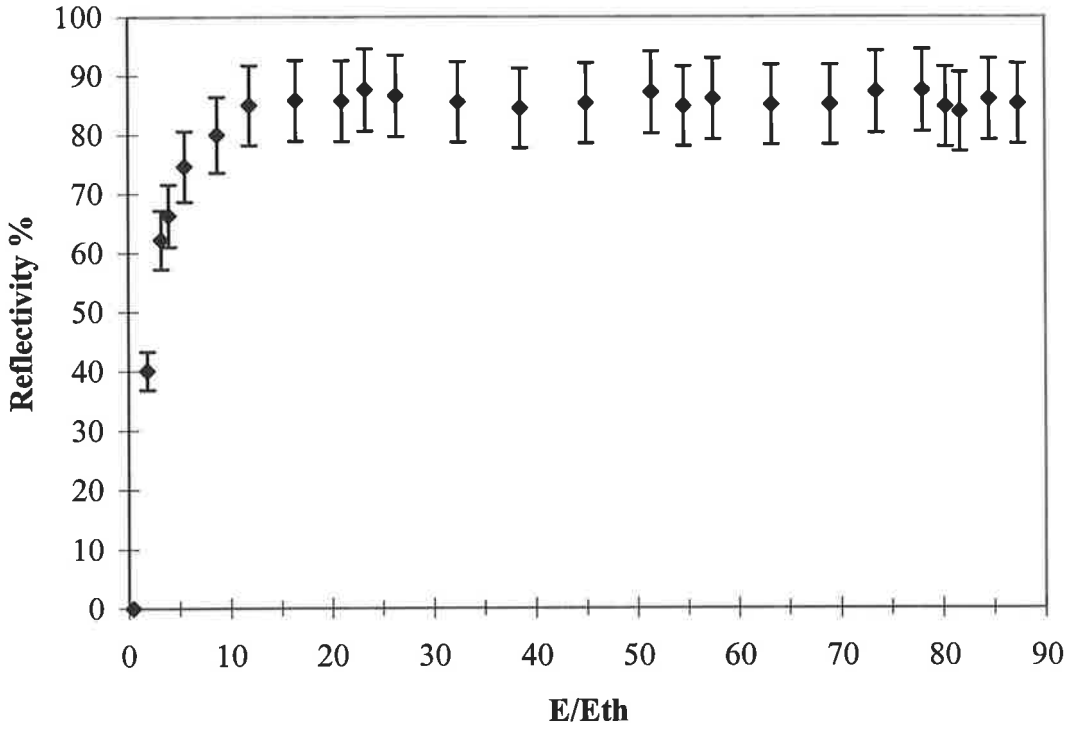

Figure 3.3.2: Diagram reflectivity of sharp rise input pulses versus input energy to threshold energy for a Freon-113 SBS cell

through appropriate choice of focusing geometry in SBS cell 1, was made to have a sharp rise and a high intensity spike at the leading edge then optical breakdown could be obtained in the SBS cell, thus reducing both reflectivity and fidelity.

The time integrated, phase fidelity is presented in figure 3.3.3, for input energies up to 86 times threshold. Again, at each input energy setting there are 99 pulses showing the average value and the standard deviation. Both the drop and variation of the fidelity value are increased as the energy increases. This is in qualitative agreement with the findings of C. Brent Dane et al.[18] for energies up to 17 times threshold with a 90-atm N_2 SBS cell. The large pulse to pulse fluctuations are attributed to the sharp rise input edge. The temporal shape difference between the

slow rise pulses of chapter 2 and the sharp rise pulses of this chapter, though large at low input energy (especially near threshold) is extremely small at energies 80 times that of threshold. In fact at high values, the input pulse energy only differs by about few percent and the temporal shape of the pulses only differs at the very start.

Some low fidelity spatial data (transverse fidelity) is also presented in figure 3.3.4 from a set of sequential pulses. These pictures were captured with a CCD camera, which had its lens focused at the far field of the SBS return beam. The observed beams had a distorted spatial structure from pulse to pulse, their divergence varied and they wondered about the location of the phase conjugate beam. This combination of errors was seen also by C. Brent Dane et al[18] and later again in this study under short coherence SBS conditions. Similar observations were made also in this present study with a SBS cell filled with SF_6 at 22-atm which has a τ_B of 16ns. All of these observations were in qualitative agreement with the findings of unsteady (i.e. transient) SBS in reference 17 where the shape of the pump pulses leading edge determined the onset of competing processes (i.e. SRS, optical breakdown) to SBS.

In the work of Ottusch et al (reference 8) poor fidelity was observed in a gas (N_2 at 90-atm) and a liquid ($TiCl_4$) SBS medium for 35 nsec duration pulses at 1.06 μm. Based on our results in chapter 2, the reduction of fidelity due to phase jumps can be discounted since $\tau_p/\tau_B<1$ in their study. Reference 18 also demonstrated poor fidelity for a gas (N_2 with τ_B=16 nsec) when the pulse risetime is smaller than the phonon relaxation time. The present study also demonstrated poor fidelity, over a larger input energy range, for a liquid ($C_2Cl_3F_3$ with τ_B=0.74 nsec) and a gas (SF_6 at 22-atm

with τ_B= 16 nsec) when the pulse leading edge is sharp and the risetime is smaller than the phonon relaxation time. Although in reference 8 "the majority of pump pulses are transform limited", no accurate indication of the temporal profile and coherence length was given and nor was the phase fidelity of these input pulses monitored throughout the measurement of the SBS fidelity. These are both important as the accurate measurement of the SBS fidelity depends on them. Further from the personal communication between C. Brent Dane et al and D. A. Rockwell[18] it become known that the laser used in reference 8 incorporated a SBS mirror, which, would produce a sharp rise input pulse. All of these findings demonstrate the importance that the input pulse leading edge has on PC fidelity and the attention that needs to be placed in the design of systems with PC mirrors.

It is clear from the results of this study that the statement in reference 8 - "the PC fidelity is best just above SBS threshold and becomes increasingly unstable as the reflectivity becomes more saturated" - is not a general statement but as shown, it only holds true under a very specific condition.

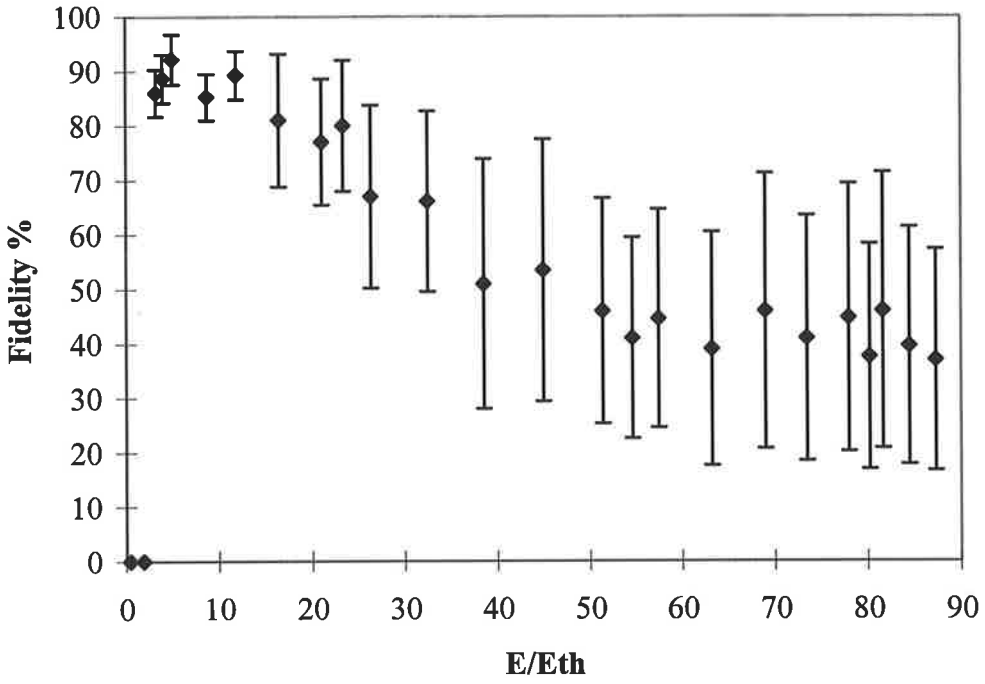

Figure 3.3.3: Diagram of Phase Fidelity vs input Energy/Threshold Energy for pulses with fast-rise edge.

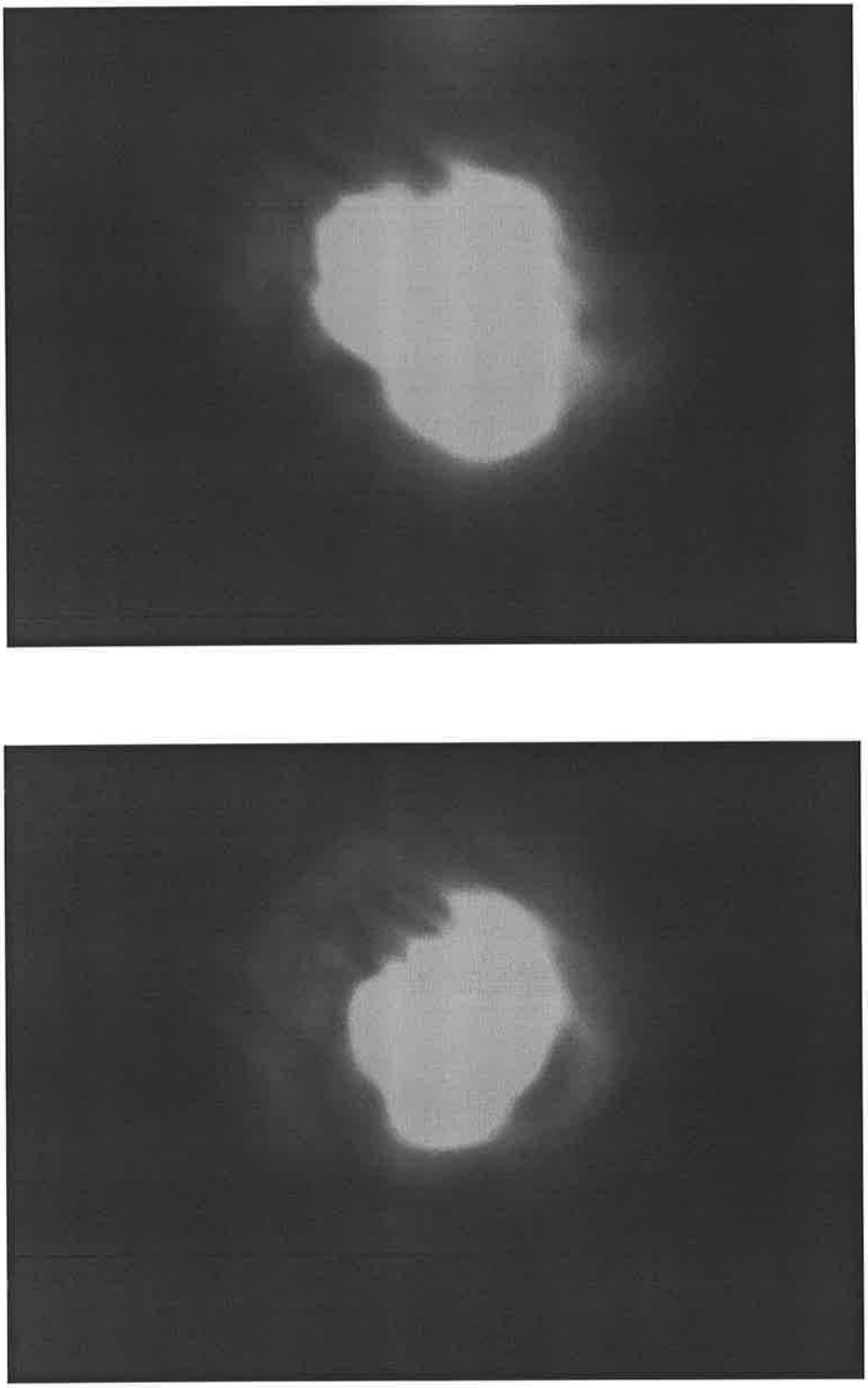

Figure 3.3.4: Pictures of some low fidelity spatial data.

3.4 Conclusion

The response of the OPC-SBS process to input pulses with fast temporal variations was investigated in this study.

Using pulses with sharp rise, ~0.2 nsec risetime, good SBS reflectivity for energies up to 86 times threshold was obtained but the corresponding PC fidelity was bad. No reliable phase conjugation was obtained as the pump energy was increased under these conditions. The long coherence length and relatively smooth input pulses did not produce any competing phenomena such as optical breakdown or Raman scattering. Thus these phenomena could not be attributed as the reason for the poor PC fidelity. When a sharp rise and a high intensity spike was present on the input pulse, only then, optical breakdown took place which resulted in bad PC fidelity again. A solution to this problem may exist in reducing the wavelength to visible or UV. This could provide better PC fidelity as the phonon relaxation time would be much reduced at those wavelengths (i.e. the smaller the phonon lifetime, the faster is the response of the medium to the rapid changes in the laser field). So what appears as a fast rise for the SBS process in one wavelength would be slower at the other shorter wavelength.

The findings of this study support these of Dane et al (reference 18) in that pulses with risetime faster than the medium's phonon relaxation time produce bad OPC-SBS. It is clear that an increase in pulse energy is not a factor in the reduction of PC SBS but rather the temporal profile of the input pulse is responsible.

3.5 References

1 R. H. Lehmberg, "Numerical study of phase conjugation in stimulated backscatter with pump depletion", Opt. Commun., Vol. 43, 369-374, 1982

2 B. Ya. Zel'dovich, N. F. Pilipetsky and V. V. Shkunov, "Principles of Phase Conjugation", Springer Series in Optical Science, Vol. 42, Springer-Verlag, p 133, 1985.

3 J. Munch, R. F. Wuerker, M. LeFebvre, S. Pfeifer, L. Marabella and M. Valley "SBS Phase Fidelity over large dynamic range of Power", OSA Annual Meeting, Paper FO4, Orlando, 1989

4 V. E. Yashin and V. I. Kryzhanovskii, "Apodization and spatial filtering of light beams in stimulated Brillouin scattering", Opt. Spectrosc., Vol. 55, No 1, 101-104, July 1983

5 L. P. Schelonka and C. M. Clayton, "Effect of focal intensity on stimulated-Brillouin -scattering reflectivity and fidelity", Optics Letters, Vol. 13, No 1, 42-44, January 1988

6 A. A. Betin, A. F. Vasil'ev, O. V. Kulagin, V. G. Manishin, and V. E. Yashin, "Phase conjugation in nonstationary stimulated Brillouin scattering of focused beams", Sov. Phys. JETP, Vol. 62, No 3, 468-476, September 1985

7 I. Yu. Anikeev, I. G. Zubarev and S. I. Mikhailov, "Scattering of noncoherent Pump radiation", Sov. J. Quantum Electron., Vol. 16, 88-90, 1986

8 J. J. Ottusch and D. A. Rockwell, "Stimulated Brillouin scattering phase-conjugation fidelity fluctuations", Optics Letters, Vol. 16, No 6, 369-371, March 15, 1991

9 A. F. Vasil'ev and V. E. Yashin, "Stimulated Brillouin scattering at high values of the excess of the pump energy above the threshold", Sov. J. Quantum Electron., Vol. 17, No 5, 644-647, May 1987

10 M. R. Osborne and M. A. O'Key, "Temporal response of stimulated Brillouin scattering phase conjugation", Optics Communications, Vol. 94, No 5, 346-352, 1 December 1992

11 G. W. Faris, M. J. Dyer and A. P. Hickman, "Transient effects on stimulated Brillouin scattering", Optics Letters, Vol. 17, No 15, 1049-1051, 1 August 1992

12 W. Kaiser and M. Maier, "Stimulated Rayleigh, Brillouin and Raman Spectroscopy", Laser Handbook, Vol. 2, edited by F.T. Arecchi and E. O Schuls-DuBois, 1077-1149, 1972

13 R. Chu, M. Kanefsky and J. Falk, "Numerical study of transient stimulated Brillouin scattering", J. Appl. Phys., Vol. 71, No 10, 4653-4658, 15 May 1992

14 R. A. Mullen, "Multiple-Short-Pulse Stimulated Brillouin Scattering for Trains of 200 ps Pulses at 1.06 μm", IEEE Journal of Quantum Electronics, Vol. 26, No 7, 1299-1303, July 1990

15 V. B. Karpov, V. V. Korobkin amd D. A. Dolgolenko, "Change in the stimulated light scattering mechanism and the quality of phase conjugation due to the effect of multiphoton absorption", Sov. J. Opt. Technol., Vol. 59, No 9, 513-517, Sept. 1992

16 V. Tosa, R. Bruzzese, C. De Lisio and S. Solimeno, "Multiphoton Absorption spectra of Freon-22 Molecules", Journal of Molecular Strucure, Vol. 267, 269-274, 1992

17 A. M. Dudov, S. B. Kormer, S. M. Kulikov, Vik. D. Nikolaev, V. V. Portnyagin and S. A. Sukharev, "Competition between nonlinear processes in gaseous SF_6 as a result of pumping by 2-nsec pulses", JETP Lett., Vol. 33, No 7, 347-351, 5 April 1981

18 C. Brent Dane, W. A. Neuman and L. A. Hackel, "Pulse-shape dependence of stimulated-Brillouin-scattering phase-conjugation fidelity for high input energies", Optics Letters, Vol. 17, No 18, 1271-1273, September 15, 1992

19 J. Munch, R. F. Wuerker and M. J. LeFebvre, "Interaction length for optical phase conjugation by stimulated Brillouin scattering: an experimental investigation", Applied Optics, Vol. 28, No 15, 3099-3105, 1 August 1989

20 D. C. Jones, M. S. Mangir, D. A. Rockwell and J. O. White, "Stimulated Brillouin scattering gain variation and transient effects in a CH_4:He binary mixture", J. Opt. Soc. Am. B, Vol. 7, 2090-2096, 1990

21 R. St. Pierre, H. Injeyan and J. Berg, "Investigation of SBS phase-conjugation fidelity fluctuations in Freon-113", CLEO'92, CTuN3, 180, 12 May 1992

22 M. J. Damzen and M. H. R. Hutchinson, "High-efficiency laser-pulse compression by stimulated Brillouin Scattering", Optics Letters, Vol. 8, No. 6, 313-315, June 1983

23 R. V. Johnson and J. H. Marburger, "Relaxation Oscillation in Stimulated Raman and Brillouin Scattering" Physical Review A, Vol. 4, No. 3, 1175-1182, September 1971

Chapter 4

Short coherence effects

4.1 Introduction

Not all lasers are capable of operating efficiently with a long coherence length and nor is it desirable in certain applications. The aim of the work covered in this section was to understand and extend the operational range of Stimulated Brillouin Scattering Optical Phase Conjugate devices. Of specific interest is the use of SBS with short coherence length pulses. Also of interest are ways of suppressing any phenomena (e.g. Raman, optical breakdown, self-focusing) that compete with the OPC-SBS process. Optical breakdown is one of these competing phenomena and its effect was observed during short coherence experiments.

A brief literature review on short coherence (broadband) SBS will be presented prior to our experimental investigation. It has been shown theoretically[1] and experimentally[2] that for coherence lengths longer than the interaction length, the SBS process is independent of the input beam spectrum. Short coherence or broadband SBS is defined by Valley[3] as SBS excited by a pump in which the bandwidth exceeds the sound decay rate or in which the pulse length is short compare to the sound decay time. Broadband SBS depends on several important length and time scales such as, the input

laser frequency, the coherence length (bandwidth), the pulse length, the Stokes frequency shift, the medium sound decay rate and the SBS interaction length. All of these parameters (considered simultaneously) can complicate the discussion of Broadband SBS and thus an attempt will be made to separate them as much as possible. In practice there are three frequency scales which are related to three spatial scales. These include, the coherence length of the input laser (l_c), the distance travelled by a photon during the lifetime of the acoustic wave (l_B) and the interaction length (l_i) for SBS.[4] A significant drop in reflectivity was observed[4] when $l_i > l_c$. For a collimated beam in a transparent medium the length of interaction is equal to the length of the cell and for a focused Gaussian beam, it is taken to be proportional to the Rayleigh range in the medium. For PC-SBS, Munch et al.[5] have shown experimentally that the effective interaction length at threshold is the shortest of the cell length, three times the coherence length or five times the Rayleigh range. The PC-SBS fidelity was also observed[5] to depend on the pump coherence length. There are also experimental observations[6] that at threshold the effective interaction length is not limited by the pump coherence length to be approximately equal to $3l_c$ but could be up to $16l_c$. Under short coherence conditions both the SBS reflectivity[7] and PC fidelity[4] have been found to be less than those of single mode, long coherence length input.[8] Good SBS conditions require that l_c be larger than l_i or l_B.[5] Most broadband lasers are also multimode and SBS would be independent of the mode structure[3,9] if the spacing between the individual laser modes is larger than the Brillouin linewidth and the bandwidth of each line results in a coherence length l_c that is much larger than the gain length $l_g = 1/GI_L$, where G is the SBS intensity gain and I_L is the input laser intensity.[10] Finally, good SBS for short coherence inputs with multiple lines, requires the consideration and avoidance of

competing effects such as nondegenerate four-wave mixing between lines and thermal heating due to absorption in the medium.[11]

The objective of this work is to characterise OPC with short coherence length pumping as well as any competing phenomena that take place during the SBS process. By obtaining the reflectivity and phase fidelity of SBS in the short coherence regime and by observing (and understanding) the competing phenomena it is hoped that techniques can be investigated that would lead to improved OPC-SBS through the reduction or elimination of these detrimental effects.

In addition to the above, a novel interferometric method for the direct, real-time measurement of the complete temporal coherence function of a pulsed laser is presented. Michelson's interferometer is modified by replacing one mirror with an inclined diffraction grating to observe interference fringes as a function of path length difference on a single pulse.[12] A computerised data acquisition method for coherence length of the infrared beam is discussed.

4.2 Experimental Technique

The simultaneous measurement of input and output pulses provide a powerful technique in probing the SBS process. This section describes the apparatus used to perform the experiments and the techniques employed to extract information from the measured scattering process.

The equipment and diagnostic tools (i.e. laser, detectors, SBS material and cells) used for this experiment are those described in section 2.2 of the long coherence chapter (see figures 2.2.2.1-2.2.5.2). The output energy of the laser pulses was governed with a $\lambda/2$ plate, plus polariser combination. Figure 4.2.1 gives a typical example of the output pulse from the laser. Similar types of pulses for SBS have been used by other researchers as well. The measurement of reflectivity and fidelity was made by obtaining time averaged near field and far field information on the laser input and SBS return beams. The reflectivity and fidelity for a SBS pulse were again calculated according to the following equations (see also section 2.2.5, equations 2.2.5.1-4):

$$\text{Reflectivity} = \frac{\text{Near Field SBS return}}{\text{Near Field Laser input}}, \text{ and}$$

$$\text{Phase Fidelity} = \frac{\text{SBS beam merit}}{\text{Laser beam merit}}$$

where we define

$$\text{beam merit} = \frac{\text{Far Field beam return through pinhole}}{\text{Near Field beam return} \times \text{T\%}}.$$

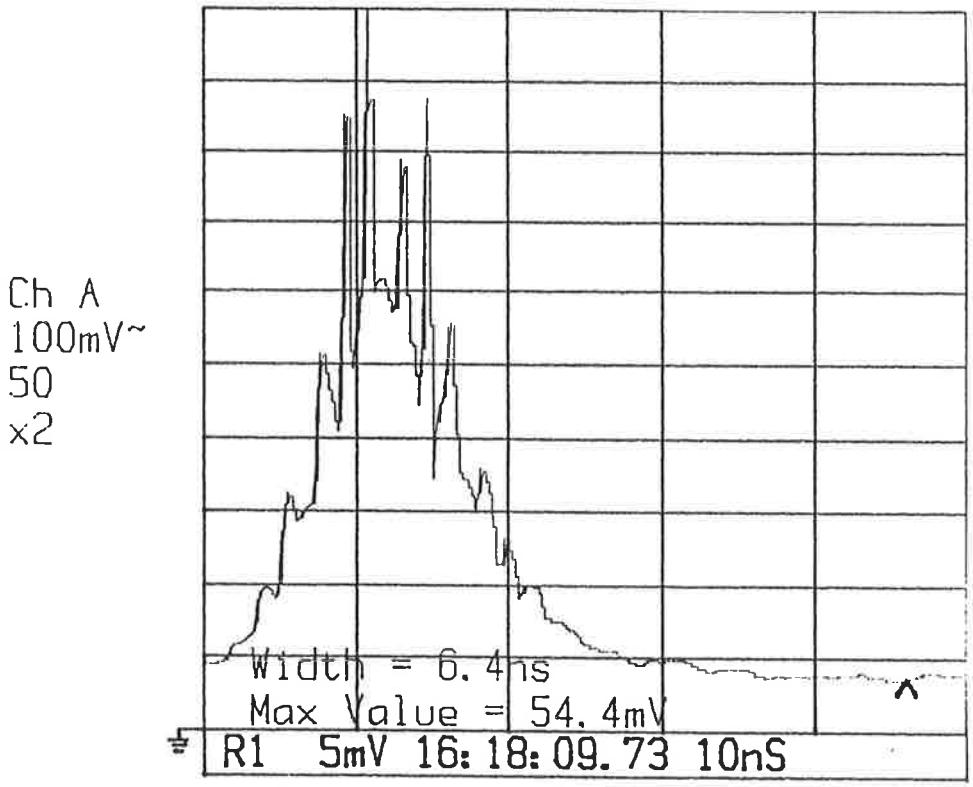

Figure 4.2.1: Plot gives a typical example of the output pulses from the laser.

4.2.1 Coherence Length Tool

In this, as in some other experiments, it is necessary to measure the complete coherence function of a single laser pulse. Until recently, the only method available was the holographic approach discussed in Reference.13. In that approach, a hologram of an inclined plane is recorded using the laser to be diagnosed. When the resulting hologram is reconstructed, the intensity distribution of the resulting image of the inclined plane can be used to determine the complete coherence properties of the laser on the single laser pulse. Although this method works well, it is limited to parts of the spectrum where holographic emulsions work, and it is neither convenient, nor real time, nor suitable for modern experiments where lasers operate at high pulse repetition rates with computerised data acquisition systems.

In this section, I shall discuss a novel approach which solves all the limitations of the holographic method while retaining the fundamental measurement capability. As we shall see, the new method is an interferometric method which records in digital form the direct interference fringes for all path length differences on a single laser pulse, as well as the transverse intensity distributions of the individual interfering beams. Although the optical layout has many similarities with the holographic method of Reference. 13, the new method differs significantly in its direct measurement of the fringe visibility as opposed to the holographic method in which the coherence function was retrieved from the brightness distribution of the reconstructed image.

The present experiments investigate the effect of short coherence lengths on SBS using a pulsed Nd:YAG laser operating at 1.06μm and a pulse repetition rate of 10 Hz.

For short and intermediate values, the coherence length is rarely exactly reproduced from pulse to pulse, due to the weak axial mode control employed. The present method measures the complete coherence function for each laser pulse at infrared wavelengths. There are other methods for measuring coherence length including the original Michelson approach,[14] etalons[15] and phase conjugate interferometers.[16] None of these methods can yield the complete coherence function on a single laser pulse, and are only suited for use on CW lasers where path lengths or etalon spacing can be scanned as a function of time. An additional method often used for single pulses is the temporal pulse shape, but this method is not reliable as discussed in Reference 13.

The temporal coherence function of a source is usually determined from an observation of the visibility of the interference fringes formed as a function of path length difference when two parts of the source are made to interfere with each other.[15] Thus, for two beams of intensity I_1 and I_2 interfering with each other with a path length difference ℓ, the normalised interference pattern $I_N(\ell)$ can yield the visibility $V(\ell)$ and hence the mutual coherence function of the two beam $\gamma_{12}(\ell)$ from

$$I_N(\ell) = \frac{I_1 + I_2 + 2\gamma_{12}(\ell)\sqrt{I_1 I_2}\cos kx}{I_1 + I_2} \qquad (4.2.1.1)$$

$$I_N(\ell) = 1 + V(\ell)\cos kx \qquad (4.2.1.2)$$

$$\text{with } V(\ell) = \frac{2\gamma_{12}(\ell)\sqrt{I_1 I_2}}{I_1 + I_2} \qquad (4.2.1.3)$$

where all intensities, are functions of the transverse coordinates (x,y), and k describes the interference pattern in one dimension (fringes parallel to y axis in this case).

This measurement is usually done for a continuous source by measuring $V(\ell)$, I_1 and I_2, for different values of ℓ in a Michelson interferometer. The challenge for a pulsed source is to include all possible values of ℓ in a single pulse. This was accomplished in the holographic method by using a diffuse inclined plane. In an interferometer an inclined specula reflector of good optical quality is needed, in order to produce recognisable interferometric fringes. Small strips of mirrors placed at different values of ℓ could be used to produce a discontinuous sample of the coherence function. A better method was chosen, making use of a blazed diffraction grating in a Littrow mount. The grating is a high quality optical element which can produce interference fringes observable with a CCD camera.

The concept is illustrated in Figure 4.2.1.1 showing a Michelson interferometer with the inclined grating in one arm. There is a line on the grating marked D, for which the path lengths of the interferometer arms are equal. Excellent fringe visibility will result from light reflected from this part of the grating. Light from other parts (E and F) on the inclined grating will take shorter or longer times to reach the interference plane on the CCD camera. The visibility of the interference fringes from these parts will therefore depend on the coherence length of the laser. The instantaneous, complete coherence function can thus be observed as the visibility of the fringes along the grating as seen on

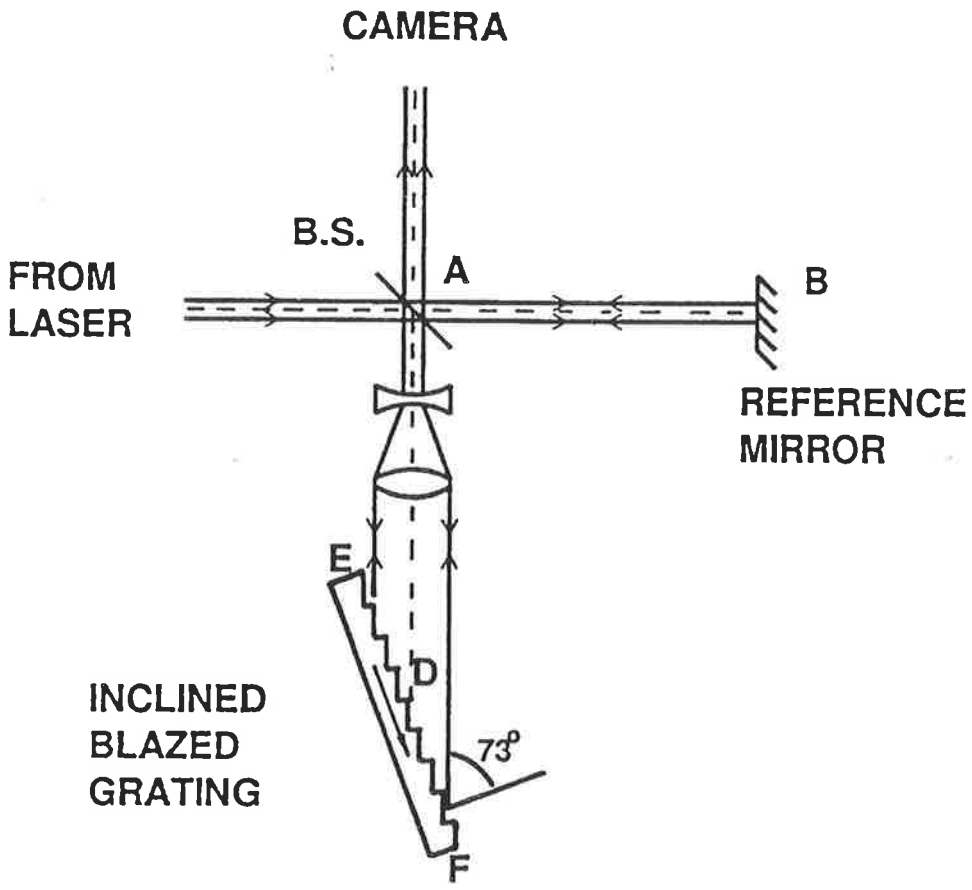

Figure 4.2.1.1: Michelson interferometer with blazed diffraction grating as one of the reflectors. The optical path lengths AB and AD are equal. Interference produced from lines E and F corresponds to shorter and longer path-length differences, respectively. B.S., beam splitter.

the TV monitor for each pulse. This direct observation of the coherence function is especially useful when adjusting intra-cavity etalons in the laser resonator to produce intermediate coherence lengths. When permanent data is required, the computer can grab and store the fringe pattern. Using appropriate masks to cover parts of the reflectors, independent measurements of slices of the intensity distribution of each of the interfering beams together with the interference pattern can be obtained on a single frame. Cross-sectional intensity profiles of the interfering beams and the interference pattern are obtained from columns of the digitised frame, and from this data the complete coherence function can be calculated.

The grating used was 210 mm long with 600 lines per mm, and blazed at 17^{o}. an inclined plane that was as long as possible was needed to be placed along the beam, and use was made of the fact that for the 90^{o} groove shape often used on gratings, the diffraction efficiency is high both at the blaze angle and its complement. The grating was thus reversed and used with an angle of incidence of 73^{o} as shown in Figure 4.2.1.1. A telescope was used to expand the beam to fill the grating. The closest and furthest points on the grating along the direction of the laser beam were separated by 200 mm, allowing coherence lengths of up to 400 mm to be measured with the set-up shown. The coherence length measurable in the system shown is limited by the length of the grating but ways to overcome this limitation were also explored.

4.2.2 Experimental Layout

The experimental set-up shown in figure 4.2.2.1 employed a delay technique to attempt to improve the phase conjugation of short coherence length pulses. This method was investigated as a possible means of reducing the high peak power of the input to the SBS cell. Using a Mach-Zehnder configuration with a 50/50 beam splitter and three mirrors, each beam's intensity was reduced to below the optical breakdown threshold. In the initial part of the experimental set-up, the path length difference in the interferometer was kept to less than 1 mm in order to avoid destructive interference. In the final part of the experimental set-up, an optical delay was introduced in one of the interferometer beams prior to recombining both beams within the SBS medium at the common focus. A 300 mm focal length lens was placed between the Mach-Zehnder and the Vertical SBS cell. The near field separation (NFS), is defined, as the ratio of the separation distance between the centre of the two beams over the beam diameter. The far field separation (FFS), is defined, as the ratio of the separation distance between the centre of the two beams at far field over the spot diameter (here FFS=0, since the beams were overlapped at the focus). The FFS was equal to zero throughout the experiment, unless otherwise stated. The optical delay consisted of glass plates with appropriate thickness. The purpose of the delay was to interlace the beating of the modes on the two beams, which in simple practical terms is similar to interlacing the teeth of two combs. In this way the peak power at the common focus is also reduced. The combined input energy of the beams at the focus did not exceed 40 mJ in the 8 nsec FWHM pulses. The SBS return of the combined pulses was sampled by reflectivity and fidelity diagnostics similar to those described in section 2.2.

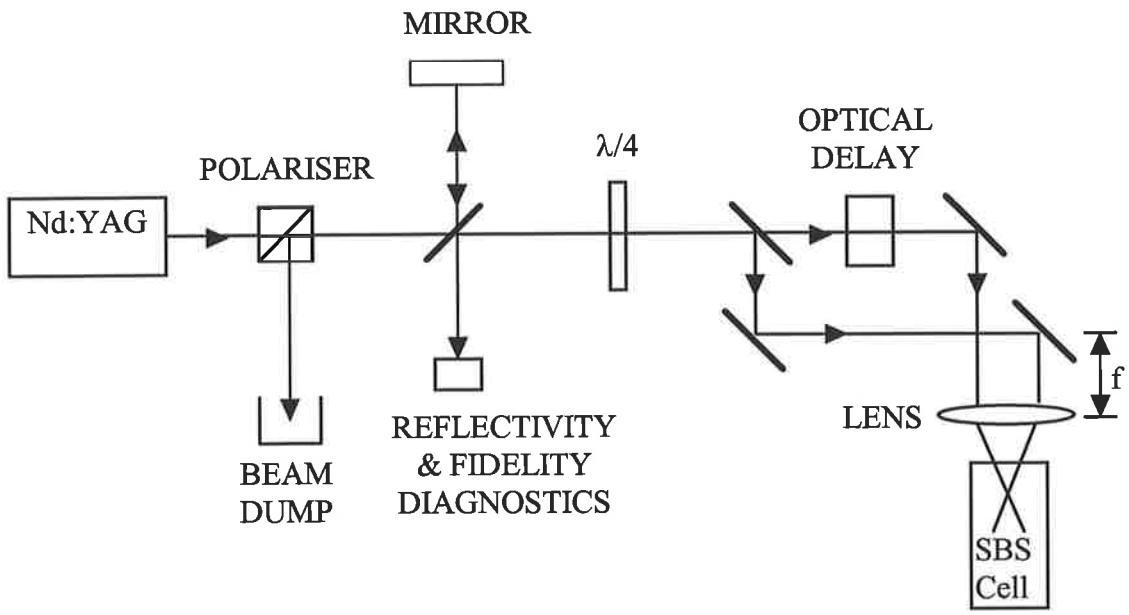

Figure 4.2.2.1: Schematic diagram of the Mach-Zehnder with optical delay configuration for the amplitude splitting and recombining of short coherence pules.

4.3 Results and Discussion

4.3.1 Coherence Length Measurement

In this section the short coherence, temporal and spatial data are discussed. The laser in standard operation (i.e. free-running mode) runs many longitudinal modes. The Q-switched operation results in a pulse width of <10 ns, and a peak optical power of tens of megawatts. The coherence length of these temporally short pulses was measured with the aid of the modified Michelson CCD interferometer (see section 4.2). A typical measurement of a short coherence-length fringe pattern is shown in figure 4.3.1.1. The uneven intensity distribution is due to transverse variations in the intensity of the two interfering beams, I_1 (x,y) and I_2 (x,y). By recording I_1 and I_2 separately, the mutual coherence function $\gamma_{12}(\ell)$ can still be obtained as discussed in the previous section. This unevenness together with the high contrast of figure 4.3.1.1 tends to mask the envelope of the interference fringes used for real time observation of the coherence length, but on a real-time TV monitor, it was readily observable. Plots of the normalised interference pattern, $1 + V(\ell) \cos kx$, for the data shown in figure 4.3.1.1, are shown in figure 4.3.1.2. In this figure, the envelope of the interference pattern is the mutual coherence function, and the coherence length is defined as the path length difference required to reduce the visibility by a factor of two as compared to the path matched condition (see references 14,15). From figure 4.3.1.2 the coherence length of the multimode pulse can be seen to be 17 mm. This length was very stable from pulse to pulse by better than 1.0 mm. The noise and lack of symmetry of the fringes shown is

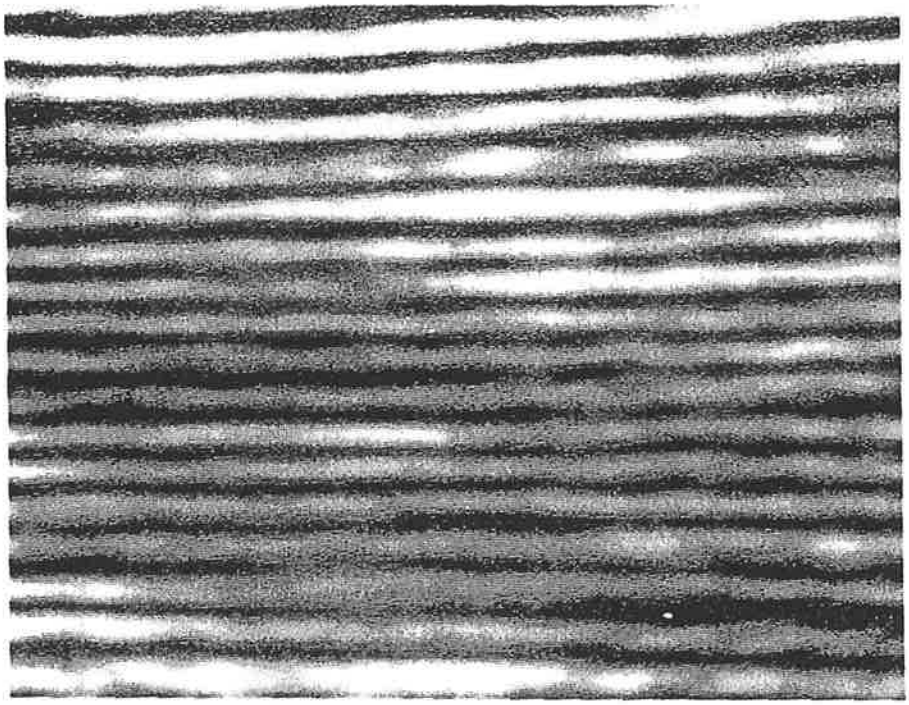

(a)

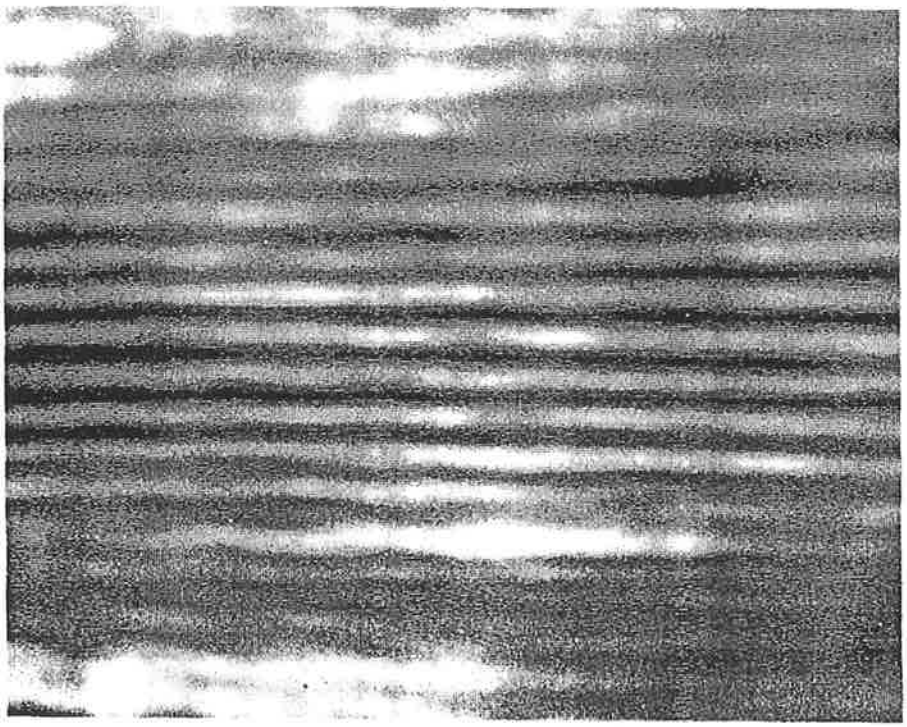

(b)

Figure 4.3.1.1: Typical interference patterns observed on the TV monitor: (a) long coherence length, (b) short coherence length. The horizontal centre line on each figure corresponds to path-matched interference. Above the centre line corresponds to shorter paths (region E in figure 4.2.1.1), and below the centre line corresponds to longer paths.

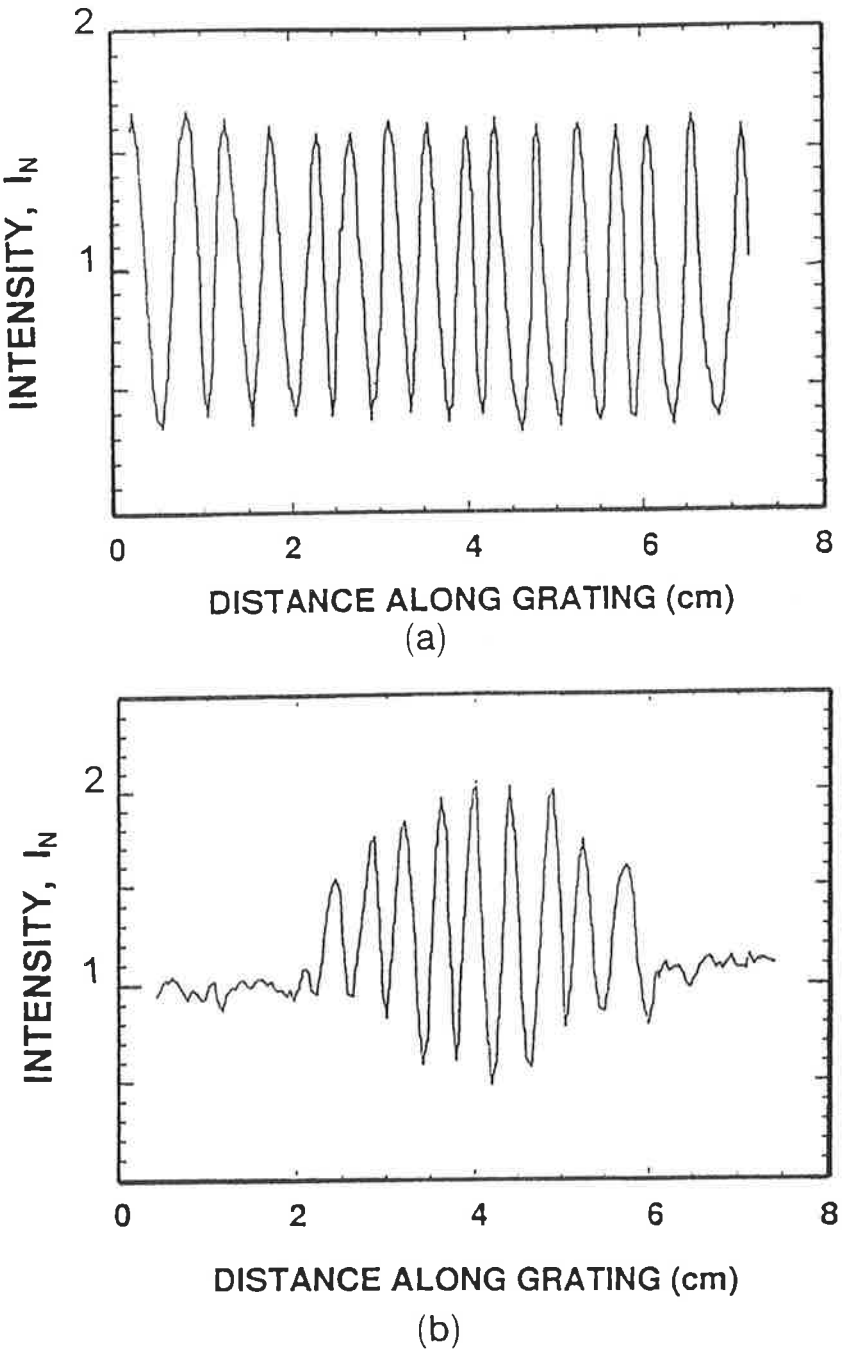

Figure 4.3.1.2: Plot of the normalised intensity distribution obtained from a single column of the digitised frame showing the resulting fringe visibility as a function of path-length difference along the grating for the interferograms shown in figure 4.3.1.1 (a) long coherence length, (b) short coherence length.

believed due to imperfections in the normalising procedure, and variations in the intensity from pulse to pulse. For our purposes, this is not considered a limitation, and can be improved by recording all intensities required on each pulse, as suggested above, and by improving the statistics by averaging adjacent pixel columns. More details relevant to this diagnostic tool and its results can be found in the published article.

4.3.2 SBS Threshold

The purpose of this experiment was to see what effect does the choice of focal length have on the SBS threshold. The behaviour of the SBS threshold power was observed under short coherence conditions. The length of interaction l_i was chosen to be smaller than the coherence length l_c of the input laser pulse. More reliable data were expected to be collected under this condition as the SBS process responds better.

The input laser beam's intensity changes when it is focused into the SBS cell. For a Gaussian beam of waist ω_0, reduced from $\omega(z)$ where

$$\omega^2(z) = \omega_0^2\left[1+\left(z/z_R\right)^2\right] \tag{4.3.1}$$

and where z_0 is the Rayleigh range

$$z_R = \pi\omega_0^2/\lambda \tag{4.3.2}$$

for an undepleted input beam the threshold intensity I_{th} value over an effective interaction length l_i in a material of SBS gain g_B satisfies the relationship

$$C = I_{th} g_B l \tag{4.3.3}$$

where C is a constant. The change of I along z is thus[5]

$$C = g_B \int_0^{+l_i} I(z)dz = \frac{2g_B P_{th}}{\pi \omega_0^2} \int_0^{+l_i} \left[1 + \left(z/z_R\right)^2\right]^{-1} dz \tag{4.3.4}$$

$$C = \frac{2g_B P_{th}}{\lambda} \tan^{-1}\left(l_i/z_R\right) \tag{4.3.5}$$

In this case, $l_i \ll z_R$ (the interaction length is shorter than the Rayleigh range), therefore, $\tan^{-1}\left(l_i/z_R\right) \approx l_i/z_R$ as $l_i/z_R \ll 1$

$$P_{th} = \frac{C\lambda z_R}{2g_B l_i} \tag{4.3.6}$$

It can be seen from this that $P_{th} \propto z_R$.

This linear relationship between the threshold power and the Rayleigh range was tested by placing a selection of lenses with focal lengths varying from 50 mm up to 500 mm. A small vertical SBS cell, filled with an appropriate amount of Freon-113 (i.e. to maintain a length of liquid that is smaller than the Rayleigh range used) was used in this experiment. Figure 4.3.2.1 shows the experimentally obtained SBS threshold power versus the Rayleigh range.

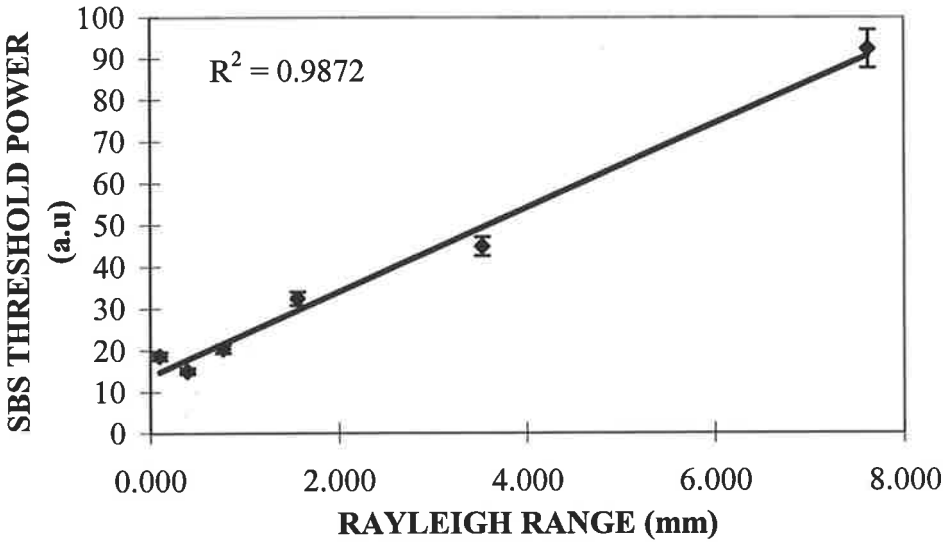

Figure 4.3.2.1 SBS threshold power versus Rayleigh range for a short coherence input beam (l_c=17 mm).

The square of the correlation coefficient R^2=0.9872 for a least squares fit shows a good agreement between the theoretical derivation for P_{th} and experiment. The SBS threshold power decreases as the Rayleigh range is reduced, or for that matter as the focal length is reduced.

4.3.3 OPC

The main objective of this work was to determine how short coherence length limits the usefulness of OPC by SBS. The experimental parameters for our data, include, a laser input bandwidth of 18 GHz, a long length of interaction (140 mm), a short Rayleigh range (<2 mm) and a high purity liquid (distilled and filtered Freon-113). As the laser input beam bandwidth, $\Delta\omega_p$ = 18 GHz, exceeds the SBS sound decay rate in the liquid, Γ=1.3 GHz, then these results fall under the broad-band SBS regime. With the experiment set up as discussed in sections 2.2 and 4.2, the energy reflectivity of the

SBS cell was measured against the pump pulse energy as a multiple of SBS threshold. This data is presented in figure 4.3.3.1. The shape of the reflectivity curve with a steep rise which gradually levels off. When comparing this to either the long coherence reflectivity (figure 2.3.1) or the theoretical prediction (figure 1.3.7) the qualitative form of the reflectivity is similar but with lower values. The measurements were done at the Pulse repetition frequencies of 4 Hz and 15 Hz. In this data, as the reflectivity started to rise above 40% at 4Hz, and 5% at 15Hz, optical breakdown took place everywhere thereafter. The optical breakdown was erratic at the lower energies but was present in

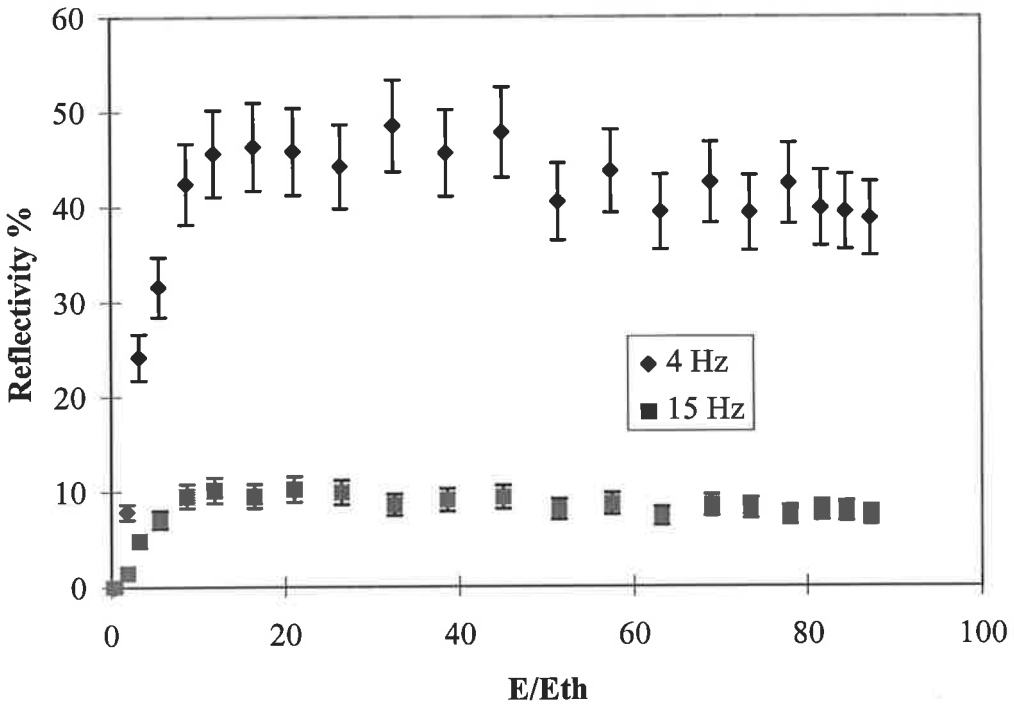

Figure 4.3.3.1: Diagram of short coherence reflectivity of Freon-113 as a function of input Energy/Threshold Energy ratio for 4 Hz and 15 Hz pulse repetition frequency.

every shot at the higher energies. The short coherence SBS threshold energy of the Freon-113 SBS cell was 3.7 mJ, which as expected (for large bandwidth and multimode beams the SBS gain is reduced)[17] was larger than that of the narrowband operation. It has been shown in reference 17 that the SBS threshold depends on the ratio of the gain length l_g=$1/g_B I_L$ to the coherence length l_c, where g_B is the SBS intensity gain and I_L is the input laser intensity. Similar reflectivity values had also been reported by others (see references 5, 6, 8, and 10).

In this experiment, at each input energy setting there are 99 pulses showing the average value and the standard deviation. Unlike the long coherence reflectivity, the data level off, bellow the 50% value and the variation is large (about 10%). Reflectivities of up to 62% have been reported by Carroll et al[18] for a broadband (15 GHz) doubled (532 nm) Nd:YAG laser at input powers of 38 times the threshold. The SBS gain has been shown in other studies to decrease rapidly with increasing input pulse bandwidth, especially for bandwidths greater than 20 GHz.[19] It has been shown that effects competing with SBS such as stimulated Raman scattering, self-focusing and optical heating depend on the input beam intensity.[20] The onset of these competitive processes is believed to be facilitated under short coherence pumping since their gain can exceed that of SBS.[9] For instance, the SRS process has a response time in the order of picoseconds and thus can respond to the intensity fluctuations of the multimode laser pulse. This low reflectivities can also be due to the very high intensities in the immediate focal volume which cause optical breakdown. The presence of optical breakdown during SBS has been seen in many other studies.[21,22,23] The propagation direction of optical breakdown generation has been shown[24] to coincide with that of the SBS and our observations agree with this (i.e. starting at or in front of the focus and

moving towards the cell entry window). For increased pulse repetition frequencies the reflectivity was reduced further due to optical breakdown. For any new train of pulses allowed to enter the SBS cell at pulse repetition frequency of 8-15 Hz only the first pulse had a higher reflectivity value. At these higher pulse repetition frequency the ion disturbance (in the focal volume) left over from the previous pulse can lower the optical breakdown threshold and thus affect the next incoming pulse.[25] Correct choice of the focusing geometry and pulse repetition frequency is important in avoiding competing effects, as these results show. For instance, increasing the focal length in turn increases the threshold energy of optical breakdown.[26] On the other hand, reducing the focal length increases the likelihood of breakdown as well helping in achieving significant SBS reflectivity. This reflectivity improvement using a broadband input beam and strong focusing was demonstrated in another study on 26 organic liquids.[27]

Some initial attempts to obtain OPC-SBS using Freon-113 that had not been distilled or filtered were a failure (even with 1 Hz pulse repetition frequency). The reflectivity in the case of contaminated liquid (micro-particles and other substances) was overcome by large optical breakdown which had a lower threshold than the SBS process. The burning of the contaminants most likely caused chemical reactions which change the properties of the liquid. These chemical changes can produce an increase in optical absorption, convection mixing, burning of new particles, and other effects. The importance of using clean, pure, clean liquids was highlighted in this study as well as in experimental studies by others.28

A number of other articles have presented good PC fidelity for broadband but only at pump intensities close to threshold and short lengths on interaction.[5,6] In fact, our

SBS results are qualitatively closer to the 45-GHz linewidth pulses of reference 29. There is good agreement between the two studies (i.e. ours and reference 29) as low SBS reflectivity and PC fidelity were obtained in the short coherence length regime. Although stable operation of the laser at intermediate bandwidths was not attempted, it was none the less possible to obtain few such pulses by momentarily blocking the injection seeding system. These intermediate bandwidth pulses (with l_c between 10 and 30 cm) had a substantially better temporal reproduction and higher SBS reflectivity than the broad bandwidth pulses.

Figure 4.3.3.2 shows the phase fidelity over a range of pump pulse energy for our 18-GHz bandwidth pulses. The fidelity overall is very low, about 10% and has a large variation. Clearly this set-up is not useful as a phase conjugator. Only near the threshold is the average value of fidelity higher but there the variation is larger.

Large fluctuations and a decrease on the average value of PC fidelity for a multimode pulse have been reported in a theoretical 3-D computer model by Litvak and Wagner.[30] In addition, numerical modelling of SBS excited by a multiline pump has shown that phase terms arising from off-resonant acoustic gratings may significantly degrade conjugation fidelity for a laser with line separations up to the order of the sound decay rate.[31] Sidorovich[32] in his theoretical modelling showed that for laser bandwidth values greater than twice that of the sound decay rate some small phase shift persists between lines, until the lines are decoupled. These phase shifts are also intensity dependent and thus may lead to a degradation of PC fidelity due to coherence loss (i.e. due to phase relations between the contributions of different hypersonic gratings produced by the interference of other pairs of spectral components of the exciting and

Stokes radiation). Delays in the response of the phonon grating between different modes result in a Stokes which also lags the input at any time thus causing the fidelity to reduce. Although there are no theoretical models that can provide a multimode SBS code utilising wave optics to model both spatial and temporal coherence, none the less, the above mentioned models provide some insight of the underlying mechanisms of SBS.

Further, in our study, by placing a lens with a smaller focal length 50 mm (instead of f=100 mm) in front of the SBS cell, a six times improvement in fidelity was achieved, but there the optical breakdown threshold was also reduced below the SBS threshold value. This is in contrast to the SBS threshold for long coherence lengths, where no optical breakdown was observed. These short coherence results are in agreement with the experimental findings of reference 5. Three reasons for this behaviour can be offered based on experimentally verified and theoretically modelled information in other studies. First, the high intensity, can cause the seeding of the SBS process to take place upstream from the focal region, thus failing to give a phase conjugate return.[4] Second, the SBS gain is reduced due to the group velocity mismatch (i.e. dispersion). Finally the temporal and spatial conjugation will be reduced when the input beam has many independent temporal modes where each mode can have its own spatial profile.[3] Experimental results by O'Key and Osborne[33] for input pulse bandwidth(2 to 800 GHz) have yielded less than 50% SBS reflectivities and poor spatial beam quality (2 to 70 x diffraction limit).

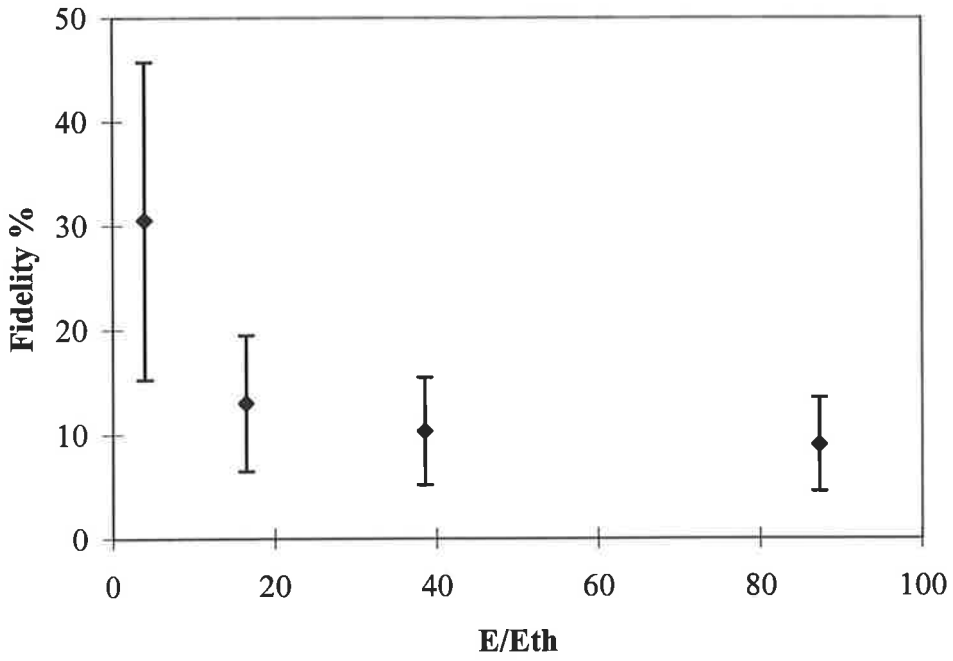

Figure 4.3.3.2: Diagram of short coherence Phase fidelity over the range of pump pulse energy as a multiple of SBS threshold.

An example of the time resolved far field and near field of the laser input and SBS return in the broad-band regime is shown in Figure 4.3.4.1. The temporal profile and width of the SBS return pulse follow approximately that of the input pulse with any temporal differences attributed to the transient SBS response, self-focusing, and possibly other competing processes. The amount of energy that the SBS far field can pass through the diffraction limited aperture is very small, due to the poor phase conjugate nature of this regime. Study of the far field pulses showed that the SBS fidelity has a temporal dependence. The reason for this may be that the input laser pulse wavefront changes faster than the phonon lifetime causing the SBS threshold to increase and the OPC fidelity to reduce.[34,35,36] Also as discussed in chapter three, fast transient effects can lead to further reductions in the fidelity. Figure 4.3.4.2 presents a typical

experimental example of the SBS return's, spatial near field profile. In this figure the SBS return has a smaller, distorted shape than either of its laser input or its long coherence SBS return, and typically from shot to shot the SBS return changes position, shape and size. In other words, the Stokes return was not the reconstructed/phase conjugate of the input laser beam. Although, similar type of pattern formations in the transverse field of multimode Stokes emission from SBS experiments have been reported by others in the presence of feedback,[37] precautions were taken in this study to avoid operation in such spatially chaotic regime.

4.3.4 Optical Breakdown and Bubble Formation

During the collection of data for the previous experiments, it was noticed that optical breakdown was prolific and some gas bubbles could be seen to rise to the top of the SBS cell. It was decided that these phenomena be more closely observed as they could interfere with the SBS process by reducing both reflectivity and fidelity.

There are two mechanisms that can cause optical breakdown, multiphoton ionisation and avalanche ionisation. In multiphoton ionisation one or more electrons are freed from the atom or molecule when the laser radiation is sufficiently intense. This can lead to the formation of a high-temperature plasma due to ionisation of the medium. Plasmas absorb optical radiation much more strongly than ordinary matter. The time to build an absorbing plasma can be much shorter than 1 ns for multiphoton ionisation.[38] The

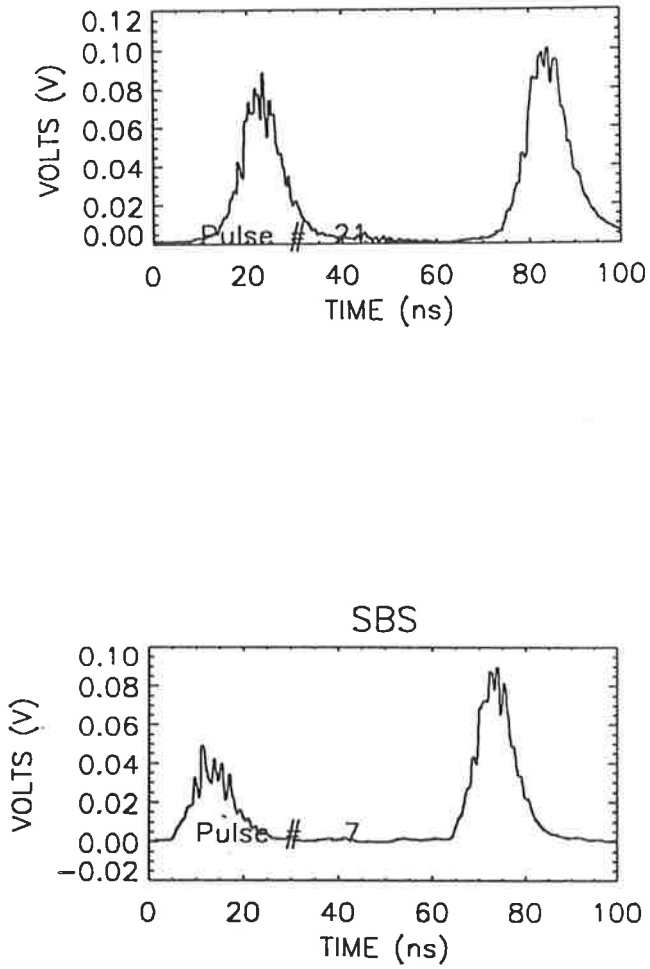

Figure 4.3.4.1: An example of the time resolved far field (left) and near field (right) of the laser input (top) and SBS return (bottom) in the broad-band regime.

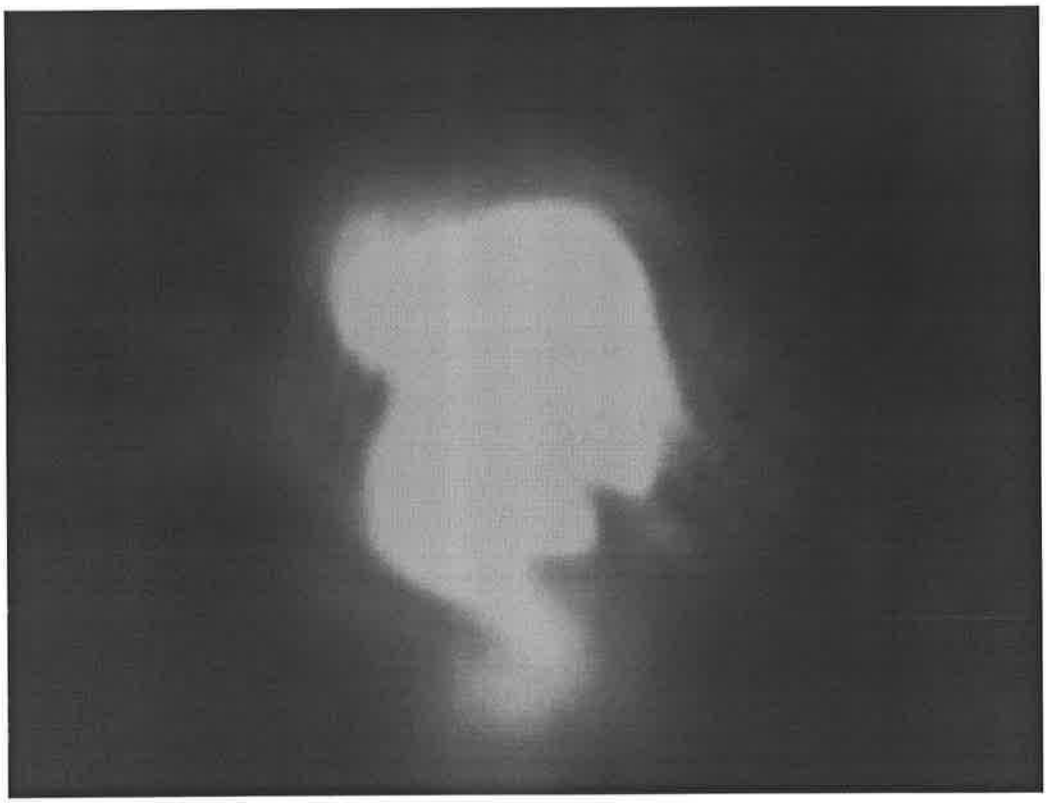

Figure 4.3.4.2: Picture presents a typical example of the spatial near field profile.

plasmas can thus be rapidly heated by the laser beam to very high temperatures, producing plasma expansion, an audible acoustic signature, a visible plasma emission (visible spark) and cavitation.[31,39] The plasma expansion can be much faster than the speed of sound in the medium thus restricting the SBS gain region. In avalanche ionisation one or more free electrons must already be present in the mediums focal volume at the beginning of the pulse.[40] If no electrons are initially present then multiphoton ionisation is believed[40,41] to be important in creating the primary electrons and so setting the stage for avalanche ionisation and optical breakdown. The process requires that the rate of free-electron production exceeds the rate of loss due to recombination and diffusion of electrons out of the mediums focal volume.[41] The rise time of avalanche breakdown depends on the initial electron concentration and the avalanche amplification rate. Avalanche amplification in liquids is high as their density of molecules is high and takes only a few tens of picoseconds until breakdown occurs.[42] Optical breakdown influences the effective interaction length which reduces the SBS reflectivity.[29] The observed (with the aid of a CCD camera) spatial extent of the plasmas varied from tens of micrometers to few millimetres and multiple plasmas for a single input pulse were not uncommon. The duration of the visible plasmas was measured with a fast Si avalanche photodiode (Newport 877) and was found to exceed that of the laser pulse and often, times of ~1 ms were observed. When the laser pulse repetition frequency was increased to 15 Hz, a continuous presence of a "spark" was obtained indicating that the duration of the plasma was equal to the interpulse time period of the laser. The fidelity reduction observed in this study in the presence of optical breakdown was mainly due to the beams cross section being partially or wholly blocked by the ion enhanced optical absorption.[36] These effects could be avoided if in SBS the acoustic grating builds up faster than the plasma density. The back-reflection from the grating

can reduce the focal intensity so that the avalanche amplification of carriers is stopped.[43] This accelerated build-up of the acoustic grating can be achieved by using sharp rise input pulses.[44] As discussed in chapter three, the sharp rise pulses would increase reflectivity but unfortunately, decrease the SBS fidelity by favouring the amplification of noise modes.[45,46] New chemical species can be created by dissociation due to optical breakdown, causing a possible increase in optical absorption. In our study even after long operating times (months) no increase in absorption or reduction in the performance of the liquid was observed (i.e. when using long coherence pulses). Further, in reference 47, it has been shown that the optical breakdown threshold of a SBS material is directly proportional to the expression $N^{2/3}/(n^2-1)$, where N is the atomic number density and n is the refractive index.

The spectrum of the back scattered and the transmitted beam was also examined for a long cell (600 mm) using a grating spectrometer. The back scattered light had a wavelength of 1.064 μm and no other wavelengths were seen. The transmitted light through the cell had spectral light at 1.064 μm and 532 nm. During optical breakdown a broad spectrum of visible wavelengths was seen superimposed on the two lines. The liquid does not normally exhibit second-order nonlinear optical effects (e.g. Second Harmonic Generation, SHG) because even-order electric dipole coefficients are zero for centrosymetric molecules.[48] Freon-113 has an electric dipole moment which is close to zero[49] and as such it should be unsuitable for SHG but under the intense laser field it's polarised sufficiently to cause the dipole moment to increase. Under this new condition a very small amount of the transmitted light was frequency doubled. In spite of its presence, SHG was not found to be an important competing process for broad-band OPC-SBS in the way optical breakdown was.

A visible plasma is not the only breakdown effect. Observation with a CCD camera revealed two types of bubbles (differentiated by size and duration) being formed. Whenever optical breakdown (plasma formation with a visible flash and an audible acoustic signature) took place, a cavitation bubble was detected. These were the larger of the two types of bubbles and moved to the top of the cell. The lifetime of these bubbles was in the order of microseconds to hundreds of milliseconds (as captured in sequential image frame on the camera). Figure 4.3.4.3 shows the formation of such bubbles which were captured with the aid of a Visible/Infrared CCD camera. Bubble formation was observed at and above the SBS threshold energy. These bubbles are initially created at or near the focus and then a series of other bubbles is created sequentially towards the front of the cell resulting in a filamentary track. The time for this process is equal to the pulse duration. The focus of the beam moves towards the front of the cell creating bubbles in the process. This behaviour is most likely due to self-focusing of the Q-switched YAG laser in the liquid since for our experimental conditions the self- focusing threshold power is about 3 times above that for SBS.[50,51] Absorption of the hypersonic wave is also known to heat the region in front of the focal waist.[52] Experiments in water by other groups, have shown that the bubble radius initially expands at 2600 m/s, reaching a radius of ~400 μm after 200 ns.[33]

The second type of bubbles observed was much smaller in diameter and had a longer lifetime within the focal volume. Figure 4.3.4.4 shows the cloud like formation of such bubbles which are only seen here because they scatter IR light to the CCD camera. These were produced near but below the SBS threshold energy. Their creation could be by diffusion of gas into the oscillating cavitation bubble.53 The intensities that

produced these bubbles were too weak to produce plasmas whose flash could be seen by a naked eye and neither was an audible acoustic signature present. The plasmas which produced these bubbles were obviously smaller, cooler and less dense than those which give out a visible flash.54 Similar bubble formation has been reported in SBS work on tropocollagen solutions55. Although the liquid used in our experiments was triple distilled and filtered the possibility of impurities/particles smaller than 200 nm still exists. The presence of impurities such as submicron particles in the SBS medium can cause the creation of bubbles.56 As the particle absorbs radiation, it heats and begins to conduct energy to the surrounding. The nucleation starts instantaneously as the surface temperature exceeds the boiling temperature. A bubble of hot gas forming around the plasma/ ionised hot particle represents a region of lower density and lower index of refraction. I suspect that bubble creation may be enhanced during SBS as the electrostrictive process can also create regions of lower density in the medium.

The following argument (based on literature) aims to show that sonoluminescence is not responsible for the creation of the observed bubbles. The spontaneous growth of bubbles has been shown[57] to depend on the radius of critical bubble (i.e. the minimum radius bubble executing harmonic radial oscillations at its resonance frequency). By assuming that the formation of critical nuclei causes the transition from Rayleigh scattering to Mie scattering, then the radius of the nucleus can be estimated to be R_{tr}= 125 nm ($R_{tr}=\lambda/2\pi n$ where λ= 1.064 μm and refractive index n= 1.36). Clouds of gas bubbles have been reported in sonoluminescence studies.[58] A literature review on the

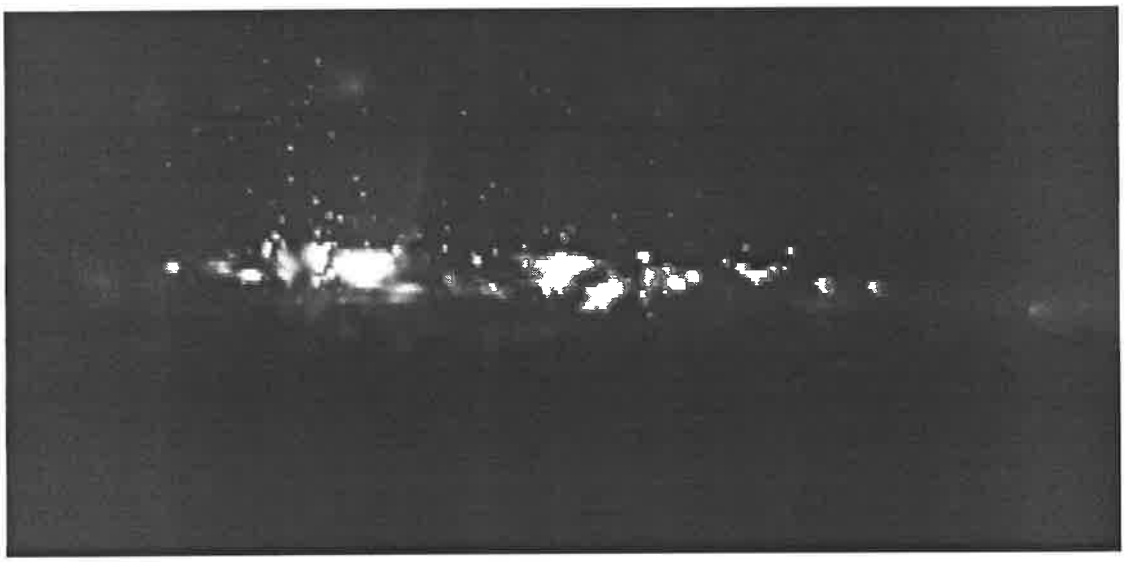

Figure 4.3.4.3: Picture presents a typical example of the formation of bubbles which were captured with the aid of a CCD camera.

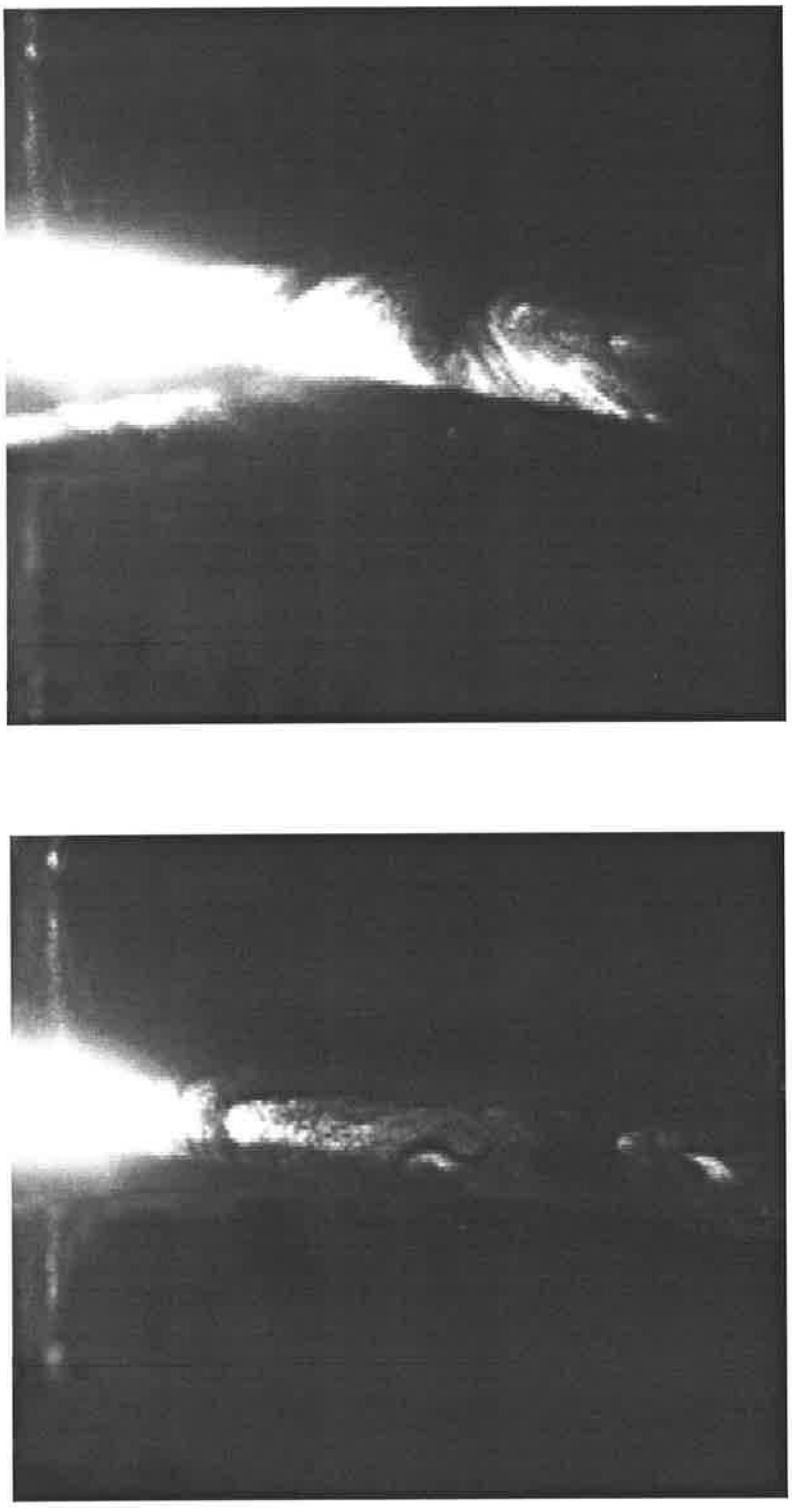

Figure 4.3.4.4: Picture shows the cloud like formation of bubbles which are only seen here because they scatter IR light to the CCD camera.

subject of sonoluminescence and cavitation bubble dynamics[59] has discounted this effect from being present in this study as the driving acoustic frequency of 1.8 GHz is well in excess of the frequency limit (~500 kHz) for parametric excitation on the surface of a bubble.[60] At 1.8 GHz a resonating bubble would need to have a radius of 1.5 nm, which is too small for it to be a bubble. length l_c, then better SBS returns should be obtained.

4.3.5 Optical Breakdown Reduction

In this study, the primary competing process in broad-band SBS is known (as discussed already in this section) and observed to be optical breakdown in the SBS cell, which is encountered due to the combined effects of tightly focused beams (short Rayleigh ranges) and the very high peak power due to the random temporal interference of many axial laser modes. The reduction of optical breakdown by control of axial modes in a Nd:YAG laser oscillator with an intracavity PC mirror has already been demonstrated.[61,62] Usually the reduction of optical breakdown has been achieved by the use of longer focal length lenses in front of the SBS cell[63] and by purifying the SBS medium. The set-up shown and described in section 4.2.2 (figure 4.2.2.1) employed a delay technique to improve phase conjugation using short coherence length. This method was investigated as a possible means of reducing the high peak power of the input to the SBS cell. Some temporal smoothing of the pulse spikes is aimed for. The near field separation was NFS=1.8 diameters and the far field separation was FFS=0. The alignment of the two beams was checked also under long coherence operation where effective OPC by SBS was achieved (similar to other studies).[18,64] This short

coherence, delay technique did not prove to be very successful. The only positive outcome was a slight decrease in the optical breakdown. The observed SBS return was accompanied by some optical breakdown, with temporally truncated pulses of reduced reflectivity (compared to long coherence results) and with a mainly non-phase conjugate return. Attempts to misalign the beams so that they overlap either in front or behind the focal plane also failed to produce a phase conjugate return. The depth of focus in the medium was also varied from the liquid surface to 55.0 mm with no significant difference in fidelity and only a slight increase in reflectivity in the 5.0 to 15 mm depth was obtained (here $l_i<l_c$). The walk-off (degradation in pointing stability) in the SBS return increased as the depth of focus increased. Some qualitative resemblance exist between the above mentioned observations and the experimental observations of reference 65 (where pulse truncation is achieved with the aid of SBS and optical breakdown). No improvements were observed for OPC with short coherence length laser pulses to date. The explanation for this, lie in the reasons given previously for the single short coherence beam (e.g. competing effects). According to the theory in reference 3, if the input laser coherence length is shorter than the gain length and if the input power fluctuations are shorter in time than the phonon relaxation time, then the SBS temporal reproduction is predicted to be bad. Further, if the input laser temporal modes have associated with them more than one spatial variations and the mode spacing is larger than the phonon relaxation rate, then the medium cannot respond to the fast changes in the spatial pattern and thus the spatial conjugation is bad. In this specific experimental study, no spatial filtering was applied to the laser input beam thus allowing the presence of temporal spatial variations. Gordeev et al.[66] showed in their study that under noncoherent SBS pumping, the fidelity was reduced due to selection of the spatial-frequency spectrum and transformation of the spatial-angular structure of the

beam. Other experimental studies[67,68] have also shown that a decreased spatial beam quality causes an increase in the SBS threshold. Under these above mentioned conditions, the broad-band gain is dramatically reduced due to group velocity mismatch (i.e. due to dispersion between pump and Stokes) and thus the fidelity of phase conjugation which is also linked to it, is also reduced (see reference 3, section III). Therefore, even though this delay technique could offer a marginal improvement as regard the optical breakdown it fell short of improving the SBS-OPC process.

4.4 Conclusion

OPC-SBS under very short coherence length was investigated as the final part of this thesis.

As part of this study a novel interferometer was designed that enabled the measurement and monitoring of the extent of the coherence length throughout the experiment. Using components found in most modern optics laboratories, we have assembled and demonstrated a simple diagnostic tool which can record the complete coherence function of a single laser pulse. The method permits real time observations of the whole visibility pattern, and is capable of producing near real time coherence functions, limited by the speed and capacity of the computer frame grabber. The method is useful over the whole range of visible and infrared wavelengths where CCD cameras and other imaging arrays function.

The SBS reflectivity for short coherence pulses was substantially reduced compared to long coherence. The short coherence PC fidelity was found to decrease with increasing energy. Although reduction of the interaction length can offer some relief, the presence of optical breakdown takes that advantage away. Increasing the pulse repetition frequency was also found to bring a reduction in both reflectivity and fidelity. The high peak power in the input pulses was suspected to cause not only optical breakdown but gas bubbles as well. The presence of other competing phenomena (e.g. SHG, feedback) was also observed and their effect on SBS considered.

An experiment was undertaken in which the effects of high peak power in SBS were reduced somewhat but with no improvement in the PC fidelity. There is an indication from this study and the other reviewed studies that temporal and spatial smoothing of the input pulse could offer an improvement in reflectivity and PC fidelity. Provided that any spatio-temporal changes in the input laser pulse are slower that the phonon relaxation time of the medium and the length of interaction is smaller than the coherence length, and competing phenomena such as optical breakdown are eliminated through appropriate choice of geometry then good OPC-SBS could possibly be obtained even in a reduced coherence length regime. Such regime would require further study for a conclusion to be drawn.

OPC-SBS for laser pulses with bandwidths broader than the mediums Brillouin bandwidth does not appear promising.

4.5 References

1 Yu. E. D'yakov, "Excitation of stimulated light scattering by broad-spectrum pumping", JETP Letters, Vol. 11, 243-246, 1970

2 V. I. Popovichev, V. V. Ragul'skii and F. S. Faizullov, "Stimulated Mandel'shtam-Brillouin scattering excited by radiation with a broad spectrum", JETP Letters, Vol. 19, No 6, 196-198, March 20, 1974

3 G. C. Valley, " A Review of Stimulated Brillouin Scattering Excited with a Broad-Band Pump Laser", IEEE Journal of Quantum Electronics, Vol. QE-22, No 5, May 1986

4 R. A. Mullen, R. C. Lind and G. C. Valley, "Observation of stimulated Brillouin scattering gain with a dual spectral-line pump", Optics Communications, Vol. 63, 123-128, 1987

5 J. Munch, R.F. Wuerker, M.J. LeFebvre "Interaction length for optical phase conjugation by SBS: an experimental investigation", Appl. Opt., Vol. 28, 3099-3105, 1989.

6 A. A. Filippo and M. R. Perrone, "Stimulated Brillouin Scattering in SF_6 with a Free-Running XeCl Laser as Pump", Appl. Phys. B, Vol. 57, 103-107, 1993

7 G. M. Davis and M. C. Gower, "Stimulated Brillouin Scattering of a KrF Laser", IEEE Journal of Quantum Electronics, Vol. 27, No 3, 496-501, March 1991

8 A. A. Filippo and M. R. Perrone, "Experimental study of Broad-Band XeCl Double-Pass Amplifier with SBS Mirror", Appl. Phys. B, Vol. 55, No 1, 71-75, July 1992

9 P Narum, M. D. Skeldon and R. W. Boyd, "Effect of laser mode structure on stimulated Brillouin scattering", IEEE Journal of Quantum Electronics, Vol. 22, No 11, 2161-2167, 1986

10 A. A. Filippo and M. R. Perrone, "Reflectivity of broad-band stimulated Brillouin scattering mirrors", Optics Communications, Vol. 91, No 5,6, 395-400, 1 August 1992

11 W. T. Whitney, M. T. Duignan and B. J. Feldman, "Stimulated Brillouin scattering and phase conjugation of multiline hydrogen fluoride laser radiation", J. Opt. Soc. Am. B, Vol. 7, No 11, 2160-2168, November 1990

12 V. Devrelis, M. O'Connor and J. Munch, "Coherence length of single laser pulses as measured by CCD interferometry", Applied Optics, Vol. 34, No 24, 5386-5389, 20 August 1995

13 R.F. Wuerker, J. Munch and L.O. Heflinger, "Coherence length measured directly by holography", Applied Optics, Vol. 28, 1015-1017, 1989.

14 A.A. Michelson, "Studies in Optics" (University of Chicago Press 1927), reissued in Phoenix Science Series., pp.34-45, 1962.

15 For an excellent review, see A.S. Marathery "Elements of Optical Coherence Theory", Wiley, N.Y., chap.5, 1987.
or W. Koechner "Solid-state Laser Engineering" 4th edition, Springer, section 5.2, 1996.

16 C. Bhan, K. Syam Sundara Rao, and P.C. Mehta, "Measurement of the Coherence Length of a laser using a holographically generated phase-conjugate wavefront", Appl. Opt., Vol. 30, no.30, 4282-4283, 1991.

17 G. Arisholm and P. Narum, "Transient Transverse Stimulated Brillouin Scattering with a Broad-Band Pump", IEEE J. Quantum Electron., Vol. 28, No 10, 2075-2083, October 1992

18 D. L. Carroll, R. Johnson, S. J. Pfeifer and R. H. Moyer, "Experimental investigation of stimulated Brillouin scattering beam combination", J. Opt. Soc. Am. B, Vol. 9, No 12, 2214-2224, December 1992

19 S. N. Dixit, "Numerical modelling of the suppression of stimulated Brillouin scattering due to finite laser bandwidth", Nonlinear Optics III, SPIE, Vol. 1626, 254-265, 1992

20 I. V. Tomov, R. Fedosejevs and D. C. D. McKen, "High-efficiency stimulated Brillouin scattering of KrF laser radiation in SF_6", Optics Letters, Vol. 9, No 9, 405-407, September 1984

21 M. R. Osborne and M. A. O'Key, "Temporal response of stimulated Brillouin scattering phase conjugation", Optics Communications, Vol. 94, 346-352, 1992

22 H. J Eichler, R. Konig, R. Menzel, H. J. Patzold and J. Schwartz, "Stimulated Brillouin scattering of broadband XeCl-laser radiation by hydrocarbon liquids", International Journal of Nonlinear Optical Physics, Vol. 2, No 2, 247-253, 1993

23 H. J Eichler, C. Jun, A. Kummrow, R. Menzel and D. Schumann, "Nd-YAG-Laser with SBS-Q-Switching mirror and repetition rate up to 50 Hz", International Journal of Nonlinear Optical Physics, Vol. 2, No 1, 187-204, 1993

24 V. S. Teslenko, "Initial Stage of Extended Laser Breakdown in Liquids", IEEE Transactions on electrical Insulation, Vol. 26, No 6, 1195-1200, December 1991

25 R. A. Mullen, "Quenching optical breakdown with an applied electric field", CLEO'90, CTHI21, p 394, 1990

26 G. N. Steinberg, "Filamentary Tracks Formed in Transparent Optical Glass by Laser Beam Self-Focusing. I. Experimental Investigation", Physical Review A, Vol. 4, No. 3, 1182-1194, September 1971

27 H. J. Eichler, R. Konig, R. Menzel, H. J. Patzold and J. Schwartz, "Stimulated Brillouin Scattering of Broadband Xe-Cl-Laser Radiation by Hydrocarbon Liquids", Int. J. Nonlin. Opt. Phys., Vol. 2, No 2, 247-253, 1993

28 H. J. Eichler, R. Konig, R. Menzel, R. Sander, J. Schwartz and H. J. Patzold, "Test of Organic SBS Liquids in the IR and UV", Int. J. Nonlin. Opt. Phys., Vol. 2, No 2, 267-270, 1993

29 M. Lefebvre, S. Pfeifer and R. Johnson, "Dependence of stimulated-Brillouin - scattering phase-conjugate correction on the far-field intensity distribution of the pump light", J. Opt. Soc. Am. B, Vol. 9, No 1, 121-131, January 1992

30 M. M. Litvak and R. J. Wagner, "Stimulated Brillouin Scatter (SBS) SIX-Code", Modeling and Simulation of Laser Systems II, SPIE, Vol. 1415, 62-71, 1991

31 D. L. Bullock, N.-M. Nguyen-Vo and S. J. Pfeifer, "Numerical Model of Stimulated Brillouin Scattering Excited by a Multiline Pump", IEEE Journal of Quantum Electronics, Vol. 30, No 3, 805-811, March 1994

32 V. G. Sidorovich, "Theory of collective processes during excitation of stimulated scattering by incoherent optical radiation", Opt. Spectrosc. (USSR), Vol. 55, No 4, 418-422, October 1983

33 M. A. O'Key and M. R. Osborne, "Broadband stimulated Brillouin scattering", Optics Communications, Vol. 89, No 2,3,4, 269-275, 1 May 1992

34 V. I. Bespalov, V. G. Manishin and G. A. Pasmanik, "Nonlinear selection of optical radiation on reflection from a stimulated Mandel'shtam-Brillouin scattering mirror", Sov. Phys. JETP, Vol. 50, No. 5, 879-886, November 1979

35 E. L. Budis, M. V. Vasilev, A. A. Leshchev, G. A. Pasmanik, V. G. Sidorovich and A. A. Shilov, "Phase conjugation of incoherent light during stimulated Brillouin scattering", Optics and spectroscopy, Vol. 53, No. 5, 550-553, November 1982

36 I. Yu Anikeev, I. G. Zubarev and S. I. Mikhailov, "Stimulated scattering of spatially incoherent optical radiation", Sov. Phys. JETP, Vol. 57, No. 5, 978-983, May 1983

37 D. S. Lim, W. Lu and R. G. Harrison, "Evidence of phase singularities and dynamic patterns in stimulated Brillouin scattering", Optics Communications, Vol. 113, 471-475, 1 January 1995

38 A. Kummrow, "Effect of optical breakdown on stimulated Brillouin scattering in focused beam cells", J. Opt. Soc. Am. B, Vol. 12, No 6, 1006-1011, June 1995

39 B. Zysset, J. G. Fujimoto and T. F. Deutsch, "Time-Resolved Measurements of Picosecond Optical Breakdown", Applied Physics B, Vol. 48, 139-147, 1989

40 Y. R. Shen, *The Principles of Nonlinear Optics*, New York: Wiley, 528-539, 1984

41 P. W. Milonni and J. H. Eberly, *Lasers*, Wiley Publications, 677-682, 1988

42 Y. S. Huo, A. J. Alcock and O. L. Bourne, "A time-resolved study of sub-nanosecond pulse generation by the combined effect of stimulated Brillouin scattering and laser induced breakdown", Applied Physics B, Vol. 38, 125-129, 1985

43 R. Menzel and H. J. Eichler, "Temporal and spatial reflectivity of focused beams in stimulated Brillouin scattering for phase conjugation", Physical Review A, Vol. 46, 7139-7149, 1992

44 R. A. Mullen, "Multiple-Short-Pulse Stimulated Brillouin Scattering for Trains of 200 ps Pulses at 1.06 μm", IEEE Journal of Quantum Electronics, Vol. 26, No 7, 1299-1303, July 1990

45 C. Brent Dane, W. A. Neuman and L. A. Hackel, "Pulse-shape dependence of stimulated-Brillouin-scettering phase-conjugation fidelity for high input energies", Optics Letters, Vol. 17, No 18, 1271-1273, September 15, 1992

46 L. A. Hackel, J. L. Miller and C. B. Dane, "Phase conjugation in a high power regenerative amplifier system", J. Nonlin. Opt. Phys., Vol. 2, 171-185, 1993

47 J. R. Bettis, "Correlation among the laser-induced breakdown threshold in solids, liquids, and gases", Applied Optics, Vol. 31, No. 18, 3448-3452, 20 May 1992

48 A. Garito, R. F. Shi and M. Wu, "Nonlinear Optics of organic and polymer materials", Physics Today, 51-57, May 1994

49 A. R. H Goodwin and G. Morrison, "Measurement of the Dipole Moment of Gaseous 1,1,1-Trichlorotrifluoroethane, 1,2-Difluoroethane, 1,1,2-Trichlorotrifluoroethane, and 2-(Difluoromethoxy)-1,1,1-trifluoroethane", The Journal of Physical Chemistry, Vol. 96, No 13, 5521-5526, 1992

50 E. L. Kerr, "Transient and Steady-State Electrostrictive Laser Beam Trapping", IEEE J. Quantum Electron., Vol. 6, No 10, 616-621, October 1970

51 E. L. Kerr, "Filamentary Track Formed in Transparent Optical Glass By Laser Beam Self-Focusing. II. Theoretical Analysis", Physical Review A, Vol. 4, No. 3, 1195-1208, September 1971

52 N. F. Andreev, E. A Khazanov, O. V. Kulagin, O. V. Palashov and G. A. Pasmanik, "Hypersonic wave absorption effect on the quality of phase conjugation by SBS", CLEO'94, CMC2, 10, 1994

53 C. C. Church, "A theoretical study of cavitation generated by an extracorporeal shock wave lithotripter", J. Acoust. Soc. Am., Vol. 86, 215-227, 1989

54 P. K. Kennedy, "A First-Order Model for Computation of Laser-Induced Breakdown Thresholds in Ocular and Aqueous Media: Part I-Theory", IEEE Journal of Quantum Electronics, Vol. 31, No 12, 2241-2249, December 1995

55 S. N. Bagrov, Yu. V. Dolgopolov, G. G. Kochemasov, S. M. Kulikov, A. V. Osipov, S. P. Smyshlyaev, S. A. Sukharev and S. N. Fedorov, "Stimulated Brillouin Scattering in tropocollagen solutions", JETP, Vol. 76, No. 2, 253-258, February 1993

56 J. A. Sell, Photothermal investigations of solids and fluids, Academic Press, Inc., Chapter 10, 1989

57 H. K. Park, C. P. Grigoropoulos, C. C. Ponn and A. C. Tam, "Optical probing of the temperature transients during pulsed-laser induced boiling of liquids", Appl. Phys. Lett., Vol. 68, No 5, 596-598, 29 January 1996

58 K. S. Suslick, D. A. Hammerton and R. E. Cline, "The sonochemical hot spot", Am. Chem. Soc., Vol. 108, 5641-5642, 1986

59 D. F. Gaitan, L. A. Crum, C. C. Church and R. A. Roy, "Sonoluminescence and bubble dynamics for a single, stable, cavitation bubble", J. Acoust. Soc. Am., Vol. 91, No 6, 3166-3183, June 1992

60 S. M. Gorskii and A. Yu. Zinov'ev, "Frequency limit of parametric wave generation on the surface of a bubble", Sov. Phys. Acoust., Vol. 33, No 5, 547-8, September-October 1987

61 M. O'Connor, V. Devrelis and J. Munch, "SBS Phase Conjugation of a Nd:YAG Laser for High Beam Quality", LASER 95, 1995

62 M. O'Connor, "Stimulated Brillouin Scattering Oscillators", Ph.D. Thesis, The University of Adelaide, 1996

63 W. L. Smith, "Laser-induced breakdown in optical materials", Optical Engineering, Vol. 17, 489-503, 1978

64 S. Sternklar, D Chomsky, S. Jackel and A. Zigler, "Misalignment sensitivity of beam combining by stimulated Brillouin scattering", Optics Letters, Vol. 15, No 9, 1 May 1990

65 S. S. Alimpiev, S. K. Vartapetov, I. A. Veselovsky, S. V. Likhansky and A. Z. Obidin, "Pulse shortening of KrF and ArF lasers in a process of optical breakdown

on a liquid surface", Optics Communications, Vol. 96, No 1,2,3, 71-74, 1 February 1993

66 A. A. Gordeev, I. Yu. Anikeev, I. G. Zubarev and S. I. Mikhailov, "Investigation of the forward and backward scattering of noncoherent Pump radiation", Sov. J. Quantum Electron., Vol. 14, No 11, 1482-1485, November 1984

67 M. R. Perrone and Y. B. Yao, "Stimulated Brillouin scattering dependence on the XeCl laser spectrum, IEEE J. Quantum Electron., Vol. 30, No 5, 1327-1331, 1994

68 H. J. Eichler, R. Menzel, R. Sander, M. Schulzke and J. Schwartz, "SBS at different wavelengths between 308 and 725 nm", Optics Communications, Vol. 121, 49-54, 15 November 1995

Chapter 5

Conclusion

In this final chapter the main achievements are re-iterated, and where appropriate, a case is made for further investigation.

I believe that a logical assessment of SBS has been made in terms of physics and that the beam fidelity in practical applications of OPC can be improved as a result of this work. The OPC-SBS provides us with a versatile reflector which possesses many useful properties.

In principle, close to one hundred percent conversion efficiency should be possible in SBS, with a corresponding high fidelity beam output. In this work it was shown that the Freon-113 SBS mirror can be used to obtain optical pulses with high reflectivity (~90%) with high fidelity (~90%) over a large input energy range. Both reflectivity and fidelity could be limited, though, by parameters such as length of interaction, pulse shape and pulse bandwidth. It is these limiting parameters which have been explored in this work.

In chapter two, the simple lens focusing scheme (i.e. SBS generator) was investigated in detail. The Stokes amplitude and phase fluctuations were attributed to the noise from which the SBS process initiates. A correlation between degradation in

OPC fidelity and SBS return phase jumps was confirmed for smoothly varying input pulses with long coherence length (3.3 m). These phase jumps were found to reduce for pulses with large input energy and small lengths of interaction, and thus a good regime for OPC-SBS was established. Over the period of this work, other researchers were reporting results of similar investigations and the general conclusion that noise can effect the SBS process in a generator is now well established. Despite the progress there are some areas which have received little attention and which may provide more opportunities for further investigations. These are: a) the experimental verification of the exact acoustic grating distribution along the interaction length for the purpose of testing and developing accurate theoretical models; b) the measurement of reflectivity and fidelity as a function of a large range of pump bandwidths rather than discrete values which are spaced well apart, should provide useful operation limits; and c) the use of bulk solid media (crystals, glasses) in OPC-SBS for incorporation into commercial systems as they do not require high pressure vessels and are not harmful to humans or environment. Certainly more work would be useful in the area of computer modeling of the SBS process. Aside from these possible direction for research, the simple lens focusing scheme has found application any many laboratories around the world (i.e. TRW, Lawrence Livermore National Laboratory) and is routinely used in MOPA configurations.

Chapter three described the dependence of the phase conjugate SBS fidelity on the shape of the input pulse. It was shown that the fidelity is substantially reduced when pulses with rise times shorter than the phonon lifetime are used, even if the coherence length is long (3.3 m). This reduction was made more pronounced as the pulse energy was increased. This effect can be thought of as the SBS systems response to an impulse

(large signal). The results of this thesis also agreed with those of other researchers which showed that in the SBS process, pump pulses with fast leading edges can enhance modes other than the phase conjugate.

Chapter four described the problems encountered in the SBS process when pulses with short coherence (<2 cm) are used. Besides the marked reduction in phase fidelity (~10%) other competing phenomena were introduced, like, optical breakdown, cool plasmas and bubbles, and even second harmonic generation. Based on these observations a technique was investigated for the reduction of optical breakdown during OPC-SBS but its success was only marginal. As an offspin of this work, a coherence length measuring diagnostic tool was developed which assisted in determining the coherence length during experiments. Overall, the SBS fidelity was tested under parameter regimes that could either degrade or improve it. This third regime of pumping (i.e. short coherence) produced the most problems and the worst results. To date a theoretical model for the numerical study of broadband transient SBS which takes focusing into account has not been developed.

There are a number of requirements which the input laser pulse must meet for the efficient production of OPC-SBS. It must not be too short, or there will be insufficient time to reach the steady state gain. If the pulse duration is less than the phonon lifetime, higher powers are required to obtain the same gain, and competing nonlinear processes such as optical breakdown and second harmonic generation are encountered. The leading edge of the input must not be to sharp compared to the phonon lifetime. The time of interaction should not exceed the phonon lifetime as phase jumps can occur in the SBS return (i.e. small immersion lengths are more desirable). Also the bandwidth of

the pulse should not be too great as to exceed the mediums SBS bandwidth. It was observed that a limit is generally reached when the coherence length of the beam becomes shorted than the interaction length. The polarisation of the pump should be well defined (i.e. linear or circular) as depolarised laser light will not be completely phase conjugated. Further, the SBS medium should be clean of any contaminants. Finally, even if all of the above conditions and more are met the SBS process will still not behave as a perfect phase conjugate mirror since the reflectivity can only approach unity but not reach it.

Provided the above mentioned requirements are met, then the SBS mirror becomes an inexpensive, high energy, phase conjugate reflector which is also capable of spectral filtering (i.e. eliminating ASE). Surely as the application of laser technology grows then the phase conjugate properties of SBS will play a part in those growing applications.

The findings from this thesis have already been applied to the theoretical development of a pump depleted, noise initiated, transient SBS numerical model that predicts the experimentally observed stochastic behaviour and has partly helped in the development work of a Nd:YAG Q-switched SBS oscillator through the better understanding of optical breakdown.

PUBLISHED PAPERS

S. Afshaarvahid, V. Devrelis and J. Munch, *The Nature of Intensity and Phase Modulations in Stimulated Brillouin Scattering*, Accepted for publication in Physical Review A, 1998

V. Devrelis, M. O'Connor, J. Munch, S. Adshaarvahid and C-J. Wei, *Experimental Investigation for the Reduction of Intensity and Phase Instabilities in Stimulated Brillouin Scattering*, Australian Optical Society 11th Conf. Proc., Adelaide, December 1997.

S. Afshaarvahid, J. Munch and V. Devrelis, *Numerical Study of Stochastic Intensity Fluctuations in Stimulated Brillouin Scattering*, Australian Optical Society 11th Conf. Proc., Adelaide, December 1997.

S. Afshaarvahid, J. Munch and V. Devrelis, *Numerical Study of Stimulated Brillouin Scattering Initiated from Noise*, CLEO/Pacific Rim'97, Chiba, ThM1, July 1997.

V. Devrelis, M. O'Connor, J. Munch, S. Adshaarvahid, C-J. Wei and A. Grisogono, *Fidelity of Optical Phase Conjugation using Stimulated Brillouin Scattering*, XX International Quantum Electronics Conference, Sydney, Technical Digest, Optical Society of America, WL59, p.165, July 1996.

M. O'Connor, V. Devrelis and J. Munch, *Phase Conjugated Nd:YAG Laser Oscillator with Stimulated Brillouin Scattering*, Proc. Int. Conference on Lasers '95, Charleston, 500-504, December 1995.

V. Devrelis, M. O'Connor and J. Munch, *Coherence Length of Single Laser Pulses by CCD Interferometry,* Applied Optics, Vol. 34, No 24, 5386-5389, August 1995.

M. O'Connor, V. Devrelis, and J. Munch, *Phase Conjugated Nd:YAG Oscillators*, Australian Optical Society 10th Conf. Proc., p. 47, Brisbane, July 1995.

J. Munch, V. Devrelis, A-M. Grisogono, M. O'Connor and C. Wei, *Phase Conjugation in Solid State Lasers,* Australian Optical Society News, Vol. 10, No. 2, 8-12, 22 June 1995.

V. Devrelis, M. O'Connor, P. Foster, J. Munch and A. Grisogono, *Phase Conjugation of Solid State Lasers,* ACOLS Conf. Proceedings, Melbourne, 236, December 1993.

M. O'Connor, V. Devrelis, P. Foster, J. Munch and A. Grisogono, *Optical Phase Conjugated Mirrors for Solid State Lasers,* Australian Optical Society Conf., Sydney, Feburary 1993.

APPENDIX 1

The Nature of Intensity and Phase Modulations in Stimulated Brillouin Scattering

Shahraam Afshaarvahid*, Vladimyros Devrelis† and Jesper Munch

Department of Physics and Mathematical Physics,

The University of Adelaide,

Adelaide, South Australia 5005, Australia

(December 30, 1997)

Abstract

The nature of SBS temporal modulations for a focused beam in a finite-length cell with homogeneous medium is examined numerically. The finite phonon lifetime produces deterministic oscillations at the threshold while the inclusion of the random noise as an initiation source of SBS leads to stochastic fluctuations in Stokes intensity and phase. A unified study of both modulations under different parameters is presented. The results indicate a large useful parameter space for excellent Stokes beam quality.

I. INTRODUCTION

The dynamics of Stimulated Brillouin Scattering (SBS) has been widely investigated because of its importance in optical phase conjugation [1,2], pulse compression [3,4] and beam combination [5–7]. SBS is a non-linear process where energy is exchanged from the laser beam to the Stokes beam through an interaction with a sound wave. When used in an

*shahraam@physics.adelaide.edu.au

†current address is: DSTO, Salisbury SA 5108, Australia

optical element, SBS is usually deployed either as an amplifier with an externally applied Stokes field, or as an SBS generator. The theory of SBS amplifiers is simpler than that of SBS generators since the Stokes field is externally applied. Whereas the analysis of SBS generators requires the inclusion of the thermal density fluctuations of the medium as the source for the initiation of the process. This stochastic initiation of SBS leads to fluctuations in the Stokes field's amplitude and phase [1,8–12]. These fluctuations are important in practical applications since they reduce the coherence length of the scattered beam [13] and have been observed to reduce the temporal and spatial fidelity of the SBS process [14–17]. Early experimental observations of the presence of phase jumps and amplitude fluctuations in SBS were reported in 1980 [18–20]. More recent theoretical and experimental investigations of these fluctuations in optical fibers have been made by Dianov et al. [9], Gaeta and Boyd [11] and Kuzin et al [21]. Their investigations showed that large scale fluctuations in the Stokes intensity occur when the transit time through the interaction region is much greater than the phonon lifetime. Intensity and phase fluctuations have been investigated experimentally also for short interaction lengths typical of a focused geometry [15,13,12,16]. Simultaneous fluctuations in the Stokes amplitude and beam quality have been observed [15] as have actual variation in the phase of the Stokes beam, measured directly by heterodyne detection [13]. In addition, the effect on these simultaneous fluctuations of experimental parameters such as the interaction length and input energy have been reported [12,16]. Numerical models have also shown simultaneous occurrence of jumps in the Stokes phase and fluctuations in the Stokes reflectivity and fidelity [8,14]. Similar fluctuations were also predicted [22,23] and observed [24,25] in stimulated Raman scattering and recognised as solitons.

Most published theoretical studies of SBS have dealt with SBS amplifiers or generators in the undepleted or steady state regime where the Stokes wave was either applied externally or initiated inside the medium from a constant or localised source. In this paper we present for the first time a single unified theoretical approach to SBS in a focused cell geometry, for the transient and depleted regimes while seeded from distributed random noise typical of

most practical applications. We have developed a numerical model to examine in detail how the scattered Stokes beam is initiated from noise and propagated through the medium, and what parameters affect its amplitude and phase modulation. We use a Gaussian random noise distribution [9,11] (both in space and time) as a source for the SBS process in order to simulate the actual thermal fluctuations in the density of the medium.

Our model predicts two kinds of amplitude modulation: a) deterministic relaxation oscillations at the threshold due to finite phonon lifetime and b) stochastic fluctuations caused by the random noise source. A new extensive examination of the behaviour of the deterministic oscillations includes the following parameters: phonon lifetime, focal length, immersion length and input energy and reveals under what parameter regimes these oscillations result in a pulse-compressed Stokes beam. This is followed by the study of stochastic fluctuations and their dependence on parameters such as phonon lifetime, immersion length, input energy and pulse duration. Although many authors identify these fluctuations as being due to phase jumps, our model shows that phase and intensity fluctuations are coupled via the nonlinear interaction, and thus occur simultaneously, denying the existence of a causal relationship to the phenomenon. This was determined by tracing the fluctuations back to the time of initiation. The parameter regime required for achieving excellent beam quality (amplitude and phase fidelity) is evaluated.

II. THEORY:

The equations describing the SBS process are derived from Maxwell's equations for the electric fields and Navier-Stokes equation for the acoustic field inside the material. Writing the electric and acoustic fields as [26]:

$$\begin{aligned} E_p &= \frac{1}{2}[\Psi_p(z,t)e^{i(\omega_p t+k_p z)} + \Psi_p^*(z,t)e^{-i(\omega_p t+k_p z)}] \\ E_s &= \frac{1}{2}[\Psi_s(z,t)e^{i(\omega_s t-k_s z)} + \Psi_s^*(z,t)e^{-i(\omega_s t-k_s z)}] \\ E_q &= \frac{1}{2}[\Psi_q(z,t)e^{i(\omega_q t+k_q z)} + \Psi_q^*(z,t)e^{-i(\omega_q t+k_q z)}] \end{aligned} \tag{1}$$

(where E_p, E_s and E_q are the pump, Stokes and the acoustic fields respectively), neglecting the transverse fields variations and using the slowly varying envelope approximation, the following coupled wave equations can be derived [27].

$$\begin{aligned}(\frac{\partial}{\partial z} - \frac{n}{c}\frac{\partial}{\partial t})\Psi_p &= ig_1\Psi_q\Psi_s \\ (\frac{\partial}{\partial z} + \frac{n}{c}\frac{\partial}{\partial t})\Psi_s &= -ig_1\Psi_q^*\Psi_p \\ (\frac{\partial}{\partial t} + \Gamma)\Psi_q &= -ig_2\Psi_p\Psi_s^*\end{aligned} \tag{2}$$

Here g_1 and g_2 are coupling coefficients, Γ is the damping rate (i.e. $\Gamma = \frac{1}{2\tau}$ where τ is the phonon lifetime of the medium) and n is the refractive index of the medium.

In order to find the equations for the amplitudes and the phases of the fields we write the complex amplitudes Ψ_μ (where $\mu = p, s, q$) as:

$$\Psi_\mu = A_\mu e^{-i\phi_\mu},$$

where A_μ and ϕ_μ are real functions. Substituting the new definition into the above equations results in a set of six coupled differential equations :

$$(\frac{\partial}{\partial z} - \frac{n}{c}\frac{\partial}{\partial t})A_p = -g_1\sin(\phi_p - \phi_s - \phi_q)A_qA_s \tag{3a}$$

$$(\frac{\partial}{\partial z} + \frac{n}{c}\frac{\partial}{\partial t})A_s = g_1\sin(\phi_s + \phi_q - \phi_p)A_qA_p \tag{3b}$$

$$(\frac{\partial}{\partial t} + \Gamma)A_q = g_2\sin(\phi_s + \phi_q - \phi_p)A_sA_p + f_1 \tag{3c}$$

$$(\frac{\partial}{\partial z} - \frac{n}{c}\frac{\partial}{\partial t})\phi_p = -g_1\cos(\phi_p - \phi_s - \phi_q)\frac{A_qA_s}{A_p} \tag{3d}$$

$$(\frac{\partial}{\partial z} + \frac{n}{c}\frac{\partial}{\partial t})\phi_s = g_1\cos(\phi_s + \phi_q - \phi_p)\frac{A_qA_p}{A_s} \tag{3e}$$

$$(\frac{\partial}{\partial t})\phi_q = g_2\cos(\phi_s + \phi_q - \phi_p)\frac{A_sA_p}{A_q} + f_2 \tag{3f}$$

To represent the noise initiation of the SBS process, we have added two Langevin forces f_1 and f_2, with spatial and temporal Gaussian distributions [11]. Both f_1 and f_2 are δ correlated functions in the sense that

$$\langle f_i(z,t) f_i^*(z',t') \rangle = Q\delta(z-z')\delta(t-t')$$

where Q is given by [10]

$$Q = \frac{2kT\rho_o\Gamma}{v^2 A}$$

Here k is the Boltzman constant, T is the temperature, ρ_o is mean density, v is the velocity of sound in the material and A is the cross sectional area of the interaction region.

For the phase locked condition (i.e. $\sin(\phi_s + \phi_q - \phi_p) = 1$) and the steady state regime of SBS (i.e ignoring all $\frac{\partial}{\partial t}A_\mu$), equation (3b) can be written as:

$$\frac{\partial}{\partial z}A_s = \frac{g_1 g_2}{\Gamma}A_p^2 A_s \tag{4}$$

which has a solution of $A_s = A_{so}\exp(\frac{g_1 g_2}{\Gamma}A_p^2 l_{imm})$ valid near threshold and without pump depletion. This leads directly to the usual expression for the steady state gain, given by $G = gI_p l_{imm}$, where I_p is the input pump intensity, l_{imm} is the active medium immersion length and $g = g_1 g_2 \Gamma^{-1}$.

Some authors (e.g. [28,29]) have used the phase locked condition for which SBS has the highest gain, i.e. $\phi_p - \phi_s - \phi_q = \frac{\pi}{2}$. When SBS starts from noise, a random noise distribution of $\phi_p - \phi_s - \phi_q$ is initially present. But as the phase-locked waves, (those with $\phi_p - \phi_s - \phi_q = \frac{\pi}{2}$), have the highest gain in the medium, they suppress other Stokes waves with unlocked-phases. By applying this condition to the equations (3), they are simplified to a set of three real coupled equations for the amplitudes. However, in order to explain the experimental observation of the simultaneous occurrence of intensity fluctuations and phase jumps [13], we have retained the complex equations since this is the only way that the phase of the Stokes field can be coupled to its intensity.

The equations (3) are nonlinear due to the terms $\sin(\phi_s + \phi_q - \phi_p)$ or $\cos(\phi_p - \phi_s - \phi_q)$. Although the behaviour of the fields and their phases is seen better by these equations, and we use them whenever we want to provide a qualitative explanation, solutions of the equations require that we rewrite them for the real and imaginary parts of the fields. Using

$$\Psi_\mu = W_\mu + iV_\mu,$$

the equations for the real and imaginary parts of the fields are:

$$\begin{aligned}
(\frac{\partial}{\partial z} - \frac{n}{c}\frac{\partial}{\partial t})W_p &= -g_1(W_qV_s + V_qW_s) \\
(\frac{\partial}{\partial z} + \frac{n}{c}\frac{\partial}{\partial t})W_s &= g_1(W_qV_p - V_qW_p) \\
(\frac{\partial}{\partial t} + \Gamma)W_q &= -g_2(W_pV_s - V_pW_s) + f_1
\end{aligned} \tag{5}$$

$$\begin{aligned}
(\frac{\partial}{\partial z} - \frac{n}{c}\frac{\partial}{\partial t})V_p &= g_1(W_qW_s - V_qV_s) \\
(\frac{\partial}{\partial z} + \frac{n}{c}\frac{\partial}{\partial t})V_s &= -g_1(W_qW_p + V_qV_p) \\
(\frac{\partial}{\partial t} + \Gamma)V_q &= -g_2(W_pW_s + V_pV_s) + f_2
\end{aligned}$$

The focusing geometry required for simulation of experiments is introduced using an approach similar to Menzel and Eichler [30]. Although, SBS is primarily used to compensate for optical aberrations, we have chosen not to include spatial aberrations in this treatment, but concentrate entirely on temporal fluctuations or "temporal fidelity" of the Stokes beam. This is important, because lack of temporal fidelity leads to degradation of the Stokes return and hence a reduction in average reflectivity and efficiency of a phase conjugated laser system [14–16]. We are thus using spatially unaberrated Gaussian beams for both pump and Stokes fields, and we have made the further approximation that both these fields have the same Gaussian beam parameters (see figure 1):

$$\omega^2(z) = \omega_o^2\left[1 + \left(\frac{(z - z_o)\lambda}{\pi\omega_o^2 n}\right)^2\right],$$

where ω_o is the radius at the waist of the beam, λ is the wavelength and n is the appropriate index of refraction as a function of z. This is a reasonable approximation in an efficient phase conjugating system where the fields are well above threshold and is justified by experimental results showing that the beam quality and divergence of the Stokes beam are indistinguishable from those of the pump beam when well above threshold. For an unaber-

rated beam this is only an approximation but is justified in our case where we concentrate on the temporal fidelity only.

As a result, the pump and Stokes intensities, $I_p = W_p^2 + V_p^2$ or $I_s = W_s^2 + V_s^2$, are changing not only because of the nonlinear interaction with the material but also because of the change in area of the beams. Keeping in mind that for a Gaussian beam the electric field amplitude has a $\omega(z)$ in the denominator, we add $-\frac{W_\nu}{\omega(z)}\frac{\partial}{\partial z}\omega(z)$ or $-\frac{V_\nu}{\omega(z)}\frac{\partial}{\partial z}\omega(z)$ to the right hand side of equations for W_ν or V_ν ($\nu = p$ or s) to represent the change in the intensity due to focussing geometry [30]. Defining

$$\Psi_\nu = \frac{\Psi'_\nu}{\omega(z)} = \frac{W'_\nu}{\omega(z)} + i\frac{V'_\nu}{\omega(z)}$$
$$\Psi'_\nu = W'_\nu + iV'_\nu$$

and hence,

$$W_\nu = \frac{W'_\nu}{\omega(z)}$$
$$V_\nu = \frac{V'_\nu}{\omega(z)},$$

it can be easily seen that $\left|\Psi'_\nu\right|^2 = |\Psi_\nu|^2 \times \omega^2(z)$ is the local power of the pump or the Stokes fields. Adding $-\frac{W_\nu}{\omega(z)}\frac{\partial}{\partial z}\omega(z)$ or $-\frac{V_\nu}{\omega(z)}\frac{\partial}{\partial z}\omega(z)$ to the right hand side of equations for W_ν or V_ν (i.e. equations (5)) and rewriting these equations for prime fields, we find:

$$(\frac{\partial}{\partial z} - \frac{n}{c}\frac{\partial}{\partial t})W'_p = -g_1(W_q V'_s + V_q W'_s) \tag{6a}$$
$$(\frac{\partial}{\partial z} + \frac{n}{c}\frac{\partial}{\partial t})W'_s = g_1(W_q V'_p - V_q W'_p) \tag{6b}$$
$$(\frac{\partial}{\partial t} + \Gamma)W_q = -\frac{g_2}{\omega^2(z)}(W'_p V'_s - V'_p W'_s) + f_1 \tag{6c}$$

$$(\frac{\partial}{\partial z} - \frac{n}{c}\frac{\partial}{\partial t})V'_p = g_1(W_q W'_s - V_q V'_s) \tag{6d}$$
$$(\frac{\partial}{\partial z} + \frac{n}{c}\frac{\partial}{\partial t})V'_s = -g_1(W_q W'_p + V_q V'_p) \tag{6e}$$
$$(\frac{\partial}{\partial t} + \Gamma)V_q = -\frac{g_2}{\omega^2(z)}(W'_p W'_s + V'_p V'_s) + f_2 \tag{6f}$$

We see that the new equations have a form similar to equations (5). The only difference is that the prime fields are the power components instead of intensity components in equations (5). The same procedure can be done for equations (3) to get the following equations for the Stokes, pump and acoustic grating power:

$$(\frac{\partial}{\partial z} - \frac{n}{c}\frac{\partial}{\partial t})A_p^{'} = -g_1 \sin(\phi_p - \phi_s - \phi_q)A_q A_s^{'} \tag{7a}$$

$$(\frac{\partial}{\partial z} + \frac{n}{c}\frac{\partial}{\partial t})A_s^{'} = g_1 \sin(\phi_s + \phi_q - \phi_p)A_q A_p^{'} \tag{7b}$$

$$(\frac{\partial}{\partial t} + \Gamma)A_q = g_2 \sin(\phi_s + \phi_q - \phi_p)\frac{A_s^{'}A_p^{'}}{\omega^2(z)} + f_1 \tag{7c}$$

The equation for the acoustic field shows how the amplitude of the field depends on the intensity of the Stokes and pump waves, implying a high acoustic field at high intensities of the pump and the Stokes fields.

Integrating the phonon fields (equations (6c) and (6f)) and substituting in the rest of the equations (6), reduces the set of equations (6a)-(6f) to four coupled differential equations for the fields amplitude. The numerical analysis starts with these four equations. An efficient noniterative algorithm is used in which Simpson's rule is applied to approximate the phonon's integral and an implicit finite differencing in time and backward differencing scheme in space are used to write the equations for discrete field amplitudes $W_p{}_j^m, V_p{}_j^m, W_s{}_j^m$ and $V_s{}_j^m$, where $m = 0, 1, 2, ...M$ are time indices ($t = m\Delta t$) and $j = 0, 1, 2, ...n + 1$ are space indices ($z = j\Delta z$) [29]. Field vectors at the time $(m + 1)\Delta t$ are defined as:

$$\overrightarrow{W_p}^{m+1} = \begin{pmatrix} W_{p\ 1} \\ W_{p\ 2} \\ . \\ . \\ . \\ W_{p\ n} \end{pmatrix}^{m+1} ; \overrightarrow{V_p}^{m+1} = \begin{pmatrix} V_{p\ 1} \\ V_{p\ 2} \\ . \\ . \\ . \\ V_{p\ n} \end{pmatrix}^{m+1}$$

$$\overrightarrow{W_s}^{m+1} = \begin{pmatrix} W_{s\ 2} \\ W_{s\ 3} \\ . \\ . \\ . \\ W_{s\ n+1} \end{pmatrix}^{m+1} ; \overrightarrow{V_s}^{m+1} = \begin{pmatrix} V_{s\ 2} \\ V_{s\ 3} \\ . \\ . \\ . \\ V_{s\ n+1} \end{pmatrix}^{m+1} ,$$

where $n+1$ is the total number of discrete points in space and $W_{p\ n+1}$, $V_{p\ n+1}$, $W_{s\ 1}$ and $V_{s\ 1}$ are the initial values at boundaries.

Using the linearization scheme defined by Chu et al. [29], we obtain the final form of the set of algebraic equations for the vector fields as:

$$\begin{aligned} A^m \overrightarrow{W_p}^{m+1} + C^m \overrightarrow{W_s}^{m+1} + D^m \overrightarrow{V_s}^{m+1} &= \overrightarrow{V} \\ E^m \overrightarrow{W_s}^{m+1} + F^m \overrightarrow{W_p}^{m+1} + G^m \overrightarrow{V_p}^{m+1} &= \overrightarrow{U} \\ A^m \overrightarrow{V_p}^{m+1} - D^m \overrightarrow{W_s}^{m+1} + C^m \overrightarrow{V_s}^{m+1} &= \overrightarrow{W} \\ E^m \overrightarrow{V_s}^{m+1} - G^m \overrightarrow{W_p}^{m+1} + F^m \overrightarrow{V_p}^{m+1} &= \overrightarrow{Z} \end{aligned} \tag{8}$$

Here, A^m, C^m, E^m, F^m, D^m, and G^m are $n \times n$ upper or lower tridiagonal matrices evaluated at time $m\Delta t$ and $\overrightarrow{V}$, $\overrightarrow{U}$, $\overrightarrow{W}$ and $\overrightarrow{Z}$ are $n \times 1$ vectors containing boundary conditions on the pump and Stokes at time $t = (m+1)\Delta t$. This set of equations can be solved numerically without the need for iteration. The matrix coefficients and vectors $\overrightarrow{V}$, $\overrightarrow{U}$, $\overrightarrow{W}$ and $\overrightarrow{Z}$ are evaluated recursively using the initial values of the Stokes and pump fields at $t = 0$. Here the field amplitudes at any time slot $m+1$ have been determined from those at the preceding time slot m. To justify the validity of the linearization assumption, we used the field amplitudes at time slot $m+1$ to re-evaluate iteratively the nonlinear coefficient involved in the differential equations. An improvement of only 4% was achieved after 5 iterations.

Solutions of equations (8) are found for a Gaussian pump pulse of the form $E_0 \exp(-2[\frac{t-t_o}{t_p}]^2)$, where t_p is the pulse width. Referring to figure 1, we apply the following

geometrical and material parameters to examine the typical results of the SBS process: cell length = 60 cm, focal length = 50 cm, immersion length = 15 cm, initial waist of the beam = 0.4 cm, gain of the medium = 0.0063 cm/MW, input energy = 320 mJ, FWHM pulse length = 20 ns, phonon lifetime = 0.85 ns and index of refraction, $n = 1.0$, with results shown in figure 2.

III. RESULTS AND DISCUSSION:

Depending on the geometry of the SBS process and the energy of the input pulse, our model results in Stokes oscillations or fluctuations similar to those observed experimentally [18–20,15–17]. The intensity modulation can be categorised into two groups: a) deterministic amplitude oscillations at the time when the energy of the pump reaches the threshold energy and b) stochastic fluctuations due to noise in amplitude and phase of the Stokes beam.

A. Deterministic Threshold Oscillation:

The finite phonon lifetime provides an energy interchange mechanism between the Stokes and laser field via the acoustic field. In the case of Gaussian pump beams, it takes some time for the energy contained in the pump to reach the threshold energy for Stokes initiation. At the threshold, the Stokes power increases very rapidly and overshoots the pump power resulting in the depletion of the pump field and reduction of gain. Because of this gain reduction the Stokes power drops, causing an increase in the pump energy which in turn causes an increase in the Stokes field again. This energy interchange between the Stokes and pump fields continues and resembles a relaxation oscillation (see figure 3). The rate of this energy interchange is controlled by the reaction time of the acoustic field, i.e. phonon lifetime. Such an energy interchange mechanism has also been discussed in Ref. [4] and [29]. Chu et al. [29] report relaxation oscillations which are visible in the transmitted pulse. However, our simulation results show that for a long cell and a geometry in which the laser

beam has been focused deeply into the cell, relaxation oscillation should be visible in the Stokes return as shown in figure 3.

In order to categorise the behaviour of threshold oscillation we use the following parameters to run the simulation: Cell length 100 cm, focal length 100 cm, immersion length 70 cm, phonon lifetime 0.85 ns, gain of the medium 0.006 cm/MW, FWHM pulse length 20 ns and input energy 114 mJ. Any changes to these parameters are specified in the caption of the figures. Figure 3 shows a typical threshold oscillation in the Stokes beam. Different parameters such as phonon lifetime, laser intensity at the focal point and immersion length affect the behaviour of the threshold oscillation. There are no phase jumps predicted corresponding to these oscillations.

1. Effect of phonon lifetime on the threshold oscillation:

If the finite phonon lifetime is responsible for the relaxation oscillation at the threshold energy, we would expect that the behaviour of the threshold oscillations depends on this parameter. Figure 4 shows the threshold oscillation for two different phonon lifetimes. Defining T_o to be the time interval over which the threshold oscillations are observable (see figure 4), our simulation predicts that T_o is reduced for long phonon lifetime (see figure 5). It is seen that for longer phonon lifetimes, oscillations in the Stokes return come to an equilibrium faster than those for short phonon lifetimes. Our model permits a detailed investigation of the above mentioned relaxation oscillation and the role of the phonon lifetime.

The acoustic field is described by equation (3c). For early times in the process, the first source term in the right hand side of the equation may be ignored and for the second term we can write $f_1 = \sum_k a_k \sin \omega_k t$. Equation (3c) can then be solved as

$$\Psi_q = \Psi_{oq} e^{-\Gamma t} + \sum_k a'_k \sin \omega_k t + \sum_k b'_k \cos \omega_k t,$$

in which $a'_k = a_k \Gamma (\Gamma^2 + \omega_k^2)^{-1}$ and $b'_k = -a_k \omega_k (\Gamma^2 + \omega_k^2)^{-1}$. In the limit of a long phonon lifetime i.e. $\Gamma \to 0 (\tau \to \infty)$ we find $a'_k = 0$ and $b'_k = -\frac{a_k}{\omega_k}$, which results in a solution of

$\Psi_q = \sum_k -\frac{a_k}{\omega_k} \cos \omega_k t$ for the acoustic field. Comparing this result with the source term f_1, it is seen that in the limit of a large phonon lifetime the medium will not respond to the rapid fluctuations in the source term, but rather responds to the integral of rapid changes. In the other limit of $\Gamma \rightarrow \infty (\tau \rightarrow 0)$, $b'_k \rightarrow 0$ and $a'_k = \frac{a_k}{\Gamma}$ which gives a solution of $\Psi_q = \sum_k \frac{a_k}{\Gamma} \sin \omega_k t$. In this case the medium can cope with the rapid changes in the source term, thus resulting in a modulated Stokes pulse. The above discussion is applicable not only for the beginning of the process but also for any rapid changes in the source fields of the acoustic field. The phonon lifetime thus represents a measure of the inertia of the acoustic field. The larger the phonon lifetime, the higher is the inertia of the acoustic field and the slower is the response of the medium to the rapid changes in the Stokes and the laser field.

2. Effect of laser intensity at the focal plane:

According to the equation (7c), the amplitude of the acoustic field depends on the intensity of the input pulse. A shorter focal length results in a higher intensity at the focal plane hence a higher power acoustic wave. As a result of this strong acoustic field, the Stokes amplitude does not reduce as quickly after overshooting, which in turn causes a shorter duration of the relaxation oscillation. This is illustrated in figure 6.

3. Effect of immersion length:

Kuzin et al [21] have discussed the influence of the depletion length, (the length over which the laser pump beam experiences most of its depletion), on the suppression of fluctuations in the Stokes field. They emphasised that if the propagation time through the depletion length $T_{l_{dep}}$ is smaller than the temporal variation of the Stokes field at the beginning of the depletion region T_s, a smoothing of the Stokes field towards the output of the cell would take place. In this case we are in the steady state regime of SBS, and can rewrite equations (3) in the phase locked condition, as

$$\frac{\partial}{\partial z} I_p = 2g I_p I_s$$
$$\frac{\partial}{\partial z} I_s = 2g I_p I_s \tag{9}$$

Moving the origin of z to the entrance of the cell and writing $I_p(z) = I_s(z) + I_l$ [31] (where I_l is a constant indicating the degree of pump depletion), we can solve the differential equations (9) to find :

$$I_s(z) = \frac{I_l I_s(0)}{I_p(0)\exp(-2gI_l z) - I_s(0)}$$

Defining the depletion length as the length over which the Stokes intensity drops to $\frac{1}{e}$ of its maximum (i.e. $I_s(l_{dep}) = \frac{1}{e} I_s(0)$), we find :

$$l_{dep} = \frac{1}{2gI_l} \ln(1 + \frac{I_l(e-1)}{I_p(0)})$$

Which can be approximated as

$$l_{dep} \approx \frac{l_{imm}}{G} \tag{10}$$

for highly depleted pump (i.e. $I_l \longrightarrow 0$), and using the definition of G.

A parallel physical explanation of conditions under which temporal fluctuations are suppressed is given by Gaeta and Boyd [11]. They discuss how a spike with temporal variation $T_s = \Gamma^{-1}$ is suppressed when $G > \Gamma T_t$ (where $T_t = n l_{imm} c^{-1}$ is the transit time and $G = g I_p l_{imm}$ is the steady state gain). This condition ($G > \Gamma T_t$) is similar to the Kuzin et al [21] condition (i.e. $T_{l_{dep}} < T_s$), if we use the depletion length given by equation (10).

Keeping constant all other parameters and varying only the immersion length, by changing the cell to lens separation, we can examine the effect of immersion length on the threshold oscillations. Figure 7 shows the behaviour of the threshold oscillation for two different immersion lengths. For a smaller immersion length, figure 7 (b), the depletion region of the pump beam is confined to a small region at the entrance of the cell resulting in a shorter relaxation oscillation.

It thus appears possible to use the advantages of a short focal length and a short immersion length to smooth out the oscillations. These conditions are confirmed to provide the

best temporal fidelity of pump pulse in SBS process, figure 8, and appear to agree with preliminary experimental results [32]. A more complete experimental investigation is planned for a later publication.

4. Pulse Compression

As mentioned previously the threshold relaxation oscillation is due to the energy interchange between the pump and the Stokes fields. We can expect to achieve pulse compression if we do not provide the appropriate amount of energy for the Stokes pulse to rebuild after the first impulse of relaxation oscillation. Figure 9 shows how the relaxation oscillation converts to a compressed pulsed as input energy is reduced from graph a) to d). The process of pulse compression can be better seen if we look at the 3D graph of the Stokes power, figure 10. At early times of the process, the center of maximum reflectivity (maximum of the Stokes pulse) is close to the focal region. This center moves towards the entrance of the cell at a later time. As a result, latter parts of the incoming pulse are traveling a shorter distance before generating the Stokes return, resulting in pulse compression [3,4].

B. Stochastic Fluctuations of Phase and Amplitude

Noise initiation of the SBS process results in large scale fluctuations in the Stokes output. These fluctuations are of stochastic nature in the sense that there is a random probability for the occurrence of the fluctuations as well as for their temporal position in the output Stokes pulse. Corresponding and simultaneous to these fluctuations in the Stokes power, there are some rapid changes in the Stokes phase (see figure 11). The simultaneous occurrence of jumps in the Stokes phase and fluctuations in the stokes power can be understood from the main equations governing SBS (equations 3). On the right hand side of these equations there are two effective gain terms, $g \sin(\ \phi_q + \phi_s - \phi_p)$ or $g \cos(\ \phi_q + \phi_s - \phi_p)$ which are affected by rapid changes in phase of the fields. Figure 11 (b) shows how the normalized effective gain $g \sin(\ \phi_q + \phi_s - \phi_p)$ suffers a reduction at the time when a phase jump occurs in the Stokes

field. Depending on the size of the phase jump and the phase behaviour of the pump and acoustic field, the effective gain can be reduced or even become negative, which interchanges the role of Stokes and pump field i.e. the pump field gains while the Stokes field depletes. This is similar to what happens in the generation of solitons in stimulated Raman scattering [33]. The final temporal position of phase jumps as well as the shape of the fluctuations in the output of the Stokes phase and power depend on how they propagate and amplify from the initiation point (focal point) towards the entrance of the cell. Stokes pulses, initiated from noise, are amplified in two main regions as they propagate towards the output of the cell. In the first region, initial amplification and spectrum narrowing of the Stokes beam growing from noise take place [20,34,35,11,36,21]. The second region of length l_{dep} (eq. 10), is where the final amplification of the Stokes beam, to a level approximately equal to the pump power occurs. The final Stokes output can be greatly affected by the dynamic processes in the depletion region. As previously discussed, this region plays a crucial role in the suppression of fluctuations in the Stokes signal when $T_{l_{dep}} < T_s$. For $T_{l_{dep}} > T_s$, however, fluctuations in the Stokes pulse experience amplification and spectrum changes, and appear in the final output [21]. It has been shown that different spectra of the fluctuations in the Stokes pulse experience different gain depending on the phonon lifetime and the length of this region [36,21]. As a result, the output spectrum of the fluctuations is different from the input when propagating through the depletion region [36,21]. Considering this and the fact that the depletion lengths l_{dep} corresponding to different temporal parts of the Stokes beam are different (see eq. 10, where the gain $G(t) = gI_p(t)l_{imm}$ is a function of time), lead to changes in the shape of fluctuations as well as the temporal position of corresponding phase jumps in propagating through the depletion region. The results from our model also display such behaviour as shown in fig. 12. It shows the temporal position of the phase jump and the beginning of the fluctuation in the figure 11 as a function of time at different positions in the cell.

The focusing geometry of the SBS cell, input energy and phonon lifetime of the material affect the phase jump fluctuations. Due to the stochastic nature of the fluctuations, the

width, magnitude and the number of fluctuations vary from pulse to pulse. As a result, we have chosen the fraction of the Stokes energy contained in the fluctuations i.e. $< \frac{E_{fluc}}{E_{output}} >$ (where <> means statistical average over all number of pulses) as the best parameter to show the importance of the fluctuations to a practical deployment of SBS in a laser system. Unless otherwise stated, the following parameters are applied for the numerical simulations: cell length = 60 cm, focal length = 60 cm, immersion length = 30 cm, phonon lifetime = 0.85 ns, input beam radius at window = 0.3 cm, gain of the medium = 0.0063 cm/MW, input energy = 119 mJ, FWHM pulse length = 20 ns and refractive index = 1.36.

1. Phonon lifetime effect on the phase jump fluctuations:

As was previously discussed, the phonon lifetime is a measure of the acoustic field inertia. For a medium with a long phonon lifetime, the acoustic field can not respond quickly to the rapid fluctuations in the noise initiated Stokes field, and it thus broadens and smoothens out the fluctuations in the Stokes field. To examine the effect of phonon lifetime on the phase jump fluctuations, the simulation model was run with different initial noise distributions for three different phonon lifetimes. The fluctuation energy (normalised to the output energy and averaged over certain number of shots) is calculated for these different phonon lifetimes. Figure 13 shows how the energy of the fluctuations decreases for higher phonon lifetime, indicating a better suppression of fluctuations for long phonon lifetimes.

2. Effect of immersion length:

As mentioned previously, the two key parameters in suppressing the fluctuations are the propagation time through the depletion region $T_{l_{dep}}$ and the temporal variation of Stokes signal T_s which reaches the depletion region. In the case when $T_{l_{dep}} < T_s$ the fluctuations in the Stokes signal are suppressed as they pass through the depletion region while in the other case, $T_{l_{dep}} > T_s$, they are magnified and appear in the final Stokes output. The depletion length l_{dep} depends (roughly) on the steady state gain G and the immersion length l_{imm} (see

equation (10)). By controlling G and l_{imm} we are thus able to change the length of depletion region. From the condition $T_{l_{dep}} > T_s$, it is clear that reducing $T_{l_{dep}}$, implies a reduction on the number of fluctuations as well as their durations in the final Stokes output.

A shorter depletion length can be obtained for a short immersion length (achieved by long cell-lens separation) and as a result, we would expect a better suppression of fluctuations. Figure 14 shows how averaged fluctuation energy $< \frac{E_{fluc}}{\overline{E}_{out}} > \%$ (normalised to output energy) changes as a function of the immersion length. We thus conclude that a small immersion length achieved by large cell to lens separation provides better suppression of fluctuations.

3. Effect of input energy:

Another parameter that can affect the depletion length is input energy. Higher input energy results in a higher gain G, which in turn reduces the depletion length, l_{dep}, of the SBS. As discussed above, we thus expect that fluctuations in the output Stokes beam have smaller duration i.e. they carry less energy. In order to examine the effect of input energy, we have studied the output Stokes beam of 500 simulated pulses with different initial noise distribution and at different energies. Considering the histogram of $\frac{E_{out}}{(\overline{E}_{out})}$ for these 500 pulses, where $\overline{E}_{out}$ is the mean energy of all output pulses, and fitting a Gaussian function to it, we find that the width of the Gaussian fit is reduced at higher energy i.e. the variation in output energy per pulse around the mean value is reduced for high energy (see figures 15). Another parameter that can show how fluctuations are suppressed for high energies is the average of the fluctuation energy (normalised to output energy). Simulation results in figure 16 show a reduction in the averaged fluctuation energy for higher input energies.

4. Effect of pulse duration:

In the above section, we kept the duration of the input pulse constant and we studied the effect of parameters such as input energy and beam area on the fluctuations. In order to

observe the role of pulse duration, we have chosen to keep the input energy of the pulse constant and reduced the pulse duration, i.e. we increased the peak injected power. Simulation results show a dramatic reduction in the number of fluctuations for short pulse durations which in turn results in a smaller averaged fluctuation energy (figure 17).

IV. CONCLUSION

To describe different kinds of temporal amplitude and phase modulations in SBS, we extended the plane-wave equations for complex fields describing SBS in a finite cell to include focusing geometry and initiation from a Gaussian random noise distributed over space and time. Two kinds of modulations were found.

(1) Deterministic relaxation oscillation at the threshold energy.

(2) Random fluctuations in the output Stokes power.

The finite phonon lifetime of a material is responsible for an energy interchange between the pump and Stokes field resulting in relaxation oscillations at the threshold. There is no modulation of the Stokes phase corresponding to these oscillations. It is predicted that materials with shorter phonon lifetimes can exhibit relaxation oscillations of longer duration than those with long phonon lifetimes. It was found that an initially stronger acoustic wave (resulting from a high focal intensity determined by the focal length of the lens) shortens the relaxation oscillations at the threshold energy since the Stokes pulse can use the energy stored in the acoustic field after initially overshooting. Also, a small immersion length achieved by a large cell to lens separation reduces the threshold relaxation oscillations. All together, short focal length, short immersion length and large phonon lifetime provide the best parameter space for removing the threshold relaxation oscillations.

SBS initiated from microscopic noise shows large scale stochastic amplitude modulation in the output Stokes beam. Simultaneous and corresponding jumps in the Stokes phase are observed. We have determined a parameter regime where this modulation is minimised or eliminated, thus predicting conditions for optimised, reliable SBS:

1) Longer phonon lifetime provides a better suppression of instabilities in the Stokes pulse.

2) Depending on the input energy and focused spot size, the pump and Stokes field can be confined to a small region near the entrance of the cell (high energies, short immersion length) or distributed towards the focal point for low energies and long immersion length. For high input energies or short immersion length the time for propagation through this region $T_{l_{dep}}$is small enough to suppress many of the fluctuations reaching this region with duration $T_s > T_{dep}$. Short immersion length achieved by large cell to lens separation is more desirable since $T_{l_{dep}}$ can be reduced more effectively and a higher reflectivity can be achieved, but will in practice be limited by optical break down of the SBS material or cell window.

3) Another parameter that can be used effectively to suppress the fluctuations is pulse duration. Our results showed that for a shorter pulse duration (i.e. higher peak power) the number of fluctuations was reduced dramatically.

REFERENCES

[1] B. Y. Zel'dovich, N. F. Pilipetsky, and V. Shkunov, *Principles of Phase Conjugation* (Springer-Verlag, Berlin, 1985).

[2] D. A. Rockwell, IEEE. J. Quantum Electron. **24**, 1124 (1988).

[3] D. T. Hon, Opt. Lett. **5**, 516 (1980).

[4] M. J. Damzen and H. Hutchinson, IEEE Journal of Quantum Electronics **19**, 7 (1983).

[5] N. G. Basov, V. F. Efimkov, I. G. Zubarev, A. V. Kotov, S. I. Mikhailov, and M. G. Smirnov, JETP Lett. **28**, 197 (1978).

[6] M. Valley, G. Lombardi, and R. Aprahamian, J. Opt. Soc. Am. B **3**, 1492 (1986).

[7] K. D. Ridley and A. M. Scott, J. Opt. Soc. Am. B **13**, 900 (1996).

[8] S. M. Wandzura, *proceedings of the Conference on Laser and Electro-Optics, Anaheim, CA, 1988* (Optical Society of America, Washington, DC, 1988), p. 8.

[9] E. M. Dianov, A. Y. Karasik, A. V. Lutchnikov, and A. N. Pilipetskii, Optical and Quantum Electronics **21**, 381 (1989).

[10] R. W. Boyd, K. Rzazewski, and P. Narum, Phys. Rev. A **42**, 5514 (1990).

[11] A. L. Gacta and R. W. Boyd, Physical Review A **44**, 3205 (1991).

[12] T. R. Moore, A. L. Gaeta, and R. W. Boyd, *Proceedings of International Quantum Electronics Conference, USA, 1993* (Optical Society of America, Washington, DC, 1993), pp. 394–395.

[13] M. S. Mangir, J. J. Ottusch, D. C. Jones, and A. Rockwell, Physical Review Letters **68**, 1702 (1992).

[14] W. P. Brown and S. M. Wandzura, *proceedings of the Conference on Laser and Electro-Optics, Anaheim, CA, 1988* (Optical Society of America, Washington, DC, 1988), p.

10.

[15] J. Munch, R. F. Wuerker, and M. J. LeFebvre, Applied Optics **28**, 3099 (1989).

[16] V. Devrelis, M. O'Connor, J. Munch, S. Afshaarvahid, C. J. Wei, and A. M. Grisogono, *Proceedings of International Quantum Electronics Conference, Sydney, Australia , 1996* (Optical Society of America, Washington, DC, 1996), p. 164.

[17] V. Devrelis, in PhD Thesis, University of Adelaide, August 1997 (unpublished).

[18] N. G. Basov, I. G. Zubarev, A. B. Miranov, S. I. Mikhailov, and A. Y. Okulov, JETP Lett. **31**, 645 (1980).

[19] M. V. Vasil'ev, A. L. Gyulameryan, A. V. Mamaev, V. V. Ragul'skii, P. M. Semenov, and V. G. Siderovich, JETP Lett. **31**, 634 (1980).

[20] V. I. Bespalov, A. A. Betin, G. A. Pasmanik, and A. A. Shilov, JETP Lett. **31**, 630 (1980).

[21] E. Kuzin, M. Petrov, and A. Fotiadi, *Principles of Phase Conjugation* (Springer-Verlag, Berlin, 1994).

[22] J. C. Englund and C. M. Bowden, Phys. Rev. Lett. **57**, 2661 (1986).

[23] C. M. Bowden and J. C. Englund, Opt. Commun. **67**, 71 (1988).

[24] Y. Akiyama, K. Midorikawa, M. Obara, and H. Tashiro, J. Opt. Soc. Am. B **8**, 2459 (1991).

[25] D. C. MacPherson, R. C. Swanson, and J. L. Carlsten, Phys. Rev. Lett. **61**, 66 (1988).

[26] W. Kaiser and M. Maier, in *"Stimulated Rayleigh, Brillouin and Raman Spectroscopy", Laser Handbook*, edited by F. T. Arecchi and E. O. Schuls-Dubis (North-Holland, Amsterdam, 1972), Vol. 2, pp. 1077–1149.

[27] G. C. Valley, IEEE Journal of Quantum Electronics **22**, 704 (1986).

[28] A. Kummrow and H. Meng, Optics Communications **83**, 342 (1991).

[29] R. Chu, M. Kanefsky, and J. Falk, J. Appl. Phys. **71**, 4653 (1992).

[30] R. Menzel and H. J. Eichler, Physical Review A **46**, 7139 (1992).

[31] C. L. Tang, J. Appl. Phys. **37**, 2945 (1966).

[32] M. O'Conor, in PhD Thesis, University of Adelaide, September 1997 (unpublished).

[33] D. C. MacPherson and J. L. Carlsten, J. Opt. Soc. Am. B **4**, 1853 (1987).

[34] Z. M. Benenson *et al.*, JETP Lett. **42**, 202 (1985).

[35] E. M. Dianov, A. Y. Karasik, A. V. Lutchnikov, and A. K. Senatorov, Sov. J. Quantum Electron **19**, 508 (1989).

[36] A. A. Fotiadi and E. A. Kuzin, *Proceedings of International Quantum Electronics Conference, USA, 1994* (Optical Society of America, Washington, DC, 1994), p. 84.

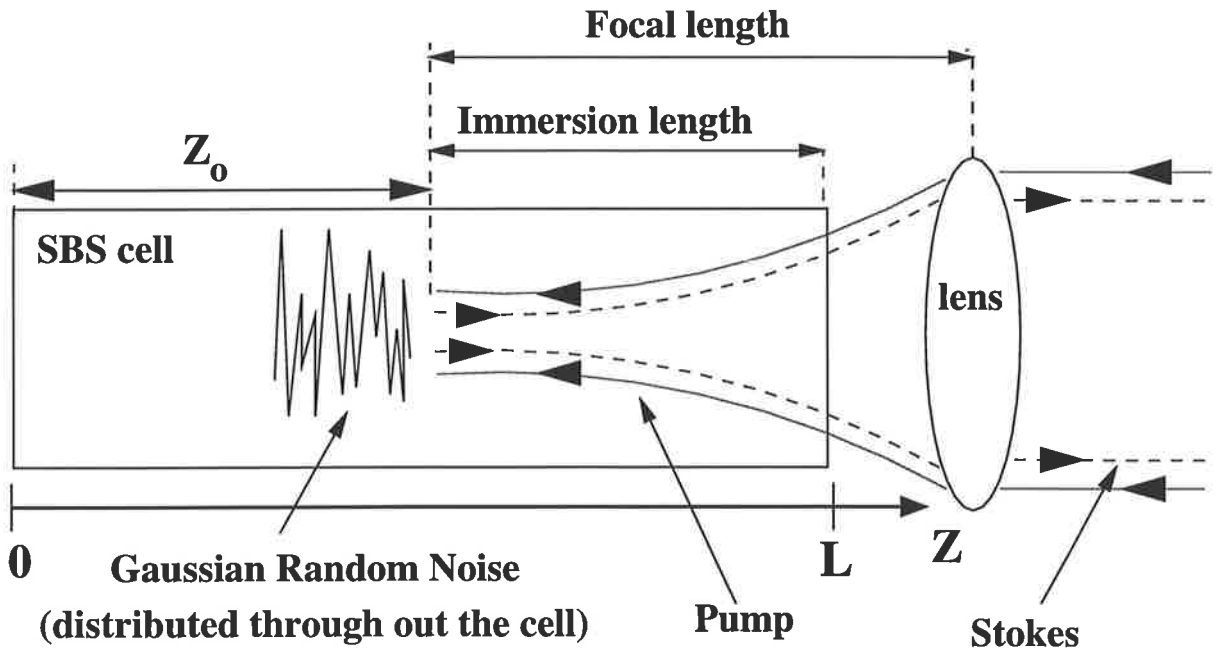

FIG. 1. The geometry used for the SBS process.

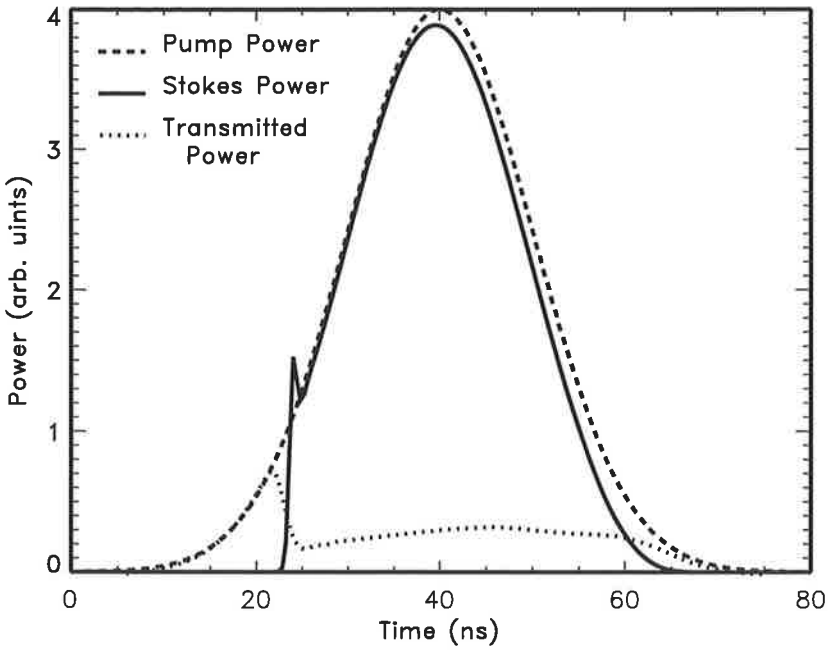

FIG. 2. Typical results for the Stokes, pump and transmitted pulse.

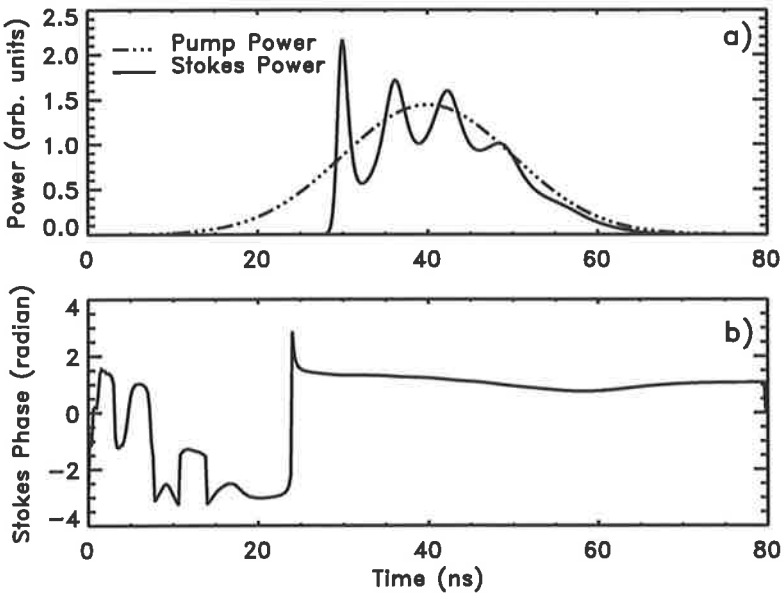

FIG. 3. (a) Typical threshold oscillation in the Stokes beam obtained for the following parameters : cell length 100 cm, focal length 100 cm, immersion length 70 cm, phonon lifetime 0.85 ns, medium gain 0.006 cm/MW, FWHM pulse length 20 ns and input energy 114 mJ. 3(b) shows no corresponding variation in the phase of the Stokes.

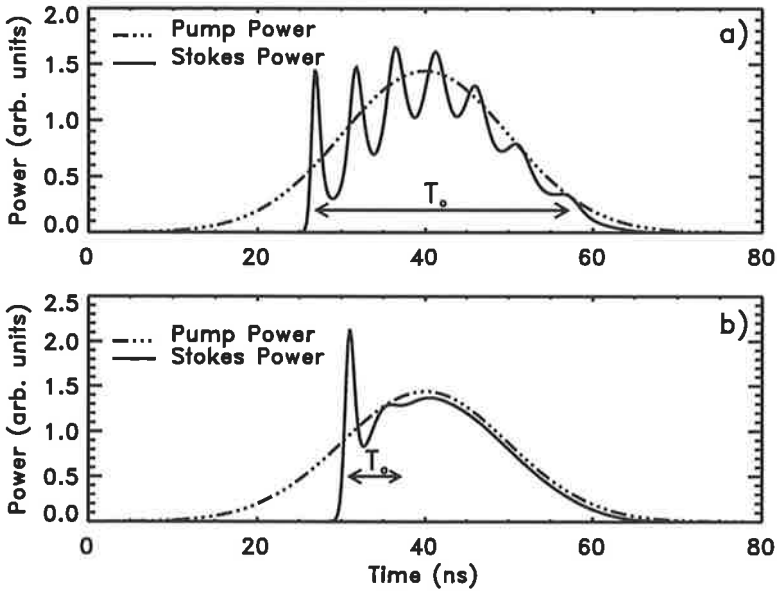

FIG. 4. Threshold oscillations are reduced for longer phonon lifetime. Graph a): phonon lifetime is 0.5 ns and graph b): phonon lifetime is 1.25 ns. Other parameters are as those of figure 3.

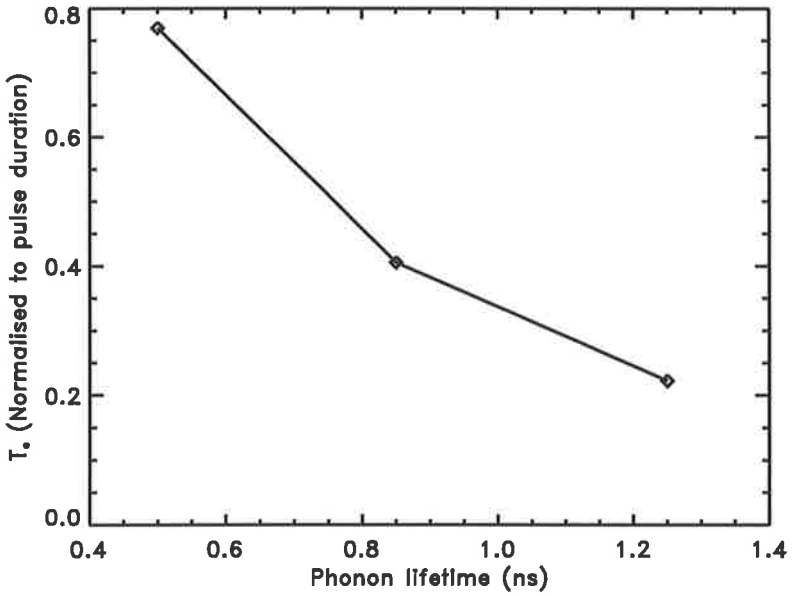

FIG. 5. A shorter relaxation oscillation is achieved for long phonon lifetime. The graph shows how T_o (a time interval over which the oscillations are visible, see figure 4.) is reduced for long phonon lifetime.

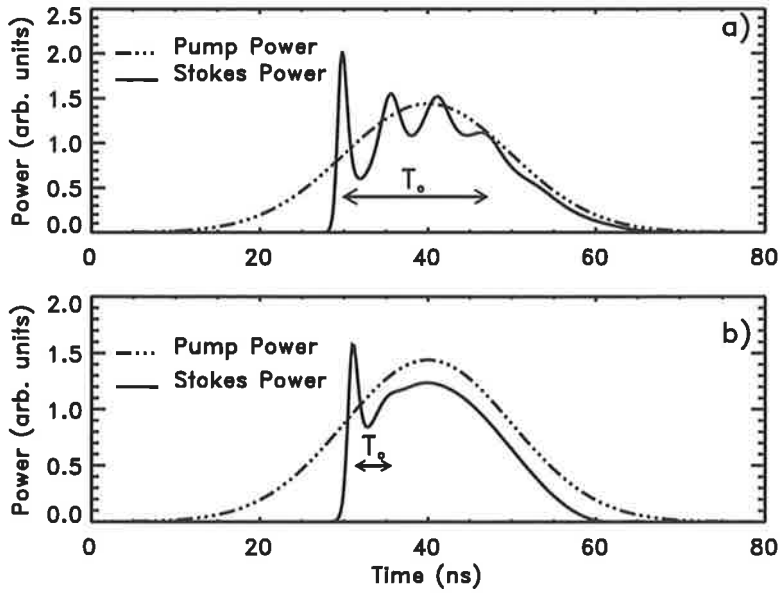

FIG. 6. Smaller focal spot (higher intensity) results in a suppression of threshold oscillations. Oscillations are reduced in graph (b) (focal length 60 cm) in comparison with graph(a) (focal length 90 cm). Other parameters as in figure 3.

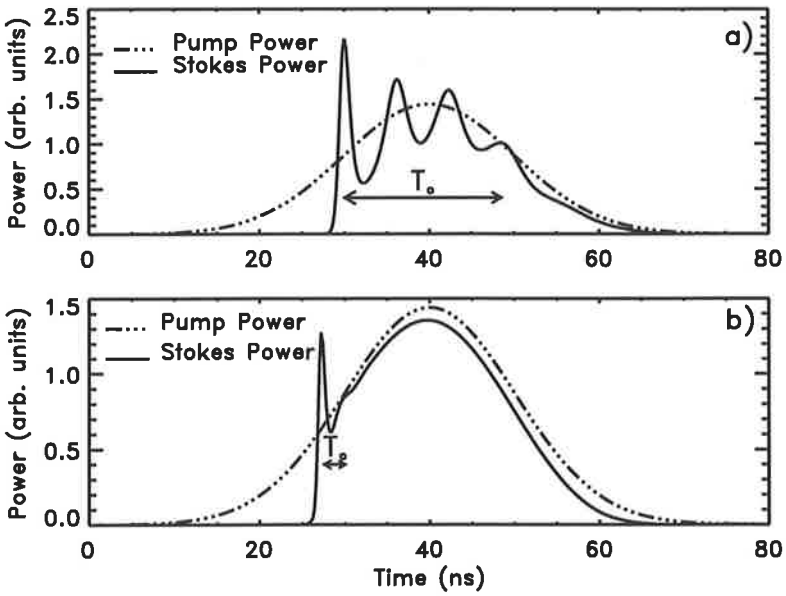

FIG. 7. Modulations present in (a) (focal length=100 cm, immersion length=40 cm) are almost suppressed in (b) (focal length=100 cm, immersion length=10 cm). Shorter immersion length provides a better suppression. Other parameters as in figure 3.

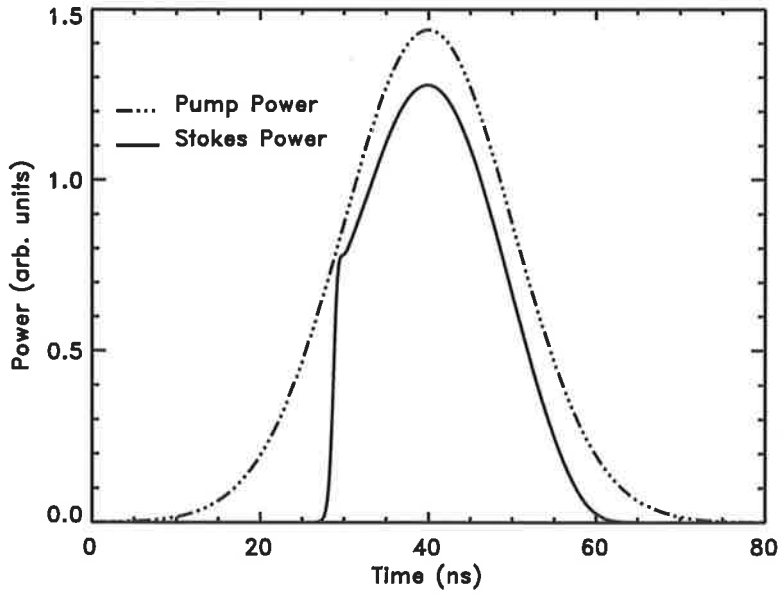

FIG. 8. Threshold oscillations disappear for short focal length and immersion length. Immersion length =20 cm and focal length =60 cm, other parameters as standard set shown in figure 3.

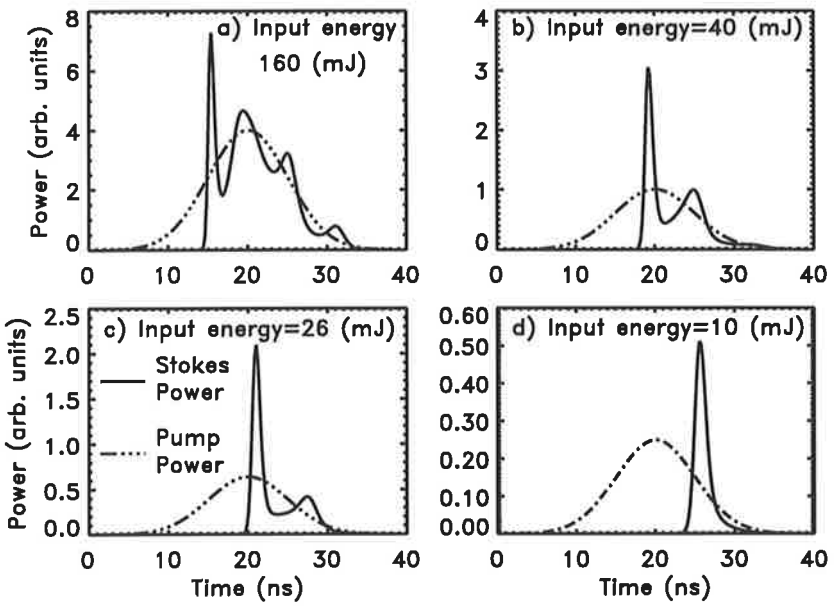

FIG. 9. Pump and Stokes power as function of time at the entrance to the cell. By reducing the pump energy, we remove extra oscillations from the threshold oscillations, resulting in a pulse compressed beam. Cell length=80 cm, focal length=80 cm and immersion length =70 cm with all other parameters as in Fig 3. In 9(d) the delay in peak Stokes and peak pump is due to the round trip time of the cell and building to threshold.

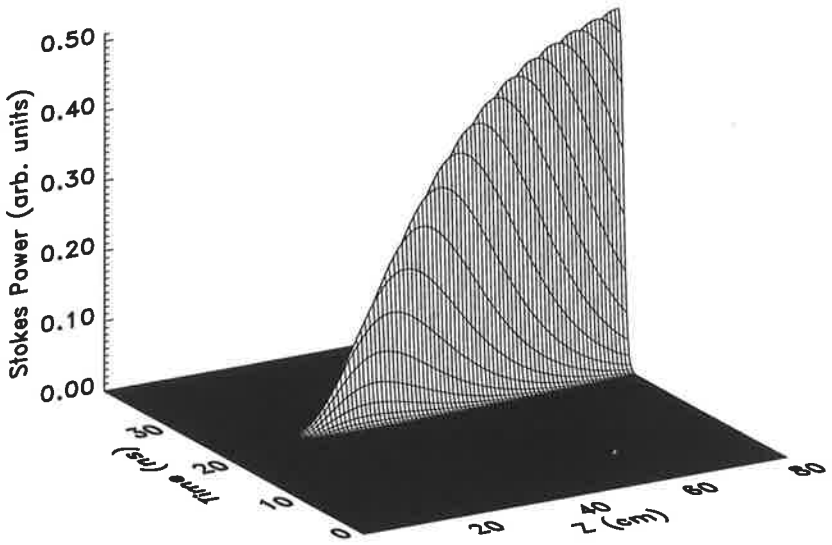

FIG. 10. 3D graph of pulse compression (graph d) in figure (9). Stokes power in time and space shows how the center of maximum reflectivity moves towards the entrance of the SBS cell (z = 80 cm) resulting in pulse compression. Parameters as in Fig 9.

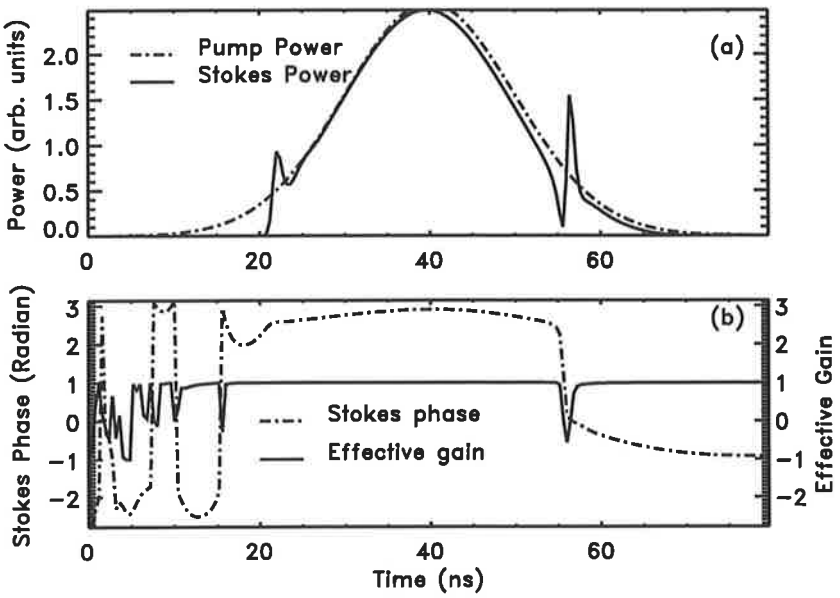

FIG. 11. Corresponding and simultaneous to each fluctuation in the Stokes output, (a), there is a jump in the Stokes phase (dashed curve in (b)). Parameters are set as: cell length 60 cm, focal length 60 cm, immersion length 30 cm, Phonon lifetime 0.85 ns, gain of the medium 0.0063 cm/MW, refractive index 1.36, FWHM pulse length 20 ns and input energy 119 mJ.

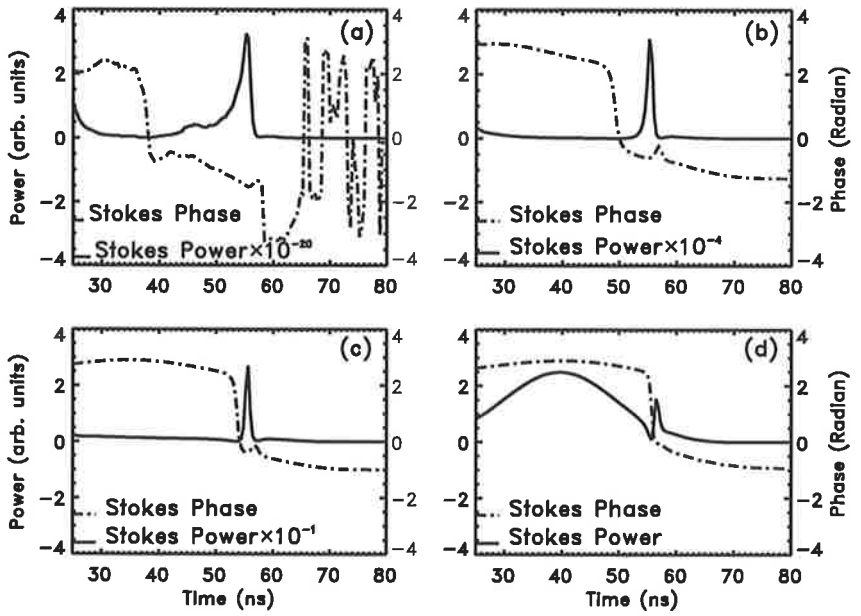

FIG. 12. The temporal position of phase jump and the beginning of the amplitude fluctuation (in figure 11) as they initiate at about $z = 0.46L$(a) inside the cell (where L is the cell length) and propagate through points $z = 0.56L$(b) and $z = 0.71L$(c) to the entrance of the cell(d).

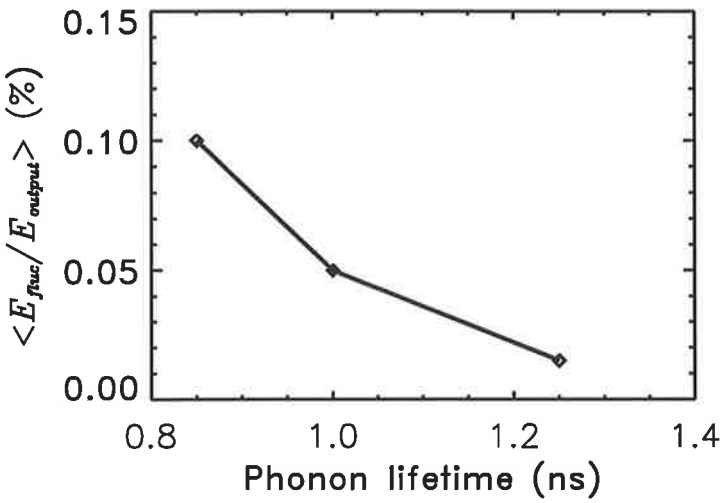

FIG. 13. Averaged fluctuation's energy (normalised to output energy) reduces for longer phonon lifetimes. Other parameters are as in figure 11.

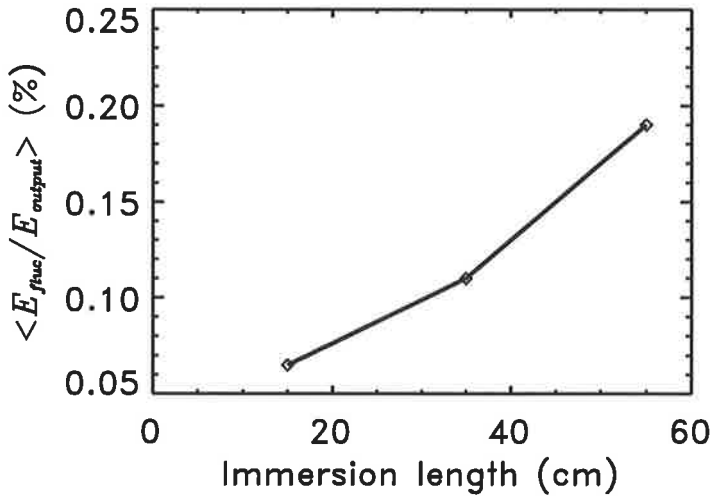

FIG. 14. The effect of the energy fluctuations, measured by $< \frac{E_{fluc}}{E_{output}} > \%$ is reduced for shorter immersion lengths (constant focal length and large cell to lens separation).

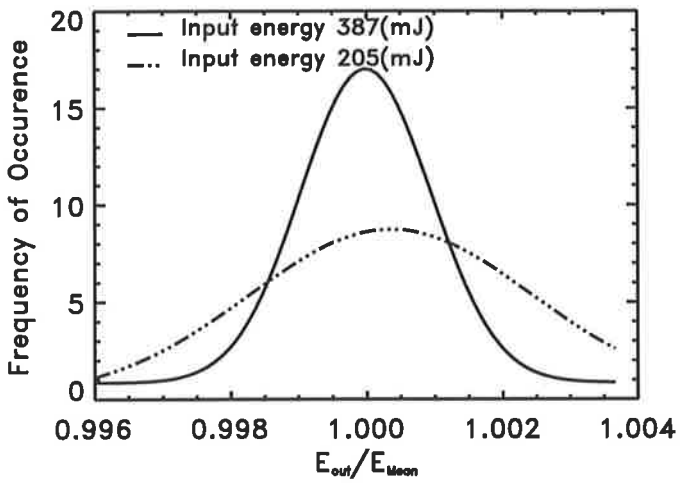

FIG. 15. Histogram of output energies (normalised to the mean) for two different energies 387 mJ and 205 mJ. Operating at high input energy reduces the effect of fluctuations.

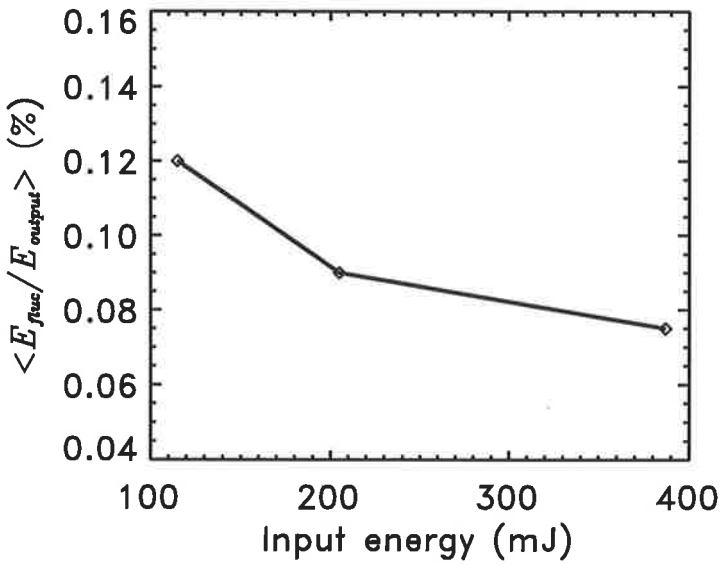

FIG. 16. A reduction in averaged fluctuation energy ($< \frac{E_{fluc}}{E_{output}} > \%$) occurs at high energies.

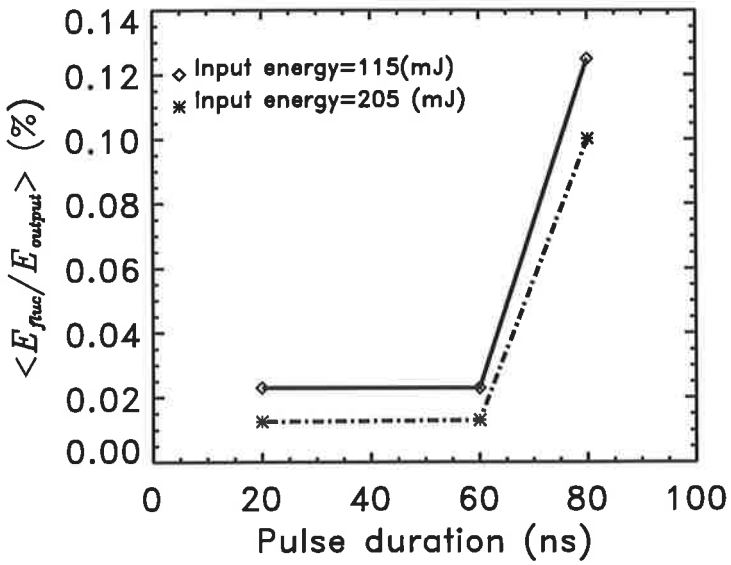

FIG. 17. For a constant energy, reducing the duration of the input pulse, dramatically suppress the fluctuation in the output Stokes. The effect of pulse duration on the suppression of fluctuations is shown for two energies: 115 mJ and 205 mJ.

APPENDIX 2

```
; Program: phase0
; Find the zero points of high-passed FFT traces, 24,05,95
; Authors: Martin O'Connor, Vladimir Devrelis and Chang-Jiang Wei
;
CLOSE,1

!P.MULTI = [0,0,3]

PRINT, 'Display on screen (1)or output a ps file (0)?'
READ, s
IF  ( s EQ 0 ) THEN BEGIN
PRINT, ' The data output is a pcl file'
SET_PLOT, 'ps'
DEVICE,filename='may18d.ps', xsize=18.0, ysize=21.0,xoff=1.0,yoff=4.0
!P.CHARSIZE = 2          &          !P.CHARTHICK = 3
!P.THICK = 3     &          !X.THICK = 3     &          !Y.THICK = 3
ENDIF ELSE BEGIN
PRINT, ' The output will be displayed in screen'
ENDELSE

n=1024                          ; number of TD data points

pm = dblarr(16)                 ; Power meter data, first 16 points
sc = dblarr(12)                 ; Scale factor
y = lonarr(32,n)   ; for 32 TD traces, each 1024 points
zz = fltarr(32,n)
t=findgen(n)                    ; time variable, 1024 points

OPENR,1,'d:\data95\may95\may18d'          ; open a data file
data = {aa17, A:dblarr(16), B:dblarr(12), $
        C1:lonarr(16384),C2:lonarr(16384)}
READF,1,data                            ; read data file into a structure

        FOR i=0, 14 DO BEGIN   ; read first 16 points power meter
        pm(i) = data.A(i)
        ENDFOR

xx = findgen(15) + 1

        FOR j= 0, 11 DO BEGIN  ; read scale factor
        sc(j) = data.B(j)
        ENDFOR

t = ((t - sc(5))*sc(1)+sc(4))*10.^9   ;normalize time as ns
dt = ((1 - sc(5))*sc(1)+sc(4))*10.^9            ;time interval in ns

        FOR m=0, 16383 DO BEGIN             ; byte-converting for TD1's traces

        dbyte = data.C1(m) AND 'FF00'X

        IF dbyte LT 0 THEN BEGIN
        dbyte = FIX((dbyte AND '7F00'X)/256) OR '0080'X
        ;Handle this having been interpreted as a signed number
        ENDIF ELSE BEGIN
        dbyte = FIX(dbyte/256)
        ENDELSE

        addbyte = data.C1(m) AND '00FF'X
```

```
        data.C1(m)= (addbyte * 256) + dbyte
        ;Count and remove interpolated data flag from data point (4000 hex)
        IF data.C1(m) GE '4000'X THEN BEGIN
        data.C1(m) = data.C1(m) - '4000'X
        ENDIF

        ENDFOR


        FOR m=0, 16383 DO BEGIN          ; byte-converting for TD2's traces

        dbyte = data.C2(m) AND 'FF00'X

        IF dbyte LT 0 THEN BEGIN
        dbyte = FIX((dbyte AND '7F00'X)/256) OR '0080'X
        ;Handle this having been interpreted as a signed number
        ENDIF ELSE BEGIN
        dbyte = FIX(dbyte/256)
        ENDELSE

        addbyte = data.C2(m) AND '00FF'X
        data.C2(m)= (addbyte * 256) + dbyte
        ;Count and remove interpolated data flag from data point (4000 hex)
        IF data.C2(m) GE '4000'X THEN BEGIN
        data.C2(m) = data.C2(m) - '4000'X
        ENDIF

        ENDFOR

yy=findgen(1024)          ;array with each element set to the value of its subscript.
yy(513:1023)=-REVERSE(yy(1:511));last 511 elements of yy a mirror image of the first 511.
FILTER=1./(1+(yy/15)^10)          ;This is a 5th order Butterworth filter with
                                  ;a cutoff of 15 cucles per total sampling period.

FOR l=0, 15 DO BEGIN              ; read 16 TD traces
n1=n-1
        FOR k=0, n1 DO BEGIN  ; read 1024 points for each trace
        y(l,k) = data.C1(k+ l*n)
        zz(l,k) = (y(l,k)-sc(0))* sc(2) + sc(3)          ; scaling
        ENDFOR


HIGHPASS=FFT(FFT(zz(l,*),1)*(1.0-FILTER),-1)  ;frequency domain high-pass filter.

hipass1 = float(highpass)
hipass1a=hipass1(100:900)
maxv=max(ABS(hipass1a))
hipass2 = hipass1/maxv

IF  ( s NE 0 ) THEN BEGIN
read,dd
ENDIF

j=50                      ;no. of zeros
zr = fltarr (j)           ;array of zeros
freq = fltarr (j)    ;frequency
aver = fltarr (j)    ;average frequency
std=fltarr(j)             ;standard frequency, a sample of five
```

```
        m = 0
        for k=1,n1 do begin
        if hipass2(k-1)*hipass2(k) LE 0.0 then begin
        m = m + 1
        zr(m-1) = k
        endif

        endfor
                i = 0
        for k=1, j-1 do begin
                if zr(k) GT 0 AND zr(k) LT 1023 then begin
                freq (k-1) = zr(k) - zr(k-1)
                IF freq(k-1) GT 0 THEN i = i+1

                endif
        endfor
sft = fltarr(i)
tsft = fltarr(i)
        stnd= total(freq(15:19))/5.0
        ave= total(freq)/(m-1)
        ;tsft(0)=(freq(0)-stnd)/stnd
tsft(0)=(freq(0)-ave)/ave
sf=0
        for k=0, i-1 do begin
                aver (k) = ave
                std (k) = stnd
                if freq(k) GT 0 then begin
                sft(k) =  (freq(k)-stnd)/stnd
                tsft(k) = sft(k) + sf
                sf = sf + sft(k)
                endif
        endfor


plot,t,zz(l,*),xrange=[0,10],xstyle=1,xtitle='TIME (ns)', $
 ytitle='POWER (a.u.)';,POS=[0.1,0.76,0.6,0.99]
fr=2.0/(freq*dt)
;fr=0.5/(freq*dt)
;fr=smooth(fr,2)
plot,(zr+0.5*ave)*dt,fr,yrange=[1,2.5],xrange=[0,10],xstyle=1,ystyle=1, $
xtitle='TIME (ns)',ytitle='BEAT FREQUENCY (GHz)';,POS=[0.1,.43,0.6,0.66]
oplot,(zr+0.5*ave)*dt, 0.5/(aver*dt)
;oplot, (zr+0.5*ave)*t, 0.5/(std*dt)
oplot,(zr+0.5*ave)*dt, 0.5/(freq*dt),psym=4
;plot,hipass2,xrange=[0,10],xstyle=1;,yrange=[-1.2,1.2],ystyle=1
plot,(zr+0.5*ave)*dt,smooth(tsft,2),xrange=[0,10],xstyle=1, $
xtitle='TIME (ns)', ytitle='PHASE (PI)';,POS=[0.1,0.1,0.6,.33]
;oplot,aver;, psym=4
;plot,hipass2;,yrange=[-.1,.1],xrange=[0,200],psym=4
;oplot,hipass2

ENDFOR

END
```

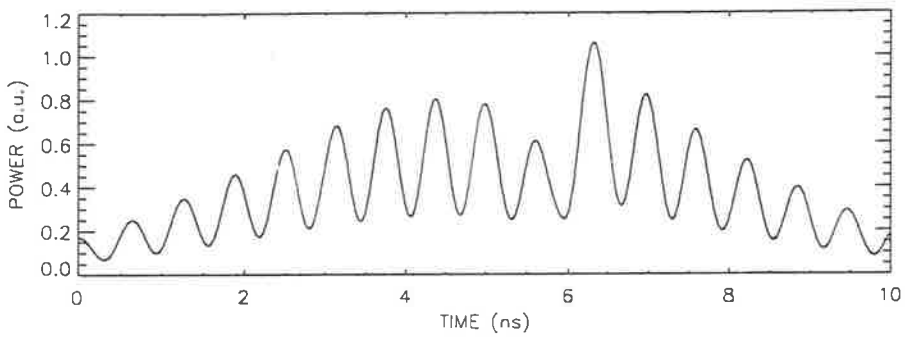
POWER (a.u.)
TIME (ns)

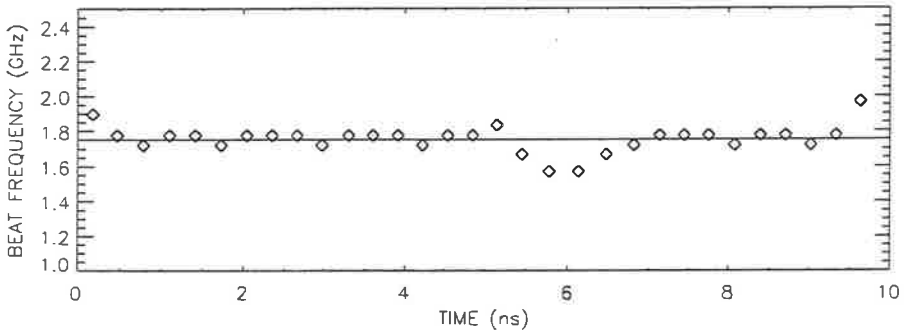
BEAT FREQUENCY (GHz)
TIME (ns)

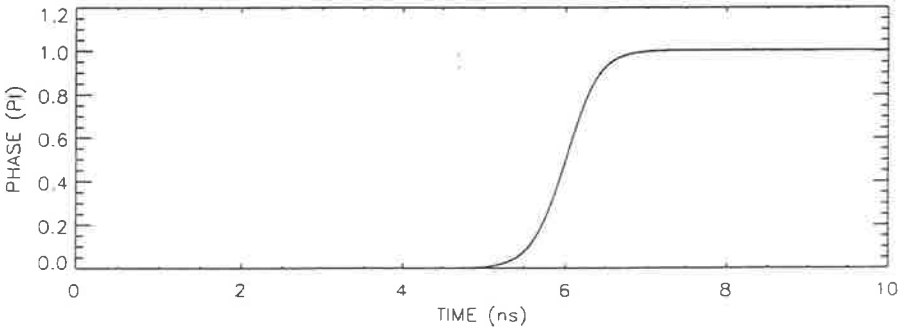
PHASE (PI)
TIME (ns)

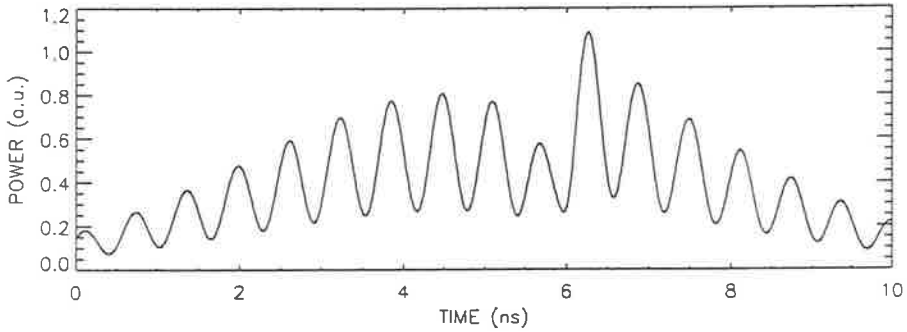
POWER (a.u.)
TIME (ns)

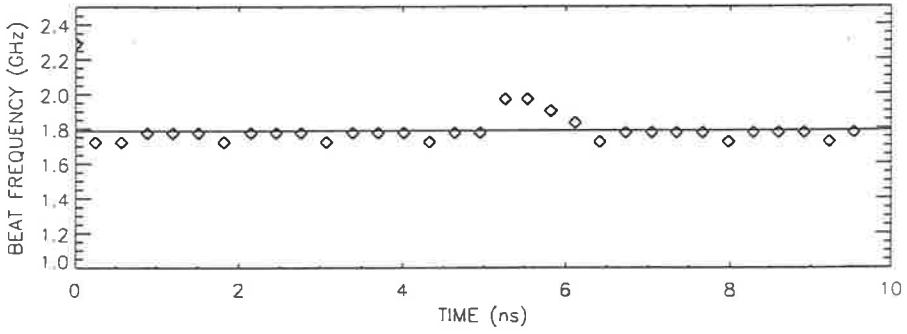
BEAT FREQUENCY (GHz)
TIME (ns)

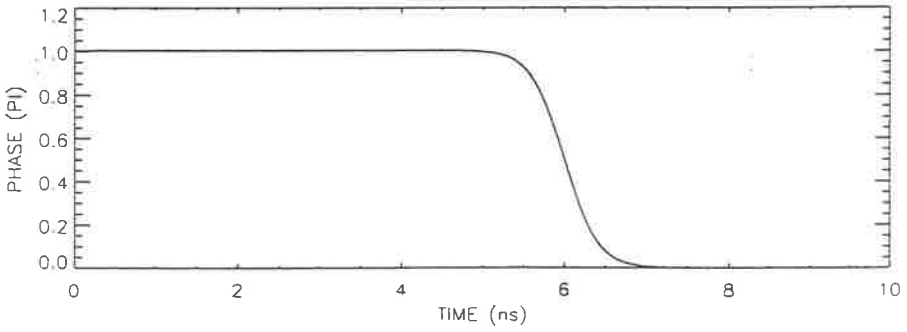
PHASE (PI)
TIME (ns)

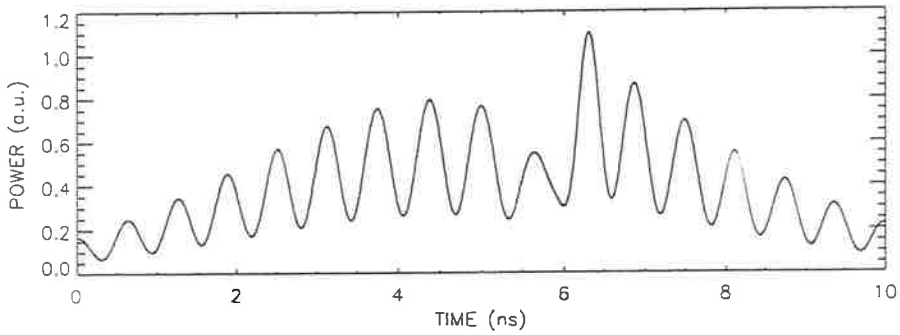
POWER (a.u.)
TIME (ns)

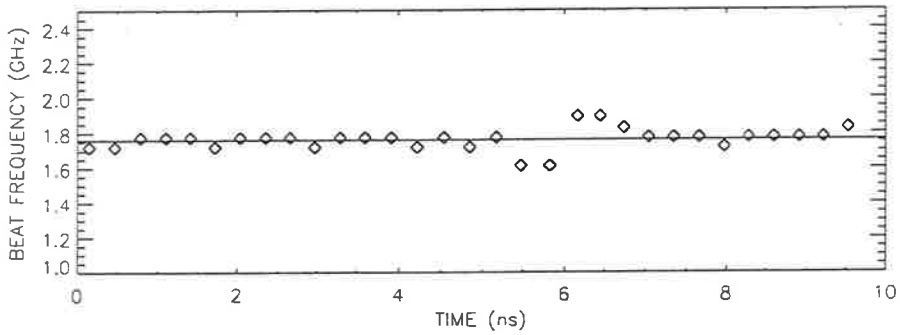
BEAT FREQUENCY (GHz)
TIME (ns)

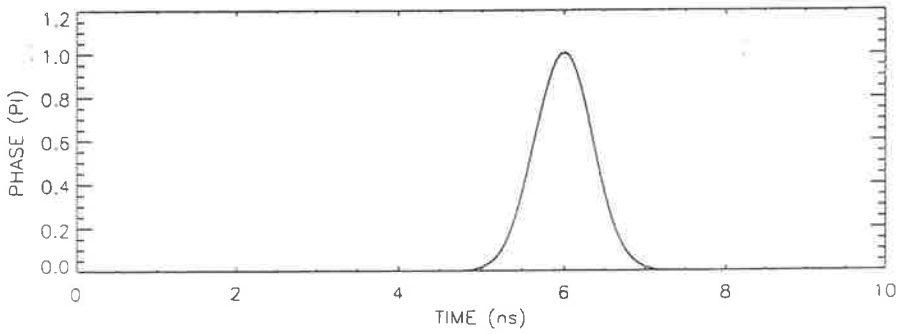
PHASE (PI)
TIME (ns)

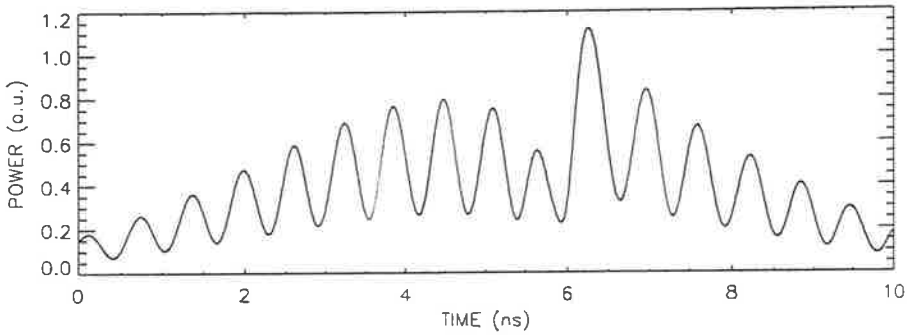
POWER (a.u.)
TIME (ns)

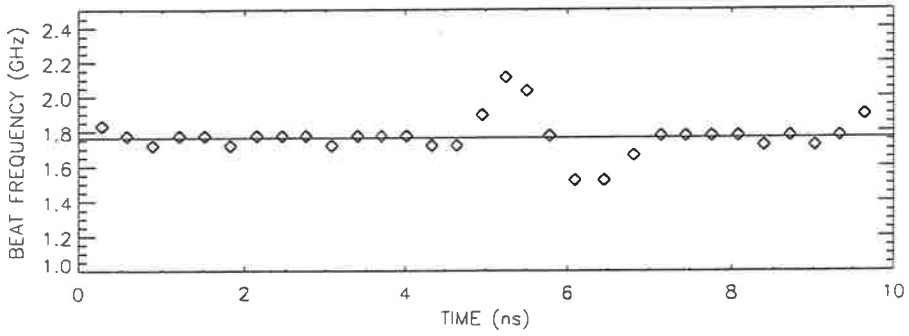
BEAT FREQUENCY (GHz)
TIME (ns)

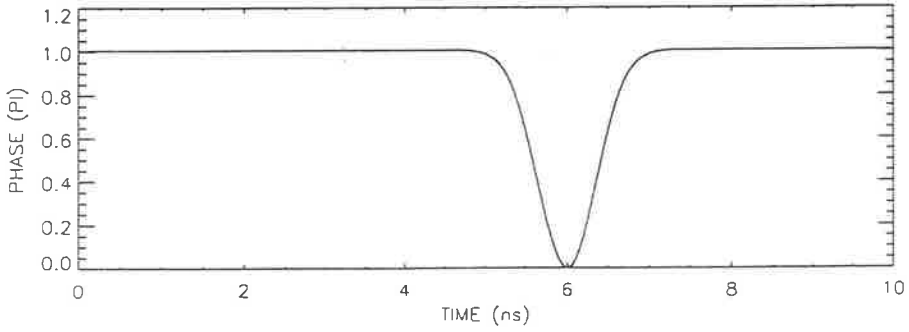
PHASE (PI)
TIME (ns)

APPENDIX 3

Devrelis, V., O'Connor, M. & Munch, J. (1995) Coherence length of single laser pulses as measured by CCD interferometry.
Applied Optics, v. 34(24), pp. 5386-5389

APPENDIX 4

Afshaarvahid, S., Munch, J. & Devrelis, V. (1997) Numerical study of stimulated Brillouin scattering initiated from noise.
Presented at: The Pacific Rim Conference on Lasers and Electro-optics, 14-18 July, Chiba, Japan.

APPENDIX 5

Munch, J., Devrelis, V. & Grissgono, A-M. (1995) Phase conjugation in solid state lasers. *Australian Optical Society news, v. 10(2), pp. 8-12*

APPENDIX 6

O'Connor, M., Devrelis, V. & Munch, J. (1995) SBS phase conjugation of a Nd:YAG laser for high beam quality.
Presented at: The International Conference on Lasers , 4-8 December, Charleston, South Carolina.